

University of Alberta

The Role of Bicarbonate Transporters in the Development of
Cardiovascular Diseases

by

Daniel Sowah

A thesis submitted to the Faculty of Graduate Studies and Research
in partial fulfillment of the requirements for the degree of

Doctor of Philosophy

In

Cell Biology

Department of Physiology

©Daniel Sowah
Spring 2014
Edmonton, Alberta

Permission is hereby granted to the University of Alberta Libraries to reproduce single copies of this thesis and to lend or sell such copies for private, scholarly or scientific research purposes only. Where the thesis is converted to, or otherwise made available in digital form, the University of Alberta will advise potential users of the thesis of these terms.

The author reserves all other publication and other rights in association with the copyright in the thesis and, except as herein before provided, neither the thesis nor any substantial portion thereof may be printed or otherwise reproduced in any material form whatsoever without the author's prior written permission.

Dedication

I wholeheartedly dedicate the volume of this work to my wife, Stella, and three kids, Manuelita, Philbert and Josiah.

Abstract

NHE1, whose activity and expression are elevated in cardiac hypertrophy, requires an acidifying pathway provided by AE3-mediated $\text{Cl}^-/\text{HCO}_3^-$ exchange to sustain its activity. Carbonic anhydrase II (CAII) interacts with NHE1 and AE3 to induce hypertrophy but the role of AE3 in hypertrophy is poorly elucidated. The present study seeks to characterize the interaction between CAII and AE1 as the prototype exchanger, and to delineate the role of AE3 in cardiac hypertrophy.

AE1, the plasma membrane $\text{Cl}^-/\text{HCO}_3^-$ exchanger of erythrocytes, interacts with CAII to maximize HCO_3^- transport. To characterize further the effect of CAII on AE1 transport, CAII-wildtype or catalytically inactive CAII-V143Y was fused to the COOH terminus of AE1 to form AE1.CAII and AE1.CAII-V143Y, respectively. When expressed in HEK293 cells, AE1.CAII had a similar $\text{Cl}^-/\text{HCO}_3^-$ exchange activity to AE1 alone, as assessed by the flux of H^+ equivalents ($87 \pm 4\%$ vs. AE1) or rate of change of $[\text{Cl}^-]_i$ ($93 \pm 4\%$ vs. AE1). Contrastingly, AE1.CAII-V143Y displayed transport rates for H^+ equivalents and Cl^- of $55 \pm 2\%$ and of $40 \pm 2\%$, versus AE1. AE1 fused to CAII-V143Y has reduced transport activity, which is compensated for during $\text{Cl}^-/\text{HCO}_3^-$ exchange by the presence of catalytically active CAII. When coexpressed with CAII-V143Y, AE1 bicarbonate transport was inhibited, whereas AE1.CAII activity was unaffected, suggesting impaired transport activity upon displacement of functional CAII from AE1 but not AE1.CAII.

The role of AE3 in hypertrophy was studied in *ae3* null mice (*ae3*^{-/-}) whose disruption did not affect cardiac function as determined by

echocardiography and blood pressure measurements. HW/BW ratio was larger in *ae3*^{+/+} compared to *ae3*^{-/-} mice. Hypertrophic stimulation with phenylephrine or angiotensin II caused a 25-30% increase in surface area, upregulated ANP and β -BHC levels, and elevated protein synthesis of wildtype cardiomyocytes but *ae3*^{-/-} cardiomyocytes were unaffected.

Our findings confirm CAII association with AE1 increases $\text{Cl}^-/\text{HCO}_3^-$ exchange activity, consistent with the HCO_3^- transport metabolon model. Additionally, AE3 operating in conjunction with CAII and NHE1 is essential in neurohormonal-stimulated hypertrophy, forming a hypertrophic transport metabolon. Thus, antagonism of AE3 is an attractive target in the treatment of cardiac hypertrophy.

Acknowledgments

I would like to extend my profound appreciation to my supervisor, Dr. Joseph Casey, for the opportunity to work in his laboratory. His guidance, words of encouragement, patience and constructive criticisms contributed immensely to the completion of my thesis and I will forever be grateful and indebted.

My thanks also go to my supervisory committee members, Dr. James Young and Dr. Peter Light for their unrelenting support during the pursuit of my PhD degree. Their suggestions and kind comments during supervisory committee meetings were invaluable and influenced positively my experiments and thesis preparation. I also express my sincere appreciation to my External Examiner, Dr. William Cole of the University of Calgary, for agreeing to be a part of my Examination Committee. Likewise I thank Dr. Larry Fliegel for deciding to serve on my Examination Committee as my Internal Examiner.

This thesis could not have been completed without the assistance and contributions by members of the Casey lab, both old and new. Their suggestions during weekly lab meetings enhanced and polished my experiments which enabled the successful completion of my thesis. Especially, I would like to thank Dr. Bernardo Alvarez who started characterizing the *ae3* knock-out and provided valuable data to set me off on that project. Also, Ms. Anita Quon deserves a mention because she introduced me to tissue culture work and also assisted in the collection of the RT-PCR data. Ms. Brittany Brown, Mr. Sam Lognathan, Drs. Danielle Johnson, Pamela Bonar, Gonzalo Vilas and Argha Basu all contributed

in various ways to create a great atmosphere in the lab for effective running of experiments.

My appreciation also goes to all the staff members at the Department of Physiology Main Office, whose hospitality and friendliness contributed positively to my degree.

Finally, I express my greatest love and appreciation to my wife, Stella, and our three lovely kids, Manuelita, Philbert and Josiah, whose unwavering support, love and care was the underpinning of my strength and motivation especially during some of the difficult moments of my PhD degree. I love them dearly.

Table of Contents

Chapter 1	1
General Introduction	1
1.1 Thesis Overview	2
1.2 Physiology of Cardiac Function.....	3
1.2.1 Regulation of $[Ca^{2+}]_i$	4
1.3 Intracellular pH Regulation.....	8
1.3.1 Proton Regulating Systems	9
1.3.1.1 Sodium/Proton Exchangers	11
1.3.1.2 Sodium/Bicarbonate Co-Transporters.....	15
1.3.1.3 The Chloride/Hydroxyl Exchanger	16
1.3.1.4 Chloride/Bicarbonate Anion Exchangers	17
1.4 Carbonic Anhydrases	25
1.5 The Bicarbonate Transport Metabolon	27
1.6 Signaling Pathways in Cardiac Hypertrophy	32
1.6.1 Signaling Pathways in Physiological Cardiac Hypertrophy.....	35
1.6.2 Signaling Mechanisms in Pathological Cardiac Hypertrophy	41
1.6.3 Concentric and Eccentric Cardiac Hypertrophy.....	52
1.6.4 Distinct Features of Cardiac Hypertrophy.....	54
1.6.4.1 Cardiac Hypertrophy and β -Myosin Heavy Chain.....	55
1.6.4.2 Natriuretic Peptides and Cardiac Hypertrophy	57
1.6.4.3 Alpha-Skeletal Actin and Cardiac Hypertrophy	58
1.7 Cardiomyopathies	59
1.8 Thesis Rationale.....	63
Chapter 2.....	122
Materials and Methods.....	122
2.1 Materials	123
2.2 Methods.....	128
2.2.1 Molecular Cloning.....	128
2.2.2 Expression of AE1 and AE1 Fusion Proteins	129

2.2.3 Immunoblotting.....	129
2.2.4 Cell Surface Biotinylation	130
2.2.5 Chloride/Bicarbonate Exchange Assays	131
2.2.6 Assays of Chloride Transport	133
2.2.7 Correction of MQAE Photobleaching.....	134
2.2.8 Calculation of Chloride Flux	135
2.2.9 Animal Care and Use	135
2.2.10 Heart Weight to Body Weight Ratio	136
2.2.11 Echocardiography.....	136
2.2.12 Blood Pressure Measurement.....	137
2.2.13 Isolation and Culture of Cardiomyocytes from Adult Mouse	137
2.2.14 Optimization of Conditions for Induction of Cardiomyocyte Hypertrophy	139
2.2.15 Assessment of Cardiomyocyte Hypertrophic Growth Using Optimal Condition.....	139
2.2.16 Real-Time Quantitative Reverse Transcription PCR (Real-Time qRT-PCR).....	140
2.2.17 Detection of Proteins by Immunoblotting	140
2.2.18 Protein Synthesis Assays.....	142
2.2.19 Measurement of pH_i in Adult Mouse Cardiomyocytes	143
2.2.20 Generation of CAII Adenoviral Constructs	144
2.2.21 Hematoxylin-Eosin Staining of Heart Sections	145
2.2.22 Statistical Analysis	146
Chapter 3.....	151
An Intramolecular Transport Metabolon Fusion of Carbonic Anhydrase II to the C-terminus of the $\text{Cl}^-/\text{HCO}_3^-$ Exchanger, AE1.....	151
3.1 Introduction.....	152
3.2 Results.....	156
3.2.1 Expression of AE1 and AE1 Fusion Proteins	156
3.2.2 Cell Surface Expression of AE1 and AE1 Fusion Proteins.....	158

3.2.3 Chloride/Bicarbonate Exchange Activity of AE1 and AE1 Fusion Proteins	161
3.2.4 Effect of CAII-V143Y on the Functional Activity of AE1.CAII.....	167
3.2.5 Effect of CAII Fusion on AE1 Chloride Transport Activity	170
3.3 Discussion	176
Bibliography	186
Chapter 4	192
Role of the Chloride/Bicarbonate Exchanger, AE3, in the Development of Cardiomyocyte Hypertrophy.....	192
4.1 Introduction.....	193
4.2 Results.....	198
4.2.1 Cardiac Development in <i>ae3^{-/-}</i> mouse	198
4.2.2 Blood Pressure and Echocardiography in <i>ae3^{-/-}</i> mice.....	199
4.2.3 Cardiomyocyte size in <i>ae3^{-/-}</i> mice.....	199
4.2.4 Effect of hypertrophic stimulation on hypertrophic molecular markers	203
4.2.5 HTM gene expression in <i>ae3^{-/-}</i> cardiomyocytes.....	208
4.2.6 Protein synthesis rate in <i>ae3^{-/-}</i> cardiomyocytes	210
4.2.7 p <i>H</i> _i regulation in <i>ae3^{-/-}</i> cardiomyocytes.....	210
4.2.8 Expression of p <i>H</i> _i regulators in <i>ae3^{-/-}</i> cardiomyocytes.....	211
4.3 Discussion	212
Bibliography.....	228
Chapter 5.....	238
Summary and Future Directions	238
5.1 Summary	239
5.2 Future Directions	245
5.2.1 An Intramolecular Transport Metabolon Fusion of Carbonic Anhydrase II to the C-terminus of the Cl ⁻ /HCO ₃ ⁻ Exchanger, AE1	245
5.2.2 Role of AE3 in the development of cardiomyocyte hypertrophy	249
Appendix.....	259
Generation of CAII Adenoviral Constructs	259
6.1 Introduction.....	260

6.2 Results and Discussion	262
6.2.1 Generation of adenoviral constructs.....	262
6.2.2 Expression of CAII proteins in cardiomyocytes	262
Bibilography	265

List of Tables

Table 2.1	Reagents
Table 2.2	Enzymes
Table 2.3	Antibodies
Table 2.4	Sequences of primers used in real time qRT-PCR
Table 3.1	Sample calculation of normalized rates of chloride/bicarbonate exchange
Table 4.1	Echocardiographic analysis of WT and <i>ae3</i> ^{-/-} mice

List of Figures

- Fig. 1.1 Schematic Representation of Cardiomyocyte Excitation-
Contraction Coupling
- Fig. 1.2 Schematic representation of the major pH regulatory transporters
in the cell
- Fig. 1.3 Topology Model of the Chloride/Bicarbonate Anion Exchanger
AE1
- Fig. 1.4 Schematic Illustration of the Bicarbonate Transport Metabolon
(BTM)
- Fig. 1.5 Schematic Representation of Cardiomyocyte Physiological
Hypertrophy
- Fig. 1.6 Schematic Representation of Pathological Hypertrophic Signaling
Pathway
- Fig. 1.7 The Hypertrophic Transport Metabolon (HTM).
- Fig. 3.1 Expression of AE1 and fusion proteins in HEK293 cells
- Fig. 3.2 Cell surface processing of AE1 fusion proteins
- Fig. 3.3 $\text{Cl}^-/\text{HCO}_3^-$ exchange activity in the absence and presence of
acetazolamide
- Fig. 3.4 Effect of acetazolamide on the rates of inward and outward
bicarbonate transport by AE1 variants
- Fig. 3.5 Effect of CAII-V143Y on AE1 and AE1.CAII $\text{Cl}^-/\text{HCO}_3^-$ activity
- Fig. 3.6 Correction of MQAE fluorescence Photobleaching

- Fig. 3.7 $\text{Cl}^-/\text{HCO}_3^-$ exchange activity of AE1 assessed by monitoring changes of $[\text{Cl}^-]_i$
- Fig. 3.8 Calibration curve to calculate Stern-Volmer Constant (K_{sv})
- Fig. 3.9 Rate of $\text{Cl}^-/\text{HCO}_3^-$ exchange of AE1 and fusion proteins, monitored by changes of $[\text{Cl}^-]_i$
- Fig. 3.10 Rate of $\text{Cl}^-/\text{NO}_3^-$ exchange by AE1 and AE1 fusion proteins
- Fig. 4.1 Heart weight to body weight ratio of wildtype ($ae3^{+/+}$), heterozygote ($ae3^{+/-}$) and knock-out ($ae3^{-/-}$) mice
- Fig. 4.2 Cross-sections of heart from wildtype ($ae3^{+/+}$) and knock-out ($ae3^{-/-}$) mice
- Fig. 4.3 Assessment of Cardiomyocyte Size
- Fig. 4.4 Optimization of Conditions for Induction of Cardiomyocyte Hypertrophy
- Fig. 4.5 Effect of hypertrophic stimuli on cardiomyocyte size
- Fig. 4.6 Effect of hypertrophic stimuli on hypertrophic marker genes
- Fig. 4.7 Effect of hypertrophic stimuli on NHE 1 and CAII Expression
- Fig. 4.8 Effect of Hypertrophic stimulation of CAII expression
- Fig. 4.9 Effect of hypertrophic stimuli on $[^3\text{H}]$ -Phe incorporation
- Fig. 4.10 Measurement of pH_i in freshly isolated cardiomyocytes
- Fig. 4.11 Expression of pH_i regulatory transporters
- Fig. 5.1 Expression of adenoviral constructs in neonatal cardiomyocytes.

List of Symbols, Nomenclature, Abbreviations

α	alpha
β	beta
μ	micro
γ	gamma
μg	microgram
α -AR	α -adrenergic receptor
AE	anion exchanger
AE3c	cardiac anion exchanger isoform 3
AE3fl	full length anion exchanger isoform 3
ANGII	angiotensin II
ANP	atrial natriuretic peptide
ATP	adenosine triphosphate
ATPase	adenosine triphosphatase
AT1	angiotensin receptor 1
ATZ	acetazolamide
β ARK1	β -adrenergic receptor kinase 1
BCECF	2'-7'-bis-(carboxyethyl)-5(6)-carboxyfluorescein
BCECF-AM	2'-7'-bis-(carboxyethyl)-5(6)-carboxyfluorescein acetoxymethyl ester
BDM	2,3-butanedione monoxime
BNP	brain natriuretic peptide
BP	blood pressure

BSA	Bovine serum albumin
BTM	bicarbonate transport metabolon
BW	body weight
CA	carbonic anhydrase
CAB	carbonic anhydrase binding motif
CaM	calmodulin
cAMP	cyclic adenosine monophosphate
cGMP	cyclic guanylyl monophosphate
Ca ²⁺	calcium ion
Cl ⁻	chloride
Cl ⁻ /HCO ₃ ⁻	chloride/bicarbonate
CMV	cytomegalovirus
CNP	C-type natriuretic peptide
CO ₂	carbon dioxide
CPTI	carnitine-palmitoyl transferase I
Ct	C-terminus or C-terminal tail
DAG	diacylglycerol
DCM	dilated cardiomyopathy
DMEM	Dulbecco's Modified Eagle's Medium
DNA	deoxyribonucleic acid
dRTA	distal renal tubular acidosis
EC	excitation-contraction coupling
eIF-4E	eukaryotic initiation factor 4E

4E-BP1	eukaryotic initiation factor 4E-binding protein 1
ET-I	endothelin I
EGFR	epidermal growth factor receptor
F	fluorescence at any given time
F ₀	fluorescence at time 0
FATP	fatty acid transport protein
FBS	fetal bovine serum
FFA	free fatty acids
g	gram
GAPDH	glyceraldehyde 3-phosphate dehydrogenase
GLUT1/4	glucose transporters 1 and 4
GPCR	G-protein coupled receptor
GST	glutathione-S-transferase
H ⁺	proton
HCM	hypertrophic cardiomyopathy
HTM	hypertrophic transport metabolon
HCO ₃ ⁻	bicarbonate ion
HEK293	human embryonic kidney 293 cells
HEPES	4-(2-hydroxyethyl)-1-piperazineethanesulfonic acid
HF	heart failure
HW	heart weight
I ⁻	iodide ion
IGF1	insulin-like growth factor 1

IgG	immunoglobulin G
IP3	inositol triphosphate
IR	ischemia-reperfusion
IVRT	isovolumic relaxation time
kDa	kiloDalton
KO	knock-out
K_{sv}	Stern-Volmer constant
KSCN	potassium thiocyanate
J_H^+	equivalent proton flux
JNK	c-Jun N-terminal kinases
m	milli
M	molar
MAPK	mitogen activated protein kinase
MCM	myocyte culture medium
MCT	monocarboxylate transporter
mg	milligram
MHC	myosin heavy chain
MQAE	<i>N</i> -(ethoxycarbonylmethyl)-6-methoxyquinolinium bromide
mRNA	messenger ribonucleic acid
mTOR	mammalian target of rapamycin
Na^+	sodium ion
NBC	sodium-bicarbonate co-transporter
NCX	sodium-calcium exchanger

NFAT	nuclear factor of activated T-cells
NHE1	sodium proton exchanger 1
Na ⁺ /K ⁺ ATPase	sodium potassium adenosine triphosphatase
NKCC	sodium potassium two chloride transporter
NO ₃ ⁻	nitrate ion
NP	natriuretic peptide
OH ⁻	hydroxyl ion
PBS	phosphate-buffered saline
PCR	polymerase chain reaction
PE	phenylephrine
PGC-1	peroxisome proliferator-activated receptor gamma co-activator-1
pH _i	intracellular pH
PIP ₂	phosphatidylinositol 1,2-bisphosphate
PIP ₃	phosphatidylinositol (3,4,5) triphosphate
PKA	protein kinase A
pK _a	acid-dissociation logarithmic constant
PKB	protein kinase B
PKC	protein kinase C
PKD	protein kinase D
PKG	protein kinase G
PLB	phospholamban
PLC	phospholipase C

PP	protein phosphatase
PPAR α	peroxisome proliferator-activated receptor alpha
PVDF	Polyvinylidene difluoride
qRT-PCR	quantitative real-time reverse transcriptase polymerase chain reaction
RAS	renin-angiotensin system
RBC	red blood cell
RyR	ryanodine receptor
SR	sarcoplasmic reticulum
SERCA	sarcoplasmic reticulum calcium ATPase
SDS	sodium dodecyl sulphate
SDS-PAGE	sodium dodecyl sulphate polyacrylamide gel electrophoresis
SHR	spontaneously hypertensive rat
SLC	solute carrier
SO $_4^{2-}$	sulphate ion
TBST	Tris-buffered saline and Tween-20
TBST-M	Tris-buffered saline and Tween-20 with milk
TCA	trichloroacetic acid
TD	transmembrane domain
TMA	trimethylamine
v/v	volume by volume
w/v	weight by volume

WT

wildtype

Chapter 1

General Introduction

1.1 Thesis Overview

Bicarbonate (HCO_3^-) is part of the major pH buffering system in cells and thus ensures normal physiological processes. The charge on HCO_3^- necessitates trans-membrane transport mediated by bicarbonate transporters, suggesting a critical role of these proteins in many cellular and biological processes. The goal of the present study was to understand the physiological roles of HCO_3^- transporters in relation to their interaction with a group of enzymes called carbonic anhydrases (CA). Accumulating evidence reveals that bicarbonate transporters interact both physically and functionally with CAs, which confers maximal transport capability to the transporters. Our objective was to probe further into this phenomenon. Specifically, the effect of fusing CA isoform II to the carboxyl terminus of the chloride/bicarbonate ($\text{Cl}^-/\text{HCO}_3^-$) anion exchanger AE1 was investigated.

The second goal of this thesis was to elucidate the role played by AE3 in the hypertrophic growth of the heart. The $\text{Cl}^-/\text{HCO}_3^-$ anion exchanger, AE3, is expressed predominantly in excitable tissues, such as retina, brain and the heart. Several lines of evidence suggest that the AE3 isoform contributes to intracellular pH (pH_i) homeostasis in the heart. In concert with the sodium/protein exchanger 1 (NHE1) and CAII, it has been proposed that AE3 activation by hypertrophic stimuli can lead to development of cardiac hypertrophy.

1.2 Physiology of Cardiac Function

The primary role of the mammalian heart is to provide continuous supply of blood to all parts of the body. In so doing, the heart supplies nutrients and oxygen to all organs to maintain their normal functions and in turn carries end-products of metabolism for excretion out of the body. The pumping action of the heart is made possible by electrical activities initiated by the natural pacemaker, the sino-atrial (SA) node (231), located in the right atrium that spread as a wave of excitation throughout the atria and the ventricles of the heart. Normal cardiac function is maintained by tight coordination between the impulse generation system, the SA node and the impulse propagation system, the Bundle of His and the Purkinje fibers (214).

Arrival of an action potential at the cardiac muscle cell surface membrane induces membrane depolarization by initially stimulating Na^+ channels, which leads to activation of voltage-dependent L-type calcium (Ca^{2+}) channels, allowing influx of extracellular Ca^{2+} (165) (Fig. 1.1). The T-type Ca^{2+} channels (274) and the $\text{Na}^+/\text{Ca}^{2+}$ exchanger (NCX) (32) are also involved with initial entry of Ca^{2+} , following membrane depolarization. The initial influx of Ca^{2+} induces further release of Ca^{2+} via the ryanodine receptors (RyR2) (318, 329) located on the sarcoplasmic reticulum (SR). The L-type Ca^{2+} channels are located in the transverse (T) tubules of the sarcoplasmic membrane and RyR2 channels are found on the SR adjacent to the T-tubules. In this manner, the local concentration of Ca^{2+} is increased to induce Ca^{2+} release through the RyR2 channels (57). The Ca^{2+} released by this phenomenon known as Ca^{2+} -induced- Ca^{2+} -release (CICR)

(57), about 10-fold the basal level of cytosolic Ca^{2+} , is responsible for the contraction of the myofibrils resulting in the contractile phase (systole) of the cardiac cycle. Myocardial contraction occurs when Ca^{2+} binds to troponin C which displaces tropomyosin, resulting in a cross-bridge formation between actin and myosin filaments (57, 318). To ensure the rhythmic beating of the heart, cardiac relaxation (diastole) occurs immediately, initiated by dissociation of Ca^{2+} from troponin C (273) followed by Ca^{2+} extrusion made possible by two mechanisms; 1. Efflux of Ca^{2+} through the sarcolemmal NCX (29, 33), which mediates the influx of 3 Na^+ ions in exchange of 1 Ca^{2+} ion (296), and 2. Sequestration of Ca^{2+} into the SR stores by the Ca^{2+} -transport ATPase, the SERCA pump (43, 57).

Cardiac function is therefore tightly regulated at various levels in order to maintain the normal function of the heart. Although the exact intricate regulatory mechanisms of cardiac function are not fully understood, most of the regulatory mechanisms involve regulation of intracellular Ca^{2+} levels (134, 317). Deviation from the normal physiological handling of $[\text{Ca}^{2+}]_i$ is detrimental to cardiac function and underlies the cause and progression of many cardiovascular diseases (235).

1.2.1 Regulation of $[\text{Ca}^{2+}]_i$

Intracellular Ca^{2+} exerts major regulatory roles in the cardiomyocytes. It is involved in intracellular signaling (30, 54), gene expression (319), regulation of mitochondrial function, excitation-contraction (EC) coupling (33) and cell death (30). As noted in the previous section, electrical activities of cardiac cells impose

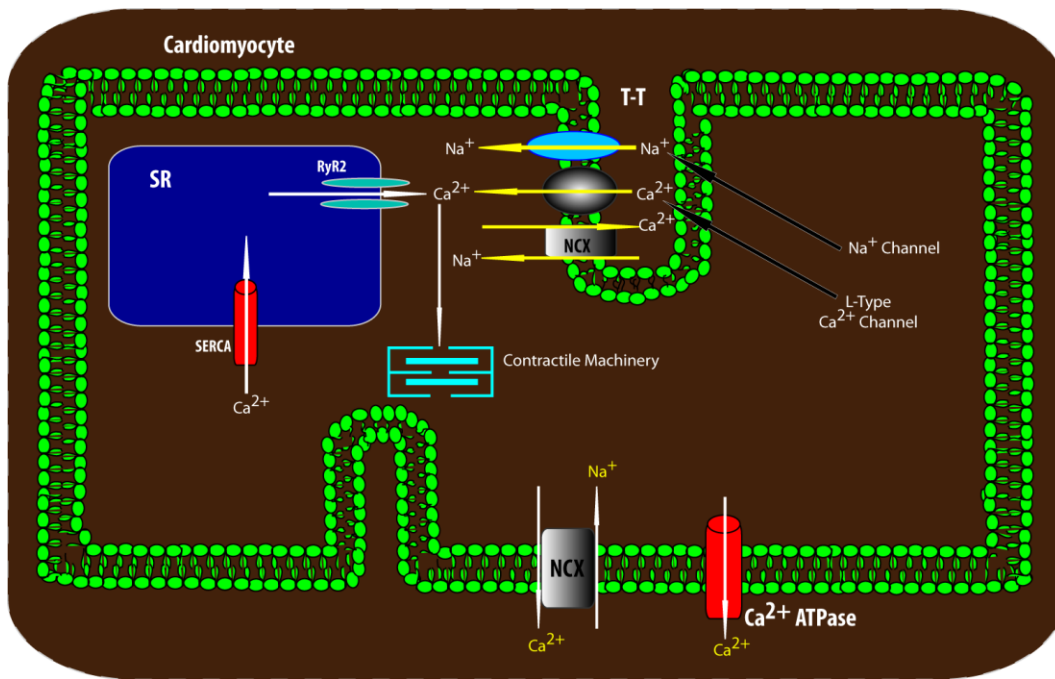


Fig. 1.1 Schematic representation of cardiomyocyte excitation-contraction coupling. An action potential induces opening of Na⁺ channels which leads to activation of voltage-dependent Ca²⁺ channels (L-type Ca²⁺ channels), both localized on the transverse tubule (T-T). The cytosol is subsequently overloaded with Ca²⁺, which causes release of Ca²⁺ from the ryanodine receptors (RyR2) located on the sarcoplasmic reticulum (SR). This intracellular Ca²⁺ interacts with the contractile apparatus, representing the systolic phase of the contractile cycle. Diastole is characterized by uptake of Ca²⁺ into the SR via the SR Ca²⁺ ATPase (SERCA) and extrusion of Ca²⁺ via the sodium-calcium exchanger (NCX) and the sarcolemmal Ca²⁺ ATPase (details in the text).

an increase in $[Ca^{2+}]_i$, resulting in the steady and continuous contractile function of the heart. This phenomenon, referred to as excitation-contraction (EC) coupling (117), must be tightly controlled since alterations in this process can lead to cardiac dysfunction and disease. Much knowledge on the regulation of $[Ca^{2+}]_i$ has accumulated over the past decade and the molecular processes are becoming increasingly understood (33, 43, 54, 57). Hormonal regulation (321, 322), influence of other cytosolic ions (123, 290) and myocardial energetics (21, 187) have all been shown to control $[Ca^{2+}]_i$. Neurohormones, including angiotensin II (ANGII), endothelin I (ET-I) and epinephrine/norepinephrine (84), influence cytosolic Ca^{2+} levels by initially interacting with sarcolemmal surface receptors referred to as G-protein coupled receptors (GPCR) leading to activation of intracellular second messenger molecules. Stimulation of β -adrenergic receptors by catecholamines for instance, increases the second messenger, cAMP (253), which in turn activates protein kinase A (PKA) (84, 253). PKA phosphorylates L-type Ca^{2+} channels and induces an increase in the opening probability of the channels (reviewed in (91)). This effect underlies the positive chronotropic and inotropic properties of β -adrenoceptor agonists. The stimulation of the α -adrenergic receptors and the angiotensin receptors by catecholamines and ANGII respectively, activate protein kinase C (PKC) (332) which have been shown to exert numerous regulatory effects on cardiac Ca^{2+} handling (detailed mechanisms will be discussed in a later section.)

Interestingly, the cardiac RyRs are under phosphorylation control by PKA, which increases Ca^{2+} release from the SR stores (196, 198). Prolonged activation

of the channel, however, leads to Ca^{2+} leak, which may cause cardiac dysfunction and heart failure (196, 198). RyRs also associate with Ca^{2+} -binding proteins such as calmodulin (320), whose interaction inhibits the channel. This suggests that at high cytosolic Ca^{2+} concentration, binding of the Ca^{2+} -calmodulin complex to RyRs negatively regulates the channel to prevent further release of Ca^{2+} from the SR (321).

The reuptake of Ca^{2+} into the SR stores through the SERCA pump is crucial in the cardiac cycle. The opening of SERCA is regulated by phospholamban (PLB) (273); phosphorylation of PLB by PKA and/or Ca^{2+} -calmodulin dependent protein kinase promotes opening of the pump (119, 201) while the channel is inhibited when PLB is dephosphorylated by protein phosphatase 1 (PP-1) (219, 284).

The sarcolemmal NCX operating in the physiological mode (forward mode), extrudes cytosolic Ca^{2+} following contraction leading to cardiac relaxation. Thus $[\text{Ca}^{2+}]_i$ and ultimately cardiac contractility depends partially on the activity of the NCX. NCX is a target of PKA (156, 332) and PKC (332) whose phosphorylation of the exchanger enhances activity. NCX is also regulated by the concentration of ions such as protons (H^+), Na^+ and Ca^{2+} . The exact mechanism of regulation of NCX by these ions is too complex to discuss here.

Abnormal handling of Ca^{2+}_i due to abnormal regulation at any step during the Ca^{2+} cycle is the hallmark of many myocardial abnormalities. Contractile dysfunction (91), arrhythmias (253) and heart failure (91) may arise as a consequence.

1.3 Intracellular pH Regulation

Due to the heart's high metabolic demands, large amounts of carbon dioxide (CO_2) are produced as a by-product of oxidative metabolism. CO_2 can diffuse across the plasma membrane and ultimately be expired via the lungs. Intracellular metabolism of CO_2 which involves interaction with H_2O , a process catalyzed by a group of enzymes called carbonic anhydrases (discussed in detail below) results in the production of large amount of protons (H^+) and proton equivalents (HCO_3^-) which will influence cardiac function (237, 238) by modulation intracellular pH. Regulation of intracellular pH (pH_i) is therefore, central to maintain normal physiological processes of the myocardium (227). pH is a measure of the hydrogen ion concentration (proton, H^+) and modulation of its concentration affects many biological processes. Organisms have therefore developed many strategies to maintain cytosolic pH within the physiological range of 7.1-7.2 intracellularly and 7.3-7.4 extracellularly (98).

Intracellular acidosis affects myocardial contractile function by reducing the delivery of Ca^{2+} to the contractile machinery as well as decreasing the sensitivity of the myofibrils to Ca^{2+} (226, 306). Metabolic acidosis as occurs during cardiac ischemic episodes impairs energy metabolism by inhibiting oxidative metabolism and thus, ATP production (285). Additionally, under diseased conditions, most of the ATP produced is harnessed to normalize the prevailing acidotic condition rather than been used to support contractile function (97, 105). Several reports show that myocardial acidosis alters cardiac efficiency (measure of cardiac work performed per amount of energy consumed by the heart)

by decreasing the efficiency of ATP production or alterations of energy usage to perform contractile work (143, 333). The latter occurs as a result of sequelae of events induced by myocardial ischemia. Myocardial ischemia inhibits the Na^+/K^+ ATPase, which regulates resting membrane potential by mediating the efflux of 3 Na^+ for 2 K^+ (31). Coupled with the activation of the cardiac NHE1, the ensuing intracellular Na^+ overload activates the reverse mode NCX which ultimately leads to intracellular Ca^{2+} accumulation (31). Consequently, myocardial ATP stores are invested to restore the ionic imbalance diverting energy away from contractile activity. Thus, myocardial intracellular acidosis exerts profound effects on overall function and pathophysiology of the heart (142, 225, 306). Understanding the source of acidosis and its regulation will enable the identification of new drug targets under disease states.

1.3.1 Proton Regulating Systems

In order to limit the changes of pH_i associated with H^+ production or consumption, three systems are employed in the cytosol. These include: 1. intracellular intrinsic buffering systems (304), 2. extrinsic buffering systems ($\text{CO}_2/\text{HCO}_3^-$ buffer system) (175, 176) and 3. activation of transporters of proton and/or proton equivalents (304, 306).

Buffer capacity is the ability of a system to resist changes in pH. Cardiac cells like all other cells are equipped with an inherent ability to withstand changes in pH_i . This affords the first line of protection against acute changes in pH_i in the cardiomyocytes and comprises two components; the intrinsic and extrinsic buffering systems. Making up the intrinsic buffer systems are the imidazole

groups of histidine residues on intracellular proteins and dipeptides (42). Proteins are able to neutralize excess protons due to the presence of histidine residues, with pKa values close to pH_i (42, 308). In sheep cardiac Purkinje fibers and the isolated ventricular cardiac cells, the intrinsic buffer capacity was estimated to be 15-20 mM per pH unit at pH_i of 7.2 (42, 308). To a lesser extent inorganic phosphate and taurine also contribute about 11 mM per pH unit at pH_i of 7.1 to the total intrinsic buffering capacity (175, 304).

The extrinsic component of the intracellular pH buffer system is offered by the $\text{CO}_2/\text{HCO}_3^-$ system (81). The formation of HCO_3^- from CO_2 is mediated by carbonic anhydrases enzymes (CAs), indicating the significant role of CAs in pH_i regulation. A separate section of the present report is devoted to CA activities and their regulation. In isolated guinea-pig ventricular myocytes, the component of the intracellular buffer capacity contributed by the CO_2 -dependent mechanism under resting conditions was $2.3 \times [\text{HCO}_3^-]_i$ at pH_i of 7.1 (175). At resting pH_i of 7.1, the cytosolic concentration of HCO_3^- is 12 mM (175). Taken together the total intracellular buffer capacity of ventricular myocytes contributed by both intrinsic and extrinsic mechanisms under a resting pH_i of 7.1 was ~56 mM.

The myocardium also expresses a number of sarcolemmal transporters which mediate the transport of H^+ and H^+ equivalents (36, 114). These transporters are categorized as proton extruders, the sodium/proton exchanger (NHE1) (36, 114) and the sodium/bicarbonate co-transporter (NBC) (73, 170), or proton loaders, the chloride/bicarbonate anion exchanger (AE) and the chloride/hydroxyl exchanger (CHE) (176, 286) (Fig. 1.2). At resting pH_i in

isolated guinea-pig ventricular myocytes all the pH regulatory transport proteins have low transport rates of ~ 0.15 mM/min (175) which suggests that they are all activated to the same extent in the steady state. Transport activities of the proton regulatory transporters are considerably elevated during increased workload when the cell is loaded with H^+ equivalents. To a smaller extent, another group of transporters referred to as the monocarboxylate transporters (MCT) are activated under certain conditions to mediate pH_i homeostasis (122, 303). A concerted interplay between activation of the pH regulatory proteins exists to ensure the maintenance of extracellular and intracellular pH within the physiological range.

1.3.1.1 Sodium/Proton Exchangers

The major mechanism by which the cardiac cell overcomes intracellular acidotic load is by activation of the sodium/proton exchanger 1 (NHE1). Members of the NHE family of proteins are integral membrane glycoproteins that catalyse the transport of one intracellular H^+ in exchange for one extracellular sodium ion (Na^+), thus normalizing pH_i under conditions of acidosis. Nine isoforms of NHEs designated NHE1-9 (64, 318) have been identified in mammalian cells and NHE1, the ubiquitously expressed isoform in most tissues is primarily found in cardiac cells (96). By maintaining pH_i at physiological levels, NHE1 plays an important role in cardiac function (95). Moreover, NHE1 activity is involved in the regulation of cell volume (242), cell growth and proliferation (133, 147) as well playing a role in cell survival and programmed cell death phenomenon known as apoptosis (171, 172).

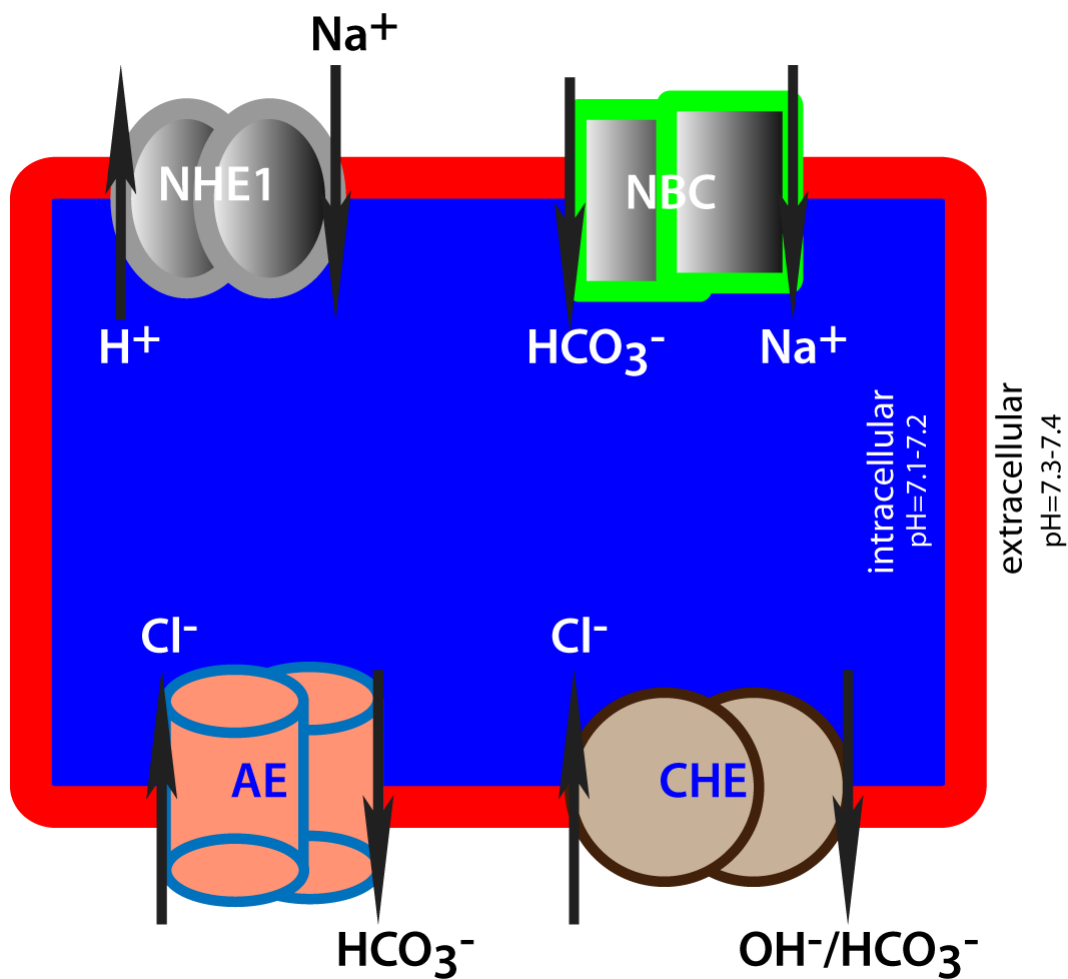


Fig. 1.2 Schematic representation of the major pH regulatory transporters in the cell. pH regulatory transporters are categorized into proton loaders, anion exchangers (AE) and chloride-hydroxyl/bicarbonate (CHE), and proton extruders, sodium-proton exchanger 1 (NHE1) and sodium-bicarbonate co-transporters (NBC). These transporters operate in concert to maintain intracellular pH at 7.1-7.2 and extracellular pH at 7.3-7.4 (details in the text).

Although the structure of NHE1 has not been fully resolved, accumulating hydropathy profiles coupled with cysteine scanning mutagenesis whereby an individual cysteine mutation is introduced into a cysteineless mutant and evaluating accessibility to sulfhydryl reactive agents, have demonstrated that NHE1 is composed of 10-12 transmembrane domains (TD) (168) with a short amino (N-) terminal domain and a large carboxyl (C-) terminal tail which are both located in the cytosol (249). These studies have also revealed an N-linked glycosylation site at N75 and a re-entrant loop at the tenth TD (173). Further details on the topology of NHE1 have been elucidated by studies in the bacterial NHE1 homologue, NhaA, albeit having a stoichiometry dissimilar to that of NHE1 in exchanging one H^+ for 2 Na^+ ions (228). Recently, a high resolution X-ray structure of NhaA has been solved (137, 228) which has enabled a 3D modeling of NHE1 structure. NhaA contains 12 TD helices with a long loop between TD 1 and 2 which contained a surface associated helix and two beta sheets responsible for dimer formation. TDs 4 and 11 contained extended regions in the center of each helix which may be responsible for transport activities of NhaA (268).

The 3D structure of NHE1 also comprises 12 TDs without the first two helices suggested by the previous model (314). The new 3D topology model also revealed that TD 9 of the previous model may be split into two helices (TD 7 and 8) and the re-entrant loop is now reassigned TD 9. The assemblage of TD 4 and 11 was similar to the crystal structure of NhaA. Two highly conserved aspartate residues (D163 and D164) on TD 5 in NhaA, responsible for cation binding were

equivalent to N266 and D267 in the eukaryotic structure. A high resolution X-structure of NHE1 is, however, far from being solved due mainly to poor overexpression of NHE1 and the difficulty in purifying the protein. Current structural studies of NHE1 therefore involve low resolution analysis of individual TDs by NMR and single particle electron microscopy. In general, these studies have demonstrated that the TD is responsible for the transport activity of NHE1 and possesses an allosteric H⁺ sensor site that confers H⁺ sensitivity to the exchanger (242, 315). The cytoplasmic C-terminus provides possibilities for regulation by various mechanisms through interaction with other cytosolic molecules (180).

The C-terminal tail interacts with cytosolic proteins and co-factors and it contains consensus sequence sites for phosphorylation by numerous protein kinases following growth factor activation (64). NHE1 is constitutively phosphorylated (261) and further phosphorylation enhances exchange activity by shifting pH sensitivity to the alkaline range (96, 262). Some of the proteins shown to interact with NHE1 include calmodulin (275), calcineurin homologue protein 1 (182), tescalin and carbonic anhydrase II (177, 179). The physiological relevance of the interaction of NHE1 with the latter will be elaborated at a later section. The phosphorylation control of NHE1 activity by pro-hypertrophic stimulants will be discussed at a later section. The many regulators of NHE1 enable the fine-tuning of the activity of the exchanger.

NHE1 is at the epicenter of many cardiovascular diseases including ischemia-reperfusion injury (20, 294), cardiac hypertrophy and heart failure (233,

266). Inhibiting the activity of NHE1 during and following an ischemic episode has proven efficacious in various ischemia-reperfusion models (reviewed in (5, 6, 150)). A plethora of experimental models of cardiac hypertrophy and heart failure have revealed promising evidence for NHE1 as an attractive therapeutic target (166, 328).

1.3.1.2 Sodium/Bicarbonate Co-Transporters

The other major mechanism by which cardiac cells regulate intracellular acidosis is through NBCs, which mediate the co-transport of Na^+ and HCO_3^- into the cell. By so doing, the reduction of pH_i is normalized by the influxed HCO_3^- , which neutralizes the H^+ ions. Since one molecule of HCO_3^- neutralizes one H^+ ion, NBCs are described as H^+ -equivalent transporters. The contribution by the NBCs to intracellular acid normalization is, however, minimal in comparison to the fraction contributed by NHE1 (61). Thus in the myocardium, alkalinizing activity is mediated by a proton extrusion mechanism (by NHE1) and a bicarbonate influx component by Na^+ - HCO_3^- symporters although NHE1 activation is the predominant pathway that induces intracellular alkalization (293, 307, 324).

In the myocardium, both the electroneutral NBC, with a stoichiometry of 1 Na^+ :1 HCO_3^- and the electrogenic NBCs, NBCe1 and NBCe2 with a stoichiometry of 1 Na^+ :2 HCO_3^- are expressed in ventricular cells of different species (rats, rabbits, guinea pigs and humans) (51, 325). By using protein immunofluorescence and confocal imaging cardiac NBC isoforms were shown to

be localized to the lateral sarcolemma, intercalated discs and T-tubules of rat ventricular myocytes (106).

The functional consequences of NBC activation in the myocardium are not fully characterized, but in rat and cat ventricular myocytes, NBC activation was shown to generate anionic repolarizing current which induced an ~25% shortening of action potential (2). A recent report (56) suggested that inhibition of the transporter by the specific inhibitor, S0859, afforded cardioprotection in ischemic-reperfused animal hearts. The exact mechanism of cardioprotection is not fully dissected, but it is believed to involve a decrease in Ca^{2+}_i overload secondary to a reduction in Na^+_i overload (154, 263). Thus, the NBC is proposed to be involved in myocardial contractility by influencing Ca^{2+}_i concentration (56).

1.3.1.3 The Chloride/Hydroxyl Exchanger

In guinea-pig ventricular myocytes a component of the intracellular pH regulatory mechanism was mediated by an unidentified chloride-dependent acid loader (286). Subsequent functional characterization revealed the acid loader as a Cl^-/OH^- exchanger that catalyses the extrusion of intracellular OH^- in exchange for extracellular Cl^- (136). The Cl^-/OH^- exchanger, now identified as SLC26A6, belongs to the SLC26 family of 11 genes (277). Adult mouse heart expresses both *slc26a3* and *slc26a6* isoforms on the sarcolemma (13). Members of the SLC26 gene are capable of mediating the exchange of other ions including HCO_3^- and SO_4^{2-} , I^- , formate and oxalate (125, 194, 195, 206). Some of the members of the SLC26 gene family are associated with genetic disorders; SLC26A2 in

chondrodysplasias, SLC26A3 is involved with diarrhea and SLC26A4 is associated with Pendred syndrome (211).

Interest in the function of SLC26A6 in cardiac function has been heightened over the past few years due to the discovery that among the $\text{Cl}^-/\text{HCO}_3^-$ anion exchangers expressed in the mouse heart, SLC26A6 is the most predominantly expressed cardiac isotype (13). The functional consequences of the high expression level of SLC26A6 in the myocardium are not evident at present.

Controversy also surrounds the electrogenicity of SLC26A6 in heart function. A recent report showed that SLC26A6 mediates an electroneutral transport of 1 OH⁻ in exchange for 1 Cl⁻ (211, 220). The role of the exchanger in disease conditions is not characterized, but its physiological role in maintaining steady state pH_i is shown in a number of experimental studies (220, 304).

1.3.1.4 Chloride/Bicarbonate Anion Exchangers

$\text{Cl}^-/\text{HCO}_3^-$ anion exchangers belong to the solute carrier 4 (SLC4) family of genes, which mediate Na⁺-independent electroneutral exchange of Cl⁻ in exchange of HCO₃⁻. The gene products designated SLC4A1-A3 (AE1-AE3) are involved with pH_i, [Cl⁻]_i and cell volume regulation (7).

Structurally, SLC4 proteins consist of three domains; a long cytoplasmic N-terminal domain of 400-700 residues, a transmembrane domain of ~500 residues which catalyses anion exchange and a short cytoplasmic C-terminus ~30-100 residues (291, 334). The topological model (Fig. 1.3) is based mainly on the

hydropathy and biochemical information obtained from studies performed on the AE1 $\text{Cl}^-/\text{HCO}_3^-$ anion exchanger isoform (291, 334).

The AE1 anion exchanger is the well-studied isoform and it is expressed mainly in the plasma membrane of red blood cells (erythroid band 3), the alpha-intercalated cells of the distal renal tubule and in the myocardium. The erythroid and the renal isoforms of AE1 are under expression regulation by two different promoters (278). AE1 comprises about 50% of the proteins found on the plasma membrane of the RBCs and is therefore known as the erythroid isoform or band 3 (70). The murine isoform has 911 amino acids sequence with a 43 kDa large intracellularly located N-terminal tail, which interacts with cytosolic proteins including glycolytic enzymes, hemoglobin and cytoskeletal proteins thus conferring structural integrity to the erythrocyte; the 55 kDa membrane domain is the functional component, which mediates transport activity (70, 120). Hydropathy plots reveal that there are about 12-14 membrane spanning regions which are involved in transport of anions (162, 163). Expression of the C-terminal membrane domain alone is capable of transport activity (283). The short C-terminal tail contains acidic amino acid residues responsible for interaction with carbonic anhydrase II forming a bicarbonate transport metabolon (243, 283, 311-313). Interestingly, the other family members, AE2 and AE3 also contain the acidic-rich motif, the carbonic anhydrase binding motif, thus forming a similar transport metabolon (see below) (283).

AE1 forms oligomers and the structural unit is a dimer although tetramers are also found (302). Until now no high resolution crystal structure of the entire

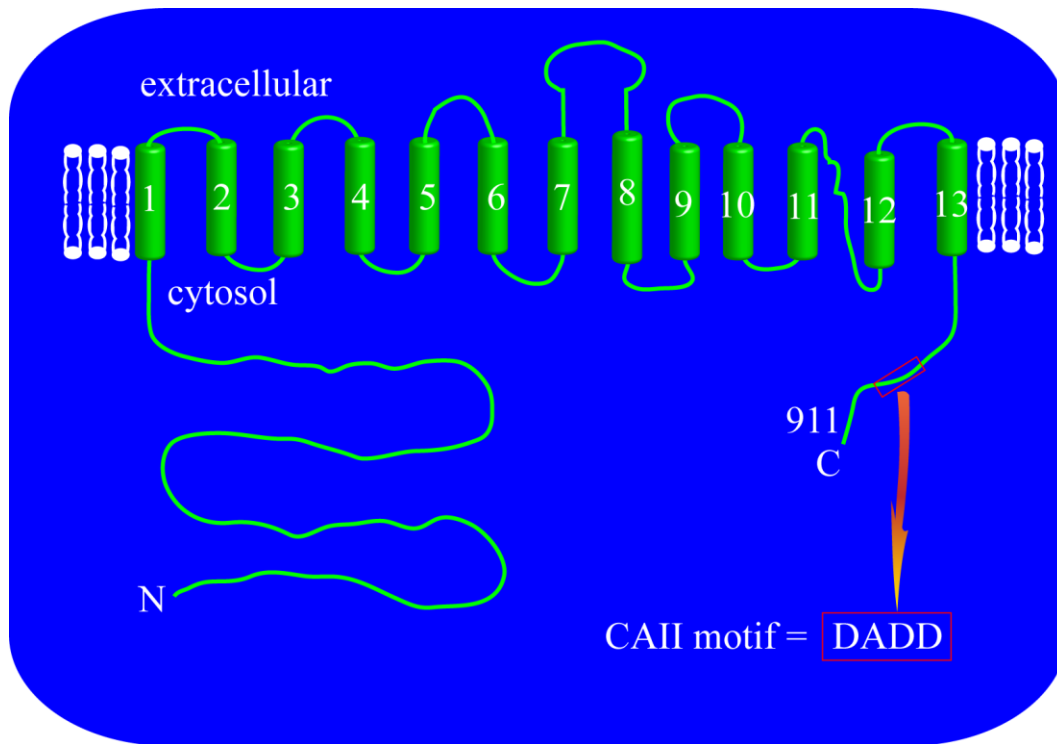


Fig. 1.3 Topology model of the chloride/bicarbonate anion exchanger AE1. AE1 consists of three main domains; a cytosolic amino (N) terminal domain which provides anchor for interaction with glycolytic enzymes and the cytoskeletal structures; a membrane domain which comprises 12-13 transmembrane regions responsible for transport activity; and a cytosolic carboxyl (C) terminal domain which contains an amino acid binding motif (DADD) for carbonic anhydrase II (CAII) (details in the text).

AE1 protein exists, but recent 3D model analysis has provided greater insight of the TD and afforded a better understanding of the transport function of AE1 and substrate binding (23, 39). A 3D homology model of the TD of AE1 based on the X-ray crystal structure of the *Escherichia coli* CIC chloride channels has been developed (39). In this manuscript, the homology model was validated by a combination of existing biochemically established spatial constraints and novel point mutations. For instance, the model suggested that dimer interfaces occur in transmembrane helices H, I, P, and Q consistent with similar helices in the *Escherichia coli* CIC chloride channel structure. Mutations of glutamate 508 (E508) of AE1 which corresponds to E148 of CIC influence transport activity of both transporters which suggests that E508 plays a major role in the functional activity of AE1. Additionally, AE1 S465, F878, I791 and F792 were shown to be part of the anion coordination site. The AE1 homology model also revealed that E681 forms an intracellular glutamate gate while the surrounding residues, F806-C885, are pore-lining.

Another 3D model based on the structure of UraA, the uracil-H⁺ cotransporter, have been developed (23). In this model further light is shed on the residues involved in anion transport of AE1. TDs 3 and 5 were shown to play a critical role in anion transport as they were proposed to line the anion exchange pathway. Residues in TD 3 may also be involved in proper folding of AE1 as revealed by cysteine scanning mutagenesis and confirmed by the 3D homology model.

There are two alternate transcripts of AE1 expressed in humans, which arise from alternative promoter usage. The erythroid isoform contains 911 residues and the kidney variant initiates at M66 (191). There are trace levels of expression in other tissues including the heart but the physiological role is unknown. Due to the different promoter usage, it has been possible to develop gene targeted mice lacking AE1 which has enabled the delineation of the functional role of AE1 in erythrocytes and kidneys. Targeted deletion of the AE1 gene in mice was characterized by a reduction of peripheral blood erythrocyte numbers, associated with enhanced Ca^{2+} entry and scrambling of cell membrane phospholipids (3). This underlies the manifestation of severe anemia and spherocytic red blood cells observed in AE1 deficient gene-targeted mice (278). Most homozygous AE1 null mice do not reach adulthood (278).

The renal AE1 isoform is located in the alpha-intercalated cells of the renal distal tubule where it plays a crucial role in bicarbonate reabsorption, thus, maintaining systemic acid-base homeostasis (70). Disruption of the renal isoform of AE1 gene was associated to distal renal tubular acidosis (dRTA) in mice (279), which is characterized by spontaneous hyperchloremic metabolic acidosis, alkaline urine without bicarbonaturia, reduced basolateral $\text{Cl}^-/\text{HCO}_3^-$ exchange activity in acid-secreting intercalated cells and nephrocalcinosis in homozygous mice (279).

Mice lacking the AE1 gene manifested cardiac hypertrophy demonstrable by increased heart weight to body weight ratio (14). This was accompanied by increased left ventricular mass, increased collagen deposition and fibrosis.

Cardiac function as revealed via echocardiography was markedly impaired. The manifestation of cardiac dysfunction was shown to be secondary to hemolytic anemia and spherocytosis, however, with no apparent role of AE1 in cardiac function (14).

Mutations in the AE1 gene have also been associated with abnormalities in the red blood cells (RBCs) and kidneys in humans. As noted above, the N-terminal cytosolic domain of erythroid AE1 by binding to ankyrin, protein 4.1 and protein 4.2 serves as an anchor for the spectrin cytoskeleton (302). RBC AE1 also associates with integral membranes including glycophorin A (GPA) and some members of the Rhesus (Rh) complex, RhAG and Rh, as well as, with some glycolytic enzymes (47, 121). Due to these many interactions, RBC AE1 plays a critical role in maintaining the membrane integrity and the biconcave structure of erythrocytes. These associations also enable AE1 to undertake its many physiological roles in erythrocytes which include facilitating the CO₂ carrying capacity of the blood and maintenance of pH homeostasis (250). Mutations in AE1 that affect the folding and trafficking to the surface membrane therefore impact the morphological and osmotic properties of the RBC (302). These mutations manifest as alterations in the shape of the RBC and underlie a number of pathological conditions in humans.

The most common of the human diseases due to defects in the AE1 gene is hereditary spherocytosis (HS) (302). As the name suggests, HS is a RBC disorder characterized by production of sphere-shaped RBC which can lead to autoimmune hemolytic anemia (86). HS is induced by mutations in the genes that encode

erythrocyte membrane proteins including ankyrin, protein 4.1, protein 4.2, spectrin and AE1 (86). Mutations in one or more of these proteins lead to binding defects between the cell membrane proteins and the cytoskeleton which give rise to spherocytes with compromised mechanical structure and osmotic fragility (70). Patients with HS present with various conditions including hemolytic anemia, jaundice and reticulocytosis (302).

Southeast Asian Ovalocytosis (SAO) is another RBC disorder which arises from deletion of nine amino acid residues which occur at the junction between the N-terminal cytosolic domain and the first transmembrane segment in the erythroid AE1. This leads to formation of oval-shaped RBCs (ovalocytosis) (70). Although mainly asymptomatic, the trait is lethal for homozygous individuals *in utero* (186). Mutations or deletions in SAO lead to endoplasmic retention of AE1 which can be rescued by co-expression of the mutant with wildtype AE1 (70).

Nine mutations which cause single amino acid substitutions in the TD of AE1 also induce a RBC-related disorder referred to as hereditary stomatocytosis (102). Each of the mutations which cause hereditary stomatocytosis, with the exception of E758K and R760Q, is characterized by extensive cation, K^+ and Na^+ , leak accompanied by a defective Cl^-/HCO_3^- exchange activity (46). Eventually, the morphological changes lead to hemolytic anemia.

Mutations in the renal Cl^-/HCO_3^- exchanger AE1 isoform are also associated with a number of kidney disorders the most common of which is dRTA (25). AE1 is expressed in the basolateral membrane of the α -intercalated cells of the distal renal tubules of the kidney where it mediates Cl^-/HCO_3^- exchange

activity (25), thereby playing an important role in mediating HCO_3^- reabsorption and urine acidification (70). Individuals with dRTA present with hypercalciuria, reduced acid excretion, nephrocalcinosis, hypokalemia and osteomalacia (70, 249). Predominantly autosomal dominant, AE1 mutations that lead to dRTA are retained intracellularly (within the ER or Golgi apparatus) or mis-targeted to the apical membrane (69, 76).

The AE2 $\text{Cl}^-/\text{HCO}_3^-$ anion exchanger is the ‘housekeeping’ isoform with widespread expression in mammalian cells. There are five N-terminal splice variants with tissue-specific expressions (summarized in (40)). AE2 is localized basolaterally in epithelial cells. The primary role of the AE2 isoform is to regulate cytosolic pH by extruding HCO_3^- in exchange for Cl^- , a process regulated by pH (8). Present in the N-terminal cytoplasmic region and the transmembrane domains of AE2 are amino acid residues that confer pH sensitivity to AE2 which distinguishes it from AE1 (9). No human hereditary disease has been linked to AE2, but AE2 knock-out mice did not survive adulthood as they showed severe growth retardation (109). No physiological function of AE2 has been demonstrated in the myocardium although AE2 transcripts have been found in the heart.

The AE3 isoform is the least studied of the electroneutral $\text{Cl}^-/\text{HCO}_3^-$ anion exchangers. It is expressed mainly in excitable tissues, including brain, retina and the heart. There are two gene products of AE3, full length AE3 (AE3fl) and the cardiac isoform (AE3c), which are products of alternate promoter usage (184, 185). The N-terminus of AE3fl comprises 270 amino acids which are replaced by

73 amino acids in AE3c (184, 185, 326). Mice lacking the AE3 gene had a greater propensity for seizures (130); point mutations in the AE3 gene led to idiopathic generalized epilepsy (309). AE3 null mice also exhibited visual impairment (12). The defects observed in these tissues were attributed to the intracellular pH regulatory role mediated by AE3.

Together with SLC26A6, the predominantly expressed bicarbonate transporter in the myocardium, AE3 regulates pH_i in the heart by inducing intracellular acidification (305). However, in response to hypertrophic stimulation, the AE3 $\text{Cl}^-/\text{HCO}_3^-$ exchanger is the isoform that is stimulated (52, 58, 60). Disruption of the AE3 gene in mice demonstrated no myocardial functional deficiency, but a double knock-out of AE3 and the $\text{Na}^+ - \text{K}^+ - \text{Cl}^- - \text{Cl}^-$ (NKCC) transporter revealed a marked impairment in cardiac function (240). Ablation of the *ae3* gene in a mouse model of cardiomyopathy hypertrophy exacerbated the loss of cardiac function (4). Taken together, this evidence suggests an important role of AE3 in cardiac function and a major focus of this thesis is to explore further the role of the AE3 $\text{Cl}^-/\text{HCO}_3^-$ anion exchanger in the development of cardiac hypertrophy.

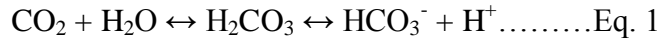
1.4 Carbonic Anhydrases

Carbonic anhydrases (CAs) are zinc metalloenzymes that play critical physiological roles. They are ubiquitously present in eukaryotes and prokaryotes and they are encoded by three distinct families of genes; 1. α -CAs are expressed mostly in vertebrates, algae and the cytoplasm of green plants, 2. β -CAs are

expressed predominantly in bacteria, algae and chloroplasts of plants and 3. γ -CAs are found in archaea and bacteria (reviewed in (111, 287)).

Fourteen α -CAs have diverse subcellular localization and tissue distribution (111, 287). Cytosolic isoforms include CAs CAI-III and CAVII; four isoforms are membrane-bound (CAV, CAIX, CAXII and CAXIV), CAV is located in the mitochondria and CAVI is secreted form.

CAs catalyze the reversible hydration of CO₂ into bicarbonate and proton (Eq. 1).



The regulation of the above equation by CAs is at the center of many physiological processes including the respiration and transport of CO₂/HCO₃⁻ between tissues and lungs. Since the primary buffer system in the human body is the CO₂/HCO₃⁻ system, CAs are involved with cytosolic and whole-body pH regulation, regulation of acid/base homeostasis and fluid secretion.

In highly metabolic tissues such as the heart, whose function is accompanied by large production of CO₂, CA catalytic activity is indispensable to maintain normal function by regulating cytosolic pH homeostasis. Of the 14 CA isozymes identified (159, 210), CAII has the highest rate of catalysis (193). Of particular importance are the numerous evidences proposing that CAs interact with bicarbonate transport proteins forming a metabolon, an interaction shown to maximize the transport rate of the transporters (27, 72, 283, 311-313), but others failed to observe a physical and/or functional consequence of CA interaction with

bicarbonate transporters (41, 192, 323). The reasons for this discrepancy will be discussed in a later discussion.

1.5 The Bicarbonate Transport Metabolon

As alluded to earlier, several lines of evidence suggest that bicarbonate transporters structurally and functionally interact with CAs to form a bicarbonate transport metabolon (BTM) (283, 311-313). A metabolon is defined as a complex of enzymes that catalyze a series of reactions in a common metabolic pathway. Thus, the product of one enzyme is channeled to the next enzyme as a substrate. The physiological relevance of a metabolon is to increase the efficiency of substrate flux across the metabolic pathway.

The continual production of CO₂ from oxidative metabolism requires an effective system for its extrusion since CO₂ is a conjugate acid and therefore its accumulation lowers cell pH leading to impairment of cellular processes. CO₂ readily diffuses out of the cell, but HCO₃⁻, the hydration product from CA catalysis, requires bicarbonate transporters to facilitate its transport. In the erythrocyte membrane, there are ~1.2 X 10⁶ copies of AE1 molecules per cell (89). Two cytosolic CA isoforms, CAI and CAII (193), are expressed in the RBCs with CAI being the predominantly expressed isoform (~85%) and CAII the more catalytically active form. Interestingly, the relative abundance of CAII (~1 million copies) is in a 1:1 stoichiometry with AE1 (292).

Considerable evidence suggests that AE1 interacts with CAII physically and functionally, a phenomenon described as the BTM (Fig. 1.4). CA isolated from bovine, a homologue of human CAII, was shown to associate with the

membrane of RBC *in vitro* (313). When AE1 was bound to an inhibitor, stilbene disulfonate, fluorescence of labeled CAII from bovine was disrupted providing the first evidence that AE1 and CAII physically interact (313). Intact red cell membranes as well as ghost membranes showed a similar redistribution of AE1 and CAII when treated with tomato lectin. Solubilized AE1 also co-immunoprecipitated with CAII (313).

Further, a solid-phase binding assay revealed that immobilized CAII binds to intact AE1 and the membrane domain of AE1, an interaction which was abolished by antiserum developed against the C-terminus (Ct) of AE1 in a dose-dependent manner (312). This suggested that Ct of AE1 plays an obligatory role in the complex formation with CAII. The binding of the Ct of AE1 to CAII was shown to be dependent on ionic strength and pH suggesting that the interaction was electrostatic in nature. Affinity chromatography assays also demonstrated that soluble CAII binds to immobilized glutathione-s-transferase-Ct (GST-Ct) with an approximate stoichiometry of 1:1 (312).

Subsequent studies performed to characterize the nature of the AE1 and CAII interaction demonstrated that the 33 residues of the AE1 Ct possessed the amino acid residues responsible for binding to CAII (312). This region contains mainly negatively acidic residues and binds to immobilized CAII on microtiter assays. Specifically, a cluster of residues, D887ADD, forms a complex with CAII with an obligatory role of L886 (312). Truncation and mutagenesis studies revealed that the absence of these residues, which form the CAII binding (CAB) motif, abolished complex formation with CAII (312). Interestingly, the cluster of

acidic residues is highly conserved among the other electroneutral $\text{Cl}^-/\text{HCO}_3^-$ exchangers, AE2 and AE3 (110, 283, 326), as well as other members of the bicarbonate family of transporters (61, 118, 241). Subsequently, it was shown that the first 20 residues of the N-terminal tail of CAII provided the localization site for binding to AE1 (311). This region is rich in positively charged amino acids, confirming that the interaction between AE1 and CAII was electrostatic in nature (312, 313).

What is the functional consequence of the physical interaction between AE1 and CAII? In HEK293 cells, inhibition of CAII activity resulted in a marked reduction in the $\text{Cl}^-/\text{HCO}_3^-$ anion exchange activity of AE1 (283). Co-expression of AE1 and the catalytically inactive CAII isoform, V143Y, caused a significant lowering of AE1 transport activity in a dose-dependent manner. $\text{Cl}^-/\text{HCO}_3^-$ anion exchange activity was abrogated in AE1 mutants that lack the ability to bind CAII. In these studies, co-expression of AE1 and CAII showed no changes in AE1 transport activity relative to AE1 alone-transfected cells. This was attributed to endogenously expressed CAII in HEK93 cells which is capable of maximizing AE1 activity (283). Additionally, in *Xenopus* oocytes, truncation of the CAB of AE1 caused a loss of $\text{Cl}^-/\text{HCO}_3^-$ anion exchange activity while preserving Cl^-/Cl^- transport activity further supporting the importance of the physical interaction for maximal transport activity (72). Taken together, these reports provide evidence to support a role of CAII in maximizing the $\text{Cl}^-/\text{HCO}_3^-$ anion exchange activity of AE1. Similar results were found with AE2 and AE3 in that the presence of catalytically active CAII facilitates the transport activity of the transporters (283).

In parotid exocrine cells, CAII inhibition by acetazolamide remarkably reduced $\text{Cl}^-/\text{HCO}_3^-$ exchange activity of AE2 (113).

Other reports have demonstrated the dependence of the Na^+ -dependent HCO_3^- co-transporters on CAII for maximal activity (27, 319). Heterologous expression of the kidney electrogenic NBC isoform, NBCe1, in oocytes showed an increased Na^+ current in a CAII dependent fashion when the transporter was operating in the 1 Na^+ :3 HCO_3^- mode (27). The enhanced activity of NBCe1 was shown to be possible when CAII forms a complex with the transporter. In that same study, injection of CAII into *Xenopus* oocytes increased current across the membrane in a fashion dependent on CAII concentration. Inhibition of CAII activity reversed the increased activity of NBCe1. Co-expression of CAII wildtype with NBCe1 enhanced the transporter activity but co-expression of NBCe1 with the catalytically inactive CAII, V143Y, showed no effect on transport activity (27). This finding lends credence to the concept that bicarbonate transporters require carbonic anhydrases for maximal activity (243, 283).

Evidence exists to suggest that the bicarbonate transport metabolon may involve an extracellular component whereby cell surface-anchored carbonic anhydrase IV interacts with extracellular loops of bicarbonate transporters (281). Expression of the inactive form of CAII, V143Y, in HEK293 cells abrogated the interaction between endogenous CAII and AE1, AE2 and AE3, concomitant to an inhibition of the transport activities of the transporters (281). The study further revealed that expression of CAIV, an extracellular CA isoform, in the presence of

V143Y, restored the transport activity of the transporters. Further characterization of the nature of the interaction between CAIV and AE1 showed that CAIV binds to AE1 via the large extracellular fourth loop (281). Later, it was demonstrated that CAIV interacts with the fourth extracellular loop of NBC1 to accelerate the rate of recovery of pH_i following imposed acid load in HEK293 cells (10). GST pull-down assays also revealed that CAIV directly interacts with the fourth extracellular loop of NBC1 at amino acid residue G767 (10). These findings present an interesting phenomenon in which maximal transport activity of the bicarbonate transporters is attained by two processes (Fig. 1.4); an intracellular component involving an interaction between CAII and the C-terminal tail of the BT and an extracellular interaction which involves the tethering of CAIV (with a catalytic rate of $\sim 8 \times 10^5 \text{ s}^{-1}$) to the fourth extracellular loop of BT. Thus, the bicarbonate transport metabolon generates a local gradient across the BT which drives the flux of HCO_3^- by a 'pull' (afforded by the extracellular component) and 'push' (mediated by the intracellular component) mechanism (205) (Fig. 1.4).

What is the physiological relevance of a bicarbonate transport metabolon? Bicarbonate transport metabolon is a nascent model which is gaining a lot of investigative attention due to its implication and relevance in biological processes. One area where a bicarbonate transport metabolon has been observed to be relevant is the respiratory system during gaseous exchange between tissues and the plasma. Upon diffusion out of the cell following oxidative metabolism, CO_2 enters the RBC where it is hydrated by CAII to produce HCO_3^- and H^+ (144).

HCO_3^- is effluxed into the plasma via the erythrocyte $\text{Cl}^-/\text{HCO}_3^-$ AE1 exchanger. In the lungs plasmalemmal AE1 catalyses the influx of HCO_3^- in exchange of Cl^- , the latter is converted to CO_2 by cytosolic CAII exits the RBC to be expired. Thus, the interaction of AE1 and CAII provides an efficient system to carry CO_2 out of the body and by so doing increases the plasma carrying capacity for CO_2 .

Conversely, other reports failed to show a physical interaction and a functional consequence of CAII interaction with bicarbonate transporters. In these studies, it was shown that CAII cannot bind to pure SLC-Ct NBCe1 peptides in solid-phase binding assays, and binding only occurred when CAII was immobilized with the soluble SLC-Ct peptide (41). Recently, it was demonstrated that NBCe1 mutant lacking the putative CAII binding site showed normal activity in *Xenopus* oocytes suggesting that the transporter does not require CAII interaction for maximal activity (192). In that study, co-expression of CAII with either wildtype NBCe1 or the mutant showed no effect of CAII on the transport activity of either transporter. These findings tend to reject the concept of a bicarbonate transport metabolon and seemed to suggest that NBCe1 does not form a complex with CAII. In the present thesis, the concept of a bicarbonate transport metabolon will be further explored in order to throw more light on the mechanism as well as the physiological and pathological relevance of the interaction between bicarbonate transporters and CAII.

1.6 Signaling Pathways in Cardiac Hypertrophy

Heart failure (HF) occurs when the heart is unable to provide adequate perfusion to the various organs of the body and manifests in patients as edema,

dyspnea and/or fatigue (129). HF is the culmination of many cardiovascular disorders and it is the leading cause of hospitalization in the elderly. Survival rate following the onset of HF is very low, thus understanding the risk factors that cause HF and the molecular events that are activated will be crucial in improving the clinical outcomes of patients. HF is induced by underlying cardiac pathologies including cardiac ischemic diseases (myocardial infarction), hypertension, valvular diseases and cardiomyopathies (48). A common feature of HF regardless of the source of the initiating insult is the enlargement of the left ventricular mass, a condition referred to as cardiac hypertrophy (99). Cardiac cells are terminally differentiated cells and in response to increased biomechanical stress, increased energetic demands or cell loss following myocardial infarction, cardiomyocytes increase their size rather than their number (224). The increase in cardiomyocyte size tend to normalize the initial wall tension and depending on the initiating stimuli, cardiac hypertrophy may improve cardiac function (physiological hypertrophy) (131) or progress to heart failure or sudden death (pathological hypertrophy) (131, 224). Physiological hypertrophy and pathological hypertrophy differ in the source of insult, the structural re-organization of myofibrils and collagen fibers (cardiac remodeling), morphological features, and the distinct molecular events elicited. Thus, delineating the distinct molecular and the subsequent effector properties of the two types of hypertrophy will promote the development of new therapeutic approaches in treating hypertrophic patients. Moreover, a better understanding of the mechanisms involved in hypertrophic growth of the heart will enhance

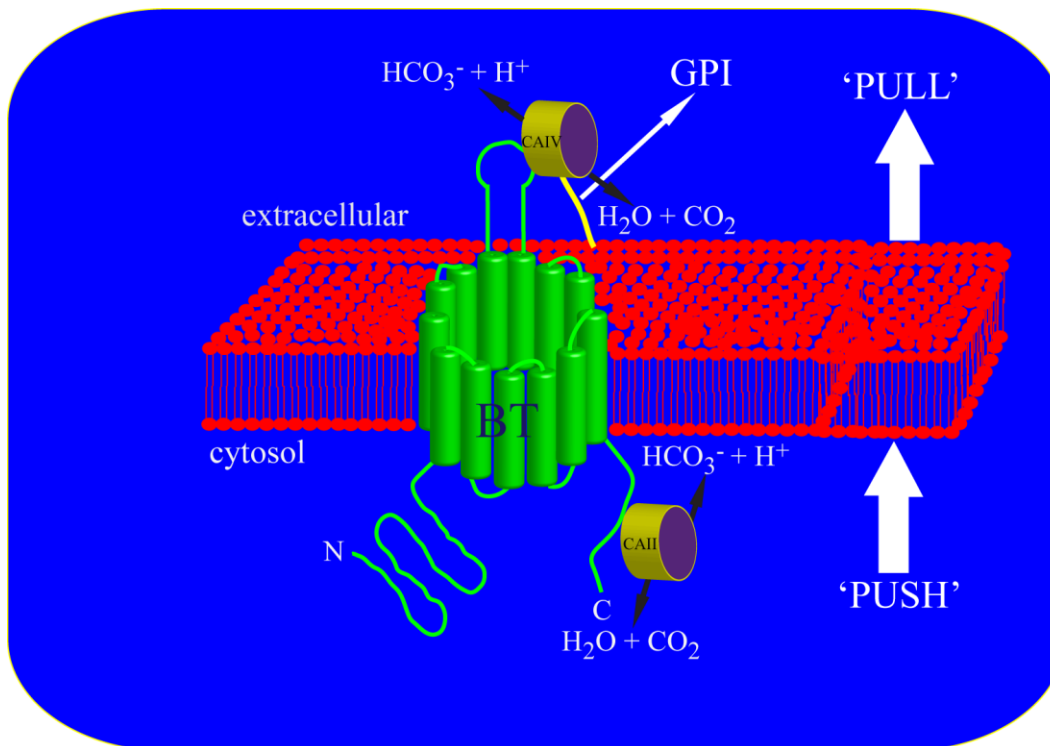


Fig. 1.4 Schematic illustration of the bicarbonate transport metabolon (BTM). Bicarbonate transporters (BT) via residues at the carboxyl (C) tail, interact intracellularly with carbonic anhydrase II (CAII) to form the intracellular component of the BTM. Production of HCO_3^- at the cytosolic surface facilitates bicarbonate efflux ('PUSH'). Extracellularly, BT via its large extracellular loop binds to carbonic anhydrase IV (CAIV) which is anchored to the surface of the plasma membrane through the glycosylphosphatidylinositol (GPI) linkage, to form the extracellular component of the BTM. The extracellular component may enhance bicarbonate transport by reducing bicarbonate concentration at the immediate vicinity of the transporter thus creating a 'PULL' mechanism (details in text).

selection of specific targets to amplify the clinically beneficial physiological hypertrophic pathways while ameliorating pathological cardiac growth.

1.6.1 Signaling Pathways in Physiological Cardiac Hypertrophy

Physiological cardiac hypertrophy, also referred to as the athlete's heart, occurs during postnatal development and is the normal physiological response of the heart to chronic training (exercise) and pregnancy (77). It is associated with increased myocardial wall mass with a proportional increase in ventricular chamber diameter (28). Physiological hypertrophy is accompanied by normal or enhanced cardiac function (204).

Various *in vitro* and animal models have been employed to delineate the distinct molecular signaling events that mediate physiological hypertrophy (104, 124). Consequently, some of the major modulators of physiological hypertrophy have been identified albeit not exhaustively. In exercise and swim-trained rat and mice hearts, about 2,534 genes were significantly altered (104). One of the well characterized pathways identified as mediating physiological hypertrophy is the growth factor signaling transduction pathway (Fig. 1.5).

Playing a key role in the postnatal development of organ and body size is the insulin-like growth factor 1 (IGF1) whose expression levels are elevated in athletes (68) as well as in the serum of chronically trained animals and humans (204, 217). IGF1 signaling was subsequently shown to mediate physiological hypertrophy using transgenic mice and knock-out studies.

IGF1 binds to its surface membrane receptors, the IGF1 receptors (IGFR), a receptor tyrosine kinase, on the cardiac cells and activates its downstream target,

phosphoinositide-3-kinase (PI3K) (Fig. 1.5). The activation of the IGF1/PI3K pathway plays a major role in cell growth and survival (217). Transgenic mice with reduced IGF1/PI3K pathway activation have reduced heart size which suggests a developmental role of the pathway in the heart (270).

Activation of IGFR by IGF1 binding leads to recruitment of PI3K to the plasma membrane via the src homology 2 (SH2) domain on the regulatory domain (101). PI3K is a heterodimeric lipid kinase which is composed of regulatory and catalytic subunits with varying isoform combinations (18). There are three classes of PI3K; Class IA/IB, Class II and Class III PI3Ks. The role of the Class II PI3K is not fully characterized; the Class III PI3K is involved in membrane trafficking events following the phosphorylation of phosphatidylinositol (PI) (101).

The catalytic domain of the members of the Class IA PI3K belong to the α , β or δ isoforms of p110; the regulatory domain expressed are p85 (α , β), p55 (α , γ) or p50 α isoforms (18). The Class IB PI3K is a heterodimer complex of p110 γ and p101 isoforms and they are activated by G-protein coupled receptors (GPCR) (18). The heart predominantly expresses p110 α and p110 γ isoforms which mediate the phosphorylation of phosphatidylinositol-4,5-diphosphate (PI-4,5-P₂) to produce PI-3,4,5-P₃. Transgenic mice with constitutively active IGF1/PI3K (p110 α) developed physiological hypertrophy compared to IGF1/PI3K (p110 γ) transgenic mice that was unresponsive to physiological hypertrophic stimuli (271). Additionally, mice lacking the regulatory subunits of PI3K (p85 α and p85 β) failed to develop hypertrophy in response to swim training

(203, 272). Contrastingly, these mice demonstrated hypertrophy in response to pressure overload (203, 272). These findings suggest that activation of p110 α and p85 α or p85 β plays a critical role in inducing adaptive hypertrophic phenotype while the p110 γ isoform induces pathological hypertrophy. PI3K activity is negatively regulated by the lipid phosphatase referred to as phosphatase and tensin homolog (PTEN), which specifically dephosphorylates P-3,4,5-P₃ to P-4,5-P₂ (271).

The cellular effects of IGF1/PI3K activation are mediated by a serine/threonine kinase, Akt (protein kinase B, PKB), which regulates a number of cellular functions in the heart and other tissues including cardiac growth, contractile function and coronary angiogenesis (271). Three mammalian Akt genes have been identified; Akt1/PKB α , Akt2/PKB β and Akt3/PKB γ . Akt1 and Akt2 are ubiquitously expressed with high expression levels in the heart, brain and lungs; Akt3 is expressed predominantly in the brain (18). Under basal conditions, Akt is located in the cytosol with its kinase domain masked by the C-terminal hydrophobic region. Akt is recruited to the plasma membrane via its N-terminus pleckstrin-homology (PH) domain following stimulation of the insulin receptors (IR) or IGFR). PI-3,4,5-P₃, generated by activated PI3K, mediates the translocation of protein kinase B (PKB/Akt1) to the plasma membrane where it is phosphorylated and stimulated by phosphoinositide-dependent kinase (PDK1) (280) at Thr308. To attain maximal activation, Akt1 is phosphorylated at Ser473 by a mechanism recently reported to be mediated by mTOR (200). Activated Akt phosphorylates a number of downstream substrates which are responsible for the myriad cellular effects observed with IR/IGFR stimulation.

Available data suggest that Akt activation in the myocardium is consistent with cardiac growth; specifically Akt1 stimulation mediates physiological hypertrophy (103, 316). During embryonic development PI3K/Akt signaling has been shown to promote cardiomyocyte differentiation and proliferation (202). Post-natally the IGF/Insulin-PI3K-Akt signaling pathway regulates regular cardiac size and development. In the insulin receptor knock-out (KO) mice, Akt signaling was abrogated, consistent with a reduction in heart size and impairment of cardiac contractile function (272). In response to pathological hypertrophic stimuli such as isoproterenol infusion or pressure overload, cardiomyocytes from insulin receptor KO mice increased in size (135). In response to swim training, Akt1 knock-out mice failed to develop hypertrophy which is sharply contrasted by the development of hypertrophy in response to pressure overload (259). These findings suggest that the IGF/Insulin-PI3K-Akt signaling pathway mediates physiological cardiac hypertrophy and is not involved in pathological development of the heart.

Downstream of Akt1 are a number of substrates which regulate the growth response to IR/IGFR activation. Germane to cardiac development are three Akt substrates namely glycogen synthase kinase-3 (GSK-3) (221), mammalian target of rapamycin (mTOR) and FOXO transcription factors (271). GSK-3 negatively regulates cardiac growth by inhibiting pro-hypertrophic transcription factors, including nuclear factor of activated T-cells (NFAT) and GATA-4 (271). The IR/IGFR-PI3K-Akt signaling pathway phosphorylates and inactivates GSK-3 thus

releasing the inhibition on hypertrophic gene expression which ultimately promotes growth in the heart (82).

Akt induced physiological hypertrophy is also mediated by mammalian target of rapamycin (mTOR) (204). mTOR, the mammalian isoform of the yeast TORs, regulates protein synthesis (by regulating translation of mRNA) and cell growth via activation of the eukaryotic initiation factor 4E (eIF-4E) binding protein 1 (4E-BP1) and the ribosomal S6 kinases (S6K1 and S6K2) (127). The drug, rapamycin, targets mTOR and ameliorates its activity, thus prevents protein translation (260). Akt mediated physiological hypertrophy development was abrogated by rapamycin treatment, which reveals that Akt-dependent hypertrophy involves mTOR (272). The role of S6K in physiological hypertrophy has not been clearly defined. Levels of the S6K1 isoform but not S6K2 were elevated in response to models of physiological hypertrophy (202). Overall, the deletion of S6Ks did not attenuate hypertrophy in various models of physiological hypertrophy (289) suggesting that more research is required to delineate the involvement of S6K in cardiac hypertrophy. Thus, in light of the aforementioned, Akt induction of physiological hypertrophy may predominantly involve mTOR activation of 4E-BP1.

FOXO, a transcription factor, is another major downstream substrate phosphorylated by Akt which is ubiquitously expressed in all tissues and subcellularly located in the nucleus (271). In the unphosphorylated state, FOXO negatively regulates genes that induce cardiac development (271) by inducing their degradation. In response to insulin stimulation, FOXO is phosphorylated

and inhibited in an Akt-dependent manner which releases the negative regulation on protein degradation and thus leads to the cardiac growth process (271). FOXO, a transcription factor, resides in the nucleus and stimulates the expression of target genes such as atrogenin and MurF1 E3 ubiquitin ligases, which mediate the regulatory activity of FOXO (259). Akt phosphorylation leads to translocation of FOXO into the cytosol and thus down-regulates protein degradation genes which preserve protein expression.

Taken together, Akt induced physiological hypertrophy is made possible by increased transcription of hypertrophic genes responsible for normal cardiac growth while inhibiting the expression of fetal genes involved in pathological hypertrophy (see below), acceleration of protein translation coupled to a reduction in protein degradation. All of these factors result in an increase in cardiac cell size without accompanying pathological consequences.

Another growth hormone whose involvement in physiological hypertrophy is becoming unraveled is the thyroid hormone (78). Thyroid hormones exert a myriad of effects on the cardiovascular system which include increasing frequency and force of cardiac systolic contraction and increasing the frequency of diastolic relaxation. That is, they increase the rate of cardiac contraction and relaxation. Conversely, thyroid hormones could also induce atrial fibrillation and increase heart rate, which are considered adverse to heart function (90). Thyroid hormones function by binding to their nuclear receptors and by so doing influences the transcription of genes responsible for the many cellular effects exerted by the hormones (327). Some of the genes activated by thyroid hormones

are involved in the normal cardiac growth and more interestingly repression of genes that activate the fetal gene program, a hallmark of the pathological phenotype of cardiac growth (78, 79).

Cardiomyocytes predominantly express two thyroid hormone receptors, TR α 1 and TR β 1, which mediate the cardiovascular influences of thyroid hormones in the heart (157). That thyroid hormones (TH) were involved with physiological hypertrophy was demonstrated in cardiomyocytes and other cell types where TH interaction with TR α 1 in the cytosol led to activation of PI3K subsequent to activation of Akt (222) (Fig. 1.5). Subsequent studies revealed increased phosphorylation of Akt, S6K and mTOR in hypertrophied rat hearts subjected to thyroxine treatment (167). Consequently, numerous studies have focused on the potential of thyroxine treatment in the setting of reversing established cardiac hypertrophy and heart failure.

It is noteworthy that despite the numerous beneficial effects of compensatory cardiac growth resulting from exercise training, overstimulation of the PI3K/Akt pathway can also lead to progression to the pathological phenotype of cardiac hypertrophy (reviewed in ref. (83)). Thus, understanding the timeline by which physiological hypertrophic stimulation will progress to maladaptive hypertrophy and the molecular events involved will be critical in maximizing the potential benefits of adaptive hypertrophy.

1.6.2 Signaling Mechanisms in Pathological Cardiac Hypertrophy

Pathological cardiac hypertrophy is characterized by increased fibrosis accompanied by apoptosis. Increased fibrosis causes the ventricular wall to

stiffen thereby impairing contractile function. Ventricular mass increases without a corresponding increase in wall diameter, thus reducing the chamber diameter and consequently cardiac output. Pathological hypertrophy often leads to detrimental outcomes manifesting as sudden death or heart failure.

In contrast to physiological hypertrophy, pathological hypertrophy occurs in response to deleterious stimuli such as chronic pressure overload (hypertension), valvular heart disease, myocardial infarction or ischemia, or cardiomyopathies resulting from diabetes or genetic mutations (reviewed in refs. (28, 53, 204)). In the pressure-overloaded myocardium, the circulating levels of angiotensin II (ANGII) (254), catecholamines (epinephrine and norepinephrine) (189) and endothelin I (ET-I), all pro-hypertrophic mediators are elevated. Additionally, in heart failure patients the myocardial renin-angiotensin system (RAS) is activated leading to increased local production of ANGI (71).

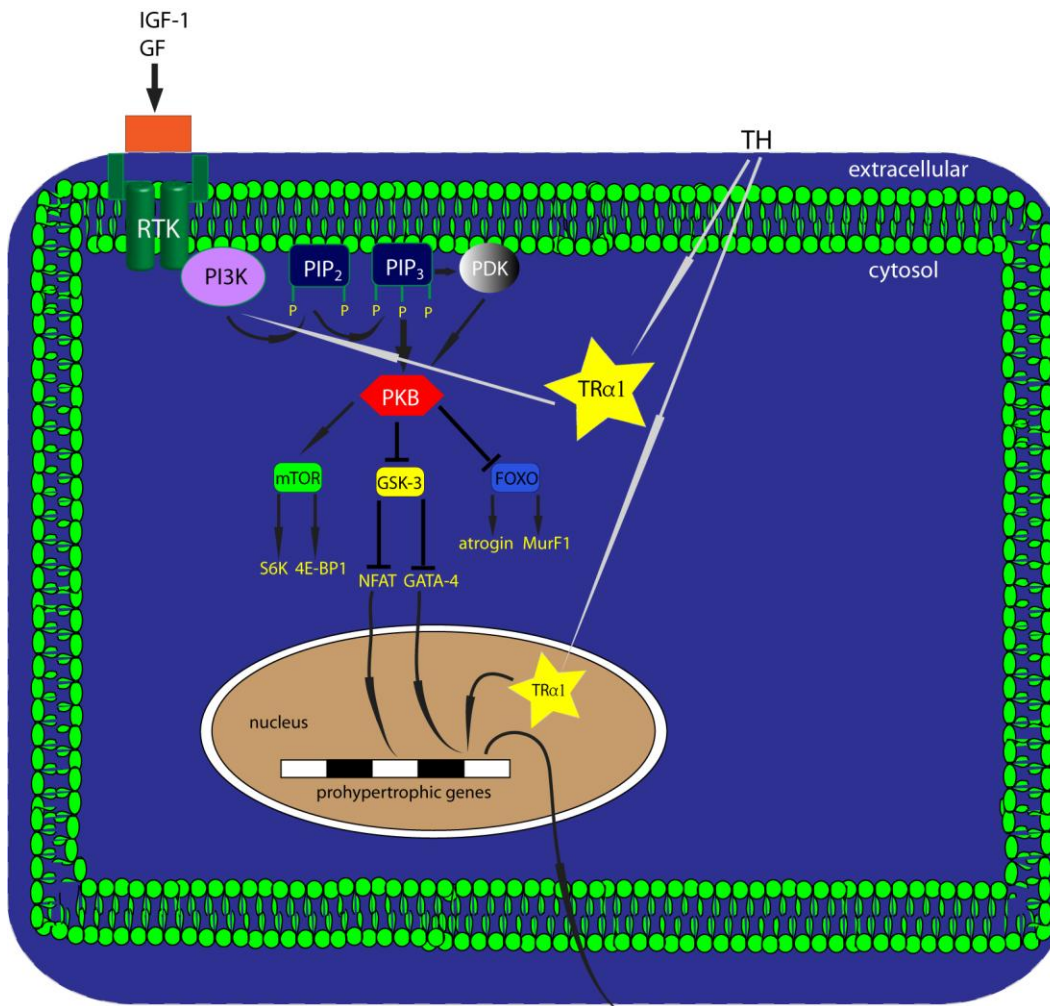
These findings led to the suggestion that the molecular pathways activated in pathological hypertrophy are in sharp contrast to the molecular events that mediate physiological hypertrophy. Delineation of the key distinct players involved in the two categories of hypertrophy has attracted a lot of attention. This is in keeping with the development of pharmacological agents that will selectively inhibit pathological hypertrophy while leaving intact the physiological growth of the heart.

Various hormonal stimuli including ANGI, PE or ET-I, exert their effects by binding of the ligand to their respective plasma membrane (guanidine) G-

protein coupled receptors (GPCRs), the most well characterized pathway implicated in the induction of pathological hypertrophy.

GPCRs are cell surface receptors with 7 transmembrane domains, which couple to intracellularly located G-proteins which are composed of three subunits, G_α , G_β and G_γ (164). In the inactive state, the G_α subunit is bound to guanine diphosphate (GDP) and to the $G_{\beta\gamma}$ subunits (Fig. 1.6). Upon ligand binding to the extracellular domain of the GPCR conformational changes result in exchange of GDP for guanine triphosphate (GTP) (223). The G_α -GTP complex dissociates from the $G_{\beta\gamma}$ subunits to influence the activity of membrane-bound enzymes as will be discussed below. There are three principal classes of heterotrimeric G-proteins namely G_s , G_q/G_{11} and G_i , which are responsible for converting the extracellular message (the ligand) into intracellular signal which results in the effector component of the transduction pathway (99). Ligands that employ GPCRs to transmit signals therefore exert widespread effects on the cardiovascular system.

Various *in vitro* and *in vivo* studies have demonstrated that these vasoactive substances induce cardiac growth. ANGII, ET-I and α -adrenergic-mediated cardiac hypertrophy involve interaction with the respective GPCR which is coupled to G_q/G_{11} (Fig. 1.5). The subsequent receptor conformational change and GDP-GTP exchange causes the $G_{\alpha q}$ -GTP complex to bind and activate phospholipase C (PLC), which is docked to the plasma membrane via lipid binding domains (108). Activated PLC hydrolyzes membrane-bound



Physiological Hypertrophy
 Increased myocardial mass
 Increase in ventricular diameter
 Normal or enhanced cardiac function

Fig. 1.5 Schematic representation of cardiomyocyte physiological hypertrophy. Insulin-like growth factor 1 (IGF-1) and growth factors (GF) bind to their surface membrane receptors, the receptor tyrosine kinase (RTK), which leads to the recruitment of phosphoinositide-3-kinase (PI3K) to the inner leaflet of the plasma membrane. PI3K phosphorylates phosphatidylinositol bisphosphate (PIP₂) to produce phosphatidylinositol (3,4,5) triphosphate (PIP₃), which causes translocation of protein kinase B (PKB) and subsequent phosphorylation and

activation of PKB by phosphoinositide-dependent kinase 1 (PDK1). PKB mediates the phosphorylation of target genes including glycogen synthase kinase 3 (GSK-3), mammalian target of rapamycin (mTOR) and FOXO transcription factors. Phosphorylated GSK-3 releases the inhibition on transcription factors such as the nuclear factor of activated T-cells (NFAT) and GATA-4, which are involved in inducing the transcription of pro-hypertrophic genes. Phosphorylation of mTOR leads to induction of protein synthesis via activation of eukaryotic initiation factor 4E (eIF-4E) binding protein 1 (4E-BP1) and the ribosomal S6 kinases (S6K). FOXO is a transcription factor which induces the transcription of genes such as atrogen and MurF1 which are responsible for protein degradation (301). Phosphorylation of FOXO by PKB inhibits its transcriptional activity. Thyroid hormones (TH) interact with thyroid receptors in the cytosol (TR α 1) which in turn activates PI3K to induce hypertrophic gene expression as described above. TH can also bind to its nuclear receptors to activate the transcription of hypertrophic genes.

phosphatidylinositol 1,2-bisphosphate (PIP₂) to produce inositol triphosphate (IP₃) and diacylglycerol (DAG). IP₃ translocates to and acts on the IP₃ receptors on the sarcoplasmic reticulum or the nuclear envelope, which leads to the release of Ca²⁺. Released Ca²⁺ binds to calmodulin (CaM), forming Ca²⁺-CaM complex, which in turn interacts with and activates calcineurin, a phosphatase. Activated calcineurin dephosphorylates its substrate, nuclear factor of activated T-cells (NFAT), a transcription factor, causing its translocation to the nucleus where it induces the transcription of pro-hypertrophic genes (reviewed in ref. (129)). In the phosphorylated state, NFAT resides in the cytosol.

DAG, which remains tethered to the inner leaflet of the plasma membrane, mediates the recruitment to the plasma membrane and subsequent activation of protein kinase C (PKC) (248). Activated PKC leads to the production of IP₃ which causes mobilization of internal Ca²⁺ as described above. Release of internal Ca²⁺ is also a potent activator of PKC in a 'feed-forward' mechanism (129). In cultured neonatal cardiomyocytes it was shown that PKC α is the isoform responsible for hypertrophy induction characterized by increased cell surface area, increased incorporation of [³H]-leucine and enhanced production of atrial natriuretic factor (ANF) (44). Additionally, dominant negative expression of PKC α suppresses agonist induced cardiomyocyte hypertrophy (44). This lends support to the critical role of PKC α involvement in the hypertrophic signaling cascade.

Downstream of PKC are the three major classes of mitogen-activated protein kinases (MAPKs), namely the extracellular signal-regulated kinase 1/2

(ERK 1/2), c-Jun N-terminal kinases (JNKs) and p38 MAPKs, whose activation was shown to be central to the PKC α -induced cardiac hypertrophy (44). MAPK activation is also mediated by elevated Ca²⁺. Agonist- or pressure-overload-induced hypertrophy was shown to be mediated by MAPK activation, a process which is abrogated by overexpression of MAPK phosphatase 1 (MKP-1) (48). There are conflicting data on the role of ERK 1/2 in the hypertrophic signaling pathway. In cultured cardiomyocytes, pharmacological inhibition of ERK 1/2 activity blunted hypertrophic growth (66), a response which could not be reproduced in other reports (239) while assessing production of ANF as a measure of cardiomyocyte hypertrophy. MAPKs are also under the phosphorylation control by other upstream kinases called MEKK and MKK. The JNK class of MAPKs is regulated by MKK4 or MKK7 which phosphorylate JNK and subsequently cause stimulation of cardiac hypertrophy genes (99). Transgenic mice with deletion of the upstream kinase, MEKK1 or adenoviral expression of MKK4 both attenuated agonist-induced hypertrophy or pressure overload hypertrophy (37, 62). On the other hand, p38 MAPKs are regulated by MKK3 and MKK6, both of which sufficiently induce hypertrophy (37). These findings suggest a critical role of the MAPKs in the PKC-mediated pathological hypertrophy and as such an important target for novel pharmacotherapy development.

Another target activated by PKC is protein kinase D (PKD). When activated, PKD phosphorylates and activates downstream transcription factors.

The ensuing translocation of the transcription factors into the nucleus leads to activation of hypertrophic genes and subsequently proteins (22).

ET-1 receptor activation by ET-1 and α -adrenergic receptor (α -AR) activation by phenylephrine (PE), an α -AR agonist, also stimulate similar molecular pathways as described for ANGII receptor activation. Pharmacological inhibition of AT₁ receptors have proven efficacious in reducing the incidence of cardiac hypertrophy in mouse and human models of hypertrophy. Cross-talk between AT₁ receptors and ET-1 production has been identified in rat cultured myocytes whereby ET-1 levels were elevated following ANGII stimulation (310). Inhibition of ET-1 receptors abolished ANGII induced cardiomyocyte hypertrophy in cultured myocytes (116).

The β 1-adrenergic receptor (β 1-AR) is the most abundant adrenergic receptor in the myocardium which underscores the important influence of adrenergic stimulation on the heart. The β 1-adrenoceptor is coupled to G α_s which stimulates adenylate cyclase (AC) leading to production of cyclic AMP (cAMP) (255).

Subsequent activation of protein kinase A (PKA) by cAMP mediates most of the cellular effects of adrenergic stimulation basically by modulating cardiac contractility and heart rate. Stimulation of the β 1-AR is normally associated with beneficial cardiac response manifested as positive chronotropic, inotropic and lusitropic effects of the heart (99). Recent findings however, suggest that β 1-adrenoceptor signaling, when chronically stimulated, could be involved in the development of cardiac hypertrophy (107, 140). The molecular underpinnings of

the adrenergic system in the development of cardiac hypertrophy have been unraveled recently. In transgenic mice, over-expression of $G_{\alpha s}$ led to enhanced β -adrenergic stimulation accompanied by development of myocardial hypertrophy, fibrosis, necrosis, and ultimately heart failure in older mice (140).

Impairment of β -adrenergic receptor function coupled to uncoupling of receptor activation and subsequent downstream effect mediate the pathologic hypertrophic effect of β -adrenergic activation. Phosphorylation of the β -adrenoceptor by β -adrenoceptor kinase 1 (β ARK1) decreases the sensitivity of the receptor to further agonist stimulation (99). Accumulating data suggest that aberrant intracellular Ca^{2+} regulation is central to the hypertrophic phenotype mediated by β -adrenergic receptor stimulation. Mutations in the ryanodine receptor 2 (RyR2) and/or hyper-phosphorylation of RyR2 by PKA resulted in abnormal handling of Ca^{2+}_i leading to heart failure in experimental models. To this end, β -receptor blockers inhibit the hyper-phosphorylated state of RyR2 leading to amelioration of heart failure (255), suggesting a role for the blockers in treatment of heart failure patients.

Several other distinct pathways that trigger the hypertrophic phenotype have been delineated in various experimental models but the extent of their involvement is beyond the scope of the present volume. The role of small GTP-binding proteins (138), matrix metalloproteinases/tissue necrotic factor α (174) and reactive oxygen species (256) signaling have all been implicated in maladaptive hypertrophic development. Moreover, various cross-talks have been shown to exist between several hypertrophic signaling pathways, which present

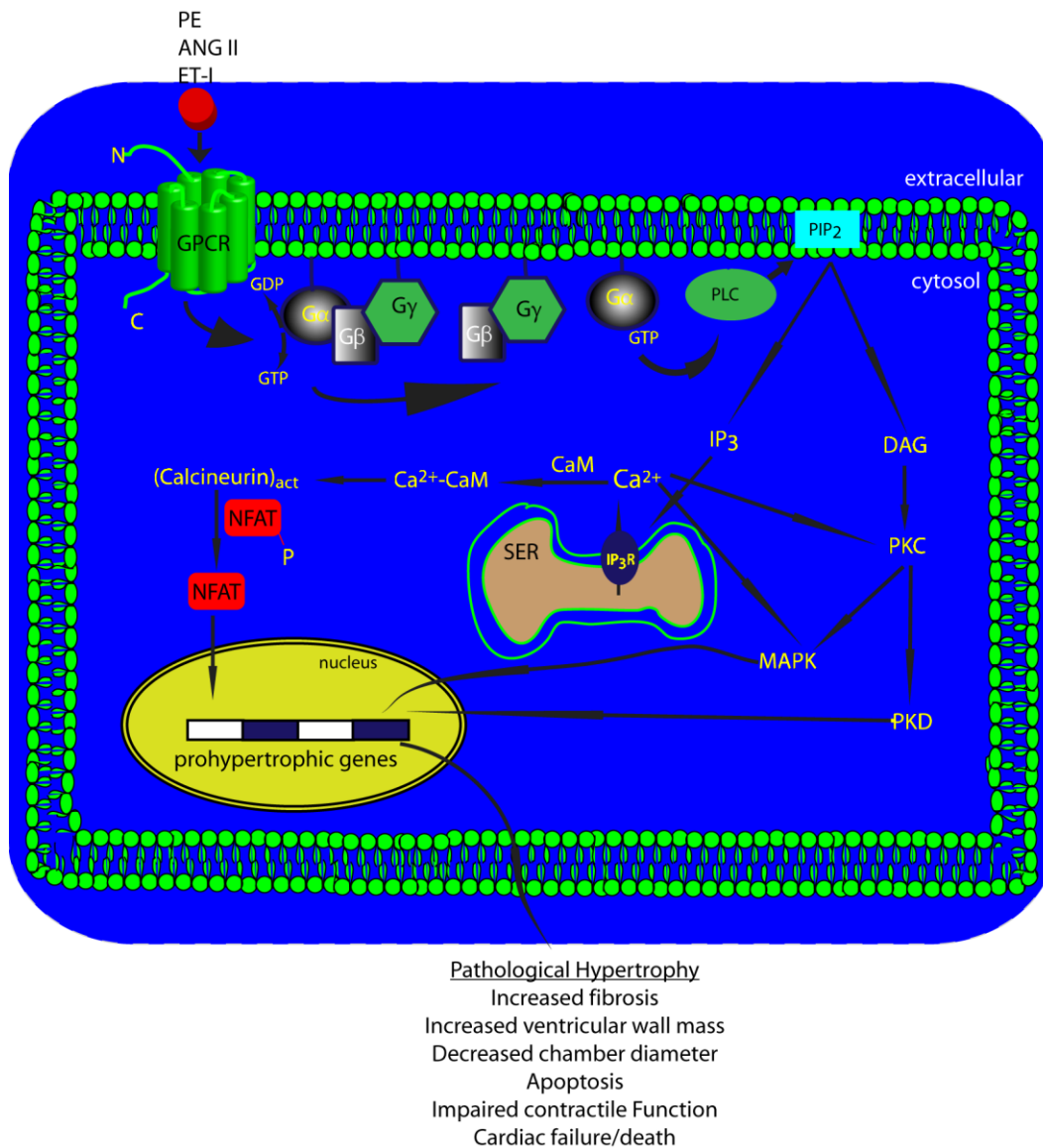


Fig. 1.6 Schematic representation of pathological hypertrophic signaling pathway. Hypertrophic agents acting via GPCR activates G-protein by inducing exchange of GDP for GTP. $G\alpha_{GTP}$ dissociates from $G\beta\gamma$ and activates PLC which in turn hydrolyzes PIP_2 to IP_3 and DAG. IP_3 interacts with IP_3R which leads to efflux of Ca^{2+} from SER. Ca^{2+} interacts with CaM forming Ca^{2+} -CaM complex which activates calcineurin, a phosphatase which dephosphorylates NFAT, leading to its translocation into the nucleus to induce the transcription of pro-hypertrophic

genes ultimately resulting in the manifestation of pathological hypertrophy. DAG activates PKC which stimulates MAPK and PKD which activate transcription factors and induction of pro-hypertrophic genes. PKC and MAPK are also activated directly by Ca^{2+} . PE, phenylephrine; ANGII, angiotensin II; ET-I, endothelin I; GPCR, guanidine protein coupled receptor; N, amino terminus; C, carboxyl terminus; GDP, guanidine diphosphate; GTP, guanidine triphosphate; PLC, phospholipase C; PIP_2 , phosphatidylinositol bisphosphate; IP_3 , inositol triphosphate; DAG, diacylglycerol; SER, sarcoendoplasmic reticulum; MAPK, mitogen activated protein kinase; PKC, protein kinase C; PKD, protein kinase D; CaM, calmodulin; $(\text{calcineurin})_{\text{act}}$, activated calcineurin; NFAT-P, phosphorylated nuclear factor of activated T cells; P, phosphorylated; IP_3R , inositol triphosphate receptor; Ca^{2+} , calcium ion.

the greatest challenge in the development of novel pharmacotherapy for the treatment of heart failure patients.

1.6.3 Concentric and Eccentric Cardiac Hypertrophy

The cardiac remodeling process is a complex adaptive mechanism in response to stimuli that exert an increased demand on the heart. Cardiac hypertrophy, whether physiological or pathological, can further be classified as concentric or eccentric depending on the source of the initiating stimuli. Characterization of hypertrophy in this manner provides additional information in delineating the underlying molecular pathway elicited by the prevailing stimulus. In concentric hypertrophy, the mass of the ventricular wall increases accompanied by a little reduction or no change in the chamber diameter (129). Sarcomeric proteins are added in a parallel fashion resulting in an increase in the wall thickness and width. Contrastingly, eccentric hypertrophy is characterized by a serial addition of sarcomeres leading to an increase in myocyte length. This causes extension of the ventricular wall (dilated chamber) accompanied by an increase in cardiac mass. It is generally accepted that concentric morphological changes of the heart are induced by pressure overload, whereas volume overload is the underlying cause for eccentric hypertrophy development (74). Additionally, varying stimuli have combinations of volume and pressure overload thus, inducing unique forms of hypertrophy (74).

Physiological hypertrophy, as noted above, is induced by factors including pregnancy and chronic exercise training (strength- and endurance-induced). Numerous reports show that endurance training (cycling and running) causes

elevation of cardiac output as well as an increase in blood pressure (236, 246). Conceivably, the heart responds by increasing both ventricular wall mass and internal diameter. The endurance-trained heart is therefore described as eccentric hypertrophic development because volume overload is the prevalent contributing factor (207). The strength-induced (e.g. weightlifting) myocardium is elicited by increased pressure overload resulting from elevation of blood pressure, with little or no effect on stroke volume and cardiac output (207). Thus, sarcomeres are added in parallel which can cause a state of physiological concentric hypertrophy because the internal diameter of the ventricles is not reduced (197, 207).

Molecular mechanisms underlying hypertrophic development induced by exercise training have been a focus of intense investigation. Activation of the ANGII receptor isoform 1 (AT1) via its effect on the systemic blood pressure (reviewed in Ref. (92)) has been implicated in mediating hypertrophy induced by exercise training. This effect occurred in the absence of any noticeable changes on the local or systemic activation of the renin-angiotensin system (RAS) suggesting a novel response of the AT1 receptors in hypertrophic development (85). Additionally, in this study, the expression level of the AT1 receptors was elevated during resistance training in adult rats. Losartan, an AT1 receptor antagonist, ameliorated hypertrophy induced by swimming and exercise trained rats. Interestingly, Angiotensin II (ANGII) level and other components of the RAS were down-regulated in the heart indicating that an alternative pathway mediates activation of AT1. Indeed, it was reported that mechanical stretch in swimming-trained mice induced activation of Akt via AT1 receptor-dependent

mechanisms (75, 331). This novel pathway involves transactivation of Akt by the epidermal growth factor receptor (EGFR) (331). From the ongoing discussion, it could be deduced that mechanical stretch induced by exercise training activates the AT1 receptors, which stimulates Akt via EGFR, leading to concentric or eccentric physiological hypertrophic development. A number of mice models of hypertrophy support a role of ANGII in inducing physiological hypertrophy via activation of EGFR (244).

In the pressure overloaded myocardium as occurs in hypertension and aortic stenosis, the increase in systolic stress induces a concentric pattern of hypertrophy. In some clinical conditions such as aortic regurgitation, an increase in diastolic wall stress induces eccentric hypertrophy leading to dilation of chamber.

1.6.4 Distinct Features of Cardiac Hypertrophy

The myocardium is influenced by a milieu of factors including biomechanical and hormonal. Changes in hemodynamic parameters often lead to adjustments in the myocardium in a process referred to as cardiac remodeling (218). As discussed above, an increase in workload or myocyte death following ischemic damage (myocardial infarction) induces changes at the molecular, cellular and structural levels to overcome the impending anomaly.

Myocardial response to biomechanical increase or stretch is increased cardiomyocyte size, in order to overcome the elevated workload (80). The prolonged exposure to the initiating stimuli translates into enlargement of the myocardium, hypertrophy (80). In pathological hypertrophy, the initiating insult

is often a diseased state such as chronic pressure overload, or ischemic heart diseases (24). Pathological hypertrophy initially appears as an adaptive or a compensatory response but prolongation of the stimuli renders the heart maladaptive, a state referred to as decompensated myocardium (24). Thus, pathological hypertrophy often leads to impairment of cardiac output and contractile activity which may proceed to heart failure and sudden death (24, 28).

Pathological cardiac hypertrophy generally leads to reactivation of the so-called fetal gene program. The re-induction of the fetal gene program involves the expression of genes that are normally associated with the fetal heart, but subsequently repressed in the adult myocardium (24, 253). The fetal phenotype of gene expression accompanies pathological hypertrophy, but has not been identified for stimuli that promote physiological hypertrophy (28, 204).

Experimentally, the expression levels of β -myosin heavy chain (β -MHC), natriuretic peptides (NPs) and α -skeletal actin have been employed as molecular hypertrophic markers to assess cardiac hypertrophic development (24, 50). Normally expressed in the developing fetal heart, the level of these biomarkers are elevated in the hypertrophied myocardium in response to pathological stimuli (24). In the present thesis, the expression levels of these biomarkers were used as one of the tools to measure cardiomyocyte hypertrophic growth in response to prohypertrophic stimuli.

1.6.4.1 Cardiac Hypertrophy and β -Myosin Heavy Chain

The contractile machinery of the heart is composed of thick filaments and thin filaments. The thick filament is mainly myosin which has two heavy chains

and four light chains. The adult rodent myocardium expresses predominantly the α -MHC isoform while the developing heart expresses the β -MHC isoform (232); in the adult human myocardium β -MHC is predominant (265). Various physiological and pathological states induce transitions between the two isoforms. In the hypertrophied myocardium and the failing heart, the level of α -MHC is depressed with an accompanying increase in the β -MHC isoform suggesting a return to the fetal isoform (208). This adaptive strategy tends to normalize the increased workload by altering the rate of contraction in the short-term but becomes maladaptive chronically.

The molecular mechanisms underlying the switch between isoforms under various conditions have not been well delineated. Studies in the rat myocardium have revealed that α_1 - and β -adrenoceptor agonists acting via the PKC- β pathway mediate expression of β -MHC (148). Another characteristic of the hypertrophic myocardium, the desensitization of the ventricles to further adrenergic stimulation, has been shown to correlate with re-emergence of β -MHC (230). A recent report in the mouse model of hypertrophy showed that the re-expression of β -MHC in the cardiomyocytes correlated with lack of response of the myocytes to further β -adrenergic stimulation (230). Additionally, interventions that abrogated cardiac hypertrophy also reduced the re-expression of β -MHC (1). These findings suggest that similar pathways may be responsible for mediating the contractile non-responsiveness and the re-expression of β -MHC. Whether β -MHC re-expression is the sole determinant of the inability of the cardiomyocytes to respond to further β -adrenergic stimulation has, however, not been established.

That β -MHC is a *bona fide* molecular marker of pathological hypertrophy has been challenged in studies which demonstrated that re-expression of β -MHC does not occur uniformly in the hypertrophied myocardium (229, 264). A recent study in the pressure overload-induced hypertrophy in the mice showed that β -MHC re-expression occurred only in non-hypertrophic cells of the myocardium (190). In general, the role of β -MHC during the hypertrophic development of the heart and its implication as a marker of hypertrophy requires further investigation.

1.6.4.2 Natriuretic Peptides and Cardiac Hypertrophy

Natriuretic peptides play important cardiovascular roles in response to wall stretch. Three isoforms have been identified; atrial natriuretic peptide (ANP), expressed mainly in the atria, brain natriuretic peptide (BNP) found in both the atria and the ventricles, and C-type natriuretic peptide (CNP) whose role in the heart is not yet defined.

ANP and BNP are expressed predominantly in the embryo and their expression levels decline in the adult heart (158). In the hypertrophied and the failing heart, however, the expression levels of these natriuretic peptides are upregulated (298). ANP and BNP exert cardiovascular effects, including vasorelaxation, diuresis and natriuresis. Clinically, an increased expression of BNP in the plasma has been found in the failing heart and has been used as a biomarker for the diagnosis of cardiac failure (298). The correlation between natriuretic peptide expression levels *in situ* and congestive heart diseases is indicative of the utility of these peptides as indicators of heart disease and cardiac hypertrophy. In *in vitro* models of hypertrophy, ANP expression levels have been

employed as a reliable indicator of cardiomyocyte hypertrophy (17, 152). In cultured cardiomyocytes endogenous ANP and BNP as well as exogenously applied natriuretic peptides were shown to be cardioprotective and anti-hypertrophic in catecholamine-induced hypertrophy (49, 132). Moreover, ANP inhibits MAPK mediated cardiomyocyte hypertrophy (49), which may suggest a protective role in reversing agonist-induced pathological hypertrophy.

ANP and BNP exert their cellular effects by acting on guanylyl cyclase (GC)-A receptors (also referred to as natriuretic peptide receptor-A), which is coupled to cyclic guanylyl monophosphate (cGMP) upregulation, which leads to the activation of protein kinase G (PKG), which in turn causes the phosphorylation and inactivation of calcineurin (reviewed in Ref. (158)). The action of ANP and BNP therefore maintains NFAT in the inactive state thereby inhibiting the induction of hypertrophic genes (158). Correspondingly, cGMP analogues demonstrate anti-hypertrophic effects in cardiomyocytes (49).

1.6.4.3 Alpha-Skeletal Actin and Cardiac Hypertrophy

Three main actin filaments are expressed sequentially in the developing myocardium. In the embryonic myocardium, the expression of α -smooth muscle actin precedes the appearance of α -skeletal actin and α -cardiac actin. Alpha-cardiac actin is predominantly expressed in the normal adult myocardium (252).

During different pathological conditions of the heart, the myocardial pattern of actin isoform expression reverts to the fetal phenotype. Many reports have shown that hypertrophic development, as well as other cardiac pathologies induce an increased expression of α -skeletal actin accompanied by a reduction in the

expression of α -cardiac actin (34). A study in the human heart during development demonstrated that the skeletal and cardiac actin isoforms expressions were diffusely distributed in the cardiomyocytes at 20 weeks of fetal life (288). Contrastingly, the α -smooth muscle actin isoform was profoundly expressed in early fetal life (288). In that same study, it was revealed that myocardial pathologies including hypertrophy, myocyte stretch and increased wall stretch, but not cardiomyopathies, were associated with an increased expression of α -skeletal actin (288).

Consistently, α -skeletal actin mRNA re-expression has been demonstrated in cardiomyocytes and whole heart models of hypertrophy including pressure overload (141) and α_1 -adrenoceptor activation (34). Thus, α -skeletal actin has been employed as a marker of cardiac hypertrophy in experimental models of hypertrophy.

In this thesis, in order to monitor hypertrophic development of cardiomyocytes of adult mice, the mRNA expression levels of α -skeletal actin, β -MHC and atrial natriuretic peptide were employed in keeping with the reactivation of the fetal gene program during hypertrophy and heart failure.

1.7 Cardiomyopathies

Cardiomyopathies generally refer to cardiac conditions in which the cardiac muscles become weak, thus reducing the ability of the heart to effectively carry out its pumping action. The etiology of cardiomyopathy can be congenital, immunological or ischemic, but the outcome is identical; the heart responds by becoming hypertrophied (24). Various forms of cardiomyopathies have been

identified in humans, but for the purposes of the present discussion, cardiomyopathies induced by aberrant expression of genes will be focused on.

Two forms of inherited cardiomyopathies exist; hypertrophic cardiomyopathy (HCM) and dilated cardiomyopathy (DCM) (218). HCM is characterized by a thickening of the left ventricular wall and narrowing of the chamber volume and functionally by diastolic dysfunction (218). DCM on the other hand manifests as enlargement of the ventricular chamber accompanied by thinning of the ventricular wall. Functionally, DCM results in defects in systolic function and development of arrhythmias (24, 218).

More than a thousand independent mutations in nine of the genes that code for sarcomeric proteins as well as their regulators have been identified to cause cardiomyopathies (245). These mutations occur in the thick filaments (β -MHC) as well as in the thin filaments (actin); regulatory proteins such as myosin light chain also demonstrate mutations that induce cardiomyopathies (245). Point mutations, missense mutations and dominant negative mutations have been shown to be involved with cardiomyopathies. The bottom line of all these mutations is the alteration of the contractile machinery to Ca^{2+} sensitivity (112, 215).

Models of HCM have consistently demonstrated increased sensitivity of cardiomyocytes to Ca^{2+} (19). This affects the overall cytosolic Ca^{2+} homeostasis, which explains the ventricular arrhythmias observed in HCM patients (19). On the other hand, DCM generally exhibits reduced sensitivity to Ca^{2+} (247). Treatments for HCM and DCM therefore include modifying the Ca^{2+} sensitivity of the myofilaments. Abrogating Ca^{2+} sensitization using blebbistatin, which

reduces the interaction between myosin and actin filaments by inhibiting ATPase activity, prevented arrhythmias associated with HCM (26). Myofilament Ca^{2+} sensitization agents such as levosimendan and omecantiv mecarbil (cardiac myosin activators) improve contractile function in DCM and heart failure (269). The shortfall in these Ca^{2+} sensitization strategies is the tendency for one form of cardiomyopathy to revert to the opposite phenotype. To overcome this detriment, an emerging therapeutic approach which involves the use of gene therapy to offset disorders associated with aberrant gene expression profile in cardiomyopathies holds much promise for the future (19). Although this strategy holds, considerable promise, the challenge of administering the gene to the target location remains a major setback. A related potential approach to treat heart failure resulting from cardiomyopathy is the use of microRNA therapy. MicroRNAs are short (~22) nucleotide RNA sequence that bind to complementary sequences in the 3' UTR of target mRNAs resulting in silencing of the target gene and suppression of their expression (139). Presently this approach is being employed in the treatment of some form of cancers (181) and holds promise in heart disease.

Since cardiomyopathies affect the overall cytosolic Ca^{2+} homeostasis, myocardial energy metabolism is significantly affected. The hypertrophic heart is characterized by a shunting of energy substrate usage from fatty acid to carbohydrate. This energy substrate switch is also apparent in cardiomyopathies, and occurs as an adaptive response to the development of hypertrophy. Inhibiting fatty acid oxidation by reducing CPT-1/2 activity has been shown to be beneficial

in experimental models of HCM (19). Metabolic energy substrate modulation is therefore emerging as an attractive therapeutic intervention in cardiomyopathies.

The molecular signaling events which mediate the evolution of cardiomyopathies to hypertrophy and heart failure are complex and still remain controversial. Targeting specific pathways in the event of cardiomyopathy have held some promise in mitigating the symptoms associated with HCM and DCM. Abolishing the renin-angiotensin-system enhances cardiac function in HCM suggesting an elevation of this system in HCM which suggests stimulation of the GPCRs as mediators of hypertrophy involving HCM (263). Indeed, in one study it was observed that myocardial aldosterone and aldosterone synthase mRNA levels were increased about 4-6 fold in HCM patients (299). Ventricular biopsies from the failing heart of humans with dilated cardiomyopathy revealed an elevated expression of carbonic anhydrase isoforms, CAII, CAIV, and CAXIV mRNAs (15). Coupled with previous findings that carbonic anhydrase expression level is increased in rat cardiomyocytes in response to ANGII (17), this suggests the possibility that carbonic anhydrase activity inhibition represents a candidate therapy to revert cardiomyopathy-associated hypertrophy. Previously, carbonic anhydrase inhibitors, due to their diuretic properties have been employed clinically to treat patients with glaucoma, seizure and osteoporosis (257). These agents, which are sulfonamides are however, non-selective in their activity against carbonic anhydrases (335). Recently, it was demonstrated that a series of novel N-substituted N'-(2-arylmethylthio-4-chloro-5-methylbenzenesulfonyl)guanidines 9-41 specifically inhibit CAIX and CAXII are effective antitumor agents (335).

This indicates the feasibility of using CA isoform specific inhibitors in the treatment of heart failure.

Taken together, cardiomyopathies induce hypertrophy by complex molecular mechanisms leading to alteration of Ca^{2+} sensitivity of the contractile machinery. The future therapeutic modalities will be enhanced by delineating the specific molecular events that precipitate hypertrophy and heart failure in HCM and DCM.

1.8 Thesis Rationale

Despite the advancement in our understanding of cardiac remodeling (following a pathological insult) and progression to heart failure, current clinical outcomes have been poor. This could be accounted for partially by the intricate network of signaling pathways involved in the remodeling process. A number of cross-talk interactions exist between the various complex mechanisms/pathways which induce hypertrophy. This leads to difficulty in identifying the most effective target in the design of pharmacotherapy. Moreover, the animal models employed in delineating the pathways that induce cardiac hypertrophy have provided conflicting data compared to the pathogenesis of the human cardiac hypertrophy and heart failure phenotype.

The search for the 'super-drug' to ameliorate cardiac hypertrophy and to limit progression to heart failure has been unrelenting in the past few years. The present treatment modalities are directed at putative targets in the deciphered signaling pathways, which have been demonstrated to mediate cardiac hypertrophy. Based on our present knowledge of the signaling mechanisms

associated with cardiac hypertrophy, some of the current therapeutic interventions include, inhibitors of cGMP phosphodiesterase (sildenafil) which have proven beneficial in animal models and are being tested in clinical trials (267); GPCR antagonists (45, 67); modulators of excitation-contraction coupling (269); and modulators of metabolic energy substrate utilization (300).

A plethora of experimental data has attempted to identify distinct signaling pathways and novel targets in cardiac hypertrophy and heart failure. The search for novel therapeutic targets still continues because of the complex mechanisms that mediate cardiac hypertrophy. Interpretation of data from studies aimed at deciphering the signaling pathways of hypertrophy from different approaches and different species has further complicated our understanding of the nature of cardiac hypertrophy. The present study seeks to contribute to the understanding of the signaling mechanism involved with pathological hypertrophy in order to identify a new target for therapeutic intervention.

Playing a central role in hypertrophic signaling is the involvement of the cardiac isoform of the Na^+/H^+ anion exchanger NHE1 (64). Several lines of evidence demonstrate that NHE1 activation is at the center of many cardiovascular disorders (100, 151). As noted earlier, NHE1 mediates the electroneutral exchange of 1 cytosolic H^+ for 1 extracellular Na^+ . The sensitivity of NHE1 to H^+ is afforded by an allosteric H^+ sensor site located within the membrane transport domain and the exchange activity is driven by the inwardly driven Na^+ gradient provided by the Na^+/K^+ ATPase (64, 96). Regulation of NHE1 by growth factors and neurohormones is determined by the cytosolic tail of

the exchanger and removal of the distal region of the cytosolic tail shifts the pH_i sensitivity to the acidic side (96). The most potent regulator of NHE 1 activity is, however, intracellular acidosis (151).

Several lines of evidence have revealed that inhibition of NHE1 activity during ischemia attenuates injury imposed by ischemia/reperfusion (149, 153). This promising strategy led to two major clinical trials, Guard During Ischemia Against Necrosis (GUARDIAN) (294) and Evaluation of the Safety and Cardioprotective Effects of Eniporide in Acute Myocardial Infarction (ESCAMI) (330). In this large study, the NHE1 inhibitor, eniporide, was administered before reperfusion therapy in patients with acute ST elevation myocardial infarction (MI). The study revealed that eniporide significantly reduced the incidence of heart failure in patients reperfused late (>4 h), but overall there was no effect on clinical outcome (death, cardiogenic shock, heart failure, life-threatening arrhythmias). The Sodium-Hydrogen Exchange Inhibition to Prevent Coronary Events in Acute Cardiac Conditions (EXPEDITION) study (38), demonstrated cardioprotective effects of cariporide, an NHE1 inhibitor, in patients with ischemic heart disease. The clinical benefits were, however, overshadowed by increased incidence of stroke, leading to the collapse of the study. The implication from these studies was that NHE1 inhibitors may not be efficacious in the treatment of ischemia-reperfusion perfusion.

NHE1 activation has also been observed in other cardiovascular disorders, including cardiac hypertrophy and heart failure (96, 151, 216). Several pro-hypertrophic (155, 199, 212) modulators and mechanical stretch (65) activate

NHE1, leading to hypertrophic growth. These factors induce a cascade of molecular signaling event that lead to activation of PKC which directly phosphorylate NHE1 or MAPKs which phosphorylate NHE1 indirectly. Moreover, phenylephrine administration activates 90-kDa ribosomal S6 kinase (RSK), which is an important modulator of NHE1 activity (209). In the cardiac overloaded rodent heart and the stretched ventricular myocytes, there was an activation of the RAS, which leads to an increased release of ANGII (88). ANGII signaling leads to increased production of endothelin, which stimulates NHE1 via action on the ET_A receptors (88, 126). These findings suggest that NHE1 plays a pivotal role in the signaling events mediated by neurohormones and mechanical stretch.

Substantial evidence suggests that NHE1 activation following mechanical stretch or hormonal activation is an early event which ultimately leads to cytosolic Na⁺ and Ca²⁺ overload and consequently induction of cardiac hypertrophy (64, 65). In the hypertrophied myocardium of the spontaneously hypertensive rats (SHR), there was an increase activation of NHE1 (233). NHE1 inhibition led to a reduction in cardiac hypertrophy and interstitial fibrosis (63). Various models of hypertrophy have demonstrated beneficial effects of NHE1 inhibition on the development of hypertrophy. Transgenic mice expressing activated NHE1 exchanger demonstrated enlargement of the heart and revealed a heightened propensity towards hypertrophic stimulation (212). In essence these studies showed that NHE1 inhibition is an attractive target for therapeutic intervention in cardiac hypertrophy and heart failure.

Since NHE1 activation leads to intracellular acid extrusion, alkalization should have normally accompanied the exchanger activation. However, NHE1 activation in the various studies was not accompanied by increased pH_i although cytosolic Na^+ was elevated (233). NHE1 inactivates under alkaline conditions, which would suggest that the autoregulatory potential of NHE1 would ‘switch off’ the exchanger activity in the face of increased stimulation unless an acidifying mechanism is simultaneously activated (275). Indeed, in the hypertrophied heart of the SHR, NHE1 hyperactivity was accompanied by a simultaneous activation of the $\text{Cl}^-/\text{HCO}_3^-$ anion exchanger (52). A report in the papillary muscles of the SHR demonstrated an increased NHE1 activity accompanied by a high pH_i under nominally $\text{HCO}_3^-/\text{CO}_2$ -free conditions (52). In the presence of HCO_3^- , pH_i was not different between papillary muscles from SHR and their Wistar-Kyoto controls, leading to the suggestion that a $\text{Cl}^-/\text{HCO}_3^-$ anion exchanger was simultaneously activated in the SHR (52). The non-specific AE inhibitor, SITS, increased the basal pH_i in the SHR in the presence of $\text{HCO}_3^-/\text{CO}_2$ confirming a hyper-activation of AE in the SHR papillary muscle.

Subsequently it was reported that ANGII enhances AE $\text{Cl}^-/\text{HCO}_3^-$ exchange activity in papillary muscles and accelerates the rate of recovery of pH_i following imposed intracellular alkalization (234). The ANGII effect was reversed by inhibition of angiotensin II receptors and AE inhibition (87). In an attempt to identify the AE isoform responsible for normalizing the pH_i in SHR papillary muscles, northern blots and hybridization probes revealed an increased expression of the full length AE3 (flAE3) isoform (59). This finding correlated

with the increased AE exchange activity found in SHR (60, 87), suggesting that fIAE3 may be the AE isoform responsible for providing the acidifying mechanism which counters the increased NHE1 activation in the myocardium of SHR.

Later it was demonstrated that infusion of anti-AE3 antibody against the extracellular loop of AE3 demonstrated an increased steady-state pH_i in the SHR myocardium relative to control (60). This provided additional support for the involvement of AE3 as an acid loader to compensate for the cytosolic alkalinization induced by NHE1 activation. To lend further credence to the observation that fIAE3 activity provides the opposite acidifying mechanism to normalize NHE1 activity, it was reported that ANGII increased $\text{Cl}^-/\text{HCO}_3^-$ anion exchange activity by enhancing only the fIAE3 isoform activity, but not SLC26A6, the predominantly expressed $\text{Cl}^-/\text{HCO}_3^-$ isoform in the myocardium (11, 13). Interestingly, this occurred by a PKC mediated phosphorylation of serine 67 of fIAE3 cytoplasmic domain (11).

Collectively, these findings suggest that hypertrophic stimulation by neurohormones induces enhanced NHE1 exchange activity, accompanied by a simultaneously increased fIAE3 anion transport activity. This would result in pH_i neutral cytosolic Na^+ overload which via mechanisms already discussed would cause cytosolic Ca^{2+} overload through the NCX. Ultimately pro-hypertrophic pathways will be stimulated resulting in cardiac hypertrophy. The exact role of AE3 in the development of cardiac hypertrophy, however, has not been well explored directly due mainly to the lack of specific pharmacological tools that attenuate or elevate AE3 functional activity.

Moreover, these findings may suggest that NHE1 and AE3 may be linked functionally in a pathway that mediates hypertrophy. The functional interaction between NHE1 and AE3 was evidenced by findings that suggested that the anion exchangers interact with CAII which provide substrates to enhance the respective transport activities. CAII catalyzes the hydration of CO₂ producing HCO₃⁻ and H⁺, the substrates for AE3 and NHE1 respectively. In a microtiter plate binding assay, CAII bound the C-terminal tail of NHE1, a finding which was confirmed by affinity binding assay by demonstrating protein-protein interaction between CAII and immobilized NHE1 fusion proteins (178). Additionally, CAII co-immunoprecipitated with NHE1 in CHO cells, which suggests a physical complex between NHE1 and CAII (178). The resultant effect of CAII physical interaction with NHE1 was an enhanced transport activity of the exchanger an effect which was reduced by the CAII inhibitor, acetazolamide (178). Subsequently, the physical interaction between CAII and NHE1 was localized to the extreme C-terminal region of NHE1 (179). Several lines of evidence also show that CAII also binds to AE3 which facilitates the anion transport activity of the exchanger (282, 283).

Involvement of CAII in the development of myocardial hypertrophy has generated considerable interest due to the findings that CAII physically and functionally interacts with NHE1 and AE exchangers. Recently, it was demonstrated that inhibition of CAII activity reversed the development of cardiomyocyte hypertrophy induced by PE and ANGII in adult and neonatal cardiomyocytes (17). The hypertrophic stimuli also caused an increased

expression of CAII in neonatal rat cardiomyocytes (17). This observation confirmed the involvement of CAII in the hypertrophic signaling cascade. These findings led to the suggestion that a functional and physical interactional complex of NHE1-CAII-AE3 may exist, which could mediate the hypertrophic stimulation by hypertrophic agonists such as ET-1, ANGII and PE.

Despite the proposed role of the AE3 $\text{Cl}^-/\text{HCO}_3^-$ anion exchanger in the regulation of steady-state pH_i , the experimental evidence to confirm its direct involvement in hypertrophic development has been lacking. However, from previous reports demonstrating cardioprotective roles of NHE1 inhibition in the context of ischemia/reperfusion injury and cardiac hypertrophy, it is reasonable to deduce that inhibition of AE3 transport activity should also afford similar beneficial effects. To determine the involvement of AE3 in cardiac function and pathogenesis, a mouse model with the *ae3* gene ablated (AE3 null, *ae3*^{-/-}) was developed (4, 240). A recent report demonstrated that disruption of the AE3 gene did not affect normal cardiac function (240). When hearts isolated from AE3 null mice were subjected to ischemia/reperfusion injury there were no significant differences in cardiac performance relative to control hearts (240). *In vivo* assessment of cardiac performance revealed that there were no differences between AE3 null mice hearts and control hearts. However, when AE3 null mice were mated with mice lacking the $\text{Na}^+-\text{K}^+-2\text{Cl}^-$ (NKCC) gene to produce *ae3*^{-/-}/*nkcc*^{-/-} double knock-out mice, cardiac contractility was greatly impaired. Additionally, hearts from the double knock-out mice demonstrated greater propensity for ischemia/reperfusion injury. These observations were attributed to

the alteration of Ca^{2+} homeostasis suggesting that both AE3 and NKCC contribute to the signaling pathways involved in regulating cytosolic Ca^{2+} . Although this study showed that AE3 may be involved in cardiac function, its absence does not improve function but rather exacerbates injury induced by ischemia/reperfusion.

In a hypertrophic cardiomyopathy model (Glu180Gly mutation in α -tropomyosin, TM180), loss of AE3 induced rapid cardiac decompensation, which progressed to heart failure (4). Ca^{2+} handling was impaired in the double mutant, TM180/*ae3*^{-/-}, hearts compared to the two mutants, *ae3*^{-/-} and TM180. From the foregoing, it may be deduced that AE3 does not play a cardioprotective role in hypertrophic cardiomyopathy and ischemia/reperfusion injury.

This thesis attempts to further delineate the role of the AE3 $\text{Cl}^-/\text{HCO}_3^-$ in the development of cardiac hypertrophy. The proposal that NHE1, CAII and AE3 operate in concert to mediate the hypertrophic effect of ANGII and PE led us to hypothesize that: *“Disrupting the gene that encodes AE3 will limit cardiomyocyte growth in response to hypertrophic stimuli”*.

The physical and potentially functional interaction between NHE1, CAII and AE3 has been termed the hypertrophic transport metabolism (HTM) (17) (Fig. 1.6). Upon stimulation by hypertrophic stimuli, activation of NHE1, CAII and AE3 will lead to a sustained ‘feed-forward’ induction of downstream hypertrophic mediators. Thus, HTM activation will present a pathological pathway that mediate hypertrophy and antagonism of either of the components involved will result in abrogation of pathological hypertrophy. Our hypothesis stemmed from accumulation of evidence which demonstrate that AE3 is the only

cardiac $\text{Cl}^-/\text{HCO}_3^-$ anion exchanger whose acid loading capability is coupled to normalizing the alkalinizing effect of NHE1 in order to maintain pH_i homeostasis. Moreover, the transport activity of AE3 is enhanced by hypertrophic stimuli via PKC (11), a pathway also shown to enhance NHE1 anion exchange activity (64, 178, 179) (Fig. 1.6). Thus, the net effect of hypertrophic stimulation is the pH_i neutral overload of Na^+ subsequently causing cytosolic Ca^{2+} overload via the NCX. Increased cytosolic Ca^{2+} stimulates downstream effectors leading to activation of NFAT which translocates to the nucleus and activates the transcription of pro-hypertrophic mediators.

From findings which revealed that NHE1 activation occurs as an early event during hypertrophic stimulation, it is also reasonable to suggest that fIAE3 activation must occur as an early event (64). Thus, we speculate in the present study that deletion of the gene that encodes AE3 will lead to an increase in pH_i following hypertrophic stimulation. Since NHE1 autoinhibits under alkaline conditions, downstream targets of hypertrophic stimulation will be downregulated which will limit cardiomyocyte growth. Thus, the deletion of the AE3 gene in adult mice will limit the development of hypertrophy in cardiomyocyte subjected to hypertrophic stimulation. These possibilities will be the focus of the present investigation.

Hypothesis

In general terms, this thesis studied the role of carbonic anhydrase in regulating the function of $\text{Cl}^-/\text{HCO}_3^-$ exchange proteins. Specifically, this document describes experiments investigating the hypotheses that:

1. Fusion of active CAII to the extreme C-terminal tail of AE1 will enhance the transport activity of the exchanger and;
2. Disruption of the AE3 gene will render cardiomyocytes isolated from adult mice less responsive to hypertrophic stimulation.

The specific objectives are:

1. To fuse either wildtype CAII or catalytically inactive CAII (CAII-V143Y) to the C-terminus of AE1 in order to determine their effect on the anion exchange activity of AE1 and;
2. To assess the response of the deletion of the mouse *ae3* gene on cardiomyocyte hypertrophic growth.

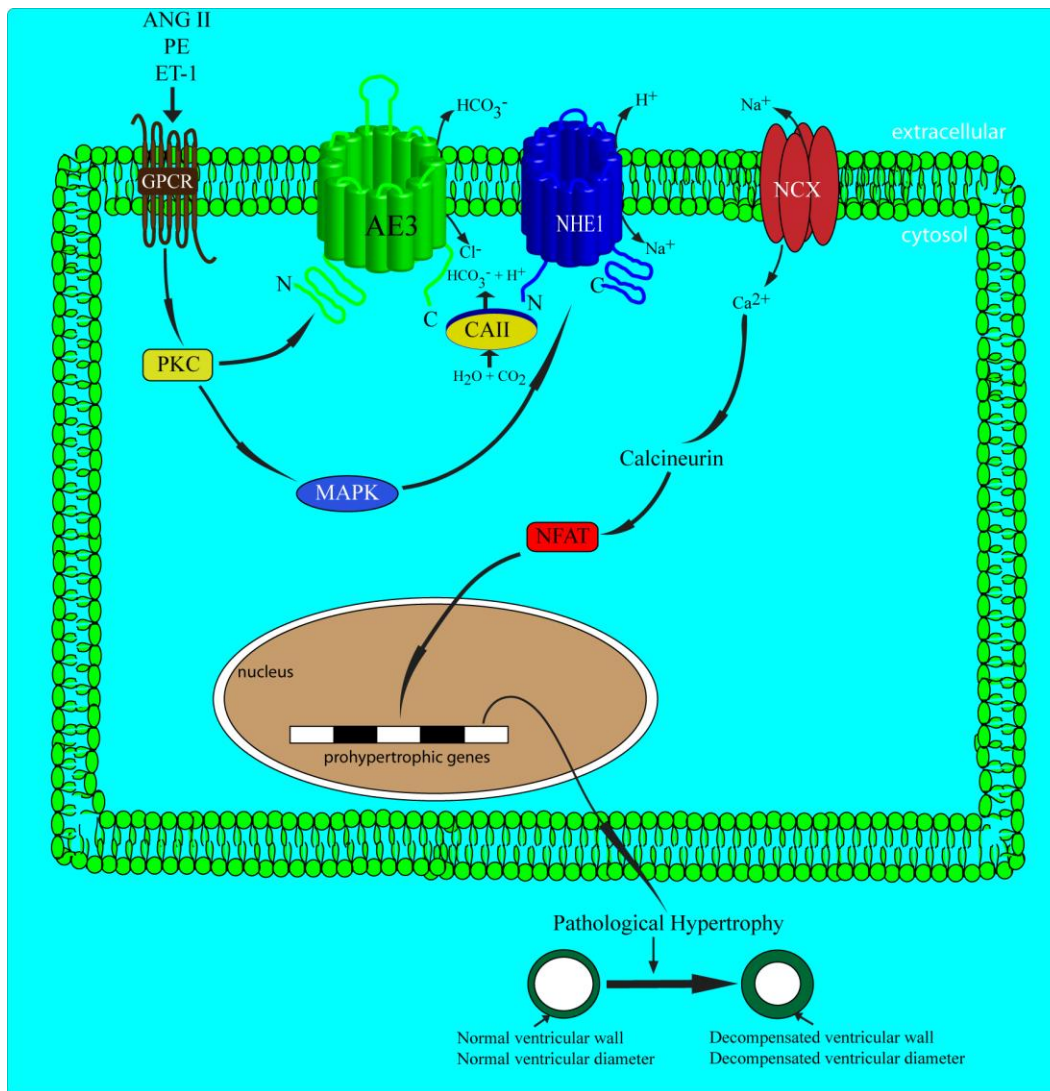


Fig. 1.7 The hypertrophic transport metabolon (HTM). Hypertrophic stimuli, angiotensin II (ANGII), phenylephrine (PE) or endothelin 1 (ET-1) bind to their guanine protein coupled receptor (GPCR) which leads to the activation of protein kinase C (PKC). PKC directly stimulates the chloride/bicarbonate anion exchanger AE3 (AE3) which mediates the exchange of chloride ion (Cl^-) and bicarbonate ion (HCO_3^-). PKC indirectly phosphorylates the sodium-proton exchanger 1 isoform (NHE1) via mitogen activated protein kinase (MAPK) facilitating the exchange of proton (H^+) for sodium ion (Na^+). The activities of

BT and NHE1 are enhanced by interaction with carbonic anhydrase II (CAII) which provides the respective substrates, HCO_3^- and H^+ for AE3 and NHE1. Consequently the cardiomyocyte is overloaded with Na^+ which activates the sodium-calcium exchanger (NCX) ultimately overloading the cytosol with calcium ion (Ca^{2+}). Increased intracellular Ca^{2+} activates calcineurin which dephosphorylates nuclear factor of activated T cells (NFAT) inducing its translocation into the nucleus. NFAT in the nucleus activates the expression of pro-hypertrophic genes which leads to induction of pathological hypertrophy characterized by increased ventricular wall mass and reduced ventricular diameter.

Bibliography

1. **Abraham WT, Gilbert EM, Lowes BD, Minobe WA, Larrabee P, Roden RL, Dutcher D, Sederberg J, Lindenfeld JA, Wolfel EE, Shakar SF, Ferguson D, Volkman K, Linseman JV, Quaife RA, Robertson AD, and Bristow MR.** Coordinate changes in Myosin heavy chain isoform gene expression are selectively associated with alterations in dilated cardiomyopathy phenotype. *Mol Med* 8: 750-760, 2002.
2. **Aiello EA, Petroff MG, Mattiazzi AR, and Cingolani HE.** Evidence for an electrogenic $\text{Na}^+\text{-HCO}_3^-$ symport in rat cardiac myocytes. *J Physiol (Lond)* 512: 137-148, 1998.
3. **Akel A, Wagner CA, Kovacikova J, Kasinathan RS, Kiedaisch V, Koka S, Alper SL, Bernhardt I, Wieder T, Huber SM, and Lang F.** Enhanced suicidal death of erythrocytes from gene-targeted mice lacking the $\text{Cl}^-/\text{HCO}_3^-$ exchanger AE1. *Am J Physiol Cell Physiol* 292: C1759-1767, 2007.
4. **Al Moamen NJ, Prasad V, Bodi I, Miller ML, Neiman ML, Lasko VM, Alper SL, Wiczorek DF, Lorenz JN, and Shull GE.** Loss of the AE3 anion exchanger in a hypertrophic cardiomyopathy model causes rapid decompensation and heart failure. *J Mol Cell Cardiol* 50: 137-146, 2011.
5. **Allen DG and Xiao XH.** Activity of the Na^+/H^+ exchanger contributes to cardiac damage following ischaemia and reperfusion. *Clin Exp Pharmacol Physiol* 27: 727-733, 2000.
6. **Allen DG and Xiao XH.** Role of the cardiac Na^+/H^+ exchanger during ischemia and reperfusion. *Cardiovasc Res* 57: 934-941, 2003.

7. **Alper SL.** Molecular physiology and genetics of Na⁺-independent SLC4 anion exchangers. *J Exp Biol* 212: 1672-1683, 2009.
8. **Alper SL.** Molecular physiology of SLC4 anion exchangers. *Exp Physiol* 91: 153-161, 2006.
9. **Alper SL, Chernova MN, and Stewart AK.** How pH regulates a pH regulator: a regulatory hot spot in the N-terminal cytoplasmic domain of the AE2 anion exchanger. *Cell Biochem Biophys* 36: 123-136, 2002.
10. **Alvarez B, Loiselle FB, C.T. S, Schwartz GJ, and Casey JR.** Direct extracellular interaction between carbonic anhydrase IV and the NBC1 Na⁺/HCO₃⁻ co-transporter. *Biochemistry* 42: 2321-2329, 2003.
11. **Alvarez BV, Fujinaga J, and Casey JR.** Molecular Basis for angiotensin II-induced increase of chloride/bicarbonate exchange in the myocardium. *Circ Research* 89: 1246-1253, 2001.
12. **Alvarez BV, Gilmour G, Mema SC, Shull GE, Casey JR, and Sauvé Y.** Blindness results from deficiency in AE3 chloride/bicarbonate exchanger. *PLoS ONE* 2: e839, 2007.
13. **Alvarez BV, Kieller DM, Quon AL, Markovich D, and Casey JR.** Slc26a6: a cardiac chloride-hydroxyl exchanger and predominant chloride-bicarbonate exchanger of the mouse heart. *J Physiol* 561: 721-734, 2004.
14. **Alvarez BV, Kieller DM, Quon AL, Robertson M, and Casey JR.** Cardiac hypertrophy in anion exchanger 1-null mutant mice with severe hemolytic anemia. *Am J Physiol Heart Circ Physiol* 292: H1301-1312, 2007.

15. **Alvarez BV, Quon AL, Mullen J, and Casey JR.** Quantification of carbonic anhydrase gene expression in ventricle of hypertrophic and failing human heart. *BMC Cardiovasc Disord* 13: 2, 2013.
16. **Alvarez BV, Shandro H, Yang Z, Vithana EN, Koh AH, Yeung K, Yong V, Kolatkar P, Palasingam P, Zhang K, J.R. C, and Aung T.** Functional characterization of a novel carbonic anhydrase 4 mutation identified in a Chinese patient with retinitis pigmentosa. *Invest Ophthalmol Vis Sci* 48: 3459-3468, 2007.
17. **Alvarez BV, Xia Y, Sowah D, Soliman D, Light P, Karmazyn M, and Casey JR.** A Carbonic Anhydrase Inhibitor Prevents and Reverts Cardiomyocyte Hypertrophy. *J Physiol* 579: 127-145, 2007.
18. **Aoyagi T and Matsui T.** Phosphoinositide-3 kinase signaling in cardiac hypertrophy and heart failure. *Curr Pharm Des* 17: 1818-1824, 2011.
19. **Ashrafian H, McKenna WJ, and Watkins H.** Disease pathways and novel therapeutic targets in hypertrophic cardiomyopathy. *Circ Res* 109: 86-96, 2011.
20. **Bak MI and Ingwall JS.** Contribution of Na^+/H^+ exchange to Na^+ overload in the ischemic hypertrophied hyperthyroid rat heart. *Cardiovasc Res* 57: 1004-1014, 2003.
21. **Balaban RS.** Cardiac energy metabolism homeostasis: role of cytosolic calcium. *J Mol Cell Cardiol* 34: 1259-1271, 2002.

22. **Balakumar P and Jagadeesh G.** Multifarious molecular signaling cascades of cardiac hypertrophy: can the muddy waters be cleared? *Pharmacol Res* 62: 365-383, 2010.
23. **Barneaud-Rocca D, Etchebest C, and Guizouarn H.** Structural model of the anion exchanger 1 (SLC4A1) and identification of transmembrane segments forming the transport site. *J Biol Chem* 288: 26372-26384, 2013.
24. **Barry SP, Davidson SM, and Townsend PA.** Molecular regulation of cardiac hypertrophy. *Int J Biochem Cell Biol* 40: 2023-2039, 2008.
25. **Battle D and Haque SK.** Genetic causes and mechanisms of distal renal tubular acidosis. *Nephrol Dial Transplant* 27: 3691-3704, 2012.
26. **Baudenbacher F, Schober T, Pinto JR, Sidorov VY, Hilliard F, Solaro RJ, Potter JD, and Knollmann BC.** Myofilament Ca^{2+} sensitization causes susceptibility to cardiac arrhythmia in mice. *J Clin Invest* 118: 3893-3903, 2008.
27. **Becker HM and Deitmer JW.** Carbonic Anhydrase II increases the activity of the human electrogenic $\text{Na}^+/\text{HCO}_3^-$ cotransporter. *J Biol Chem* 282: 13508-13521, 2007.
28. **Bernardo BC, Weeks KL, Pretorius L, and McMullen JR.** Molecular distinction between physiological and pathological cardiac hypertrophy: experimental findings and therapeutic strategies. *Pharmacol Ther* 128: 191-227, 2010.
29. **Bers DM.** Altered cardiac myocyte Ca regulation in heart failure. *Physiology (Bethesda)* 21: 380-387, 2006.

30. **Bers DM.** Calcium cycling and signaling in cardiac myocytes. *Annu Rev Physiol* 70: 23-49, 2008.
31. **Bers DM, Barry WH, and Despa S.** Intracellular Na⁺ regulation in cardiac myocytes. *Cardiovasc Res* 57: 897-912, 2003.
32. **Bers DM, Christensen DM, and Nguyen TX.** Can Ca entry via Na-Ca exchange directly activate cardiac muscle contraction? *J Mol Cell Cardiol* 20: 405-414, 1988.
33. **Bers DM and Despa S.** Cardiac myocytes Ca²⁺ and Na⁺ regulation in normal and failing hearts. *J Pharmacol Sci* 100: 315-322, 2006.
34. **Bishopric NH, Simpson PC, and Ordahl CP.** Induction of the skeletal alpha-actin gene in alpha 1-adrenoceptor-mediated hypertrophy of rat cardiac myocytes. *J Clin Invest* 80: 1194-1199, 1987.
35. **Biwersi J and Verkman AS.** Cell-permeable fluorescent indicator for cytosolic chloride. *Biochemistry* 30: 7879-7883, 1991.
36. **Blatter LA and McGuigan JA.** Intracellular pH regulation in ferret ventricular muscle. The role of Na-H exchange and the influence of metabolic substrates. *Circ Res* 68: 150-161, 1991.
37. **Bogoyevitch MA, Gillespie-Brown J, Ketterman AJ, Fuller SJ, Ben-Levy R, Ashworth A, Marshall CJ, and Sugden PH.** Stimulation of the stress-activated mitogen-activated protein kinase subfamilies in perfused heart. p38/RK mitogen-activated protein kinases and c-Jun N-terminal kinases are activated by ischemia/reperfusion. *Circ Res* 79: 162-173, 1996.

38. **Bolli R.** The role of sodium-hydrogen ion exchange in patients undergoing coronary artery bypass grafting. *J Card Surg* 18 Suppl 1: 21-26, 2003.
39. **Bonar P, Schneider HP, Becker HM, Deitmer JW, and Casey JR.** Three-dimensional model for the human $\text{Cl}^-/\text{HCO}_3^-$ exchanger, AE1, by homology to the E. coli ClC protein. *J Mol Biol* 425: 2591-2608, 2013.
40. **Bonar PT and Casey JR.** Plasma membrane $\text{Cl}^-/\text{HCO}_3^-$ exchangers: structure, mechanism and physiology. *Channels (Austin)* 2: 337-345, 2008.
41. **Boron WF.** Evaluating the role of carbonic anhydrases in the transport of HCO_3^- -related species. *Biochim Biophys Acta* 1804: 410-421, 2010.
42. **Boutra C, Powell T, and Vaughan-Jones RD.** Comparison of intracellular pH transients in single ventricular myocytes and isolated ventricular muscle of guinea-pig. *J Physiol* 424: 343-365, 1990.
43. **Bouyer P, Zhou Y, and Boron WF.** An increase of intracellular calcium concentration that is induced by basolateral CO_2 in the rabbit renal proximal tubule. *Am J Physiol Renal Physiol* 17: 17, 2003.
44. **Braz JC, Bueno OF, De Windt LJ, and Molkenin JD.** PKC alpha regulates the hypertrophic growth of cardiomyocytes through extracellular signal-regulated kinase1/2 (ERK1/2). *J Cell Biol* 156: 905-919, 2002.
45. **Bristow MR.** beta-adrenergic receptor blockade in chronic heart failure. *Circulation* 101: 558-569, 2000.
46. **Bruce LJ.** Hereditary stomatocytosis and cation-leaky red cells-recent developments. *Blood Cells Mol Dis* 42: 216-222, 2009.

47. **Bruce LJ, Beckmann R, Ribeiro ML, Peters LL, Chasis JA, Delaunay J, Mohandas N, Anstee DJ, and Tanner MJ.** A band 3-based macrocomplex of integral and peripheral proteins in the red cell membrane. *Blood* 101: 4180-4188, 2003.
48. **Bueno OF, De Windt LJ, Lim HW, Tymitz KM, Witt SA, Kimball TR, and Molckentin JD.** The dual-specificity phosphatase MKP-1 limits the cardiac hypertrophic response in vitro and in vivo. *Circ Res* 88: 88-96, 2001.
49. **Calderone A, Thaik CM, Takahashi N, Chang DL, and Colucci WS.** Nitric oxide, atrial natriuretic peptide, and cyclic GMP inhibit the growth-promoting effects of norepinephrine in cardiac myocytes and fibroblasts. *J Clin Invest* 101: 812-818, 1998.
50. **Cameron VA and Ellmers LJ.** Minireview: natriuretic peptides during development of the fetal heart and circulation. *Endocrinology* 144: 2191-2194, 2003.
51. **Camilion de Hurtado MC, Alvarez BV, Perez NG, and Cingolani HE.** Role of an electrogenic $\text{Na}^+\text{-HCO}_3^-$ cotransport in determining myocardial pH_i after an increase in heart rate. *Circ Res* 79: 698-704, 1996.
52. **Camilion de Hurtado MC, Alvarez BV, Perez NG, Ennis IL, and Cingolani HE.** Angiotensin II activates Na^+ -independent $\text{Cl}^-\text{-HCO}_3^-$ exchange in ventricular myocardium. *Circ Res* 82: 473-481, 1998.
53. **Camilion de Hurtado MC, Portiansky EL, Perez NG, Rebolledo OR, and Cingolani HE.** Regression of cardiomyocyte hypertrophy in SHR following chronic inhibition of the Na^+/H^+ exchanger. *Cardiovasc Res* 53: 862-868, 2002.

54. **Cartwright EJ, Mohamed T, Oceandy D, and Neyses L.** Calcium signaling dysfunction in heart disease. *Biofactors* 37: 175-181, 2011.
55. **Casey JR, Ding Y, and Kopito RR.** The role of cysteine residues in the erythrocyte plasma membrane anion exchange protein, AE1. *J Biol Chem* 270: 8521-8527, 1995.
56. **Ch'en FF, Villafuerte FC, Swietach P, Cobden PM, and Vaughan-Jones RD.** S0859, an N-cyanosulphonamide inhibitor of sodium-bicarbonate cotransport in the heart. *Br J Pharmacol* 153: 972-982, 2008.
57. **Chakraborti S, Das S, Kar P, Ghosh B, Samanta K, Kolley S, Ghosh S, Roy S, and Chakraborti T.** Calcium signaling phenomena in heart diseases: a perspective. *Mol Cell Biochem* 298: 1-40, 2007.
58. **Chiappe de Cingolani G, Morgan P, C M-W, Casey JR, Fujinaga J, Camili3n de Hurtado M, and Cingolani H.** Expression of the Cl⁻/HCO₃⁻ anion exchanger mRNA in the hypertrophied myocardium of spontaneously hypertensive rat. *Cardiovascular Research* 51: 71-79, 2001.
59. **Chiappe de Cingolani G, Morgan P, Mundina-Weilenmann C, Casey J, Fujinaga J, Camilion de Hurtado M, and Cingolani H.** Hyperactivity and altered mRNA isoform expression of the Cl⁻/HCO₃⁻ anion-exchanger in the hypertrophied myocardium. *Cardiovasc Res* 51: 71-79, 2001.
60. **Chiappe de Cingolani GE, Ennis IL, Morgan PE, Alvarez BV, Casey JR, and Camilion de Hurtado MC.** Involvement of AE3 isoform of Na⁺-independent Cl⁻/HCO₃⁻ exchanger in myocardial pH_i recovery from intracellular alkalization. *Life Science* 78: 3018-3026, 2006.

61. **Choi I, Romero MF, Khandoudi N, Bril A, and Boron WF.** Cloning and characterization of a human electrogenic $\text{Na}^+\text{-HCO}_3^-$ cotransporter isoform (hhNBC). *Am J Physiol* 276: C576-584, 1999.
62. **Choukroun G, Hajjar R, Fry S, del Monte F, Haq S, Guerrero JL, Picard M, Rosenzweig A, and Force T.** Regulation of cardiac hypertrophy in vivo by the stress-activated protein kinases/c-Jun NH(2)-terminal kinases. *J Clin Invest* 104: 391-398, 1999.
63. **Cingolani HE and Camilion De Hurtado MC.** $\text{Na}^+\text{-H}^+$ exchanger inhibition: a new antihypertrophic tool. *Circ Res* 90: 751-753, 2002.
64. **Cingolani HE and Ennis IL.** Sodium-hydrogen exchanger, cardiac overload, and myocardial hypertrophy. *Circulation* 115: 1090-1100, 2007.
65. **Cingolani HE, Perez NG, Aiello EA, Ennis IL, Garcarena CD, Villa-Abrille MC, Dulce RA, Caldiz CI, Yeves AM, Correa MV, Nolly MB, and Chiappe de Cingolani G.** Early signals after stretch leading to cardiac hypertrophy. Key role of NHE-1. *Front Biosci* 13: 7096-7114, 2008.
66. **Clerk A, Michael A, and Sugden PH.** Stimulation of the p38 mitogen-activated protein kinase pathway in neonatal rat ventricular myocytes by the G protein-coupled receptor agonists, endothelin-1 and phenylephrine: a role in cardiac myocyte hypertrophy? *J Cell Biol* 142: 523-535, 1998.
67. **Cohn JN and Tognoni G.** A randomized trial of the angiotensin-receptor blocker valsartan in chronic heart failure. *N Engl J Med* 345: 1667-1675, 2001.
68. **Conlon I and Raff M.** Size control in animal development. *Cell* 96: 235-244, 1999.

69. **Cordat E.** Unraveling trafficking of the kidney anion exchanger 1 in polarized MDCK epithelial cells. *Biochem Cell Biol* 84: 949-959, 2006.
70. **Cordat E and Casey JR.** Bicarbonate transport in cell physiology and disease. *Biochem J* 417: 423-439, 2009.
71. **Crowley SD, Gurley SB, Herrera MJ, Ruiz P, Griffiths R, Kumar AP, Kim HS, Smithies O, Le TH, and Coffman TM.** Angiotensin II causes hypertension and cardiac hypertrophy through its receptors in the kidney. *Proc Natl Acad Sci U S A* 103: 17985-17990, 2006.
72. **Dahl NK, Jiang L, Chernova MN, Stuart-Tilley AK, Shmukler BE, and Alper SL.** Deficient HCO_3^- transport in an AE1 mutant with normal Cl^- transport can be rescued by carbonic anhydrase II presented on an adjacent AE1 protomer. *J Biol Chem* 278: 44949-44958, 2003.
73. **Dart C and Vaughan-Jones RD.** Na^+ - HCO_3^- symport in the sheep cardiac Purkinje fibre. *J Physiol* 451: 365-385, 1992.
74. **de Simone G.** Concentric or Eccentric Hypertrophy: How Clinically Relevant Is the Difference? *Hypertension* 43: 714-715, 2004.
75. **DeBosch B, Treskov I, Lupu TS, Weinheimer C, Kovacs A, Courtois M, and Muslin AJ.** Akt1 is required for physiological cardiac growth. *Circulation* 113: 2097-2104, 2006.
76. **Devonald MA, Smith AN, Poon JP, Ihrke G, and Karet FE.** Non-polarized targeting of AE1 causes autosomal dominant distal renal tubular acidosis. *Nat Genet* 21: 21, 2003.

77. **Dickhuth HH, Rocker K, Mayer F, Konig D, and Korsten-Reck U.** [Endurance training and cardiac adaptation (athlete's heart)]. *Herz* 29: 373-380, 2004.
78. **Dillmann W.** Cardiac hypertrophy and thyroid hormone signaling. *Heart Fail Rev* 15: 125-132, 2010.
79. **Dillmann WH.** Cellular action of thyroid hormone on the heart. *Thyroid* 12: 447-452, 2002.
80. **Distefano G and Sciacca P.** Molecular pathogenesis of myocardial remodeling and new potential therapeutic targets in chronic heart failure. *Ital J Pediatr* 38: 41, 2012.
81. **Do E, Ellis D, and Noireaud J.** Intracellular pH and intrinsic H⁺ buffering capacity in normal and hypertrophied right ventricle of ferret heart. *Cardiovasc Res* 31: 729-738, 1996.
82. **Doble BW and Woodgett JR.** GSK-3: tricks of the trade for a multi-tasking kinase. *J Cell Sci* 116: 1175-1186, 2003.
83. **Dorn GW.** The Fuzzy Logic of Physiological Cardiac Hypertrophy. *Hypertension* 49: 962-970, 2007.
84. **Dorn GW, 2nd and Force T.** Protein kinase cascades in the regulation of cardiac hypertrophy. *J Clin Invest* 115: 527-537, 2005.
85. **Dostal DE.** The cardiac renin-angiotensin system: novel signaling mechanisms related to cardiac growth and function. *Regul Pept* 91: 1-11, 2000.

86. **Eber S and Lux SE.** Hereditary spherocytosis-defects in proteins that connect the membrane skeleton to the lipid bilayer. *Semin Hematol* 41: 118-141, 2004.
87. **Ennis IL, Alvarez BV, Camilion de Hurtado MC, and Cingolani HE.** Enalapril induces regression of cardiac hypertrophy and normalization of pH_i regulatory mechanisms. *Hypertension* 31: 961-967, 1998.
88. **Ennis IL, Garciarena CD, Perez NG, Dulce RA, Camilion de Hurtado MC, and Cingolani HE.** Endothelin isoforms and the response to myocardial stretch. *Am J Physiol* 288: H2925-2930, 2005.
89. **Fairbanks G, T.L. Steck, and Wallach. DFH.** Electrophoretic analysis of the major polypeptides of the human erythrocyte membrane. *Biochemistry* 10: 2606-2617, 1971.
90. **Fazio S, Palmieri EA, Lombardi G, and Biondi B.** Effects of thyroid hormone on the cardiovascular system. *Recent Prog Horm Res* 59: 31-50, 2004.
91. **Feldman DS, Carnes CA, Abraham WT, and Bristow MR.** Mechanisms of disease: beta-adrenergic receptors-alterations in signal transduction and pharmacogenomics in heart failure. *Nat Clin Pract Cardiovasc Med* 2: 475-483, 2005.
92. **Fernandes T, Soci UPR, and Oliveira EM.** Eccentric and concentric cardiac hypertrophy induced by exercise training: microRNAs and molecular determinants. *Brazilian Journal of Medical and Biological Research* 44: 836-847, 2011.

93. **Fischer AH, Jacobson KA, Rose J, and Zeller R.** Cutting sections of paraffin-embedded tissues. *CSH Protoc* 2008: 4987, 2008.
94. **Fischer AH, Jacobson KA, Rose J, and Zeller R.** Hematoxylin and eosin staining of tissue and cell sections. *CSH Protoc* 2008: 4986, 2008.
95. **Fliegel L.** Regulation of the Na⁺/H⁺ exchanger in the healthy and diseased myocardium. *Expert Opin Ther Targets* 13: 55-68, 2009.
96. **Fliegel L and Karmazyn M.** The cardiac Na-H exchanger: a key downstream mediator for the cellular hypertrophic effects of paracrine, autocrine and hormonal factors. *Biochem Cell Biol* 82: 626-635, 2004.
97. **Folmes CD, Sowah D, Clanachan AS, and Lopaschuk GD.** High rates of residual fatty acid oxidation during mild ischemia decrease cardiac work and efficiency. *J Mol Cell Cardiol* 47: 142-148, 2009.
98. **Frelin C, Vigne P, Ladoux A, and Lazdunski M.** The regulation of the intracellular pH in cells from vertebrates. *Eur J Biochem* 174: 3-14, 1988.
99. **Frey N and Olson EN.** Cardiac hypertrophy: the good, the bad, and the ugly. *Annu Rev Physiol* 65: 45-79, 2003.
100. **Frolich O and Karmazyn M.** The Na-H exchanger revisited: an update on Na-H exchange regulation and the role of the exchanger in hypertension and cardiac function in health and disease. *Card Res* 36: 138-148, 1997.
101. **Fruman DA, Meyers RE, and Cantley LC.** Phosphoinositide kinases. *Annu Rev Biochem* 67: 481-507, 1998.
102. **Frumence E, Genetet S, Ripoche P, Iolascon A, Andolfo I, Le Van Kim C, Colin Y, Mouro-Chanteloup I, and Lopez C.** Rapid Cl⁻/HCO₃⁻

exchange kinetics of AE1 in HEK293 cells and hereditary stomatocytosis red blood cells. *Am J Physiol Cell Physiol* 305: C654-662, 2013.

103. **Fukuda A, Tanaka M, Yamada Y, Muramatsu K, Shimano Y, and Nishino H.** Simultaneous optical imaging of intracellular Cl^- in neurons in different layers of rat neocortical slices: advantages and limitations. *Neurosci Res* 32: 363-371, 1998.

104. **Galindo C, Skinner M, Errami M, Olson LD, Watson D, Li J, McCormick J, McIver L, Kumar N, Pham T, and Garner H.** Transcriptional profile of isoproterenol-induced cardiomyopathy and comparison to exercise-induced cardiac hypertrophy and human cardiac failure. *BMC Physiology* 9: 23, 2009.

105. **Gandhi M, Finegan BA, and Clanachan AS.** Role of glucose metabolism in the recovery of postischemic LV mechanical function: effects of insulin and other metabolic modulators. *Am J Physiol Heart Circ Physiol* 294: H2576-2586, 2008.

106. **Garciarena CD, Ma YL, Swietach P, Huc L, and Vaughan-Jones RD.** Sarcolemmal localisation of Na^+/H^+ exchange and $\text{Na}^+-\text{HCO}_3^-$ co-transport influences the spatial regulation of intracellular pH in rat ventricular myocytes. *J Physiol* 591: 2287-2306, 2013.

107. **Gaudin C, Ishikawa Y, Wight DC, Mahdavi V, Nadal-Ginard B, Wagner TE, Vatner DE, and Homcy CJ.** Overexpression of Gs alpha protein in the hearts of transgenic mice. *J Clin Invest* 95: 1676-1683, 1995.

108. **Gautel M.** The sarcomere and the nucleus: functional links to hypertrophy, atrophy and sarcopenia. *Adv Exp Med Biol* 642: 176-191, 2008.
109. **Gawenis LR, Ledoussal C, Judd LM, Prasad V, Alper SL, Stuart-Tilley AK, Woo AL, Grisham C, Sanford LP, Doetschman T, Miller ML, and Shull GE.** Mice with a targeted disruption of the AE2 Cl⁻/HCO₃⁻ exchanger are achlorhydric. *J Biol Chem* 279: 30531-30539, 2004.
110. **Gehrig H, Müller W, and Appelhans H.** Complete nucleotide sequence of band 3-related anion transport protein AE2 from human kidney. *Biochim Biophys Acta* 1130: 326-328, 1992.
111. **Gilmour KM.** Perspectives on carbonic anhydrase. *Comp Biochem Physiol A Mol Integr Physiol* 157: 193-197, 2010.
112. **Gomes AV, Harada K, and Potter JD.** A mutation in the N-terminus of troponin I that is associated with hypertrophic cardiomyopathy affects the Ca²⁺-sensitivity, phosphorylation kinetics and proteolytic susceptibility of troponin. *J Mol Cell Cardiol* 39: 754-765, 2005.
113. **Gonzalez-Begne M, Nakamoto T, Nguyen HV, Stewart AK, Alper SL, and Melvin JE.** Enhanced formation of a HCO₃⁻ transport metabolon in exocrine cells of Nhe1^{-/-} mice. *J Biol Chem* 282: 35125-35132, 2007.
114. **Grace AA, Kirschenlohr HL, Metcalfe JC, Smith GA, Weissberg PL, Cragoe EJ, Jr., and Vandenberg JI.** Regulation of intracellular pH in the perfused heart by external HCO₃⁻ and Na⁺-H⁺ exchange. *Am J Physiol* 265: H289-298, 1993.

115. **Graham FL, Smiley J, Russell WC, and Nairn R.** Characteristics of a human cell line transformed by DNA from human adenovirus type 5. *J Gen Virol* 52: 59-72, 1977.
116. **Gray MO, Long CS, Kalinyak JE, Li HT, and Karliner JS.** Angiotensin II stimulates cardiac myocyte hypertrophy via paracrine release of TGF-beta 1 and endothelin-1 from fibroblasts. *Cardiovasc Res* 40: 352-363, 1998.
117. **Greenstein JL and Winslow RL.** Integrative systems models of cardiac excitation-contraction coupling. *Circ Res* 108: 70-84, 2011.
118. **Grichtchenko, II, Choi I, Zhong X, Bray-Ward P, Russell JM, and Boron WF.** Cloning, characterization, and chromosomal mapping of a human electroneutral Na⁺-driven Cl⁻/HCO₃⁻ exchanger. *J Biol Chem* 276: 8358-8363, 2001.
119. **Grimm M and Brown JH.** Beta-adrenergic receptor signaling in the heart: role of CaMKII. *J Mol Cell Cardiol* 48: 322-330, 2010.
120. **Grinstein S, Ship S, and Rothstein A.** Anion transport in relation to proteolytic dissection of band 3 protein. *Biochim Biophys Acta* 507: 294-304, 1978.
121. **Groves JD and Tanner MJ.** Glycophorin A facilitates the expression of human Band 3-mediated anion transport in *Xenopus* oocytes. *J Biol Chem* 267: 22163-22170, 1992.
122. **Halestrap AP, Wang X, Poole RC, Jackson VN, and Price NT.** Lactate transport in heart in relation to myocardial ischemia. *Am J Cardiol* 80: 17A-25A, 1997.

123. **Harrison SM, Frampton JE, McCall E, Boyett MR, and Orchard CH.** Contraction and intracellular Ca^{2+} , Na^+ , and H^+ during acidosis in rat ventricular myocytes. *Am J Physiol* 262: C348-357, 1992.
124. **Hasenfuss G.** Animal models of human cardiovascular disease, heart failure and hypertrophy. *Cardiovasc Res* 39: 60-76, 1998.
125. **Hastbacka J, de la Chapelle A, Mahtani MM, Clines G, Reeve-Daly MP, Daly M, Hamilton BA, Kusumi K, Trivedi B, and Weaver A.** The diastrophic dysplasia gene encodes a novel sulfate transporter: positional cloning by fine-structure linkage disequilibrium mapping. *Cell* 78: 1073-1087, 1994.
126. **Haworth RS, McCann C, Snabaitis AK, Roberts NA, and Avkiran M.** Stimulation of the plasma membrane Na^+/H^+ exchanger NHE1 by sustained intracellular acidosis. Evidence for a novel mechanism mediated by the ERK pathway. *J Biol Chem* 278: 31676-31684, 2003.
127. **Hay N and Sonenberg N.** Upstream and downstream of mTOR. *Genes Dev* 18: 1926-1945, 2004.
128. **He TC, Zhou S, da Costa LT, Yu J, Kinzler KW, and Vogelstein B.** A simplified system for generating recombinant adenoviruses. *Proc Natl Acad Sci U S A* 95: 2509-2514, 1998.
129. **Heineke J and Molkentin JD.** Regulation of cardiac hypertrophy by intracellular signalling pathways. *Nat Rev Mol Cell Biol* 7: 589-600, 2006.
130. **Hentschke M, Wiemann M, Hentschke S, Kurth I, Hermans-Borgmeyer I, Seidenbecher T, Jentsch TJ, Gal A, and Hubner CA.** Mice with

a targeted disruption of the $\text{Cl}^-/\text{HCO}_3^-$ exchanger AE3 display a reduced seizure threshold. *Mol Cell Biol* 26: 182-191, 2006.

131. **Hilfiker-Kleiner D, Landmesser U, and Drexler H.** Molecular Mechanisms in Heart Failure: Focus on Cardiac Hypertrophy, Inflammation, Angiogenesis, and Apoptosis. *J Am Coll Cardiol* 48: A56-66, 2006.

132. **Horio T, Nishikimi T, Yoshihara F, Matsuo H, Takishita S, and Kangawa K.** Inhibitory regulation of hypertrophy by endogenous atrial natriuretic peptide in cultured cardiac myocytes. *Hypertension* 35: 19-24, 2000.

133. **Horvat B, Taheri S, and Salihagic A.** Tumour cell proliferation is abolished by inhibitors of Na^+/H^+ and $\text{HCO}_3^-/\text{Cl}^-$ exchange. *Eur J Cancer* 29A: 132-137, 1992.

134. **Houser SR and Margulies KB.** Is depressed myocyte contractility centrally involved in heart failure? *Circ Res* 92: 350-358, 2003.

135. **Hu P, Zhang D, Swenson L, Chakrabarti G, Abel ED, and Litwin SE.** Minimally invasive aortic banding in mice: effects of altered cardiomyocyte insulin signaling during pressure overload. *Am J Physiol Heart Circ Physiol* 285: H1261-1269, 2003.

136. **Hun Leem C and Vaughan-Jones RD.** Chloride-hydroxyl exchange in the guinea-pig ventricular myocyte: no role for bicarbonate. *J Mol Cell Cardiol* 29: 2483-2489, 1997.

137. **Hunte C, Screpanti E, Venturi M, Rimon A, Padan E, and Michel H.** Structure of a Na^+/H^+ antiporter and insights into mechanism of action and regulation by pH. *Nature* 435: 1197-1202, 2005.

138. **Hunter JJ, Tanaka N, Rockman HA, Ross J, Jr., and Chien KR.** Ventricular expression of a MLC-2 ν -ras fusion gene induces cardiac hypertrophy and selective diastolic dysfunction in transgenic mice. *J Biol Chem* 270: 23173-23178, 1995.
139. **Huynh K, Bernardo BC, McMullen JR, and Ritchie RH.** Diabetic Cardiomyopathy: Mechanisms and New Treatment Strategies Targeting Antioxidant Signaling Pathways. *Pharmacol Ther*, 2014.
140. **Iwase M, Bishop SP, Uechi M, Vatner DE, Shannon RP, Kudej RK, Wight DC, Wagner TE, Ishikawa Y, Homcy CJ, and Vatner SF.** Adverse effects of chronic endogenous sympathetic drive induced by cardiac GS alpha overexpression. *Circ Res* 78: 517-524, 1996.
141. **Izumo S, Nadal-Ginard B, and Mahdavi V.** Protooncogene induction and reprogramming of cardiac gene expression produced by pressure overload. *Proc Natl Acad Sci U S A* 85: 339-343, 1988.
142. **Jaswal JS, Gandhi M, Finegan BA, Dyck JR, and Clanachan AS.** Inhibition of p38 MAPK and AMPK restores adenosine-induced cardioprotection in hearts stressed by antecedent ischemia by altering glucose utilization. *Am J Physiol Heart Circ Physiol* 293: H1107-1114, 2007.
143. **Jaswal JS, Keung W, Wang W, Ussher JR, and Lopaschuk GD.** Targeting fatty acid and carbohydrate oxidation-a novel therapeutic intervention in the ischemic and failing heart. *Biochim Biophys Acta* 1813: 1333-1350, 2011.
144. **Jennings ML.** Structure and function of the red blood cell anion transport protein. *Annu Rev Biophys Biophys Chem* 18: 397-430, 1989.

145. **Jennings ML, Anderson MP, and Monaghan R.** Monoclonal antibodies against human erythrocyte Band 3 protein: localization of proteolytic cleavage sites and stilbenedisulfonate-binding lysine residues. *J Biol Chem* 261: 9002-9010, 1986.
146. **Johnson DE and Casey JR.** Cytosolic H⁺ microdomain developed around AE1 during AE1-mediated Cl⁻/HCO₃⁻ exchange. *J Physiol* 589: 1551-1569, 2011.
147. **Kapus A, Grinstein S, Wasan S, Kandasamy R, and Orłowski J.** Functional characterization of three isoforms of the Na⁺/H⁺ exchanger stably expressed in Chinese hamster ovary cells. ATP dependence, osmotic sensitivity, and role in cell proliferation. *J Biol Chem* 269: 23544-23552, 1994.
148. **Kariya K, Farrance IK, and Simpson PC.** Transcriptional enhancer factor-1 in cardiac myocytes interacts with an alpha 1-adrenergic- and beta-protein kinase C-inducible element in the rat beta-myosin heavy chain promoter. *J Biol Chem* 268: 26658-26662, 1993.
149. **Karmazyn M.** Amiloride enhances postischemic ventricular recovery: possible role of Na⁺-H⁺ exchange. *Am J Physiol* 255: H608-615, 1988.
150. **Karmazyn M.** The myocardial sodium-hydrogen exchanger (NHE) and its role in mediating ischemic and reperfusion injury. *Keio J Med* 47: 65-72, 1998.
151. **Karmazyn M, Kilic A, and Javadov S.** The role of NHE-1 in myocardial hypertrophy and remodelling. *J Mol Cell Cardiol* 44: 647-653, 2008.
152. **Karmazyn M, Liu Q, Gan XT, Brix BJ, and Fliegel L.** Aldosterone increases NHE-1 expression and induces NHE-1-dependent hypertrophy in neonatal rat ventricular myocytes. *Hypertension* 42: 1171-1176, 2003.

153. **Karmazyn M and Moffat MP.** Role of Na^+/H^+ exchange in cardiac physiology and pathophysiology: mediation of myocardial reperfusion injury by the pH paradox. *Card Res* 27: 914-924, 1993.
154. **Khandoudi N, Albadine J, Robert P, Krief S, Berrebi-Bertrand I, Martin X, Bevensee MO, Boron WF, and Bril A.** Inhibition of the cardiac electrogenic sodium bicarbonate cotransporter reduces ischemic injury. *Cardiovasc Res* 52: 387-396, 2001.
155. **Khandoudi N, Ho J, and Karmazyn M.** Role of Na^+/H^+ exchange in mediating effects of endothelin-1 on normal and ischemic/reperfused hearts. *Circ Res* 75: 369-378, 1994.
156. **Kimura J, Ono T, Sakamoto K, Ito E, Watanabe S, Maeda S, Shikama Y, Yatabe MS, and Matsuoka I.** $\text{Na}^+/\text{Ca}^{2+}$ exchanger expression and its modulation. *Biol Pharm Bull* 32: 325-331, 2009.
157. **Kinugawa K, Jeong MY, Bristow MR, and Long CS.** Thyroid hormone induces cardiac myocyte hypertrophy in a thyroid hormone receptor α 1-specific manner that requires TAK1 and p38 mitogen-activated protein kinase. *Mol Endocrinol* 19: 1618-1628, 2005.
158. **Kishimoto I, Tokudome T, Horio T, Garbers DL, Nakao K, and Kangawa K.** Natriuretic Peptide Signaling via Guanylyl Cyclase (GC)-A: An Endogenous Protective Mechanism of the Heart. *Curr Cardiol Rev* 5: 45-51, 2009.
159. **Kivela A, Parkkila S, Saarnio J, Karttunen TJ, Kivela J, Parkkila AK, Waheed A, Sly WS, Grubb JH, Shah G, Tureci O, and Rajaniemi H.**

Expression of a novel transmembrane carbonic anhydrase isozyme XII in normal human gut and colorectal tumors. *Am J Pathol* 156: 577-584, 2000.

160. **Knauf PA, Law FY, Leung TW, and Atherton SJ.** Relocation of the Disulfonic Stilbene Sites of AE1 (Band 3) on the Basis of Fluorescence Energy Transfer Measurements. *Biochemistry* 43: 11917-11931, 2004.

161. **Koncz C and Daugirdas JT.** Use of MQAE for measurement of intracellular [Cl⁻] in cultured aortic smooth muscle cells. *Am J Physiol* 267: H2114-2123, 1994.

162. **Kopito RR and Lodish HF.** Primary structure and transmembrane orientation of the murine anion exchange protein. *Nature* 316: 234-238, 1985.

163. **Kopito RR and Lodish HL.** Structure of the murine anion exchange protein. *J Cell Biochem* 29: 1-17, 1985.

164. **Kroeze WK, Sheffler DJ, and Roth BL.** G-protein-coupled receptors at a glance. *Journal of Cell Science* 116: 4867-4869, 2003.

165. **Kubalova Z.** Inactivation of L-type calcium channels in cardiomyocytes. Experimental and theoretical approaches. *Gen Physiol Biophys* 22: 441-454, 2003.

166. **Kusumoto K, Haist JV, and Karmazyn M.** Na⁺/H⁺ exchange inhibition reduces hypertrophy and heart failure after myocardial infarction in rats. *Am J Physiol Heart Circ Physiol* 280: H738-745, 2001.

167. **Kuzman JA, Gerdes AM, Kobayashi S, and Liang Q.** Thyroid hormone activates Akt and prevents serum starvation-induced cell death in neonatal rat cardiomyocytes. *J Mol Cell Cardiol* 39: 841-844, 2005.

168. **Kyte J and Doolittle RF.** A simple method for displaying the hydrophobic character of a protein. *J Mol Biol* 157: 105-132, 1982.
169. **Laemmli UK.** Cleavage of structural proteins during assembly of the head of bacteriophage T4. *Nature* 227: 680-685, 1970.
170. **Lagadic-Gossmann D, Buckler KJ, and Vaughan-Jones RD.** Role of bicarbonate in pH recovery from intracellular acidosis in the guinea-pig ventricular myocyte. *J Physiol* 458: 361-384, 1992.
171. **Lang F, Ritter M, Gamper N, Huber S, Fillon S, Tanneur V, Leppl-Wienhues A, Szabo I, and Gulbins E.** Cell volume in the regulation of cell proliferation and apoptotic cell death. *Cell Physiol Biochem* 10: 417-428, 2000.
172. **Lang F, Shumilina E, Ritter M, Gulbins E, Vereninov A, and Huber SM.** Ion channels and cell volume in regulation of cell proliferation and apoptotic cell death. *Contrib Nephrol* 152: 142-160, 2006.
173. **Lee BL, Sykes BD, and Fliegel L.** Structural and functional insights into the cardiac Na⁺/H⁺ exchanger. *J Mol Cell Cardiol* 61: 60-67, 2013.
174. **Lee RT.** Matrix metalloproteinase inhibition and the prevention of heart failure. *Trends Cardiovasc Med* 11: 202-205, 2001.
175. **Leem CH, Lagadic-Gossmann D, and Vaughan-Jones RD.** Characterization of intracellular pH regulation in the guinea-pig ventricular myocyte. *J Physiol (Lond)* 517: 159-180, 1999.
176. **Leem CH and Vaughan-Jones RD.** Sarcolemmal mechanisms for pH_i recovery from alkalosis in the guinea-pig ventricular myocyte. *J Physiol (Lond)* 509: 487-496, 1998.

177. **Li X, Alvarez B, Casey JR, Reithmeier RA, and Fliegel L.** Carbonic anhydrase II binds to and enhances activity of the Na⁺/H⁺ exchanger. *J Biol Chem* 277: 36085-36091, 2002.
178. **Li X, Alvarez B, Casey JR, Reithmeier RAF, and Fliegel L.** Carbonic Anhydrase II Binds to and Enhances Activity of the Na⁺/H⁺ Exchanger. *J Biol Chem* 277: 36085-36091, 2002.
179. **Li X, Liu Y, Alvarez BV, Casey JR, and Fliegel L.** A novel carbonic anhydrase II binding site regulates NHE1 activity. *Biochemistry* 45: 2414-2424, 2006.
180. **Li X, Prins D, Michalak M, and Fliegel L.** Calmodulin dependent binding to the NHE1 Cytosolic Tail Mediates Activation of the Na⁺/H⁺ Exchanger by Ca²⁺ and Endothelin. *Am J Physiol Cell Physiol*, 2013.
181. **Li Y and Zhang T.** Targeting Cancer Stem Cells by Curcumin and Clinical Applications. *Cancer Lett*, 2014.
182. **Lin X and Barber DL.** A calcineurin homologous protein inhibits GTPase-stimulated Na-H exchange. *Proc Natl Acad Sci U S A* 93: 12631-12636, 1996.
183. **Link AJ and Labaer J.** Trichloroacetic Acid (TCA) Precipitation of Proteins. *Cold Spring Harbor Protocols* 2011: 993-994, 2011.
184. **Linn SC, Askew GR, Menon AG, and Shull GE.** Conservation of an AE3 Cl⁻/HCO₃⁻ exchanger cardiac-specific exon and promotor region and AE3 mRNA expression patterns in murine and human hearts. *Circ Res* 76: 584-591, 1995.

185. **Linn SC, Kudrycki KE, and Shull GE.** The predicted translation product of a cardiac AE3 mRNA contains an N-terminus distinct from that of the brain AE3 Cl⁻/HCO₃⁻ exchanger. *J Biol Chem* 267: 7927-7935, 1992.
186. **Liu SC, Jarolim P, Rubin HL, Palek J, Amato D, Hassan K, Zaik M, and Sapak P.** The homozygous state for the band 3 protein mutation in Southeast Asian Ovalocytosis may be lethal. *Blood* 84: 3590-3591, 1994.
187. **Liu T and O'Rourke B.** Regulation of mitochondrial Ca²⁺ and its effects on energetics and redox balance in normal and failing heart. *J Bioenerg Biomembr* 41: 127-132, 2009.
188. **Lohi H, Kujala M, Kerkela E, Saarialho-Kere U, Kestila M, and Kere J.** Mapping of five new putative anion transporter genes in human and characterization of SLC26A6, a candidate gene for pancreatic anion exchanger. *Genomics* 70: 102-112, 2000.
189. **Lohse MJ, Engelhardt S, and Eschenhagen T.** What is the role of beta-adrenergic signaling in heart failure? *Circ Res* 93: 896-906, 2003.
190. **Lopez JE, Myagmar BE, Swigart PM, Montgomery MD, Haynam S, Bigos M, Rodrigo MC, and Simpson PC.** beta-myosin heavy chain is induced by pressure overload in a minor subpopulation of smaller mouse cardiac myocytes. *Circ Res* 109: 629-638, 2011.
191. **Low PS.** Structure and function of the cytoplasmic domain of Band 3: center of erythrocyte membrane-peripheral protein interactions. *Biochim Biophys Acta* 864: 145-167, 1986.

192. **Lu J, Daly CM, Parker MD, Gill HS, Piermarini PM, Pelletier MF, and Boron WF.** Effect of human carbonic anhydrase II on the activity of the human electrogenic $\text{Na}^+/\text{HCO}_3^-$ cotransporter NBCe1-A in *Xenopus* oocytes. *J Biol Chem* 281: 19241-19250, 2006.
193. **Maren TH.** Carbonic anhydrase: chemistry, physiology, and inhibition. *Physiol Rev* 47: 595-781, 1967.
194. **Markovich D.** Physiological roles and regulation of mammalian sulfate transporters. *Physiol Rev* 81: 1499-1533, 2001.
195. **Markovich D, Bissig M, Sorribas V, Hagenbuch B, Meier PJ, and Murer H.** Expression of rat renal sulfate transport systems in *Xenopus laevis* oocytes. Functional characterization and molecular identification. *J Biol Chem* 269: 3022-3026, 1994.
196. **Marks AR.** Ryanodine receptors/calcium release channels in heart failure and sudden cardiac death. *J Mol Cell Cardiol* 33: 615-624, 2001.
197. **Martin CE, Shaver JA, Leon DF, Thompson ME, Reddy PS, and Leonard JJ.** Autonomic mechanisms in hemodynamic responses to isometric exercise. *J Clin Invest* 54: 104-115, 1974.
198. **Marx SO, Reiken S, Hisamatsu Y, Jayaraman T, Burkhoff D, Rosemlit N, and Marks AR.** PKA phosphorylation dissociates FKBP12.6 from the calcium release channel (ryanodine receptor): defective regulation in failing hearts. *Cell* 101: 365-376, 2000.

199. **Matsui H, Barry WH, Livsey C, and Spitzer KW.** Angiotensin II stimulates sodium-hydrogen exchange in adult rabbit ventricular myocytes. *Cardiovasc Res* 29: 215-221, 1995.
200. **Matsui T and Rosenzweig A.** Convergent signal transduction pathways controlling cardiomyocyte survival and function: the role of PI 3-kinase and Akt. *J Mol Cell Cardiol* 38: 63-71, 2005.
201. **Mattiazzi A, Mundina-Weilenmann C, Guoxiang C, Vittone L, and Kranias E.** Role of phospholamban phosphorylation on Thr17 in cardiac physiological and pathological conditions. *Cardiovasc Res* 68: 366-375, 2005.
202. **McDevitt TC, Laflamme MA, and Murry CE.** Proliferation of cardiomyocytes derived from human embryonic stem cells is mediated via the IGF/PI 3-kinase/Akt signaling pathway. *J Mol Cell Cardiol* 39: 865-873, 2005.
203. **McMullen JR.** Phosphoinositide 3-kinase(p110[alpha]) plays a critical role for the induction of physiological, but not pathological, cardiac hypertrophy. *Proc Natl Acad Sci USA* 100: 12355-12360, 2003.
204. **McMullen JR and Jennings GL.** Differences between pathological and physiological cardiac hypertrophy: novel therapeutic strategies to treat heart failure. *Clin Exp Pharmacol Physiol* 34: 255-262, 2007.
205. **McMurtrie HL, Cleary HJ, Alvarez BV, Loiselle FB, Sterling D, Morgan PE, Johnson DE, and Casey JR.** The bicarbonate transport metabolon. *J Enzyme Inhib Med Chem* 19: 231-236, 2004.
206. **Melvin JE, Park K, Richardson L, Schultheis PJ, and Shull GE.** Mouse down-regulated in adenoma (DRA) is an intestinal $\text{Cl}^-/\text{HCO}_3^-$ exchanger

and is up-regulated in colon of mice lacking the NHE3 Na⁺/H⁺ exchanger. *J Biol Chem* 274: 22855-22861, 1999.

207. **Mihl C, Dassen WR, and Kuipers H.** Cardiac remodelling: concentric versus eccentric hypertrophy in strength and endurance athletes. *Neth Heart J* 16: 129-133, 2008.

208. **Miyata S, Minobe W, Bristow MR, and Leinwand LA.** Myosin heavy chain isoform expression in the failing and nonfailing human heart. *Circ Res* 86: 386-390, 2000.

209. **Moor AN, Gan XT, Karmazyn M, and Fliegel L.** Activation of Na⁺/H⁺ exchanger-directed protein kinases in the ischemic and ischemic-reperfused rat myocardium. *J Biol Chem* 276: 16113-16122, 2001.

210. **Mori K, Ogawa Y, Ebihara K, Tamura N, Tashiro K, Kuwahara T, Mukoyama M, Sugawara A, Ozaki S, Tanaka I, and Nakao K.** Isolation and characterization of CAXIV, a novel membrane-bound carbonic anhydrase from mouse kidney. *J Biol Chem* 274: 15701-15705, 1999.

211. **Mount DB and Romero MF.** The SLC26 gene family of multifunctional anion exchangers. *Pflugers Arch* 447: 710-721, 2004.

212. **Mraiche F, Oka T, Gan XT, Karmazyn M, and Fliegel L.** Activated NHE1 is required to induce early cardiac hypertrophy in mice. *Basic Res Cardiol* 106: 603-616, 2011.

213. **Munkonge F, Alton EW, Andersson C, Davidson H, Dragomir A, Edelman A, Farley R, Hjelte L, McLachlan G, Stern M, and Roomans GM.**

Measurement of halide efflux from cultured and primary airway epithelial cells using fluorescence indicators. *J Cyst Fibros* 3 Suppl 2: 171-176, 2004.

214. **Munshi NV.** Gene regulatory networks in cardiac conduction system development. *Circ Res* 110: 1525-1537, 2012.

215. **Murphy RT, Mogensen J, Shaw A, Kubo T, Hughes S, and McKenna WJ.** Novel mutation in cardiac troponin I in recessive idiopathic dilated cardiomyopathy. *Lancet* 363: 371-372, 2004.

216. **Nakamura TY, Iwata Y, Arai Y, Komamura K, and Wakabayashi S.** Activation of Na⁺/H⁺ exchanger 1 is sufficient to generate Ca²⁺ signals that induce cardiac hypertrophy and heart failure. *Circ Res* 103: 891-899, 2008.

217. **Neri Serneri GG, Boddì M, Modesti PA, Cecioni I, Coppo M, Padeletti L, Michelucci A, Colella A, and Galanti G.** Increased cardiac sympathetic activity and insulin-like growth factor-I formation are associated with physiological hypertrophy in athletes. *Circ Res* 89: 977-982, 2001.

218. **Nicol RL, Frey N, and Olson EN.** From the sarcomere to the nucleus: role of genetics and signaling in structural heart disease. *Annu Rev Genomics Hum Genet* 1: 179-223, 2000.

219. **Nicolaou P, Hajjar RJ, and Kranias EG.** Role of protein phosphatase-1 inhibitor-1 in cardiac physiology and pathophysiology. *J Mol Cell Cardiol* 47: 365-371, 2009.

220. **Niederer SA, Swietach P, Wilson DA, Smith NP, and Vaughan-Jones RD.** Measuring and modeling chloride-hydroxyl exchange in the Guinea-pig ventricular myocyte. *Biophys J* 94: 2385-2403, 2008.

221. **O'Neill BT and Abel ED.** Akt1 in the cardiovascular system: friend or foe? *J Clin Invest* 115: 2059-2064, 2005.
222. **Ojamaa K.** Signaling mechanisms in thyroid hormone-induced cardiac hypertrophy. *Vascul Pharmacol* 52: 113-119, 2010.
223. **Oldham WM and Hamm HE.** Heterotrimeric G protein activation by G-protein-coupled receptors. *Nat Rev Mol Cell Biol* 9: 60-71, 2008.
224. **Olson EN.** A decade of discoveries in cardiac biology. *Nat Med* 10: 467-474, 2004.
225. **Omar MA, Wang L, and Clanachan AS.** Cardioprotection by GSK-3 inhibition: role of enhanced glycogen synthesis and attenuation of calcium overload. *Cardiovasc Res* 86: 478-486, 2010.
226. **Orchard CH, Hamilton DL, Astles P, McCall E, and Jewell BR.** The effect of acidosis on the relationship between Ca^{2+} and force in isolated ferret cardiac muscle. *J Physiol* 436: 559-578, 1991.
227. **Orchard CH and Kentish JC.** Effects of changes of pH on the contractile function of cardiac muscle. *Am J Physiol* 258: C967-981, 1990.
228. **Padan E, Kozachkov L, Herz K, and Rimon A.** NhaA crystal structure: functional-structural insights. *J Exp Biol* 212: 1593-1603, 2009.
229. **Pandya K, Kim HS, and Smithies O.** Fibrosis, not cell size, delineates beta-myosin heavy chain reexpression during cardiac hypertrophy and normal aging in vivo. *Proc Natl Acad Sci U S A* 103: 16864-16869, 2006.

230. **Pandya K, Porter K, Rockman HA, and Smithies O.** Decreased beta-adrenergic responsiveness following hypertrophy occurs only in cardiomyocytes that also re-express beta-myosin heavy chain. *Eur J Heart Fail* 11: 648-652, 2009.
231. **Park DS and Fishman GI.** The cardiac conduction system. *Circulation* 123: 904-915, 2011.
232. **Peng HB, Wolosewick JJ, and Cheng PC.** The development of myofibrils in cultured muscle cells: a whole-mount and thin-section electron microscopic study. *Dev Biol* 88: 121-136, 1981.
233. **Perez NG, Alvarez BV, Camilion de Hurtado MC, and Cingolani HE.** pH_i regulation in myocardium of the spontaneously hypertensive rat. Compensated enhanced activity of the $Na^+ - H^+$ exchanger. *Circ Res* 77: 1192-1200, 1995.
234. **Perez NG, de Hurtado MC, and Cingolani HE.** Reverse mode of the $Na^+ - Ca^{2+}$ exchange after myocardial stretch: underlying mechanism of the slow force response. *Circ Res* 88: 376-382, 2001.
235. **Pieske B, Maier LS, Bers DM, and Hasenfuss G.** Ca^{2+} handling and sarcoplasmic reticulum Ca^{2+} content in isolated failing and nonfailing human myocardium. *Circ Res* 85: 38-46, 1999.
236. **Pluim BM, Zwinderman AH, van der Laarse A, and van der Wall EE.** The Athlete's Heart. *Circulation* 101: 336-344, 2000.
237. **Poole-Wilson PA.** Acidosis and contractility of heart muscle. *Ciba Found Symp* 87: 58-76, 1982.

238. **Poole-Wilson PA.** Is early decline of cardiac function in ischaemia due to carbon-dioxide retention? *Lancet* 2: 1285-1287, 1975.
239. **Post GR, Goldstein D, Thuerauf DJ, Glembotski CC, and Brown JH.** Dissociation of p44 and p42 mitogen-activated protein kinase activation from receptor-induced hypertrophy in neonatal rat ventricular myocytes. *J Biol Chem* 271: 8452-8457, 1996.
240. **Prasad V, Bodi I, Meyer JW, Wang Y, Ashraf M, Engle SJ, Doetschman T, Sisco K, Nieman ML, Miller ML, Lorenz JN, and Shull GE.** Impaired cardiac contractility in mice lacking both the AE3 $\text{Cl}^-/\text{HCO}_3^-$ exchanger and the NKCC1 $\text{Na}^+-\text{K}^+-2\text{Cl}^-$ cotransporter: effects on Ca^{2+} handling and protein phosphatases. *J Biol Chem* 283: 31303-31314, 2008.
241. **Pushkin A, Abuladze N, Lee I, Newman D, Hwang J, and Kurtz I.** Cloning, tissue distribution, genomic organization, and functional characterization of NBC3, a new member of the sodium bicarbonate cotransporter family. *J Biol Chem* 274: 16569-16575, 1999.
242. **Putney LK, Denker SP, and Barber DL.** The changing face of the Na^+/H^+ exchanger, NHE1: structure, regulation, and cellular actions. *Annu Rev Pharmacol Toxicol* 42: 527-552, 2002.
243. **Reithmeier RAF.** A membrane metabolon linking carbonic anhydrase with chloride/bicarbonate anion exchangers. *Blood cells, Molecules and Diseases* 27: 85-89, 2001.

244. **Reudelhuber TL, Bernstein KE, and Delafontaine P.** Is angiotensin II a direct mediator of left ventricular hypertrophy? Time for another look. *Hypertension* 49: 1196-1201, 2007.
245. **Richard P, Charron P, Carrier L, Ledeuil C, Cheav T, Pichereau C, Benaiche A, Isnard R, Dubourg O, Burban M, Gueffet JP, Millaire A, Desnos M, Schwartz K, Hainque B, and Komajda M.** Hypertrophic cardiomyopathy: distribution of disease genes, spectrum of mutations, and implications for a molecular diagnosis strategy. *Circulation* 107: 2227-2232, 2003.
246. **Rivera-Brown AM and Frontera WR.** Principles of exercise physiology: responses to acute exercise and long-term adaptations to training. *PM R* 4: 797-804, 2012.
247. **Robinson P, Griffiths PJ, Watkins H, and Redwood CS.** Dilated and hypertrophic cardiomyopathy mutations in troponin and alpha-tropomyosin have opposing effects on the calcium affinity of cardiac thin filaments. *Circ Res* 101: 1266-1273, 2007.
248. **Rockman HA, Koch WJ, and Lefkowitz RJ.** Seven-transmembrane-spanning receptors and heart function. *Nature* 415: 206-212, 2002.
249. **Rodriguez-Soriano J.** New insights into the pathogenesis of renal tubular acidosis-from functional to molecular studies. *Pediatr Nephrol* 14: 1121-1136, 2000.
250. **Romero MF, Fulton CM, and Boron WF.** The SLC4 family of HCO₃⁻ transporters. *Pflugers Arch* 447: 496-509, 2004.

251. **Ruetz S, Lindsey AE, Ward CL, and Kopito RR.** Functional activation of plasma membrane anion exchangers occurs in a pre-Golgi compartment. *J Cell Biol* 121: 37-48, 1993.
252. **Ruzicka DL and Schwartz RJ.** Sequential activation of alpha-actin genes during avian cardiogenesis: vascular smooth muscle alpha-actin gene transcripts mark the onset of cardiomyocyte differentiation. *J Cell Biol* 107: 2575-2586, 1988.
253. **Sabbah HN.** Biologic rationale for the use of beta-blockers in the treatment of heart failure. *Heart Fail Rev* 9: 91-97, 2004.
254. **Sadoshima J, Xu Y, Slayter HS, and Izumo S.** Autocrine release of angiotensin II mediates stretch-induced hypertrophy of cardiac myocytes in vitro. *Cell* 75: 977-984, 1993.
255. **Salazar NC, Chen J, and Rockman HA.** Cardiac GPCRs: GPCR signaling in healthy and failing hearts. *Biochim Biophys Acta* 1768: 1006-1018, 2007.
256. **Sam F, Kerstetter DL, Pimental DR, Mulukutla S, Tabae A, Bristow MR, Colucci WS, and Sawyer DB.** Increased reactive oxygen species production and functional alterations in antioxidant enzymes in human failing myocardium. *J Card Fail* 11: 473-480, 2005.
257. **Sambhara D and Aref AA.** Glaucoma management: relative value and place in therapy of available drug treatments. *Ther Adv Chronic Dis* 5: 30-43, 2014.

258. **Sambrano GR, Fraser I, Han H, Ni Y, O'Connell T, Yan Z, and Stull JT.** Navigating the signalling network in mouse cardiac myocytes. *Nature* 420: 712-714, 2002.
259. **Sandri M, Sandri C, Gilbert A, Skurk C, Calabria E, Picard A, Walsh K, Schiaffino S, Lecker SH, and Goldberg AL.** Foxo transcription factors induce the atrophy-related ubiquitin ligase atrogin-1 and cause skeletal muscle atrophy. *Cell* 117: 399-412, 2004.
260. **Sarbassov DD, Ali SM, and Sabatini DM.** Growing roles for the mTOR pathway. *Curr Opin Cell Biol* 17: 596-603, 2005.
261. **Sardet C, Fafournoux P, and Pouyssegur J.** Alpha-thrombin, epidermal growth factor, and okadaic acid activate the Na⁺/H⁺ exchanger, NHE-1, by phosphorylating a set of common sites. *J Biol Chem* 266: 19166-19171, 1991.
262. **Sardet C, Franchi A, and Pouyssegur J.** Molecular cloning, primary structure, and expression of the human growth factor-activatable Na⁺/H⁺ antiporter. *Cell* 56: 271-280, 1989.
263. **Schafer C, Ladilov YV, Siegmund B, and Piper HM.** Importance of bicarbonate transport for protection of cardiomyocytes against reoxygenation injury. *Am J Physiol Heart Circ Physiol* 278: H1457-1463, 2000.
264. **Schiaffino S, Samuel JL, Sassoon D, Lompre AM, Garner I, Marotte F, Buckingham M, Rappaport L, and Schwartz K.** Nonsynchronous accumulation of alpha-skeletal actin and beta-myosin heavy chain mRNAs during early stages of pressure-overload-induced cardiac hypertrophy demonstrated by in situ hybridization. *Circ Res* 64: 937-948, 1989.

265. **Schier JJ and Adelstein RS.** Structural and enzymatic comparison of human cardiac muscle myosins isolated from infants, adults, and patients with hypertrophic cardiomyopathy. *J Clin Invest* 69: 816-825, 1982.
266. **Schussheim AE and Radda GK.** Altered Na⁺-H⁺ exchange activity in the spontaneously hypertensive perfused rat heart. *J Mol Cell Cardiol* 27: 1475-1481, 1995.
267. **Scoote M, Poole-Wilson PA, and Williams AJ.** The therapeutic potential of new insights into myocardial excitation-contraction coupling. *Heart* 89: 371-376, 2003.
268. **Screpanti E and Hunte C.** Discontinuous membrane helices in transport proteins and their correlation with function. *J Struct Biol* 159: 261-267, 2007.
269. **Shen YT, Malik FI, Zhao X, Depre C, Dhar SK, Abarzua P, Morgans DJ, and Vatner SF.** Improvement of cardiac function by a cardiac Myosin activator in conscious dogs with systolic heart failure. *Circ Heart Fail* 3: 522-527, 2010.
270. **Shioi T, Kang PM, Douglas PS, Hampe J, Yballe CM, Lawitts J, Cantley LC, and Izumo S.** The conserved phosphoinositide 3-kinase pathway determines heart size in mice. *EMBO J* 19: 2537-2548, 2000.
271. **Shiojima I and Walsh K.** Regulation of cardiac growth and coronary angiogenesis by the Akt/PKB signaling pathway. *Genes Dev* 20: 3347-3365, 2006.
272. **Shiojima I, Yefremashvili M, Luo Z, Kureishi Y, Takahashi A, Tao J, Rosenzweig A, Kahn CR, Abel ED, and Walsh K.** Akt signaling mediates

postnatal heart growth in response to insulin and nutritional status. *J Biol Chem* 277: 37670-37677, 2002.

273. **Simmerman HK and Jones LR.** Phospholamban: protein structure, mechanism of action, and role in cardiac function. *Physiol Rev* 78: 921-947, 1998.

274. **Sipido KR, Carmeliet E, and Van de Werf F.** T-type Ca^{2+} current as a trigger for Ca^{2+} release from the sarcoplasmic reticulum in guinea-pig ventricular myocytes. *J Physiol* 508 (Pt 2): 439-451, 1998.

275. **Slepkov E and Fliegel L.** Structure and function of the NHE1 isoform of the Na^+/H^+ exchanger. *Biochem Cell Biol* 80: 499-508, 2002.

276. **Smith PK, Krohn RI, Hermanson GT, Mallia AK, Gartner FH, Provenzano MD, Fujimoto EK, Goeke NM, Olson BJ, and Klenk DC.** Measurement of protein using bicinchoninic acid. *Anal Biochem* 150: 76-85, 1985.

277. **Soleimani M, Greeley T, Petrovic S, Wang Z, Amlal H, Kopp P, and Burnham CE.** Pendrin: an apical $\text{Cl}^-/\text{OH}^-/\text{HCO}_3^-$ exchanger in the kidney cortex. *Am J Physiol Renal Physiol* 280: F356-364, 2001.

278. **Southgate CD, Chishti AH, Mitchell B, Yi SJ, and Palek J.** Targeted disruption of the murine erythroid band 3 gene results in spherocytosis and severe haemolytic anaemia despite a normal membrane skeleton. *Nat Genet* 14: 227-230, 1996.

279. **Stehberger PA, Shmukler BE, Stuart-Tilley AK, Peters LL, Alper SL, and Wagner CA.** Distal renal tubular acidosis in mice lacking the AE1 (band3) $\text{Cl}^-/\text{HCO}_3^-$ exchanger (slc4a1). *J Am Soc Nephrol* 18: 1408-1418, 2007.

280. **Stephens L, Anderson K, Stokoe D, Erdjument-Bromage H, Painter GF, Holmes AB, Gaffney PR, Reese CB, McCormick F, Tempst P, Coadwell J, and Hawkins PT.** Protein kinase B kinases that mediate phosphatidylinositol 3,4,5-trisphosphate-dependent activation of protein kinase B. *Science* 279: 710-714, 1998.
281. **Sterling D, Alvarez BV, and Casey JR.** The extracellular component of a transport metabolon: Extracellular loop 4 of the human AE1 $\text{Cl}^-/\text{HCO}_3^-$ exchanger binds carbonic anhydrase IV. *J Biol Chem* 277: 25239-25246, 2002.
282. **Sterling D and Casey JR.** Transport activity of AE3 chloride/bicarbonate anion-exchange proteins and their regulation by intracellular pH. *Biochem J* 344 Pt 1: 221-229, 1999.
283. **Sterling D, Reithmeier RA, and Casey JR.** A Transport Metabolon. Functional Interaction of Carbonic Anhydrase II and Chloride/Bicarbonate Exchangers. *J Biol Chem* 276: 47886-47894, 2001.
284. **Sulakhe PV and Vo XT.** Regulation of phospholamban and troponin-I phosphorylation in the intact rat cardiomyocytes by adrenergic and cholinergic stimuli: roles of cyclic nucleotides, calcium, protein kinases and phosphatases and depolarization. *Mol Cell Biochem* 149-150: 103-126, 1995.
285. **Suleymanlar G, Zhou HZ, McCormack M, Elkins N, Kucera R, Reiss OK, and Shapiro JI.** Mechanism of impaired energy metabolism during acidosis: role of oxidative metabolism. *Am J Physiol* 262: H1818-1822, 1992.

286. **Sun B, Leem CH, and Vaughan-Jones RD.** Novel chloride-dependent acid loader in the guinea-pig ventricular myocyte: part of a dual acid-loading mechanism. *J Physiol* 495 (Pt 1): 65-82, 1996.
287. **Supuran CT.** Carbonic anhydrase inhibitors. *Bioorg Med Chem Lett* 20: 3467-3474, 2010.
288. **Suurmeijer AJ, Clement S, Francesconi A, Bocchi L, Angelini A, Van Veldhuisen DJ, Spagnoli LG, Gabbiani G, and Orlandi A.** Alpha-actin isoform distribution in normal and failing human heart: a morphological, morphometric, and biochemical study. *J Pathol* 199: 387-397, 2003.
289. **Takewaki S, Kuro-o M, Hiroi Y, Yamazaki T, Noguchi T, Miyagishi A, Nakahara K, Aikawa M, Manabe I, Yazaki Y, and et al.** Activation of Na⁺-H⁺ antiporter (NHE-1) gene expression during growth, hypertrophy and proliferation of the rabbit cardiovascular system. *J Mol Cell Cardiol* 27: 729-742, 1995.
290. **Takimoto E, Yao A, Toko H, Takano H, Shimoyama M, Sonoda M, Wakimoto K, Takahashi T, Akazawa H, Mizukami M, Nagai T, Nagai R, and Komuro I.** Sodium calcium exchanger plays a key role in alteration of cardiac function in response to pressure overload. *FASEB J* 16: 373-378, 2002.
291. **Tanner MJ.** The structure and function of band 3 (AE1): recent developments (review). *Mol Membr Biol* 14: 155-165, 1997.
292. **Tashian RE and Carter ND.** Biochemical genetics of carbonic anhydrase. *Adv Hum Genet* 7: 1-56, 1976.

293. **Ten Hove M, Nederhoff MG, and Van Echteld CJ.** Relative contributions of Na^+/H^+ exchange and $\text{Na}^+/\text{HCO}_3^-$ cotransport to ischemic Na_i^+ overload in isolated rat hearts. *Am J Physiol Heart Circ Physiol* 288: H287-292, 2005.
294. **Theroux P, Chaitman BR, Danchin N, Erhardt L, Meinertz T, Schroeder JS, Tognoni G, White HD, Willerson JT, and Jessel A.** Inhibition of the sodium-hydrogen exchanger with cariporide to prevent myocardial infarction in high-risk ischemic situations. Main results of the GUARDIAN trial. Guard during ischemia against necrosis (GUARDIAN) Investigators. *Circulation* 102: 3032-3038, 2000.
295. **Thomas JA, Buchsbaum RN, Zimniak A, and Racker E.** Intracellular pH measurements in Ehrlich ascites tumor cells utilizing spectroscopic probes generated in situ. *Biochemistry* 18: 2210-2218, 1979.
296. **Toth A, Kiss L, Varro A, and Nanasi PP.** Potential therapeutic effects of $\text{Na}^+/\text{Ca}^{2+}$ exchanger inhibition in cardiac diseases. *Curr Med Chem* 16: 3294-3321, 2009.
297. **Towbin H, Staehelin T, and Gordon J.** Electrophoretic transfer of proteins from polyacrylamide gels to nitrocellulose sheets: procedure and some applications. *Proc Natl Acad Sci* 76: 4350-4354, 1979.
298. **Tsutamoto T, Wada A, Maeda K, Hisanaga T, Maeda Y, Fukai D, Ohnishi M, Sugimoto Y, and Kinoshita M.** Attenuation of compensation of endogenous cardiac natriuretic peptide system in chronic heart failure: prognostic

role of plasma brain natriuretic peptide concentration in patients with chronic symptomatic left ventricular dysfunction. *Circulation* 96: 509-516, 1997.

299. **Tsybouleva N, Zhang L, Chen S, Patel R, Lutucuta S, Nemoto S, DeFreitas G, Entman M, Carabello BA, Roberts R, and Marian AJ.**

Aldosterone, through novel signaling proteins, is a fundamental molecular bridge between the genetic defect and the cardiac phenotype of hypertrophic cardiomyopathy. *Circulation* 109: 1284-1291, 2004.

300. **Turer AT, Malloy CR, Newgard CB, and Podgoreanu MV.** Energetics and metabolism in the failing heart: important but poorly understood. *Curr Opin Clin Nutr Metab Care* 13: 458-465, 2010.

301. **Tzivion G, Dobson M, and Ramakrishnan G.** FoxO transcription factors; Regulation by AKT and 14-3-3 proteins. *Biochim Biophys Acta* 1813: 1938-1945, 2011.

302. **van den Akker E, Satchwell TJ, Williamson RC, and Toye AM.** Band 3 multiprotein complexes in the red cell membrane; of mice and men. *Blood Cells Mol Dis* 45: 1-8, 2010.

303. **Vandenberg JI, Metcalfe JC, and Grace AA.** Mechanisms of pH_i recovery after global ischemia in the perfused heart. *Circ Res* 72: 993-1003, 1993.

304. **Vaughan-Jones RD and Spitzer KW.** Role of bicarbonate in the regulation of intracellular pH in the mammalian ventricular myocyte. *Biochem Cell Biol* 80: 579-596, 2002.

305. **Vaughan-Jones RD, Spitzer KW, and Swietach P.** Intracellular pH regulation in heart. *J Mol Cell Cardiol*, 2008.

306. **Vaughan-Jones RD, Spitzer KW, and Swietach P.** Intracellular pH regulation in heart. *J Mol Cell Cardiol* 46: 318-331, 2009.
307. **Vaughan-Jones RD, Villafuerte FC, Swietach P, Yamamoto T, Rossini A, and Spitzer KW.** pH-Regulated Na^+ influx into the mammalian ventricular myocyte: the relative role of Na^+ - H^+ exchange and Na^+ - HCO_3^- Co-transport. *J Cardiovasc Electrophysiol* 17 Suppl 1: S134-S140, 2006.
308. **Vaughan-Jones RD and Wu ML.** pH dependence of intrinsic H^+ buffering power in the sheep cardiac Purkinje fibre. *J Physiol* 425: 429-448, 1990.
309. **Vilas GL, Johnson DE, Freund P, and Casey JR.** Characterization of an epilepsy-associated variant of the human $\text{Cl}^-/\text{HCO}_3^-$ exchanger AE3. *Am J Physiol Cell Physiol* 297: C526-536, 2009.
310. **Villa-Abrille MC, Cingolani HE, Garcarena CD, Ennis IL, and Aiello EA.** [Angiotensin II-induced endothelin-1 release in cardiac myocytes]. *Medicina (B Aires)* 66: 229-236, 2006.
311. **Vince JW, Carlsson U, and Reithmeier RA.** Localization of the $\text{Cl}^-/\text{HCO}_3^-$ anion exchanger binding site to the amino-terminal region of carbonic anhydrase II. *Biochemistry* 39: 13344-13349, 2000.
312. **Vince JW and Reithmeier RA.** Identification of the Carbonic Anhydrase II Binding Site in the $\text{Cl}^-/\text{HCO}_3^-$ Anion Exchanger AE1. *Biochemistry* 39: 5527-5533, 2000.
313. **Vince JW and Reithmeier RAF.** Carbonic anhydrase II binds to the carboxyl-terminus of human band 3, the erythrocyte $\text{Cl}^-/\text{HCO}_3^-$ exchanger. *J Biol Chem* 273: 28430-28437, 1998.

314. **Wakabayashi S, Pang T, Su X, and Shigekawa M.** A novel topology model of the human Na⁺/H⁺ exchanger isoform 1. *J Biol Chem* 275: 7942-7949, 2000.
315. **Wakabayashi S, Shigekawa M, and Pouyssegur J.** Molecular physiology of vertebrate Na⁺/H⁺ exchangers. *Physiol Rev* 77: 51-74, 1997.
316. **Wang AY, Wang M, Lam CW, Chan IH, Zhang Y, and Sanderson JE.** Left ventricular filling pressure by Doppler echocardiography in patients with end-stage renal disease. *Hypertension* 52: 107-114, 2008.
317. **Wehrens XH, Lehnart SE, Huang F, Vest JA, Reiken SR, Mohler PJ, Sun J, Guatimosim S, Song LS, Rosembliit N, D'Armiento JM, Napolitano C, Memmi M, Priori SG, Lederer WJ, and Marks AR.** FKBP12.6 deficiency and defective calcium release channel (ryanodine receptor) function linked to exercise-induced sudden cardiac death. *Cell* 113: 829-840, 2003.
318. **Wehrens XH and Marks AR.** Molecular determinants of altered contractility in heart failure. *Ann Med* 36 Suppl 1: 70-80, 2004.
319. **Williams RS and Rosenberg P.** Calcium-dependent gene regulation in myocyte hypertrophy and remodeling. *Cold Spring Harb Symp Quant Biol* 67: 339-344, 2002.
320. **Xiao B, Sutherland C, Walsh MP, and Chen SR.** Protein kinase A phosphorylation at serine-2808 of the cardiac Ca²⁺-release channel (ryanodine receptor) does not dissociate 12.6-kDa FK506-binding protein (FKBP12.6). *Circ Res* 94: 487-495, 2004.

321. **Xiao RP.** Beta-adrenergic signaling in the heart: dual coupling of the beta₂-adrenergic receptor to G_s and G_i proteins. *Sci STKE* 2001: re15, 2001.
322. **Xiao RP, Cheng H, Zhou YY, Kuschel M, and Lakatta EG.** Recent advances in cardiac beta₂-adrenergic signal transduction. *Circ Res* 85: 1092-1100, 1999.
323. **Yamada H, Horita S, Suzuki M, Fujita T, and Seki G.** Functional role of a putative carbonic anhydrase II-binding domain in the electrogenic Na⁺-HCO₃⁻ cotransporter NBCe1 expressed in *Xenopus* oocytes. *Channels (Austin)* 5: 106-109, 2011.
324. **Yamamoto T, Shirayama T, Sakatani T, Takahashi T, Tanaka H, Takamatsu T, Spitzer KW, and Matsubara H.** Enhanced activity of ventricular Na⁺-HCO₃⁻ cotransport in pressure overload hypertrophy. *Am J Physiol Heart Circ Physiol* 293: H1254-1264, 2007.
325. **Yamamoto T, Swietach P, Rossini A, Loh SH, Vaughan-Jones RD, and Spitzer KW.** Functional diversity of electrogenic Na⁺-HCO₃⁻ cotransport in ventricular myocytes from rat, rabbit and guinea pig. *J Physiol* 562: 455-475, 2005.
326. **Yannoukakos D, Stuart-Tilley A, Fernandez HA, Fey P, Duyk G, and Alper SL.** Molecular cloning, expression, and chromosomal localization of two isoforms of the AE3 anion exchanger from human heart. *Circ Res* 75: 603-614, 1994.

327. **Yen PM, Ando S, Feng X, Liu Y, Maruvada P, and Xia X.** Thyroid hormone action at the cellular, genomic and target gene levels. *Mol Cell Endocrinol* 246: 121-127, 2006.
328. **Yoshida H and Karmazyn M.** Na⁺/H⁺ exchange inhibition attenuates hypertrophy and heart failure in 1-wk postinfarction rat myocardium. *Am J Physiol Heart Circ Physiol* 278: H300-304, 2000.
329. **Zalk R, Lehnart SE, and Marks AR.** Modulation of the ryanodine receptor and intracellular calcium. *Annu Rev Biochem* 76: 367-385, 2007.
330. **Zeymer U, Suryapranata H, Monassier JP, Opolski G, Davies J, Rasmanis G, Linszen G, Tebbe U, Schroder R, Tiemann R, Machnig T, and Neuhaus KL.** The Na⁺/H⁺ exchange inhibitor eniporide as an adjunct to early reperfusion therapy for acute myocardial infarction. Results of the evaluation of the safety and cardioprotective effects of eniporide in acute myocardial infarction (ESCAMI) trial. *J Am Coll Cardiol* 38: 1644-1650, 2001.
331. **Zhai P, Galeotti J, Liu J, Holle E, Yu X, Wagner T, and Sadoshima J.** An angiotensin II type 1 receptor mutant lacking epidermal growth factor receptor transactivation does not induce angiotensin II-mediated cardiac hypertrophy. *Circ Res* 99: 528-536, 2006.
332. **Zhang YH and Hancox JC.** Regulation of cardiac Na⁺-Ca²⁺ exchanger activity by protein kinase phosphorylation--still a paradox? *Cell Calcium* 45: 1-10, 2009.
333. **Zhou L, Huang H, McElfresh TA, Prosdocimo DA, and Stanley WC.** Impact of anaerobic glycolysis and oxidative substrate selection on contractile

function and mechanical efficiency during moderate severity ischemia. *Am J Physiol Heart Circ Physiol* 295: H939-H945, 2008.

334. **Zhu Q, Lee DW, and Casey JR.** Novel topology in C-terminal region of the human plasma membrane anion exchanger, AE1. *J Biol Chem* 278: 3112-3120, 2003.

335. **Zolnowska B, Slawinski J, Pogorzelska A, Chojnacki J, Vullo D, and Supuran CT.** Carbonic anhydrase inhibitors. Synthesis, and molecular structure of novel series N-substituted N'-(2-arylmethylthio-4-chloro-5-methylbenzenesulfonyl)guanidines and their inhibition of human cytosolic isozymes I and II and the transmembrane tumor-associated isozymes IX and XII. *Eur J Med Chem* 71C: 135-147, 2013.

Chapter 2

Materials and Methods

2.1 Materials

Most of the compounds employed in this study were purchased from Sigma-Aldrich and Invitrogen. The less common compounds are shown in Table 2.1 below. Molecular biology tools (restriction enzymes, oligonucleotides, etc.) and antibodies used for immunoblotting are given in Tables 2.2 and 2.3 below.

Table 2.1 Reagents

Name	Source
Mouse Laminin	Invitrogen, Canada
2'-7'-bis-(carboxyethyl)-5(6)-carboxyfluorescein acetoxymethyl ester (BCECF-AM)	Sigma-Aldrich, Oakville, ON, Canada
2,3-butanedione monoxime (BDM)	Sigma-Aldrich, Canada
Taurine	Sigma-Aldrich, Canada
Nigericin	Sigma-Aldrich, Canada
Angiotensin II	Sigma-Aldrich, Canada
Phenylephrine	Sigma-Aldrich, Canada
Trimethylamine (TMA)	Sigma-Aldrich, Canada
Bovine serum albumin (BSA)	Sigma-Aldrich, Canada
Dulbecco's Modified Eagle's Medium Nutrient Mixture with F-12 HAM	Invitrogen, Canada
Fetal bovine serum (FBS)	Invitrogen, Canada
Sodium pentobarbital	Invitrogen, Canada
Tributyltin chloride	Sigma-Aldrich, Canada
Poly-L-lysine	Sigma-Aldrich, Canada
<i>N</i> -(ethoxycarbonylmethyl)-6-methoxyquinolinium bromide (MQAE)	Molecular Probes, Eugene, OR

Table 2.1 Reagents (cont'd)

Protease inhibitor cocktail	Roche Diagnostics, Indianapolis, IN
Polyvinylidene difluoride (PVDF) membranes	Millipore, Billerica, MA
Calf serum	Invitrogen, Canada
Protease XIV	Sigma-Aldrich, Canada
Collagenase B	Roche, Mannheim, Germany
Collagenase D	Roche, Mannheim, Germany
Penicillin-streptomycin	Invitrogen, Canada
L-glutamine	Invitrogen, Canada
Insulin-transferrin-selenite (ITS)	Sigma-Aldrich, Canada
Phenylephrine (PE)	Sigma-Aldrich, Canada
Angiotensin II (ANGII)	Sigma-Aldrich, Canada
Acetazolamide (ATZ)	Sigma-Aldrich, Canada

Table 2.2 Enzymes

<i>Nhe I</i>	New England Biolabs, Mississauga, ON, Canada
<i>Xho I</i>	New England Biolabs, Mississauga, ON, Canada
<i>EcoR I</i>	New England Biolabs, Mississauga, ON, Canada
Mung Bean exonuclease	New England Biolabs, Mississauga, ON, Canada
<i>Xba I</i>	New England Biolabs, Mississauga, ON, Canada
<i>Pme I</i>	New England Biolabs, Mississauga, ON, Canada
<i>EcoR V</i>	New England Biolabs, Mississauga, ON, Canada
DNA Ligase	New England Biolabs, Mississauga, ON, Canada

Table 2.3 Antibodies

Donkey anti-rabbit IgG conjugated to horseradish peroxidase	GE Healthcare, Little Chalfont, UK
Sheep anti-mouse IgG conjugated to horseradish peroxidase	GE Healthcare, Little Chalfont, UK
Rabbit polyclonal anti-CAII antibody	Santa Cruz Biotechnology, San Diego, CA, USA
Goat polyclonal anti-ANP antibody	Santa Cruz Biotechnology, San Diego, CA, USA
Monoclonal anti-GAPDH antibody	Santa Cruz Biotechnology, San Diego, CA, USA
Monoclonal anti- β -actin antibody	Sigma, St Louis, MO, USA
Rabbit anti-NHE1 polyclonal	Chemicon, Temucula, CA, USA

Table 2.4 Sequences of primers used in real time qRT-PCR

Target Gene	Sequence	
<i>Anp</i>	F:	5'-TCCAGGCCATATTGGAGCAAATCC-3'
	R:	5'-TCCAGGTGGTCTAGCAGGTTCTTG-3'
β - <i>mhc</i>	F:	5'-GAGACGGAGAATGGCAAGAC-3'
	R:	5'-AAGCGTAGCGCTCCTTGAG-3'
<i>Caii</i>	F:	5'-CTCTGCTGGAATGTGTGACCT-3'
	R:	5'-GCGTACGGAAATGAGACATCTGC-3'
<i>Nhe1</i>	F:	5'-TTTTCACCGTCTTTGTGCAG-3'
	R:	5'-TGTGTGGATCTCCTCGTTGA-3'
<i>Gapdh</i>	F:	5'-CCTCGTCCCGTAGACAAAAT-3'
	R:	5'-TGATGGCAACAATCTCCACT-3'

Anp, atrial natriuretic peptide; β -*mhc*, beta myosin heavy chain; *Caii*, carbonic anhydrase II; *Nhe1*, sodium proton exchanger isoform 1; *Gapdh*, glyceraldehyde 3-phosphate dehydrogenase.

2.2 Methods

2.2.1 Molecular Cloning

pJRC9 (55), encoding human full length erythrocyte AE1, was used as a template to amplify the coding sequence for AE1 using the AE1 forward primer, 5'-GCCGGCTAGCATGGAGGAGCTGCAGGATG-3', which contains an *NheI* restriction site and the AE1 reverse primer, 5'-CCAGTGATGGGAACCACCCACAGGCATGGCCACTTCGTC-3', which encodes two glycine residues and the 5' end of CAII. The stop codon of AE1 and the start codon of CAII were eliminated from the AE1 reverse primer. The coding sequence of wild-type human CAII and the CAII-V143Y mutant were amplified using the plasmids, pJRC36 (283) (containing CAII) and pDS14 (283) (containing CAII-V143Y), with the forward primer, 5'-GACGAAGTGGCCATGCCTGTGGGTGGTTCCCATCACTGGGGGTACGG-3', which contains the 3' end of AE1 cDNA without the stop codon of AE1 and the start codon of CAII, and the CAII reverse primer, 5'-GCCGCTCGAGTTATTTGAAGGAAGCTTTGATTTGCC-3', containing an *XhoI* site. In the next round of PCR, the coding sequences of AE1 and CAII, obtained above, were used as templates with AE1 forward primer and CAII reverse primer to generate a fused gene product. This was then cloned into the *NheI* and *XhoI* sites of the mammalian expression vector, pcDNA 3.1(+), to obtain pDAS3 (encoding AE1.CAII insert) and pDAS4 (encoding AE1.CAII-V143Y).

2.2.2 Expression of AE1 and AE1 Fusion Proteins

AE1, AE1.CAII and AE1.CAII-V143Y were expressed in HEK293 cells by transient transfection (115), using the calcium phosphate precipitate method (251). The cells were incubated at 37 °C in DMEM, supplemented with 5% fetal bovine serum and 5% calf serum, in a 5% CO₂ incubator. Two days following transfection, cells were washed with PBS (140 mM NaCl, 3 mM KCl, 6.5 mM Na₂HPO₃, 1.5 mM KH₂PO₃, pH 7.4) and lysed with 2x SDS-PAGE sample buffer (10% (v/v) glycerol, 2% (w/v) SDS, 2% β-mercaptoethanol, 0.5% (w/v) bromophenol blue, 75 mM Tris, pH 6.8, containing protease inhibitor cocktail).

2.2.3 Immunoblotting

Protein samples (20 µg), whose concentrations were determined by the BCA assay (276) were resolved by SDS-PAGE on 10% acrylamide gels (169). Proteins were transferred onto PVDF membranes by electrophoresis for 1 h at 100 V in transfer buffer (10% (v/v) methanol, 25 mM Tris, and 192 mM glycine) (297). PVDF membranes were blocked in TBST-M (TBST (137 mM NaCl, 20 mM Tris, 0.1% (v/v) Tween 20, pH 7.5), containing 5% (w/v) nonfat dry milk) for 30 min (162). Immunoblots were incubated with rabbit polyclonal N-terminal anti-AE1 antibody (1:5000) or anti-AE1 monoclonal antibody, IVF12 (145) (1:1000) in TBST-M, for 16 h at 4 °C. Immunoblots were washed with TBST buffer and incubated with TBST-M containing either donkey anti-rabbit IgG conjugated to horseradish peroxidase (1:2000) or sheep anti-mouse IgG conjugated to horseradish peroxidase (1:3000) for 1 h at 20 °C. Immunoblots

were washed in TBST and visualized using ECL reagents (Perkin Elmer) and Kodak Imaging Station 440CF (Kodak, NY), as previously described (16). Proteins were quantified by densitometry using Kodak Molecular Imaging Software v4.0.3 (Kodak, NY). Immunoblots were stripped by incubating in 10 ml of stripping buffer (2% (w/v) SDS, 62.5 mM Tris, 100 mM β -mercaptoethanol, pH 6.8) at 50 °C for 10 min, with occasional shaking, followed by three washes with TBST. Membranes were incubated with monoclonal anti- β -actin antibody (Santa Cruz Biotechnology, CA, USA) (1:2000) for 1 h at room temperature, washed with TBST and incubated with sheep anti-mouse IgG conjugated to horseradish peroxidase (1:3000) for 1 h.

2.2.4 Cell Surface Biotinylation

To determine the proportion of protein processed to the cell surface, HEK293 cells grown in 100 mm dishes, were transiently transfected with AE1, AE1.CAII, AE1.CAII-V143Y or empty vector and subjected to cell surface biotinylation assays, as described previously (282). Forty-eight hours post-transfection, cells were carefully rinsed with 4 °C PBS, washed with borate buffer (154 mM NaCl, 7.2 mM KCl, 1.8 mM CaCl₂, 10 mM boric acid, pH 9.0), and then incubated with borate buffer containing Sulfo-NHS-SS-Biotin (0.5 mg/ml) at 4 °C for 20 min. Reactions were stopped by the addition of 4 °C quenching buffer (192 mM glycine, 25 mM Tris, pH 8.3) followed by three washes with the quenching buffer. Cells were lysed by adding 500 μ l 4 °C immunoprecipitation buffer (IPB) (1% (w/v) deoxycholic acid, 1% (w/v) Triton X-100, 0.1% (v/v) SDS,

150 mM NaCl, 1 mM EDTA, 10 mM Tris-Cl, pH 7.5, with protease inhibitor cocktail). Lysates were centrifuged at 16,000 x g for 20 min. Supernatant was divided into two equal halves and one half was retained for immunoblotting (total protein). Immobilized streptavidin agarose resin (100 μ l) (Thermo Scientific, IL, USA) (2 mg/ml streptavidin resin in PBS, containing 2 mM NaN₃) was added to half of the lysate and incubated overnight at 4 °C while rocking. Samples were centrifuged at 8000 x g for 2 min, and 250 μ l of supernatant (unbound protein), was collected for subsequent protein detection. SDS-PAGE sample buffer was added to the total protein and the unbound protein samples prior to analyses by SDS-PAGE immunoblotting, as described above. Immunoblots were stripped (as described above) and re-probed with monoclonal anti-GAPDH antibody (Santa Cruz, CA, USA) (1:2000). The percentage of protein at the cell surface, calculated as $((\text{Total protein} - \text{Unbound protein})/\text{Total protein}) * 100\%$, was corrected for GAPDH biotinylation.

2.2.5 Chloride/Bicarbonate Exchange Assays

HEK293 cells were transiently transfected with AE1, AE1.CAII, AE1.CAII-V143Y or pcDNA and grown on poly-L-lysine-coated glass coverslips. Forty-eight hours post-transfection, coverslips were rinsed in serum-free DMEM and incubated for 20 min in serum-free DMEM, containing 2 μ M BCECF-AM. Ringer's buffer (5 mM glucose, 5 mM potassium gluconate, 1 mM calcium gluconate, 1 mM MgSO₄, 2.5 mM NaH₂PO₄, 25 mM NaHCO₃, 10 HEPES, pH 7.4), with either 140 mM NaCl or 140 mM sodium gluconate, was pre-equilibrated by continuously bubbling with 5% CO₂/ balance air. Coverslips,

mounted in fluorescence cuvettes, were perfused with the Cl⁻-containing Ringer's buffer until steady-state fluorescence was achieved, followed by perfusion in Cl⁻-free gluconate-containing Ringer's buffer and finally perfusion in Cl⁻-containing buffer. Cells were illuminated at wavelengths of 440 nm and 502.5 nm and the fluorescence emission was recorded at 528.7 nm, using a Photon Technologies International fluorimeter. Calibration was performed using the high potassium/nigericin technique (295) at three known pH values around 6.5, 7.0 and 7.5 and fluorescent ratios were converted to pH_i. In all assays that used nigericin, the compound was exhaustively removed by perfusion of the system with 70% ethanol, followed by water. Rates of change of pH_i were assessed by linear regression (Kaleidagraph software) of the first minute of pH_i change following solution change to Cl⁻-free Ringer's buffer. Background activity of HEK293 cells was corrected by subtracting the transport activity of cells transfected with vector alone from the total rate. The effect of acetazolamide on the measured rate of Cl⁻/HCO₃⁻ exchange was assessed by performing Cl⁻/HCO₃⁻ exchange assays. Following incubation with Cl⁻-containing Ringer's buffer cells were perfused with Cl⁻-containing Ringer's buffer, containing 100 μM acetazolamide and the assay was repeated with all buffers supplemented with 100 μM acetazolamide.

In some assays cells were co-transfected with AE1 or AE1.CAII and varied amounts of CAII-V143Y cDNA. Following each Cl⁻/HCO₃⁻ exchange assay, cells from the dish that contained the coverslips used for transport assays were collected and probed for AE1 and CAII on immunoblots. Expression of

CAII-V143Y was determined by densitometry of the immunoblots, probed with anti-CAII antibody. Since the cells endogenously expressed WT CAII, the amount of CAII-V143Y was determined by subtracting the amount of CAII in cells transfected with 0 μg CAII-V143Y cDNA, from the CAII abundance in cells transfected with CAII-V143Y cDNA.

Flux of proton equivalents (J_{H^+}) was calculated as $\Delta\text{pH}/\text{min} \times \text{total buffer capacity}$ (β_{total}), where $\beta_{\text{total}} = \beta_{\text{intrinsic}} + \beta_{\text{HCO}_3^-}$. $\beta_{\text{intrinsic}}$ at the initial time of pH change was used in calculations. $\beta_{\text{intrinsic}}$ for transfected HEK293 cells was recently reported by our laboratory over a range of pH values (146) and $\beta_{\text{HCO}_3^-}$ was $2.3 \times [\text{HCO}_3^-]$ (25 mM), which is 57.5 mM.

2.2.6 Assays of Chloride Transport

The rate of chloride transport was monitored using a fluorescent dye method previously described (161, 213), with slight modifications. HEK293 cells were grown and transfected on poly-L-lysine-coated coverslips, as described above. Forty-eight hours post-transfection, coverslips were rinsed in serum-free DMEM and then incubated in a hypotonic solution (2.5 mM glucose, 2.5 mM potassium gluconate, 70 mM NaCl, 0.5 mM calcium gluconate, 0.5 mM MgSO_4 , 1.8 mM NaH_2PO_4 , 12.5 mM NaHCO_3 , 5 mM HEPES, pH 7.4), containing 5 mM MQAE-AM for 5 min at 37 °C. Coverslips were then rinsed with the hypotonic solution and mounted in fluorimeter cuvettes. Excitation wavelength was 350 nm and emission was recorded at 460 nm. Two different types of Cl^- transport assays

were performed $\text{Cl}^-/\text{NO}_3^-$ exchange assays in the nominal absence of $\text{CO}_2/\text{HCO}_3^-$ and $\text{Cl}^-/\text{HCO}_3^-$ exchange assays in the presence of $\text{CO}_2/\text{HCO}_3^-$.

In $\text{Cl}^-/\text{NO}_3^-$ exchange assays, cells were perfused with Cl^- -containing Ringer's buffer until steady-state fluorescence was achieved and then switched to a Cl^- -free gluconate-containing Ringer's buffer. To measure the rate of $\text{Cl}^-/\text{NO}_3^-$ exchange, perfusion was switched to NO_3^- -containing Ringer's buffer, containing 140 mM NaNO_3 , and then back to the Cl^- -containing Ringer's buffer after reaching a plateau. MQAE fluorescence was calibrated against $[\text{Cl}^-]_i$, using the double ionophore technique with nigericin (10 μM), and tributyltin (10 μM) (103). The calibration solutions contained final Cl^- concentrations of 20, 50 and 80 mM, with NO_3^- as the substitute anion. At the end of the experiment, 150 mM potassium thiocyanate (KSCN) was added to completely quench the MQAE fluorescence in order to correct for the background fluorescence.

$\text{Cl}^-/\text{HCO}_3^-$ exchange assays were performed with solutions gassed with 5% CO_2 /balance air. Perfusion was switched to a Cl^- -free gluconate-containing Ringer's buffer, containing 25 mM NaHCO_3 upon reaching a steady-state. Calibration of $[\text{Cl}^-]_i$ and quenching of MQAE fluorescence were performed as in $\text{Cl}^-/\text{NO}_3^-$ exchange assays above.

2.2.7 Correction of MQAE Photobleaching

Untransfected HEK293 cells were grown on poly-L-lysine-coated glass coverslips and incubated in a 5% CO_2 incubator at 37 °C for forty-eight hours. Cells were loaded with MQAE-AM as described under *Assays for Chloride Transport*. Cells were mounted in fluorescence cuvettes and fluorescence was

monitored with wavelengths 350 nm (excitation) and 460 nm (emission). Relative fluorescence intensity (F/F_0), where F is fluorescence at time (t) and F_0 is the fluorescence at time 0, was plotted against time, representing photobleaching. An exponential decay equation of the form

$$Y = \text{Span} * \exp(-K * X) + \text{Plateau}$$

was fitted to the data, where fluorescence starts at $\text{Span} + \text{Plateau}$ and decays to Plateau with rate constant K . The half-life is $0.69/K$. The inverse of this decay equation was applied to all the MQAE fluorescence experimental data to correct for photobleaching.

2.2.8 Calculation of Chloride Flux

Fluorescence intensity was converted to $[\text{Cl}^-]_i$ by determining the Stern-Volmer constant for Cl^- (K_{sv}) using the $[\text{Cl}^-]_i$ calibration curve, as described previously (35). The MQAE fluorescence was related to the $[\text{Cl}^-]_i$ by the following equation (213)

$F_0/F_{\text{Cl}} = 1 + [\text{Cl}^-]_i * K_{sv}$, where F_0 is the fluorescence in the absence of Cl^- after background correction; F_{Cl} is the fluorescence in the presence of Cl^- after background correction.

2.2.9 Animal Care and Use

All procedures involving animals were performed in accordance with the guidelines established by the Canadian Council on Animal Care and the University of Alberta Animal Care and Use Committee. Experiments were performed using *ae3* null mice in a C57BL/6 background. The *ae3* null strain has

been previously described and characterized (240). Age-matched WT mice from separate breedings were used as controls.

2.2.10 Heart Weight to Body Weight Ratio

Adult male mice, 1-3 month old, were weighed and anesthetized with sodium pentobarbital (50 mg/kg) by intraperitoneal injection. Upon reaching surgical plane, the heart was quickly removed after performing midsection thoracotomy and rinsed in 4 °C phosphate buffer saline (PBS: 140 mM NaCl, 3 mM KCl, 6.5 mM Na₂HPO₄, 1.5 mM KH₂PO₄, pH 7.4). Ventricles were separated from atria and blood vessels, blotted dry and the wet ventricular weight was measured. Heart weight to body weight ratio (HW/BW) was then calculated by dividing the weight of the ventricles by the weight of the whole animal.

2.2.11 Echocardiography

Echocardiographic assessment of cardiac performance in *WT* and *ae3^{-/-}* mice was performed by the Cardiovascular Research Centre Core Facility (University of Alberta). Mice were subjected to mild anesthesia by isoflurane inhalation and echocardiography parameters were measured using a Vevo 770 High-Resolution Imaging System with a 30-MHz transducer (RMV-707B; Visual Sonics, Toronto). M-mode images and a four chamber view allowed for the calculation of wall measurements, ejection fraction, fractional shortening, and mitral velocities (E and A). Mitral valve tissue motion (E') was measured using Tissue Doppler taken from the mitral septal annulus.

2.2.12 Blood Pressure Measurement

Non-invasive blood pressure measurements were performed by the Cardiovascular Research Centre Core Facility (University of Alberta). Mice were comfortably restrained in a 26 °C warming chamber (IITC Life Science) for ~15 min prior to taking blood-pressure (BP) measurements. Tail-cuff sensors were secured on the tail to occlude the blood flow, and connected to the recording device. Systolic and diastolic pressure, heart rate, blood volume and flow were obtained, using CODA6 software (Kent Scientific Corporation, Connecticut, USA).

2.2.13 Isolation and Culture of Cardiomyocytes from Adult Mouse

Cardiomyocytes from adult mouse hearts were isolated and cultured with modifications of a published protocol (14, 258). Briefly, adult mice were euthanized with sodium pentobarbital (50 mg/kg body mass) by intraperitoneal injection. Upon reaching surgical plane, midsection thoracotomy was performed and hearts were quickly excised and placed in 4 °C perfusion solution, containing in mM: 120 NaCl, 5.4 KCl, 1.2 MgSO₄, 5.6 glucose, 10 2,3-butanedione monoxime (BDM) (Sigma), 5 taurine (Sigma), 1.2 NaH₂PO₄, 10 HEPES, pH 7.4. Extra-cardiac tissues were removed and hearts were subjected to retrograde perfusion with perfusion solution to remove excess blood. Perfusion was switched for 15 min to perfusion solution at 37 °C, supplemented with 0.5 mg/ml collagenase type B (Roche), 0.5 mg/ml collagenase type D (Roche), 0.02 mg/ml protease XIV (Roche) and 50 μM CaCl₂. Ventricles, partially digested at this

stage, were removed, cut into several pieces (about 0.02 cm), and digested further in the same enzyme digestion solution by gentle trituration with a transfer pipette. Once the ventricles were completely digested via trituration, enzymatic digestion was abolished by addition of Digestion stop buffer I (perfusion solution, containing 10% (v/v) fetal bovine serum (FBS) (GIBCO) and 50 μ M CaCl_2). Lysates settled under gravity for 10 min at room temperature and pellets were resuspended in myocyte stopping buffer II (perfusion solution, containing 5% (v/v) FBS and 50 μ M CaCl_2). Samples were transferred to 60 mm tissue culture dish and calcium levels were increased by addition of CaCl_2 to obtain final concentrations of (μ M) 62, 112, 212, 500 and 1000, sequentially at 4 min intervals at 20 °C. Cells were transferred to a 14 ml culture tube and allowed to sediment for 10 min under gravity. Cells were resuspended in myocyte culture medium (Dulbecco's Modified Eagle's Medium/Nutrient Mixture F12-Ham (Sigma), supplemented with 10 mM BDM, 5% (v/v) FBS, 1% penicillin (GIBCO), 10 mM BDM, and 2 mM L-glutamine (GIBCO)). Myocytes were plated at a density of $(0.5-1) \times 10^4$ cells/cm² onto 35 mm culture dishes, pre-coated for 2 h with 10 μ g/ml mouse laminin (Invitrogen) in PBS. Cells were incubated at 37 °C in a 5% CO₂ incubator for 1 h at which point medium was replaced with Dulbecco's Modified Eagle's Medium/Nutrient Mixture F12-Ham, containing 10 mM BDM, 1% penicillin, 2 mM L-glutamine, 0.1 mg/ml bovine serum albumin, and 1x ITS Liquid Media Supplement (Sigma). The entire culture procedure was carried out in a sterile laminar flow hood.

2.2.14 Optimization of Conditions for Induction of Cardiomyocyte

Hypertrophy

Following isolation and culture for 3 h, 6 h, 12 h, 18 h and 24 h, cardiomyocytes were subjected to hypertrophic stimulation by adding 10 μ M PE or 1 μ M ANGI; another group (control) was treated with solvent carrier (Fig. 4.4). Cardiomyocytes were incubated for further 24 h. Hypertrophy was assessed by analysis of cell surface area of cardiomyocyte images taken pre- and post-treatment with the hypertrophic agonists. Images of characteristic rod-shaped cardiomyocytes collected with a QICAM fast-cooled 12-bit color camera (QImaging Corporation) were used for analysis. Image analyses were performed with Image-Pro Plus software (Media Cybernetics) to measure cell surface area. Each group contained between 100-200 cells. Cell surface area (% relative to control) = Surface area (post-treatment)/Surface area (pre-treatment) X 100.

2.2.15 Assessment of Cardiomyocyte Hypertrophic Growth Using

Optimal Condition

Cardiomyocytes were isolated and cultured from adult hearts as described above. Following 18 h of culture, myocytes were treated with solvent carrier (control), 10 μ M PE or 1 μ M ANGI for further 24 h. Hypertrophy was assessed by analysis of cell surface area of cardiomyocyte images taken pre- and post-treatment with the hypertrophic agonists as described above.

2.2.16 Real-Time Quantitative Reverse Transcription PCR (Real-Time qRT-PCR)

Cardiomyocytes were prepared and treated as above. At the end of the culture period, medium was aspirated and cardiomyocytes were harvested in 350 μ l Buffer RLT (Qiagen). RNA was extracted from the lysates with an RNeasy Plus Mini Kit, as per manufacturer's instructions (Qiagen). RNA samples (100 ng) were reverse transcribed, following the manufacturer's instructions for SuperScript IITM reverse transcriptase (Invitrogen). Real-time qRT-PCR was performed in a Rotorgene 3000 real time thermal cycler (Corbett Research), using a reaction mix containing: 5 μ l template cDNA, 12 μ l 2x Rotor-Gene SYBR Green PCR Master Mix (Rotor-Gene SYBR Green PCR Kit, Qiagen), and 1 μ M of each primer. Data were obtained and analyzed, using Rotor Gene 6.0.14 software. Cycle threshold (Ct) values were obtained for carbonic anhydrase II (CAII), NHE1, atrial natriuretic peptide (ANP), β -MHC and glyceraldehyde-3-phosphate dehydrogenase (GAPDH). Primers (Table 1) were designed, using Primer3 (<http://Frodo.wi.mit.edu/primer3/>).

2.2.17 Detection of Proteins by Immunoblotting

Cardiomyocytes, isolated and cultured from adult mouse hearts, were subjected to drug intervention as described above. Twenty-four hour following treatment, medium was aspirated and myocytes were washed with 4 °C PBS. Cells were lysed with SDS-PAGE sample buffer (10% (v/v) glycerol, 2% (w/v) SDS, 2% 2-mercaptoethanol, 0.001% (w/v) bromophenol blue, 65 mM Tris, protease

inhibitors (1 $\mu\text{g/ml}$ pH 6.8) and lysates were heated 5 min at 65 °C. Protein concentrations were determined by the bicinchoninic acid (Pierce Biotechnology) assay (276), and 20 μg of protein was resolved by SDS-PAGE on 10% acrylamide gels. Proteins were transferred onto PVDF membranes by electrophoresis for 1 h at 100 V in transfer buffer (10% (v/v) methanol, 25 mM Tris, and 192 mM glycine). PVDF membranes were blocked for 30 min with 5% (w/v) nonfat dry milk/ 0.1% (v/v) Tween 20 in TBS (137 mM NaCl, 20 mM Tris, pH 7.5). Immunoblots were incubated with rabbit polyclonal anti-CAII antibody (Santa Cruz Biotechnology; 1:1000), anti-AE1 monoclonal antibody, IVF12 (1:1000) (145), rabbit anti-human SLC26A6 (1:1000) (188), or rabbit polyclonal anti-NHE1 antibody (1:1000) (17) in TBST-M for 16 h at 4 °C. Immunoblots were washed with TBST (TBS, containing 0.1% (v/v) Tween 20) and incubated with donkey anti-rabbit IgG conjugated to horseradish peroxidase (Santa Cruz Biotechnology; 1:2000) or mouse anti-goat IgG conjugated to horseradish peroxidase (Santa Cruz Biotechnology; 1:2000) for 1 h at room temperature. Immunoblots were washed in TBST and visualized, using ECL reagents (Perkin Elmer) and a Kodak Imaging Station 440CF (Kodak, Rochester, NY). Proteins were quantified by densitometry, using Kodak Molecular Imaging software (version 4.0.3; Kodak). Immunoblots were stripped by incubating in 10 ml of stripping buffer (2% (w/v) SDS, 10 mM 2-mercaptoethanol, 62.5 mM Tris, pH 6.8) at 50°C for 10 min with occasional shaking, followed by three washes with TBST. Membranes were incubated with mouse monoclonal anti- β -actin antibody (Santa Cruz Biotechnology; 1:2000) for 1 h at 20 °C, washed with TBST, and

incubated with sheep anti-mouse IgG conjugated to horseradish peroxidase (Santa Cruz Biotechnology; 1:3000) for 1 h. Immunoblots were washed and visualized again, as described above.

2.2.18 Protein Synthesis Assays

Cardiomyocytes were prepared and subjected to hypertrophic stimulation as above. Radiolabeled phenylalanine ($[^3\text{H}]$ -Phe, 1 $\mu\text{Ci/ml}$, (Perkin Elmer)) was added immediately after drug intervention and cells were incubated for another 24 h. Proteins were precipitated, using trichloroacetic acid (TCA) as described previously with some modifications (183). Medium was carefully aspirated and 500 μl of 0.5% (v/v) Triton X-100, containing protease inhibitor cocktail (Roche) were added. Lysates were transferred into 1.5 ml microcentrifuge tubes and TCA (100%: 500 g in 350 ml H_2O) was added to each tube to a final concentration of 40% (v/v). Samples were incubated at 4 $^\circ\text{C}$ for 30 min, after which proteins were sedimented by centrifugation at 12 682 x g for 15 min at 4 $^\circ\text{C}$. Pellets were resuspended by adding 200 μl acetone (-20 $^\circ\text{C}$) and sedimented again by centrifugation, as above, for 10 min. The acetone wash was repeated one more time, and the pellets air dried for 20 min at room temperature. Pellets were resuspended in 200 μl of 0.2 M NaOH, 1% (w/v) SDS. Scintillation fluid (Pelkin Elmer) (3.5 ml) was added to each sample and the radioactivity of $[^3\text{H}]$ -Phe was counted in a Beckman LS6500 liquid scintillation counter.

2.2.19 Measurement of pH_i in Adult Mouse Cardiomyocytes

The protocol was as described previously with minor modifications (51, 52). Briefly, cardiomyocytes were isolated as described above and cultured on laminin-coated glass coverslips. Approximately 2 h later, cells were loaded with 2 μM BCECF-AM (Sigma-Aldrich, Canada) for 30 min at 37 °C. Coverslips were placed in an Attofluor cell chamber (Invitrogen, Canada), then transferred onto the stage of a Leica DMIRB microscope. Perfusion with HCO_3^- Ringer's buffer solution (in mM: 128.3 NaCl, 4.7 KCl, 1.35 CaCl_2 , 20.23 NaHCO_3 , 1.05 MgSO_4 and 11 glucose, pH 7.4) was initiated at 3.5 ml/min. Solutions were bubbled with 5% CO_2 -balanced air. Intracellular alkalosis was induced by switching to a HCO_3^- Ringer's solution, containing, 20 mM trimethylamine (TMA) (Sigma) and perfusion was continued for 3 min. Perfusion was switched back to the HCO_3^- Ringer's buffer solution. pH_i of individual cardiomyocytes was measured by photometry at excitation wavelengths of 502.5 nm and 440 nm with a Photon Technologies International (PTI, Lawrenceville, NJ, USA) Deltascan monochromator. Emission wavelength, 528.7 nm, was selected, using a dichroic mirror and narrow range filter (Chroma Technology Corp., Rockingham, VT, USA) and was measured with a PTI D104 photometer. At the end of experiments, pH_i was clamped by the high K^+ /Nigericin technique (295) in calibration solutions containing, 140 mM, 1 mM MgCl_2 , 2 mM EGTA, 10 mM HEPES, 11 mM glucose and 20 mM BDM. Three pH standards spanned a range of 6.5-7.5. Steady-state pH_i was measured from the pH_i value prior to induction of alkalosis.

Rate of pH_i recovery was measured by linear regression from first min of recovery from imposed alkalosis.

To evaluate the effect of $\text{CO}_2/\text{HCO}_3^-$ on pH_i recovery, perfusion was performed in a HEPES buffer solution (HEPES replaced NaHCO_3 in the HCO_3^- buffer described above) in the nominal absence of HCO_3^- .

2.2.20 Generation of CAII Adenoviral Constructs

Adenoviral constructs, pDAS1 and pDAS2, containing the wildtype human CAII and mutant CAII (V143Y), respectively, were generated following the approach described previously (128). pDAS1 was obtained by subcloning CAII from pJRC36 (283), which has both the translated and untranslated regions of hCAII, into the adenoviral shuttle vector, pAdTRACK-CMV, which is under the influence of the cytomegalovirus (CMV) promoter. pJRC36 was initially digested with the restriction enzyme, EcoR I. Following gel purification, the linearized product was subjected to Mung Bean exonuclease digestion to create a blunt end. The final fragment was digested with Xba I to isolate the hCAII gene and subsequently subcloned into the Xba I and EcoR V sites of pAdTRACK-CMV to generate pDAS1. pDAS2 was constructed by a similar strategy using the plasmid vector, pDS14 (283), containing V143Y, the catalytically inactive CAII. Success of cloning was confirmed by DNA sequencing performed at the DNA sequencing core facility at the University of Alberta, Edmonton.

The resultant plasmids, pDAS1 and pDAS2, were each digested with Pme I and then co-transformed into *E. coli* cells, containing the backbone adenoviral plasmid, pAdEasy-1.

2.2.21 Hematoxylin-Eosin Staining of Heart Sections

Hematoxylin and eosin (HE) staining was performed on longitudinal (LS) and transverse sections (TS) of wildtype and *ae3* null adult mouse heart, using previously described protocols (93, 94). Briefly, paraffin-embedded hearts were sectioned into 3 μm slices, which were trimmed and floated onto a water bath at 42 °C, containing 50 mg/l of gelatin while gently stretching the cut sections to avoid wrinkles. Poly-L-lysine coated microscope slides were dipped under the meniscus of the water bath and a tissue slice was carefully mounted onto it. Sections were then allowed to air-dry overnight at 20 °C, after which the slide was placed on its edge in an oven and baked for 15 min at 60 °C. Sections were deparaffinized by successively immersing them for 5 min with agitation in xylene, 100% ethanol and 70% ethanol, and rehydrated in Tris-EDTA buffer (1 mM EDTA, 0.05% Tween 20, 10 mM Tris, pH 9.0) for 1 min. Slides were rinsed in distilled water for 1 min with agitation. Slides were dipped in Mayer's hematoxylin solution (1.0 g/l hematoxylin (Sigma), sodium iodate (0.2 g/l), aluminum ammonium sulfate·12 H₂O (50 g/l), chloral hydrate (50 g/l) and citric acid (1 g/l), agitated for 30 s and rinsed in water for 1 min. Slides were stained in 1% eosin Y solution (1% eosin Y aqueous solution, Fisher) for 30 s with agitation. Sections were dehydrated by successively immersing it twice in 95% ethanol and twice in 100% ethanol for 30 s each. Ethanol was extracted twice in xylene followed by addition of two drops of mounting medium (Canada Balsam, Sigma) after which the section was covered with a coverslip. Images of transverse and longitudinal sections were taken using a Kodak EasyShare Digital Camera

(Kodak) and photos of whole hearts were collected with a Panasonic Lumix camera without zoom magnification. The thickness of the ventricular wall and chamber diameter of the images of the TS and LS were measured using Image-Pro Plus software (Media Cybernetics).

2.2.22 Statistical Analysis

Data are expressed as mean \pm S.E. Statistical analyses were performed using paired *t*-test or ANOVA where appropriate, and values were considered significant with $p < 0.05$.

Bibliography

1. **Alvarez BV, Kieller DM, Quon AL, Robertson M, and Casey JR.** Cardiac hypertrophy in anion exchanger 1-null mutant mice with severe hemolytic anemia. *Am J Physiol Heart Circ Physiol* 292: H1301-1312, 2007.
2. **Alvarez BV, Shandro H, Yang Z, Vithana EN, Koh AH, Yeung K, Yong V, Kolatkar P, Palasingam P, Zhang K, J.R. C, and Aung T.** Functional characterization of a novel carbonic anhydrase 4 mutation identified in a Chinese patient with retinitis pigmentosa. *Invest Ophthalmol Vis Sci* 48: 3459-3468, 2007.
3. **Alvarez BV, Xia Y, Sowah D, Soliman D, Light P, Karmazyn M, and Casey JR.** A Carbonic Anhydrase Inhibitor Prevents and Reverts Cardiomyocyte Hypertrophy. *J Physiol* 579: 127-145, 2007.
4. **Biwersi J and Verkman AS.** Cell-permeable fluorescent indicator for cytosolic chloride. *Biochemistry* 30: 7879-7883, 1991.
5. **Camilion de Hurtado MC, Alvarez BV, Perez NG, and Cingolani HE.** Role of an electrogenic $\text{Na}^+\text{-HCO}_3^-$ cotransport in determining myocardial pH_i after an increase in heart rate. *Circ Res* 79: 698-704, 1996.
6. **Camilion de Hurtado MC, Alvarez BV, Perez NG, Ennis IL, and Cingolani HE.** Angiotensin II activates Na^+ -independent $\text{Cl}^-\text{-HCO}_3^-$ exchange in ventricular myocardium. *Circ Res* 82: 473-481, 1998.
7. **Casey JR, Ding Y, and Kopito RR.** The role of cysteine residues in the erythrocyte plasma membrane anion exchange protein, AE1. *J Biol Chem* 270: 8521-8527, 1995.

8. **Fischer AH, Jacobson KA, Rose J, and Zeller R.** Cutting sections of paraffin-embedded tissues. *CSH Protoc* 2008: 4987, 2008.
9. **Fischer AH, Jacobson KA, Rose J, and Zeller R.** Hematoxylin and eosin staining of tissue and cell sections. *CSH Protoc* 2008: 4986, 2008.
10. **Fukuda A, Tanaka M, Yamada Y, Muramatsu K, Shimano Y, and Nishino H.** Simultaneous optical imaging of intracellular Cl^- in neurons in different layers of rat neocortical slices: advantages and limitations. *Neurosci Res* 32: 363-371, 1998.
11. **Graham FL, Smiley J, Russell WC, and Nairn R.** Characteristics of a human cell line transformed by DNA from human adenovirus type 5. *J Gen Virol* 52: 59-72, 1977.
12. **He TC, Zhou S, da Costa LT, Yu J, Kinzler KW, and Vogelstein B.** A simplified system for generating recombinant adenoviruses. *Proc Natl Acad Sci U S A* 95: 2509-2514, 1998.
13. **Jennings ML, Anderson MP, and Monaghan R.** Monoclonal antibodies against human erythrocyte Band 3 protein: localization of proteolytic cleavage sites and stilbenedisulfonate-binding lysine residues. *J Biol Chem* 261: 9002-9010, 1986.
14. **Johnson DE and Casey JR.** Cytosolic H^+ microdomain developed around AE1 during AE1-mediated $\text{Cl}^-/\text{HCO}_3^-$ exchange. *J Physiol* 589: 1551-1569, 2011.
15. **Kopito RR and Lodish HF.** Primary structure and transmembrane orientation of the murine anion exchange protein. *Nature* 316: 234-238, 1985.

16. **Laemmli UK.** Cleavage of structural proteins during assembly of the head of bacteriophage T4. *Nature* 227: 680-685, 1970.
17. **Link AJ and Labaer J.** Trichloroacetic Acid (TCA) Precipitation of Proteins. *Cold Spring Harbor Protocols* 2011: 993-994, 2011.
18. **Lohi H, Kujala M, Kerkela E, Saarialho-Kere U, Kestila M, and Kere J.** Mapping of five new putative anion transporter genes in human and characterization of SLC26A6, a candidate gene for pancreatic anion exchanger. *Genomics* 70: 102-112, 2000.
19. **Munkonge F, Alton EW, Andersson C, Davidson H, Dragomir A, Edelman A, Farley R, Hjelte L, McLachlan G, Stern M, and Roomans GM.** Measurement of halide efflux from cultured and primary airway epithelial cells using fluorescence indicators. *J Cyst Fibros* 3 Suppl 2: 171-176, 2004.
20. **Prasad V, Bodi I, Meyer JW, Wang Y, Ashraf M, Engle SJ, Doetschman T, Sisco K, Nieman ML, Miller ML, Lorenz JN, and Shull GE.** Impaired cardiac contractility in mice lacking both the AE3 $\text{Cl}^-/\text{HCO}_3^-$ exchanger and the NKCC1 $\text{Na}^+-\text{K}^+-2\text{Cl}^-$ cotransporter: effects on Ca^{2+} handling and protein phosphatases. *J Biol Chem* 283: 31303-31314, 2008.
21. **Ruetz S, Lindsey AE, Ward CL, and Kopito RR.** Functional activation of plasma membrane anion exchangers occurs in a pre-Golgi compartment. *J Cell Biol* 121: 37-48, 1993.
22. **Sambrano GR, Fraser I, Han H, Ni Y, O'Connell T, Yan Z, and Stull JT.** Navigating the signalling network in mouse cardiac myocytes. *Nature* 420: 712-714, 2002.

23. **Smith PK, Krohn RI, Hermanson GT, Mallia AK, Gartner FH, Provenzano MD, Fujimoto EK, Goeke NM, Olson BJ, and Klenk DC.** Measurement of protein using bicinchoninic acid. *Anal Biochem* 150: 76-85, 1985.
24. **Sterling D and Casey JR.** Transport activity of AE3 chloride/bicarbonate anion-exchange proteins and their regulation by intracellular pH. *Biochem J* 344 Pt 1: 221-229, 1999.
25. **Sterling D, Reithmeier RA, and Casey JR.** A Transport Metabolon. Functional Interaction of Carbonic Anhydrase II and Chloride/Bicarbonate Exchangers. *J Biol Chem* 276: 47886-47894, 2001.
26. **Thomas JA, Buchsbaum RN, Zimniak A, and Racker E.** Intracellular pH measurements in Ehrlich ascites tumor cells utilizing spectroscopic probes generated in situ. *Biochemistry* 18: 2210-2218, 1979.
27. **Towbin H, Staehelin T, and Gordon J.** Electrophoretic transfer of proteins from polyacrylamide gels to nitrocellulose sheets: procedure and some applications. *Proc Natl Acad Sci* 76: 4350-4354, 1979.

Chapter 3

An Intramolecular Transport Metabolon Fusion of Carbonic Anhydrase II to the C- terminus of the Cl⁻/HCO₃⁻ Exchanger, AE1

A version of this chapter has been previously published as Sowah, D., and Casey, J.R. (2011) An Intramolecular Transport Metabolon: Fusion of Carbonic Anhydrase II to the C-terminus of the Cl⁻/HCO₃⁻ Exchanger, AE1, *Am. J. Physiol.*, **301**, C336-46.

3.1 Introduction

Regulation of intracellular pH (pH_i) is critical to maintain cellular functions. pH_i regulatory mechanisms include the $\text{CO}_2/\text{HCO}_3^-$ buffer system and plasma membrane $\text{Cl}^-/\text{HCO}_3^-$ exchange proteins. CO_2 is the by-product of oxidative metabolism and readily diffuses across most plasma membranes. HCO_3^- is generated from CO_2 by a group of metalloenzymes, carbonic anhydrases (CAs) (31), which catalyze the reaction $\text{CO}_2 + \text{H}_2\text{O} \leftrightarrow \text{H}_2\text{CO}_3$, which in turn is part of the equilibrium $\text{H}_2\text{CO}_3 \leftrightarrow \text{HCO}_3^- + \text{H}^+$. Mammalian cells express 16 isoforms of CA, found in the cytosol (CAI, CAII, CAIII, CAVII, CAXIII), membrane-associated (CAIV, CAIX, CAXII, CAXIV, CAXV), in the mitochondria (CAV) and secreted into saliva and milk (CAVI) (31).

HCO_3^- is membrane-impermeant, so its transport across the plasma membrane is mediated by HCO_3^- transporters, which are integral membrane proteins. HCO_3^- transporters serve crucial physiological roles, including the regulation of pH_i (3) and cell volume (9). HCO_3^- transporters are classified into two Solute carrier (SLC, in Human Genome Organization nomenclature) families SLC4 and SLC26 (7). The SLC4 family functionally and phylogenetically divides into the electroneutral $\text{Cl}^-/\text{HCO}_3^-$ anion exchangers (AE) and the Na^+ -dependent HCO_3^- co-transporters (2, 7). Members of the electroneutral $\text{Cl}^-/\text{HCO}_3^-$ exchangers include SLC4A1-SLC4A3 (AE1-AE3) (2, 7), which share 53-56% amino acid identity (28).

AE1, the focus of the present study, mediates the trans-plasma membrane exchange of Cl^- for HCO_3^- at up to $5 \times 10^4 \text{ s}^{-1}$, a process stimulated by the

transmembrane gradient of substrate anions (14). AE1, also known as Band 3, comprises 50% of integral membrane protein in the red blood cell (RBC) (1, 23, 33, 34). In erythrocytes AE1 works reversibly to facilitate bicarbonate efflux in peripheral capillaries and bicarbonate efflux as the cell passes through the lungs (7). A truncated version of AE1, lacking the N-terminal 65 amino acids, is found in the kidney (kAE1), where it effluxes bicarbonate from the type-A intercalated cell into the blood (7). Human erythrocyte AE1 is a 911 amino acid protein defined by two domains, a 43 kDa cytosolic N-terminal domain and a 55 kDa transmembrane domain (7). The N-terminal cytoplasmic domain interacts with the cytoskeleton to maintain the biconcave shape of RBCs (19), and binds to some glycolytic enzymes and hemoglobin (19). The transmembrane domain, which alone is responsible for the anion exchange activity of the protein, consists of 12-14 membrane-spanning regions (39).

Growing evidence indicates that within the extreme C-terminal cytoplasmic 39 amino acids is a region, which physically interacts with CAII (26, 30, 37). Solid phase binding assays revealed that AE1 binds to immobilized CAII and the binding is dependent on pH and ionic strength (35-37). Truncation and mutagenesis studies revealed that the CAII binding (CAB) motif on the C-terminal tail of AE1 is an acidic-enriched sequence, LD887ADD (36, 37). The 17 amino acid N-terminal tail of CAII, rich in histidine, is responsible for binding to AE1's CAB (35). Lending further support to this physical linkage, CAII could be co-immunoprecipitated with AE1 in the epithelia of fish gills (32), as well as with solubilized AE1 from erythrocyte membranes (32, 36, 37).

Several lines of evidence now suggest that the physical interaction between AE1 and CAII increases $\text{Cl}^-/\text{HCO}_3^-$ exchange activity. Inhibition of CAII activity decreased the rate of flux of HCO_3^- across the plasma membrane (30). Moreover, when AE1 was co-transfected with the catalytically-inactive CAII mutant, CAII-V143Y, AE1 anion exchange activity was impaired (30). Since CAII-V143Y binds to AE1 with an affinity similar to CAII (30), these findings suggested that the CAII mutant exerted a dominant negative effect by displacing endogenous CAII from AE1, thereby reducing the local rate of $\text{CO}_2/\text{HCO}_3^-$ catalysis at the surface of AE1. Studies in *Xenopus laevis* oocytes revealed that mutation of the acidic CAB site on AE1 reduced $\text{Cl}^-/\text{HCO}_3^-$ exchange activity, without effect on the capacity to carry out Cl^-/Cl^- exchange and over-expression of CAII increased $\text{Cl}^-/\text{HCO}_3^-$ exchange activity, without effect on Cl^-/Cl^- exchange activity (8).

Interestingly, the CAB motif is present in all of the members of the AE family (8, 30) and among members of the $\text{Na}^+/\text{HCO}_3^-$ co-transporter family (6, 24). The rate of transport of HCO_3^- by the electrogenic $\text{Na}^+-\text{HCO}_3^-$ co-transporter (NBCe1) was enhanced when CAII was bound to the transporter (24). When co-expressed with NBCe1 in *X. laevis* oocytes, CAII increased the NBCe1 activity as measured by membrane current and the rate of cytosolic rise of Na^+ , a process reversed by the addition of the CAII inhibitor, ethoxzolamide (6). Interestingly, the activity of NBCe1, remained unaltered when it was co-expressed with CAII-V143Y (6), suggesting that active CAII is required for full NBCe1 transport activity.

The physical and functional complex between CAII and HCO_3^- transporters forms a HCO_3^- transport metabolon, which maximizes HCO_3^- flux across the membrane (5, 8, 13, 22, 26, 29, 30). Although the mechanism by which CAII enhances transport activity is not fully elucidated, CAII may concentrate the substrate, HCO_3^- , at the transport site, thereby leading to an increase in the rate of transmembrane movement of HCO_3^- . In contrast, when CAII was fused to the C-terminal tail of NBCe1 and expressed in *X. laevis* oocytes, the rate of transport was not affected (20). Moreover, in the same study, when NBCe1 was co-expressed with CAII, the activity of NBCe1 was not enhanced.

In the present study, we fused CAII to the C-terminal cytoplasmic tail of AE1 (AE1.CAII) to generate an intramolecular transport metabolon. As a control we also fused the catalytically-inactive mutant, CAII-V143Y, to AE1 (AE1.CAII-V143Y). The rate of HCO_3^- efflux was assessed by monitoring the rate of change of pH_i , using the pH-sensitive dye, BCECF, or measuring coupled Cl^- flux by monitoring the rate of change of intracellular Cl^- ($[\text{Cl}^-]_i$) using the Cl^- -sensitive dye, MQAE. Taken together, our data provide support for the existence of a bicarbonate transport metabolon, in which association with CAII facilitates the $\text{Cl}^-/\text{HCO}_3^-$ exchange efficiency of AE1.

3.2 Results

3.2.1 Expression of AE1 and AE1 Fusion Proteins

An intramolecular transport metabolon was generated by fusion of CAII to the C-terminus of AE1 linked by two glycine residues, to enable flexibility of the fusion protein (Fig. 3.1A). As a control, the catalytically-inactive CAII mutant, CAII-V143Y (12), was also fused to the C-terminus of AE1. Cell lysates from cells transfected with AE1, AE1.CAII, AE1.CAII-V143Y or vector alone were probed with an antibody directed against the N-terminal domain of AE1 (Fig. 3.1B). Usually the monoclonal antibody, IVF12 (15), is used to detect AE1, but since its epitope is the C-terminus of AE1 we found that IVF12 did not accurately report expression of AE1.CAII, because of partial epitope disruption. In vector alone-transfected cells, no immunoreactive material was detected, indicating specificity of the anti-AE1 antibody. A prominent band near 100 kDa was detected in lysates from cells transfected with AE1, consistent with the molecular weight of AE1 (101 kDa), while lysates from cells expressing AE1.CAII or AE1.CAII-V143Y revealed a band of approximately 125 kDa, consistent with the predicted mass of an AE1.CAII fusion protein (125 kDa). The immunoblot was also probed for actin, which serves as a marker for the amount of cell material present in each sample, to allow quantification of the amount of AE1 in each cell (e.g. Table 3.1).

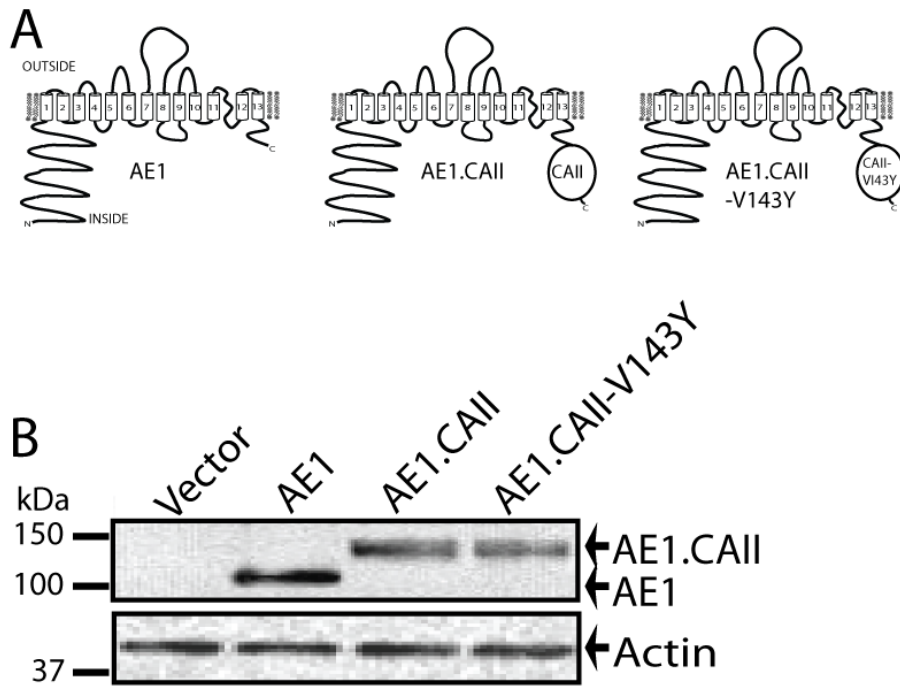


Fig. 3.1. Expression of AE1 and fusion proteins in HEK293 cells. A, Schematic diagrams representing AE1, AE1.CAII and AE1.CAII-V143Y, residing in the plasma membrane. Numbered boxes indicate transmembrane segments. N- and C-termini of proteins are labeled. Cytosolic and outside surfaces of cell are shown. B, HEK293 cells were transiently transfected with pcDNA3.1 (Vector) and cDNA coding AE1, AE1.CAII or AE1.CAII-V143Y. Lysates prepared from the cells were probed on immunoblots for AE1 with anti-AE1 rabbit polyclonal antibody directed against the N-terminal cytoplasmic domain of AE1, and were re probed for β -actin, using an anti- β -actin monoclonal antibody.

3.2.2 Cell Surface Expression of AE1 and AE1 Fusion Proteins

The efficiency of processing to the cell surface varies between different membrane proteins. Mutagenesis of regions on the C-terminal tail of AE1 can affect the processing of the protein to the cell surface (10, 25). To determine the effect of fusion of CAII or CAII-V143Y to the C-terminus of AE1, we measured the fraction of AE1 at the cell surface, using a cell surface biotinylation assay. HEK293 cells were transiently transfected with AE1, AE1.CAII or AE1.CAII-V143Y, and treated with a membrane-impermeant biotinylation reagent. Abundance of AE1 immunoreactive material was assessed in cell lysates (total protein) and in the lysate following removal of biotinylated proteins (unbound protein), using streptavidin resin (Fig. 3.2A). Biotinylated cell surface protein was assessed by the difference between total and unbound protein. To examine the degree of spurious labeling of cytosolic proteins, lysates were probed for the cytosolic marker, GAPDH. The fraction of biotin-labeled GAPDH was $6\pm 2\%$ (n=4), as determined by densitometric analysis, representing the non-specific background for the assay. The amount of wildtype AE1 at the plasma membrane was approximately 38% (Fig. 3.2B), comparable to previous data (30). Fusion of AE1 to CAII or CAII-V143Y, however, reduced the proportion of AE1 fusion at the cell surface by about 35% relative to AE1 alone (i.e. about 25% of the fusion protein was at the cell surface, Fig. 3.2B). Fusion of CAII or CAII-V143Y to the C-terminus of AE1 therefore impairs the processing of the protein to the cell surface. Subsequent assays of AE1 anion transport activity were corrected for the amount of AE1, or AE1 fusion protein processed to the cell surface (Table 3.1).

Table 3.1 Sample calculation of normalized rates of chloride/bicarbonate exchange

	AE1	AE1.CAII	AE1.CAII-V143Y
Rate of pH change ($\Delta\text{pH}_i/\text{min}$)	0.62	0.30	0.16
Fraction of AE1 variant at cell surface	0.39	0.28	0.25
Amount of AE1 in cell lysate (pixels)	19431	17621	18866
Amount of actin in cell lysate (pixels)	5990	6290	6388
Amount of AE1 per cell (arbitrary units)	3.2	2.8	2.9
Relative number of cell surface AE1 molecules	1.27	0.78	0.73
Initial pH_i	7.22	7.20	7.23
Buffer capacity at initial pH_i ($\text{mM H}^+/\text{pH}$)	65	65	65
H^+ equivalent Flux, J_{H^+} (mM/min)	40.3	19.5	10.4
Normalized H^+ equivalent Transport Rate	31.7	25.0	14.2

Rates of pH_i change were determined in $\text{Cl}^-/\text{HCO}_3^-$ assays of HEK293 cells transfected with the named AE1 variant cDNA. In parallel the fraction of AE1 processed to the cell surface of HEK293 cells was measured. After each anion exchange assay, cells from the dish holding the coverslip used in the assay were solubilized and assayed for the amount of AE1 present and actin present on

immunoblots. Actin served as a surrogate for the number of cells present in the dish, assuming that actin abundance is proportional to cell number in the sample. The amount of AE1/cell= amount of AE1/Amount of Actin. The relative number of AE1 variant molecules at the cell surface= Amount of AE1/cell x Fraction at cell surface. Intrinsic buffer capacity at pH 7.20-7.23 is 7.4 mM/pH (16) and the component arising from bicarbonate is 57.5 mM, for a total of 65 mM/pH. Normalized H⁺ equivalent transport rate= H⁺ equivalent Flux/ Relative number of AE1 variant molecules at cell surface.

3.2.3 Chloride/Bicarbonate Exchange Activity of AE1 and AE1 Fusion Proteins

Previous studies in our laboratory showed that association of CAII with AE1 enhances the rate of $\text{Cl}^-/\text{HCO}_3^-$ exchange (30). To examine further the role of CAII in modulating AE1 function, we measured the transport activity of AE1 alone and the fusion proteins, AE1.CAII and AE1.CAII-V143Y. Transfected HEK293 cells, loaded with the pH indicator dye, BCECF-AM, were alternately perfused with Cl^- -containing or Cl^- -free gluconate buffer, in the presence of $\text{CO}_2/\text{HCO}_3^-$. Rise of pH_i upon switching to the gluconate buffer indicates entry of HCO_3^- into the cell, as AE1 mediates efflux of Cl^- in exchange for HCO_3^- (Fig. 3.3A). Rate of change of pH_i was measured by linear regression of the initial rate of HCO_3^- efflux upon switching to the Cl^- -free buffer. The functional activity of any transport protein is dependent upon the number of molecules of the transporter present at the plasma membrane. The rate of $\text{Cl}^-/\text{HCO}_3^-$ exchange activity was, thus, normalized by the amount of AE1 per cell as determined by densitometry of immunoblots normalized for actin (Fig. 3.1) and the fraction of AE1 at the cell surface determined by cell surface biotinylation assay (Fig. 3.2B). An example of data treatment is presented in Table 3.1.

Fusion of CAII-V143Y to AE1 (AE1.CAII-V143Y) reduced the $\text{Cl}^-/\text{HCO}_3^-$ exchange activity to $55\pm 2\%$ vs. AE1 (Fig. 3.3B). Fusion of CAII to AE1 (AE1.CAII) increased transport activity relative to AE1.CAII-V143Y, yielding activity that was statistically indistinguishable from AE1 ($87\pm 4\%$ vs. AE1) (Fig. 3.3B). Since the only difference between AE1.CAII and AE1.CAII-V143Y is a

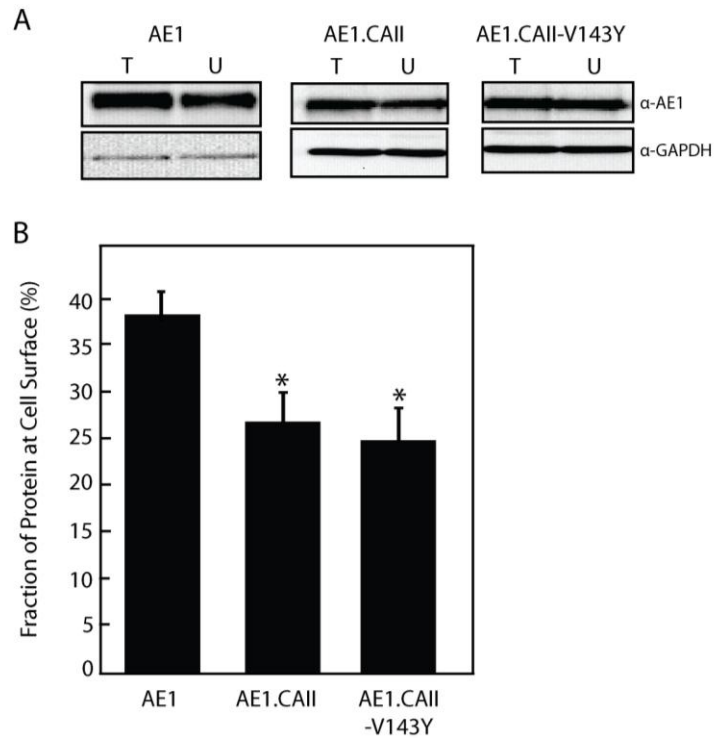


Fig. 3.2. Cell surface processing of AE1 fusion proteins. HEK293 cells were transiently transfected with cDNA coding for AE1, AE1.CAII or AE1.CAII-V143Y. Cells were incubated with sulfo-NHS-SS-biotin at 4 °C for 20 min and detergent lysates of cells were prepared. One-half of the supernatant was retained to assess the total amount of protein (T) and the other half was incubated with streptavidin resin. The supernatant and unbound protein (U) were retained for SDS-PAGE. A, Immunoblots were probed for AE1 with rabbit polyclonal anti-AE1 antibody and then reprobed with anti-GAPDH antibody. B, Densitometric analysis of the fraction of protein present at cell surface, calculated as $((T-U)/T)*100\%$, and corrected for GAPDH biotinylation, $n=4$. * Indicates statistically significant compared to AE1 alone, by one-way ANOVA.

point mutation that renders CAII-V143Y catalytically-inactive, we conclude that maximal AE1 $\text{Cl}^-/\text{HCO}_3^-$ exchange activity requires interaction with active CAII.

Another strategy to determine the role of CAII in the transport activity of the AE1 variants is to inhibit CAII activity, using acetazolamide (ATZ). $\text{Cl}^-/\text{HCO}_3^-$ exchange assays were performed in the absence, then presence of 100 μM ATZ, a concentration sufficient for maximal reduction of AE1 $\text{Cl}^-/\text{HCO}_3^-$ exchange activity (30) (Fig. 3.3A and Fig. 3.4). $\text{Cl}^-/\text{HCO}_3^-$ exchange activity differs in the absence and presence of ATZ (Fig. 3.3A and Fig. 3.4). Most significantly whereas there is no statistical difference between $\text{Cl}^-/\text{HCO}_3^-$ exchange rates of AE1 and AE1.CAII in the absence of ATZ (Fig. 3.3B), transport activity of the two proteins differs significantly upon CA inhibition (Fig. 3.3C). Also, inhibition of CA activity suppresses the bicarbonate transport rate difference between AE1.CAII and AE1.CAII-V143Y (Fig. 3.3C). From these data we conclude that AE1.CAII and AE1.CAII-V143Y have similar levels of anion transport activity, which is less than AE1 alone. Active CAII fused to AE1 allows AE1.CAII to have activity indistinguishable from AE1 alone in the absence of ATZ. The transport activity defect of AE1.CAII-V143Y is not rescued by the inactive CAII fused to it.

We performed additional analysis of the effect of ATZ on transport activity, examining the rate of HCO_3^- transport in HCO_3^- influx and efflux mode (Fig. 3.4). The data reveal that the rate of HCO_3^- efflux is slower than the rate of HCO_3^- influx. Nonetheless, the conclusions drawn in considering only the rate of HCO_3^- influx (Fig. 3.3) are also seen when considering HCO_3^- efflux.

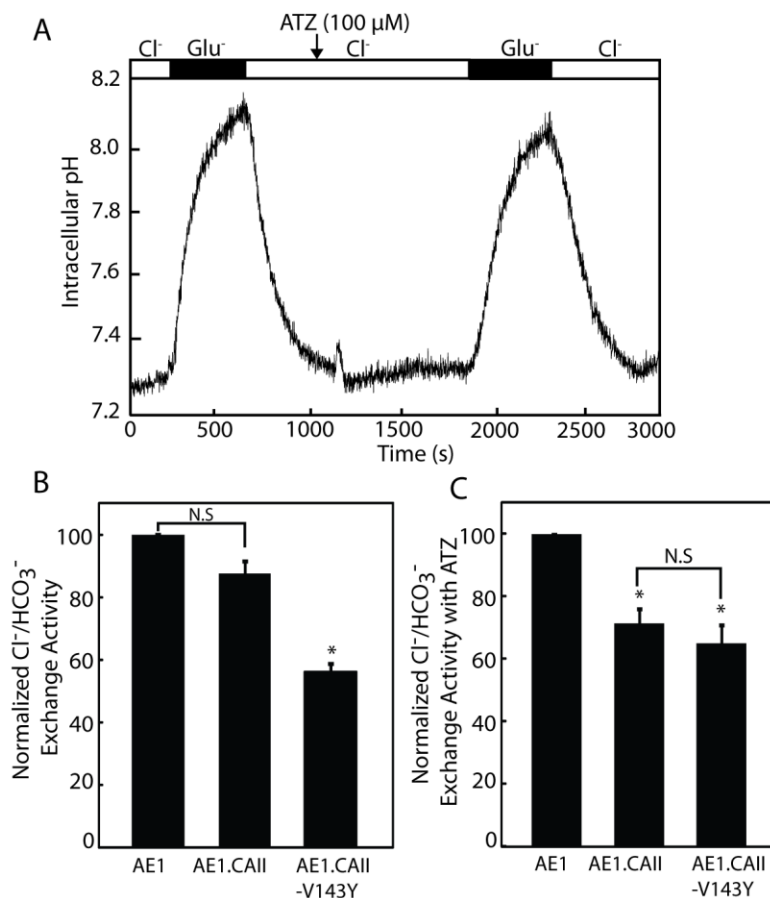


Fig. 3.3 $\text{Cl}^-/\text{HCO}_3^-$ exchange activity in the absence and presence of acetazolamide. HEK293 cells, grown on glass coverslips and transfected with cDNA coding for AE1, AE1.CAII or AE1.CAII-V143Y were loaded with BCECF-AM and subjected to $\text{Cl}^-/\text{HCO}_3^-$ exchange assays. A, Representative data for AE1-transfected cells. Cells were perfused alternately with Cl^- -containing Ringer's buffer (open bar) or Ringer's buffer with gluconate replacing Cl^- (Glu^- , filled bar), in the presence of HCO_3^- . Perfusion was switched to Cl^- -containing Ringer's buffer containing acetazolamide (100 μM ATZ) (arrow) and the cells incubated for 10 min followed by another cycle of alternate Ringer's buffer perfusion with buffers containing 100 μM ATZ. B, Transport activity was assessed by linear regression of the initial rate of change of pH_i after changing to

Cl⁻-free buffer, in the absence of ATZ. Transport activities were expressed as a percentage of Cl⁻/HCO₃⁻ exchange of AE1 alone-transfected cells and normalized to the amount of AE1 variant at the cell surface ($n=4$). (See Table I for a sample calculation). C, Transport rates in the presence of ATZ were determined as described in Panel B. N.S. no significant difference. * Indicates statistically significant, compared to AE1 alone, by one-way ANOVA.

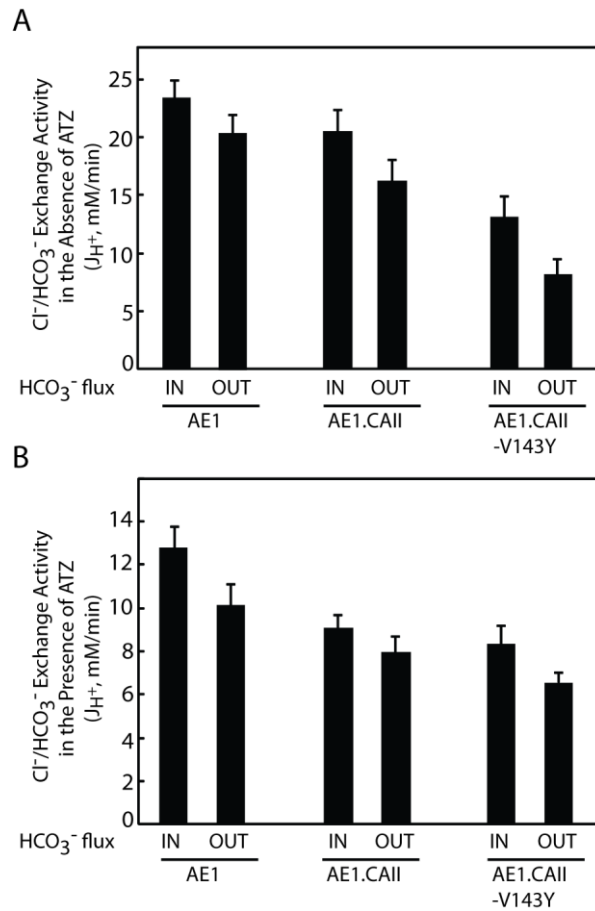


Fig. 3.4. Effect of acetazolamide on the rates of inward and outward bicarbonate transport by AE1 variants. HEK293 cells transfected with AE1, AE1.CAII or AE1.CAII-V143Y cDNAs, were grown on glass coverslips. Two days post-transfection, cells were loaded with BCECF-AM and subjected to Cl⁻/HCO₃⁻ exchange assays in the absence (A), then presence of 100 μM ATZ (B). Rate of HCO₃⁻ influx (IN) was determined by linear regression of the initial rate of HCO₃⁻ flux upon switching to Cl⁻-free Ringer's solution, while HCO₃⁻ efflux (OUT) was measured upon reperfusion with Cl⁻-containing Ringer's solution. Data represent summary of HCO₃⁻ flux in the absence (A) and presence (B) of 100 μM ATZ ($n=4$).

3.2.4 Effect of CAII-V143Y on the Functional Activity of AE1.CAII

Over-expression of the catalytically-inactive mutant CAII was previously found to suppress the $\text{Cl}^-/\text{HCO}_3^-$ exchange activity of AE1 (30), possibly by displacing endogenous CAII from binding to AE1. To determine the effect of CAII-V143Y on the transport activity of AE1.CAII, $\text{Cl}^-/\text{HCO}_3^-$ exchange assays were performed on cells transfected with a constant amount of AE1 or AE1.CAII cDNA and an increasing amount of CAII-V143Y (Fig. 3.5). We earlier found that HEK293 cells endogenously express CAII at a level near-stoichiometric with AE1 in AE1-transfected cells. Over-expression of WT CAII did not increase the rate of AE1-mediated $\text{Cl}^-/\text{HCO}_3^-$ exchange, suggesting that the cells expressed sufficient endogenous CAII to maximally activate AE1 bicarbonate transport activity (30).

CAII-V143Y reduced the $\text{Cl}^-/\text{HCO}_3^-$ exchange activity of AE1 in a dose-dependent manner (Fig. 3.5B), consistent with previous findings (30). In contrast, AE1.CAII anion exchange activity was unaffected by varying the amount of CAII-V143Y (Fig. 3.5B). The data suggest either 1) the presence of CAII fusion to AE1 prevents binding of free CAII to the CAB site in the AE1 C-terminus (since CAII-V143Y had no effect on the transport activity of AE1.CAII), or 2) CAII can bind to the CAB site, but is without effect as the presence of CAII fused to AE1 C-terminus provides sufficient CA activity to activate maximally the $\text{Cl}^-/\text{HCO}_3^-$ exchange rate of AE1.CAII.

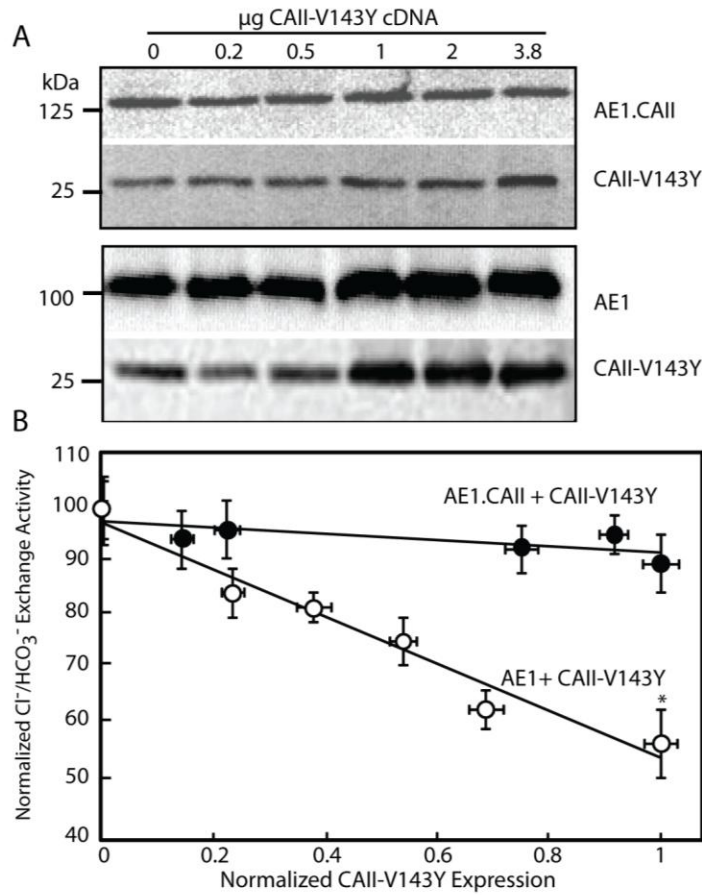


Fig. 3.5 Effect of CAII-V143Y on AE1 and AE1.CAII Cl⁻/HCO₃⁻ activity. HEK293 cells were transiently co-transfected with cDNA coding for AE1 (3.8 μg) or AE1.CAII (3.8 μg) and increasing amount of CAII-V143Y and grown on glass coverslips. A, Cell lysates from cells co-transfected with CAII-V143Y and AE1.CAII (top panels) or AE1 (bottom panels) were probed on immunoblots with anti-AE1 and anti-CAII antibodies as indicated. B, Transfected cells were loaded with BCECF-AM, placed in fluorescence cuvettes and subjected to Cl⁻/HCO₃⁻ exchange assays by monitoring pH_i. Activity was expressed as a percentage of AE1 alone (open circles) or AE1.CAII (filled circles). Data were corrected for background activity of vector-transfected cells and for the level of AE1

expression at the cell surface. The amount of CAII-V143Y expressed in cells used for transport assays (as expressed as the X-axis) was determined as described in methods, n=4. * Indicates statistically significant, compared to AE1.CAII.

3.2.5 Effect of CAII Fusion on AE1 Chloride Transport Activity

Assays of $\text{Cl}^-/\text{HCO}_3^-$ exchange activity that monitor changes of pH_i are not straightforward to interpret as they integrate the rate of HCO_3^- transport and HCO_3^- metabolism by cytosolic CAII. To assay $\text{Cl}^-/\text{HCO}_3^-$ exchange activity independent of pH_i measurements, we evaluated Cl^- transport using a membrane-impermeant Cl^- -sensitive dye, MQAE-AM, whose AM ester structure allows intracellular accumulation as cytosolic esterases cleave the compound to the membrane-impermeant MQAE (38). MQAE is not a ratiometric dye, meaning that we could not internally correct for photobleaching (Fig. 3.6, uncorrected). To correct for this photobleaching we continuously monitored the fluorescence of MQAE-loaded non-transfected HEK293 (Fig. 3.6). We fitted the rate of photobleaching to an exponential decay equation. The inverse of this equation was then used to correct the fluorescence data for photobleaching. Following correction for photobleaching, MQAE fluorescence in HEK293 cells was relatively flat (Fig. 3.6). Fluorescence in the initial 150 s decayed, even following correction for photobleaching (Fig. 3.6, corrected). Since data in this time period was not used in the measurements of rates of change of intracellular Cl^- , this would not affect the rates of transport measured here. All Cl^- transport assay data described below has been corrected for photobleaching.

Transfected cells were incubated with MQAE-AM and $\text{Cl}^-/\text{HCO}_3^-$ exchange assays were performed in $\text{CO}_2/\text{HCO}_3^-$ -containing medium, by alternate perfusion with a Cl^- -containing Ringer's buffer or Cl^- -free gluconate-containing Ringer's buffer (Fig. 3.7). Switching to Cl^- -free buffer established an outward-

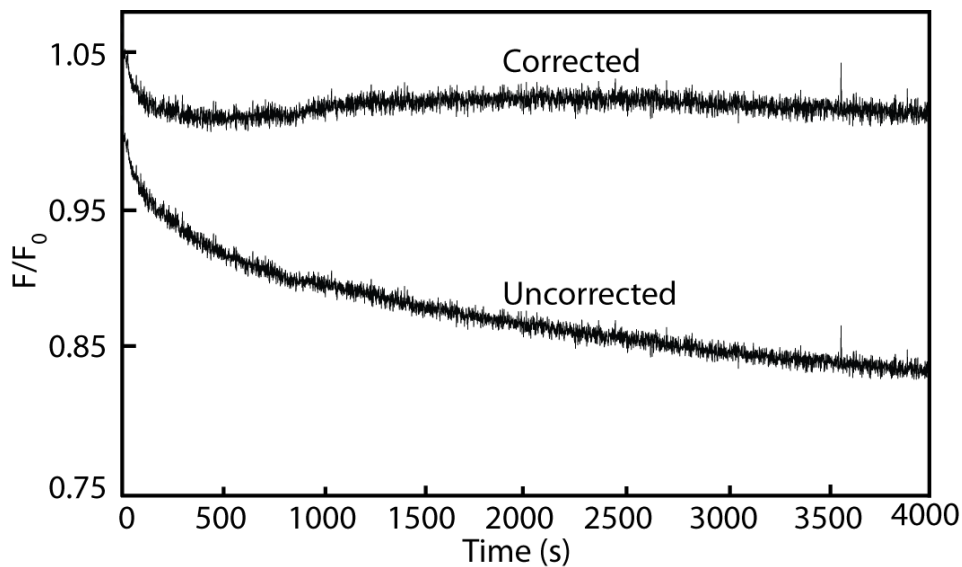


Fig. 3.6. Correction of MQAE fluorescence Photobleaching. Untransfected HEK293 cells were grown on poly-L-lysine-coated glass coverslips. Cells were loaded with MQAE-AM as described under Assays for Chloride Transport (Materials and Methods). Coverslips were mounted in fluorescence cuvettes and subjected to perfusion with Ringer's buffer, containing $\text{CO}_2/\text{HCO}_3^-$. Cells were illuminated at 350 nm and emission was recorded at 460 nm (uncorrected). A first order exponential decay curve of F/F_0 versus time was fitted to the raw data (Uncorrected) and the extent of photobleaching was corrected for photobleaching (Corrected), using the resultant exponential decay equation as described under Correction for MQAE Photobleaching (Materials and Methods).

directed Cl^- gradient, allowing AE1 to facilitate Cl^- efflux in exchange for HCO_3^- influx. Upon switching to the gluconate-containing buffer, the $[\text{Cl}^-]_i$ decreased (Fig. 3.7); $[\text{Cl}^-]_i$ returned to baseline after switching to the Cl^- -containing buffer (Fig. 3.7). After each assay of AE1 Cl^- transport, measurements of MQAE fluorescence were converted to $[\text{Cl}^-]_i$ by generating a Stern-Volmer curve (Fig. 3.8). Use of a double ionophore calibration technique with high K^+ -nigericin and tributyltin, enabled the clamping of $[\text{Cl}^-]_i$ to medium $[\text{Cl}^-]$. The calculated K_{sv} for Cl^- in HEK293 cells, $19 \pm 3 \text{ M}^{-1}$ (Fig. 3.8), was comparable to previous values (18).

We followed the rate of change of $[\text{Cl}^-]_i$ as cells were alternately exposed to Ringer's buffer with 140 mM or 0 mM Cl^- in the presence of $\text{CO}_2/\text{HCO}_3^-$ (Figs. 3.9A-C). In this case, change of the Cl^- gradient will drive $\text{Cl}^-/\text{HCO}_3^-$ exchange. In Cl^- -containing Ringer's buffer, steady-state intracellular Cl^- was in the 85-90 mM range (Figs. 3.9-3.10, initial open bar), consistent with the reported resting $[\text{Cl}^-]$ in HEK293 cells (60-100 mM) (17). The rate of Cl^- transport was measured from the initial rate of decrease of $[\text{Cl}^-]_i$ after switching to the Cl^- -free Ringer's buffer, and was normalized for the expression of AE1 at the cell surface (Fig. 3.9D). The rate of change of $[\text{Cl}^-]_i$ associated with vector alone-transfected cells was subtracted from rates measured for AE1 and AE1 fusion protein expressing cells. AE1.CAII had $\text{Cl}^-/\text{HCO}_3^-$ exchange activity indistinguishable from AE1 alone ($93 \pm 4\%$ versus AE1, $p < 0.2$) (Fig. 3.9D). Interestingly, this mirrored the results seen in $\text{Cl}^-/\text{HCO}_3^-$ exchange assays, that measured the rate of change of pH_i (Fig. 3.3B).

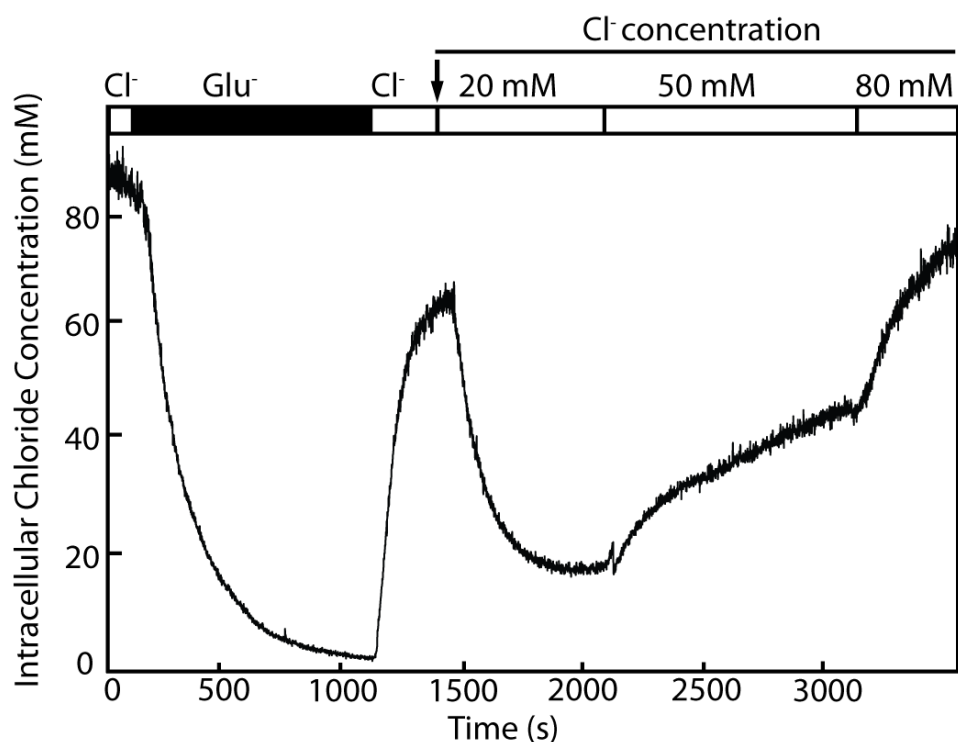


Fig. 3.7. $\text{Cl}^-/\text{HCO}_3^-$ exchange activity of AE1 assessed by monitoring changes of $[\text{Cl}^-]_i$. AE1-transfected HEK293 cells were loaded with the Cl^- -sensitive dye, MQAE-AM. Coverslips were mounted in a fluorescence cuvette and subjected to $\text{Cl}^-/\text{HCO}_3^-$ exchange assay. Cells were perfused initially with a Cl^- -containing Ringer's buffer (open bar) and switched to Ringer's buffer in which Cl^- was replaced by gluconate (Glu^- , filled bar), in the presence of HCO_3^- , then switched to Cl^- -containing buffer again. MQAE fluorescence was calibrated against $[\text{Cl}^-]_i$ by sequential perfusion in calibration buffers, containing varied $[\text{Cl}^-]$ (20, 50 and 80 mM, starting at arrow) in the presence of the ionophores, tributyltin and nigericin. At the end of the experiment, fluorescence was quenched by addition of 150 mM KSCN.

Fusion of CAII-V143Y to AE1, however, impaired $\text{Cl}^-/\text{HCO}_3^-$ exchange activity relative to AE1 alone ($40\pm 2\%$ *versus* AE1) as assessed by monitoring $[\text{Cl}^-]_i$ (Fig.3.9D). Importantly, the rate of $\text{Cl}^-/\text{HCO}_3^-$ exchange of AE1.CAII-V143Y was approximately half that of AE1.CAII, when measuring Cl^- flux. This indicates that the presence of catalytically-active CAII fused to AE1 nearly doubles the rate of $\text{Cl}^-/\text{HCO}_3^-$ transport (relative to AE1.CAII-V143Y), when measuring the rate of coupled Cl^- transport in $\text{Cl}^-/\text{HCO}_3^-$ assays.

In addition to mediating the transport of the physiological substrates, Cl^- and HCO_3^- , AE1 also transports other anions including NO_3^- , I^- and SO_4^{2-} (14). Thus far, our data indicate that fusion of CAII-V143Y to the C-terminal tail of AE1 impairs $\text{Cl}^-/\text{HCO}_3^-$ exchange activity relative to AE1 alone and relative to the AE1.CAII-wildtype. The simplest explanation for the lowered activity of AE1.CAII-V143Y is that CAII-V143Y is catalytically inactive, and that the loss of carbonic anhydrase activity reduces $\text{Cl}^-/\text{HCO}_3^-$ exchange activity. Another possibility, however, is that fusion of CAII-V143Y to AE1 caused misfolding of the transporter, thus reducing its functional activity. To test this possibility, HEK293 cells expressing AE1, AE1.CAII or AE1.CAII-V143Y were subjected to $\text{Cl}^-/\text{NO}_3^-$ exchange assays by monitoring $[\text{Cl}^-]_i$ using MQAE fluorescence, as described above (Figs. 3.10A-C). Fusion of CAII or CAII-V143Y to AE1 reduced the rate of $\text{Cl}^-/\text{NO}_3^-$ exchange by the same amount relative to activity of AE1 alone-transfected cells (Fig. 3.10D). This indicates that fusion of either form of CAII to AE1 compromises transport activities of AE1 to the same degree, *in assays that are independent of carbonic anhydrase activity*.

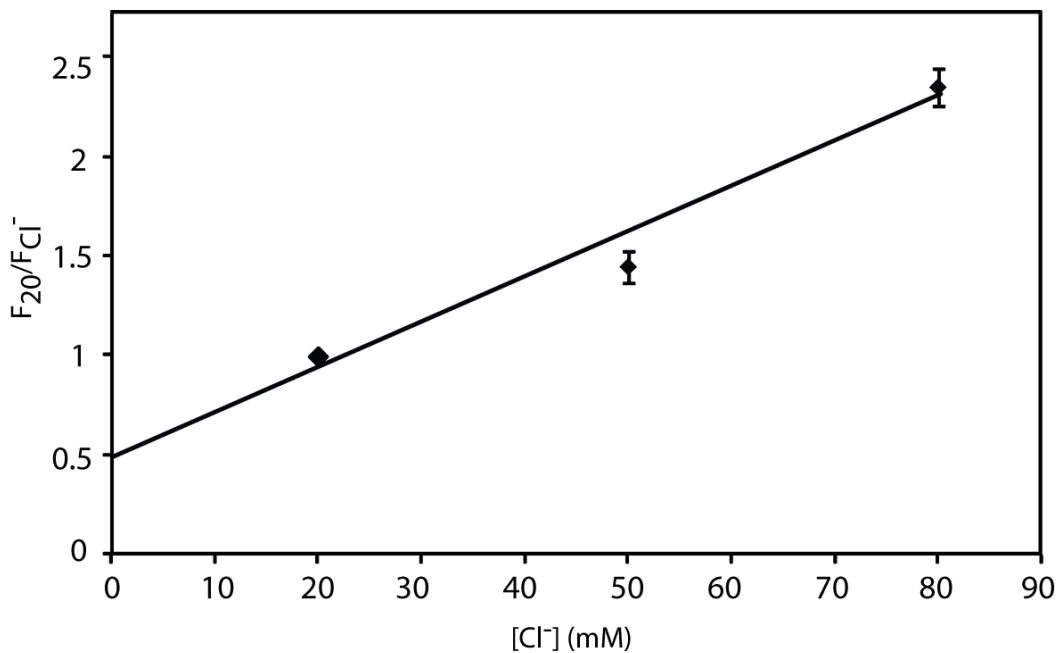


Fig. 3.8. Calibration curve to calculate Stern-Volmer Constant (K_{sv}). Transfected HEK293 cells, grown on glass coverslips, were loaded with the Cl^- -sensitive dye, MQAE, and subjected to $\text{Cl}^-/\text{HCO}_3^-$ exchange assays as described under *Assays of Chloride Transport*. Following the assays, cells were perfused with Ringer's buffer with varied concentrations of KCl, in the presence of the Cl^- ionophore, nigericin/tributyltin. Raw data were corrected for photobleaching. F_{20} is the MQAE fluorescence in the presence of 20 mM Cl^- after subtraction of background (F in the presence of KSCN); F_{Cl^-} is the MQAE fluorescence in the presence of intracellular Cl^- after subtraction of background fluorescence. Each symbol represents the mean \pm SEM for 5 independent experiments.

3.3 Discussion

In this study, we have provided evidence that association of CAII with the C-terminus of AE1 increases the rate of $\text{Cl}^-/\text{HCO}_3^-$ exchange, as shown by the effect of fusion of CAII to AE1. Previous studies revealed that the AE1 C-terminal tail binds cytosolic CAII (30, 35-37), which increases the rate of $\text{Cl}^-/\text{HCO}_3^-$ exchange by approximately 40% (30). In contrast, studies of the electrogenic $\text{Na}^+/\text{HCO}_3^-$ co-transporter, NBCe1, suggested that fusion of CAII to the C-terminus of NBCe1 did not affect the rate of $\text{Na}^+/\text{HCO}_3^-$ co-transport (20). To determine whether AE1 might be activated by CAII in a way that NBCe1 is not, we fused human CAII to the C-terminus of AE1. The results presented here revealed that fusion of CAII to AE1 increases AE1 $\text{Cl}^-/\text{HCO}_3^-$ exchange activity by about two-fold, when compared to fusion of catalytically-dead CAII-V143Y to AE1. Importantly, this increase in transport activity was observed in $\text{Cl}^-/\text{HCO}_3^-$ exchange assays that followed changes of both intracellular pH and intracellular Cl^- .

This work provides further evidence for a bicarbonate transport metabolon, the physical complex of a bicarbonate transporter with a carbonic anhydrase enzyme, which together facilitates coupled $\text{CO}_2/\text{HCO}_3^-$ metabolism and HCO_3^- transport (30). The bicarbonate transport metabolon model states that association of CAII with the surface of AE1 should activate AE1 transport activity. In anion exchange assays that were independent of carbonic anhydrase activity ($\text{Cl}^-/\text{HCO}_3^-$ assays in the presence of ATZ and $\text{Cl}^-/\text{NO}_3^-$ exchange assays) AE1.CAII and AE1.CAII-V143Y had indistinguishable

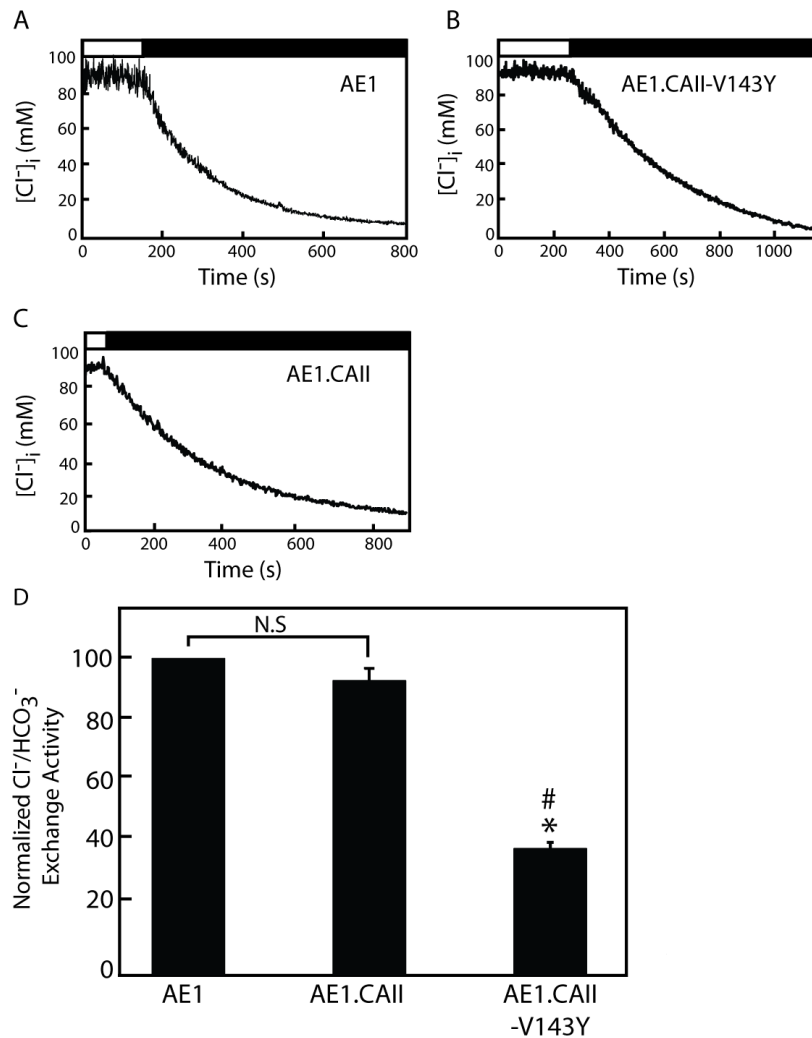


Fig. 3.9. Rate of Cl⁻/HCO₃⁻ exchange of AE1 and fusion proteins, monitored by changes of [Cl⁻]_i. HEK293 cells were transiently transfected with cDNA encoding AE1 (A), AE1.CAII-V143Y (B) or AE1.CAII (C) and grown on glass coverslips. Forty-eight hours following transfection, cells were loaded with MQAE-AM, mounted in fluorescence cuvettes and perfused alternately with Cl⁻-containing (open bar) or Cl⁻-free (filled bar) Ringer's buffer, in the presence of HCO₃⁻. After converting fluorescence measurement to [Cl⁻]_i, the rate of Cl⁻/HCO₃⁻ exchange was assessed by the linear portion after switching to Cl⁻-free buffer. D, Cl⁻/HCO₃⁻ exchange activity normalized for amount of protein at the cell surface and

expressed as percentage of AE1 alone-transfected cells ($n=4$). * indicates statistically significant, compared to AE1; # indicates statistically significant, compared to AE1.CAII, by one-way ANOVA.

rates of transport that were significantly lower than AE1. Fusion of CAII, whether WT or mutant, thus compromises AE1 anion transport activity. In contrast, anion transport assays dependent on functional CAII ($\text{Cl}^-/\text{HCO}_3^-$ assays in the absence of ATZ and $\text{Cl}^-/\text{HCO}_3^-$ exchange assays that monitored rates of pH_i or $[\text{Cl}]_i$ change) revealed that AE1.CAII had much higher transport activity than AE1.CAII-V143Y, activity that was indistinguishable from AE1 alone. Viewed in this light, the presence of CAII catalysis at the surface of AE1 potentiated AE1 $\text{Cl}^-/\text{HCO}_3^-$ exchange activity, lending support to the bicarbonate transport metabolon model.

The simplest explanation for these results is that fusion of CAII to the AE1 C-terminus adversely affected the anion transport activity of AE1.CAII and AE1.CAII-V143Y. AE1.CAII and AE1.CAII-V143Y differ only by a point mutation that abrogates CAII-V143Y catalysis. The increased $\text{Cl}^-/\text{HCO}_3^-$ exchange activity of AE1.CAII can thus only be explained by the presence of catalytically-active CAII fused to its C-terminus. Support for this interpretation is provided by assays of $\text{Cl}^-/\text{NO}_3^-$ exchange, which revealed that AE1.CAII and AE1.CAII-V143Y had the same level of $\text{Cl}^-/\text{NO}_3^-$ exchange activity and that this level was much lower than AE1 alone. The reduction in transport activity of the two AE1 fusion proteins suggests that the presence of CAII at the AE1 C-terminus was detrimental to AE1's ability to transport anions. Since we normalized transport rates of AE1 and AE1 fusion proteins for differences in cell surface expression, the transport activity defect does not arise from differences in cell surface expression. We therefore speculate that the presence

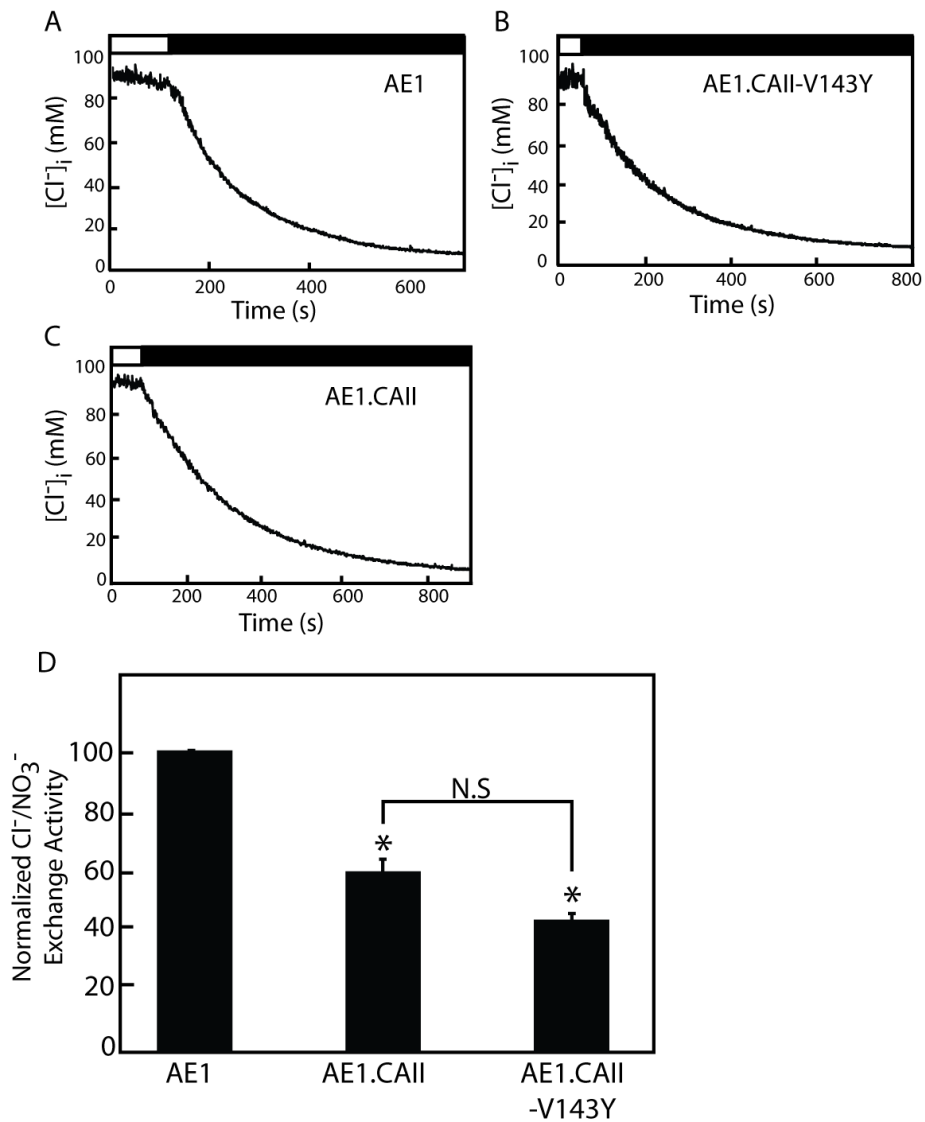


Fig. 3.10. Rate of Cl⁻/NO₃⁻ exchange by AE1 and AE1 fusion proteins. HEK293 cells were transiently transfected with cDNA encoding AE1 (A), AE1.CAII-V143Y (B) or AE1.CAII (C) and grown on glass coverslips. The cells were loaded with MQAE-AM dye, mounted in fluorescence cuvettes and subjected to Cl⁻/NO₃⁻ exchange assays. Cells were perfused alternately with a Cl⁻-containing (open bar) or NO₃⁻-containing (filled bar) Ringer's buffer, in the absence of HCO₃⁻. After converting fluorescence measurement to [Cl⁻]_i, the rate of Cl⁻/NO₃⁻

exchange was assessed by linear regression after switching to NO_3^- buffer. D, Cl^- / NO_3^- exchange activity normalized for total AE1 expression at the cell surface and expressed as percentage of AE1 alone-transfected cells ($n=4$). * indicates statistically significant, compared to AE1, by one-way ANOVA.

of CAII fused to the AE1 C-terminus reduced the conformational flexibility of AE1 during its transport cycle, or presented a steric barrier to substrate anion access. There is no evidence to suggest that CAII-V143Y has a structure significantly different from CAII-wildtype since the mutation is in the catalytic cleft (12), not on the surface and CAII-V143Y is unaltered in its ability to bind AE1 (30). The observation that fusion of wildtype or catalytically-inactive CAII to AE1 resulted in the same level of $\text{Cl}^-/\text{NO}_3^-$ exchange activity provides further evidence that CAII catalysis at the surface of AE1 stimulates AE1 transport activity. That is, CAII activity is required to potentiate $\text{Cl}^-/\text{HCO}_3^-$ exchange but not $\text{Cl}^-/\text{NO}_3^-$ exchange. In experiments that removed or mutated the CAB site in AE1, similar results were found, where the CAB mutations decreased $\text{Cl}^-/\text{HCO}_3^-$ exchange activity, but left Cl^-/Cl^- exchange activity intact (8).

In these experiments, we have studied an “intramolecular transport metabolon”. That is, the fusion of the transport protein to the enzyme that metabolizes the transported substrate has produced a protein with two coupled enzymatic activities in one molecule. Precedent is found in eight bacterial species that span four bacterial kingdoms, in which integral membrane proteins have fused to their C-terminus a protein that appears to be a carbonic anhydrase (11). In this bioinformatic study (11), a member of the SulP family of sulfate transporters was observed to have a carbonic anhydrase homologue fused into a single open reading frame (11). SulP contains the STAS domain present in members of the SLC26 family of $\text{Cl}^-/\text{HCO}_3^-$ exchangers. While it has not been shown experimentally, the implication of the study is that the SulP protein may be

a bicarbonate transporter, with fused carbonic anhydrase activity, representing an intramolecular transport metabolon. A caveat is that in fish carbonic anhydrase is required for sulfate secretion (27), possibly suggesting that SulP could be involved in sulfate transport. Interestingly in bacteria other possible intramolecular transport metabolons are found. For example, a SulP sulfate permease transporter is fused to a thiosulfatecyanide sulfotransferase enzyme, suggesting that localization of metabolic enzymes to the surface of a transport protein is a common feature in bacterial biology. Although the bacterial intramolecular transport metabolons have not been subjected to functional study, our data suggests that intramolecular fusion of the metabolic enzyme and the transporter will increase the coupled metabolic/transport flux. Intramolecular transport metabolons have not been reported in eukaryotes except those artificially constructed ((20) and the present report), as far as we can find. It may be that expression of the CA enzyme and HCO_3^- transporter in separate genes, rather than into a single gene, affords an additional mode of regulation in eukaryotes, either at the expression level or by modulation of the interaction of the CA with the bicarbonate transporter (4).

These results support the concept of a bicarbonate transport metabolon, but stand in conflict with studies of NBCe1, in which fusion of CAII to the protein's C-terminus were without effect on NBCe1 HCO_3^- transport activity (20). The data presented here do not fundamentally disagree with the report on NBCe1-CAII fusion, in that we also showed that CAII fusion did not affect the rate of HCO_3^- transport. What differed here, and changed the interpretation of

the data, was the control fusion of catalytically-dead CAII-V143Y to AE1, a control that was not included in the study of NBCe1 fused to CAII.

In the present study, CAII was fused to the C-terminus of AE1 (V911), leaving the endogenous CAB site (L886-D890) available for occupancy by a free CAII molecule. CAII-V143Y is able to bind to the CAB site and reduces $\text{Cl}^-/\text{HCO}_3^-$ exchange activity of AE1, by acting in a dominant negative manner to compete with endogenous CAII-wildtype from its binding site on AE1 (30). Consistent with the previous report (30), we found that over-expression of CAII-V143Y at levels approximately five-fold higher than endogenous CAII in HEK293 cells, dramatically decreased the activity of AE1 in a dose-dependent manner. In contrast, the transport activity of AE1.CAII was unaffected by CAII-V143Y expression. This finding can be interpreted in two ways 1. The amount of CAII fused to the C-terminus of AE1.CAII is sufficient to maximally activate $\text{Cl}^-/\text{HCO}_3^-$ exchange activity. This is reasonable given that in red blood cells (21) and in AE1-transfected HEK293 cells (30) the stoichiometry of AE1CAII expression is about 11, suggesting that one CAII/AE1 maximizes transport activity. Moreover, the catalytic rate of CAII is $10^6 \cdot \text{s}^{-1}$, which is much faster than the maximum transport activity of AE1 (5×10^4 anions. s^{-1}), so one CAII associated with AE1 provides an excess of substrate. 2. Fusion of CAII sterically hinders the ability of a second CAII to bind the CAB site or that fused CAII binds to that available CAII binding site on AE1. These two possibilities are not mutually exclusive. The data therefore leave open the possibility that a

second CAII might bind the CAB site, but if so it does not increase the rate of HCO_3^- transport by AE1.CAII.

Here, we have presented data that support the concept of the bicarbonate transport metabolon association of a carbonic anhydrase enzyme with a bicarbonate transporter to facilitate coupled $\text{CO}_2/\text{HCO}_3^-$ metabolism and HCO_3^- transport. This serves to reduce the diffusional distance, hence, enhancing the transport activity of the HCO_3^- transporter. Fusion of catalytically-active CAII to the C-terminus of AE1 increased the rate of $\text{Cl}^-/\text{HCO}_3^-$ exchange in comparison to fusion of catalytically-inactive CAII. This “intramolecular transport metabolon” is reminiscent of those found in many bacteria (11), so our data provide support for the effect of these gene fusions found in bacteria. Our data show that $\text{Cl}^-/\text{HCO}_3^-$ exchange activity is activated by localization of CAII to the surface of AE1, as proposed in the bicarbonate transport metabolon model.

Bibliography

1. **Alper SL.** The Band 3-related anion exchanger family. *Annu Rev Physiol* 53: 549-564, 1991.
2. **Alper SL.** Molecular physiology of SLC4 anion exchangers. *Exp Physiol* 91: 153-161, 2006.
3. **Alper SL, Chernova MN, and Stewart AK.** How pH regulates a pH regulator: a regulatory hot spot in the N-terminal cytoplasmic domain of the AE2 anion exchanger. *Cell Biochem Biophys* 36: 123-136, 2002.
4. **Alvarez BV, Kieller DM, Quon AL, Markovich D, and Casey JR.** Slc26a6: A cardiac chloride/hydroxyl exchanger and predominant chloride/bicarbonate exchanger of the heart. *J Physiol* 561: 721-734, 2004.
5. **Alvarez BV, Vilas GL, and Casey JR.** Metabolon disruption: a mechanism that regulates bicarbonate transport. *EMBO J* 24: 2499-2511, 2005.
6. **Becker HM and Deitmer JW.** Carbonic Anhydrase II increases the activity of the human electrogenic $\text{Na}^+/\text{HCO}_3^-$ cotransporter. *J Biol Chem* 282: 13508-13521, 2007.
7. **Cordat E and Casey JR.** Bicarbonate transport in cell physiology and disease. *Biochem J* 417: 423-439, 2009.
8. **Dahl NK, Jiang L, Chernova MN, Stuart-Tilley AK, Shmukler BE, and Alper SL.** Deficient HCO_3^- transport in an AE1 mutant with normal Cl^- transport can be rescued by carbonic anhydrase II presented on an adjacent AE1 protomer. *J Biol Chem* 278: 44949-44958, 2003.

9. **Davies SL, Best L, and Brown PD.** HCO₃⁻-dependent volume regulation in alpha-cells of the rat endocrine pancreas. *Pflugers Arch* 458: 621-629, 2009.
10. **Dhermy D, Burnier O, Bourgeois M, and Grandchamp B.** The red blood cell band 3 variant (band 3Biceetrel:R490C) associated with dominant hereditary spherocytosis causes defective membrane targeting of the molecule and a dominant negative effect. *Mol Membr Biol* 16: 305-312, 1999.
11. **Felce J and Saier MH, Jr.** Carbonic anhydrases fused to anion transporters of the SulP family: evidence for a novel type of bicarbonate transporter. *J Mol Microbiol Biotechnol* 8: 169-176, 2004.
12. **Fierke CA, Calderone TL, and Krebs JF.** Functional consequences of engineering the hydrophobic pocket of carbonic anhydrase II. *Biochemistry* 30: 11054-11063, 1991.
13. **Gonzalez-Begne M, Nakamoto T, Nguyen HV, Stewart AK, Alper SL, and Melvin JE.** Enhanced formation of a HCO₃⁻ transport metabolon in exocrine cells of Nhe1^{-/-} mice. *J Biol Chem* 282: 35125-35132, 2007.
14. **Jennings ML.** Structure and function of the red blood cell anion transport protein. *Annu Rev Biophys Biophys Chem* 18: 397-430, 1989.
15. **Jennings ML, Anderson MP, and Monaghan R.** Monoclonal antibodies against human erythrocyte Band 3 protein: localization of proteolytic cleavage sites and stilbenedisulfonate-binding lysine residues. *J Biol Chem* 261: 9002-9010, 1986.

16. **Johnson DE and Casey JR.** Cytosolic H⁺ Microdomain Developed Around AE1 During AE1-Mediated Cl⁻/HCO₃⁻ Exchange. *J Physiol* In Press, 2011.
17. **Lamprecht G, Baisch S, Schoenleber E, and Gregor M.** Transport properties of the human intestinal anion exchanger DRA (down-regulated in adenoma) in transfected HEK293 cells. *Pflugers Arch* 449: 479-490, 2005.
18. **Lamprecht G, Baisch S, Schoenleber E, and Gregor M.** Transport properties of the human intestinal anion exchanger DRA (down-regulated in adenoma) in transfected HEK293 cells.
19. **Low PS.** Structure and function of the cytoplasmic domain of Band 3: center of erythrocyte membrane-peripheral protein interactions. *Biochim Biophys Acta* 864: 145-167, 1986.
20. **Lu J, Daly CM, Parker MD, Gill HS, Piermarini PM, Pelletier MF, and Boron WF.** Effect of human carbonic anhydrase II on the activity of the human electrogenic Na⁺/HCO₃⁻ cotransporter NBCe1-A in *Xenopus* oocytes. *J Biol Chem* 281: 19241-19250, 2006.
21. **Maren TH.** Carbonic anhydrase: chemistry, physiology, and inhibition. *Physiol Rev* 47: 595-781, 1967.
22. **McMurtrie HL, Cleary HJ, Alvarez BV, Loiselle FB, Sterling D, Morgan PE, Johnson DE, and Casey JR.** The bicarbonate transport metabolon. *J Enzyme Inhib Med Chem* 19: 231-236, 2004.

23. **Passow H.** Molecular aspects of Band 3-mediated anion transport across the red blood cell membrane. *Rev Physiol Biochem Pharmacol* 103: 61-223, 1986.
24. **Pushkin A, Abuladze N, Gross E, Newman D, Tatishchev S, Lee I, Fedotoff O, Bondar G, Azimov R, Ngyuen M, and Kurtz I.** Molecular mechanism of kNBC1-carbonic anhydrase II interaction in proximal tubule cells. *J Physiol* 559: 55-65, 2004.
25. **Quilty JA and Reithmeier RA.** Trafficking and folding defects in hereditary spherocytosis mutants of the human red cell anion exchanger. *Traffic* 1: 987-998, 2000.
26. **Reithmeier RAF.** A membrane metabolon linking carbonic anhydrase with chloride/bicarbonate anion exchangers. *Blood cells, Molecules and Diseases* 27: 85-89, 2001.
27. **Renfro JL, Maren TH, Zeien C, and Swenson ER.** Renal sulfate secretion is carbonic anhydrase dependent in a marine teleost, *Pleuronectes americanus*. *Am J Physiol* 276: F288-294, 1999.
28. **Romero MF, Fulton CM, and Boron WF.** The SLC4 family of HCO_3^- transporters. *Pflugers Arch* 447: 496-509, 2004.
29. **Sterling D, Brown N, Supuran CT, and Casey JR.** The functional and physical relationship between the downregulated in adenoma bicarbonate transporter and carbonic anhydrase II. *Am J Physiol* 283: C1522-1529, 2002.

30. **Sterling D, Reithmeier RA, and Casey JR.** A Transport Metabolon. Functional Interaction of Carbonic Anhydrase II and Chloride/Bicarbonate Exchangers. *J Biol Chem* 276: 47886-47894, 2001.
31. **Supuran CT.** Carbonic anhydrases--an overview. *Curr Pharm Des* 14: 603-614, 2008.
32. **Tang CH and Lee TH.** The novel correlation of carbonic anhydrase II and anion exchanger 1 in gills of the spotted green pufferfish, *Tetraodon nigroviridis*. *J Exp Zool A Ecol Genet Physiol* 307: 411-418, 2007.
33. **Tanner MJ.** Molecular and cellular biology of the erythrocyte anion exchanger (AE1). *Semin Hematol* 30: 34-57, 1993.
34. **Tanner MJ.** The structure and function of band 3 (AE1): recent developments (review). *Mol Membr Biol* 14: 155-165, 1997.
35. **Vince JW, Carlsson U, and Reithmeier RA.** Localization of the $\text{Cl}^-/\text{HCO}_3^-$ anion exchanger binding site to the amino-terminal region of carbonic anhydrase II. *Biochemistry* 39: 13344-13349, 2000.
36. **Vince JW and Reithmeier RA.** Identification of the Carbonic Anhydrase II Binding Site in the $\text{Cl}^-/\text{HCO}_3^-$ Anion Exchanger AE1. *Biochemistry* 39: 5527-5533, 2000.
37. **Vince JW and Reithmeier RAF.** Carbonic anhydrase II binds to the carboxyl-terminus of human band 3, the erythrocyte $\text{Cl}^-/\text{HCO}_3^-$ exchanger. *J Biol Chem* 273: 28430-28437, 1998.
38. **Woll E, Gschwentner M, Furst J, Hofer S, Buemberger G, Jungwirth A, Frick J, Deetjen P, and Paulmichl M.** Fluorescence-optical

measurements of chloride movements in cells using the membrane-permeable dye diH-MEQ. *Pflugers Arch* 432: 486-493, 1996.

39. **Zhu Q and Casey JR.** The substrate anion selectivity filter in the human erythrocyte $\text{Cl}^-/\text{HCO}_3^-$ exchange protein, AE1. *J Biol Chem* 279: 23565-23573, 2004.

Chapter 4

Role of the Chloride/Bicarbonate Exchanger, AE3, in the Development of Cardiomyocyte Hypertrophy

A manuscript version of this chapter is in preparation for submission as:
Role of the Chloride/Bicarbonate Exchanger, AE3, in the Development of
Cardiomyocyte Hypertrophy.

Daniel Sowah, Brittany F. Brown, Anita Quon, Bernardo V. Alvarez, and Joseph
R. Casey

Brittany F. Brown assisted in the preparation of the manuscript.

Anita Quon contributed to the collection of the RT-PCR data.

Dr. Bernardo V. Alvarez provided the HW/BW data.

Cardiovascular Core Facility, University of Alberta, provided measurements of
cardiac function.

4.1 Introduction

Cardiovascular diseases remain a major cause of death worldwide despite progress in disease outcomes of patients (47). Heart failure (HF) is the common end-stage of many cardiovascular disorders and has a prevalence of 5.8 million in the USA and about 23 million worldwide (16, 31). Annually 550,000 new cases of HF arise in the USA. The intricate molecular events resulting in heart failure remain incompletely understood, but enlargement of cardiac contractile cells (cardiomyocyte hypertrophy) in response to various stimuli is central to the progression to heart failure (27). Cardiac cells are terminally differentiated cells that respond to increased stress by increasing their size rather than mitotically dividing to increase their number (41).

Cardiovascular events that increase myocardial stress (workload) chronically induce hypertrophic growth. Pressure overload, myocardial infarction, obesity, pregnancy or exercise can independently trigger molecular mechanisms culminating in increased cardiomyocyte size. Cardiac hypertrophy occurs to normalize the elevated demand on the myocardium, and can be physiological or pathological depending on the source of the initiating stimuli (34). Physiological hypertrophy prevails in healthy individuals during increased physical activities or in pregnant women. Pathological hypertrophy results from prolonged elevated blood pressure (pressure overload), ischemia accompanied by changes in Ca^{2+} handling, or genetic abnormalities. Initially, pathological hypertrophic growth compensates for the decline in contractile function but ultimately the myocardium becomes decompensated from sustained exposure to the initiating stimuli.

Understanding the distinct pathways mediating cardiac hypertrophic development has potential to identify new drug targets for the management of heart failure.

Intracellular pH (pH_i) regulation is paramount in maintaining normal cardiac function (20, 22). Plasma membrane transporters involved in maintaining pH_i at physiological levels in the heart include the Na^+ - H^+ exchanger (NHE1), Na^+ - HCO_3^- co-transporters (NBC), and $\text{Cl}^-/\text{HCO}_3^-$ exchangers (60, 61). Cytosolic acidification or hormonal stimulation activate NHE1, which facilitates electroneutral Na^+/H^+ exchange, to alkalinize the cytosol (26). Accumulating evidence suggests that NHE1 expression level and activity increase in hypertrophy (58, 63). In the hypertrophied myocardium of the spontaneously hypertensive rats (SHR), there was an increased activation of NHE1 (52) and NHE1 inhibition reduced cardiac hypertrophy and interstitial fibrosis (21). Transgenic mice expressing activated NHE1 exchanger had enlargement of the heart and increased sensitivity to hypertrophic stimulation (50). Since NHE1 activation induces acid extrusion, alkalinization should accompany NHE1 activation. NHE1 activation was not, however, accompanied by increased pH_i , although cytosolic Na^+ was elevated (52). Moreover, under alkaline conditions, NHE1 activity is self-inhibited, which suggests that an acidifying mechanism running counter to NHE1 is necessary for sustained NHE1 activation (24, 32, 33, 35). Indeed, $\text{Cl}^-/\text{HCO}_3^-$ exchange mediated by AE3 provides this acidifying pathway (20, 22, 61).

The heart expresses three $\text{Cl}^-/\text{HCO}_3^-$ exchanger isoforms: AE1, AE2 and AE3 (8, 61). SLC26A6 is expressed in the heart (7, 38, 44), which may facilitate

the Cl⁻/OH⁻ exchanger (CHE) reported to occur there (51). Two AE3 variants, AE3 full length (AE3fl) and cardiac AE3 (AE3c) are expressed in the heart; AE3fl is also expressed in the brain and retina (3, 4, 17). Phenylephrine (PE) and angiotensin II (ANGII), acting on their G-protein-coupled receptors (GPCRs), activate AE3fl via protein kinase C (PKC). Interestingly, PKC can indirectly activate NHE1 via MAPK-dependent mechanisms (18). Moreover, carbonic anhydrase II (CAII), another modulator of the PE-dependent hypertrophic growth, interacts with both NHE1 and AE3 to provide their respective transport substrates, H⁺ and HCO₃⁻ (8).

CAII activation was recently found to be important in the induction of cardiomyocyte hypertrophy. In isolated rat cardiomyocytes, inhibition of CAII catalytic activity reduced PE and ANGII-induced cardiomyocyte hypertrophy (11). Additionally, infection of neonatal rat cardiomyocytes with adenoviral constructs encoding catalytically inactive CAII mutant, CAII-V143Y, reduced the response of the cardiomyocytes to hypertrophic stimuli, suggested to arise from a dominant negative mode of action (15). Cardiomyocytes from CAII-deficient mice had physiological hypertrophy, but were unresponsive to hypertrophic stimulation (15). Finally, expression of CAII and CAIV was elevated in the hypertrophic ventricles from failing human hearts, indicating that elevation of carbonic anhydrases is a feature of heart failure in people (9). Taken together, these findings show that CAII plays a role in the development of cardiomyocyte hypertrophy.

Several reports revealed that CAII physically and functionally interacts with $\text{Cl}^-/\text{HCO}_3^-$ anion exchangers to enhance the transport activity of anion exchangers forming a bicarbonate transport metabolon (13, 29, 55, 56), although some reports have questioned the significance of CAII interaction with AE1 (1, 45, 53). CAII also interacts physically and functionally with NHE1 to increase the exchange activity (42, 43). These observations suggest that simultaneous stimulation of AE3 and NHE1 coupled with enhanced CAII activity during hypertrophic intervention may be involved in the hypertrophic signaling triggered by PE, ANGII or endothelin I (ET-I).

Accumulating evidence suggests a significant role of AE3 in cardiac function. AE3 $\text{Cl}^-/\text{HCO}_3^-$ exchange activity is involved in cardiac contractility by altering cardiac Ca^{2+} handling (54). Moreover, disruption of the *ae3* gene in mice resulted in an exacerbated cardiac function and precipitated heart failure in hypertrophic cardiomyopathy mice (2). Taken together, these findings suggest that the AE3 $\text{Cl}^-/\text{HCO}_3^-$ exchanger is critical in heart growth and function but the exact mechanism remains unknown.

In the present study, we examined the role of AE3 in cardiomyocyte hypertrophy, using AE3-deficient (*ae3*^{-/-}) mice. Cardiac growth parameters and fetal gene reactivation were measured in the presence of pro-hypertrophic stimulation in cardiomyocytes from *ae3*^{-/-} mice. We also examined the role of AE3 in cardiomyocyte steady state pH_i , using the *ae3*^{-/-} mice. Our results indicate that *ae3* deletion prevents cardiomyocyte hypertrophy and reduces the rate of pH_i

recovery in cardiomyocytes, reinforcing the importance of AE3 in cardiovascular pH regulation and the development of cardiomyocyte hypertrophy.

4.2 Results

4.2.1 Cardiac Development in *ae3*^{-/-} mouse

To examine the role of AE3 in heart development, we characterized age-matched wildtype (WT) and *ae3*^{-/-} mice (~three months old). Breeding yielded Mendelian ratios of litters of both WT and *ae3*^{-/-} mice, indicating that loss of the AE3 does not affect prenatal survival. While the body weights of age-matched WT and *ae3*^{-/-} mice were not significantly different (Fig. 4.1A), the difference in heart weights between the groups was statistically significant (Fig. 4.1B). As a result, the HW/BW ratio, an index of cardiac hypertrophy, was reduced in the *ae3*^{-/-} mice relative to their WT counterparts (Fig. 4.1C and 4.1D), suggesting that AE3 has a role in heart growth. To determine the ventricular wall thickness and chamber diameter of transverse and longitudinal sections of the heart, images were analyzed by Image-Pro Plus software. Our data revealed no differences in the wall thickness (WT, TS: 1.1±0.02 mm, LS: 0.97±0.04 mm vs. KO, TS: 0.96±0.03 mm, LS: 0.95±0.03 mm, *n*=3) and the chamber diameter (WT, TS: 2.4±0.06 mm, LS: 3.5±0.05 mm vs. KO, TS: 2.2±0.04 mm, LS: 3.2±0.06 mm, *n*=3) of WT (left panel) and *ae3* null (right panel) hearts stained with hematoxylin/eosin (Fig. 4.2A-C). Interestingly, these findings mirrored results from the echocardiography measurements shown in Table 4.1.

4.2.2 Blood Pressure and Echocardiography in *ae3*^{-/-} mice

Cardiovascular performance of *age-matched WT* and *ae3*^{-/-} mice was assessed by echocardiography. No major variations in cardiovascular functional parameters between WT and *ae3*^{-/-} mice (~three months old) were observed, except for a significant decrease in the mitral value E/A ratio in *ae3*^{-/-} mice (Table 4.1). While this would suggest that more blood is entering the ventricle during the atrial systolic phase than during ventricular relaxation, other parameters of diastolic cardiac function (E/E' ratio, IVRT) were unaffected. It is therefore unlikely that *ae3*^{-/-} exhibit diastolic dysfunction. Systemic blood pressure measurements were also performed using the non-invasive tail cuffing approach. No significant difference in the systemic blood pressure of WT and *ae3*^{-/-} mice was observed (Table 4.1). Overall, these observations suggest that loss of AE3 does not affect cardiovascular performance under basal conditions.

4.2.3 Cardiomyocyte size in *ae3*^{-/-} mice

Previous studies demonstrated that cardiomyocytes isolated from adult mice are not susceptible to culturing as they lose their typical rod-shaped morphology within a few hours of staying in a culture medium (37). To determine the response of cardiomyocytes to hypertrophic intervention with PE and ANGII, we first have to establish optimal conditions to culture cardiomyocytes from adult mice. To achieve this, cardiomyocytes isolated from adult mice were cultured at various intervals (3 h, 6 h, 12 h, 18 h and 24 h) and subjected to hypertrophic stimulation with PE (10 μ M) or ANGII (1 μ M) as

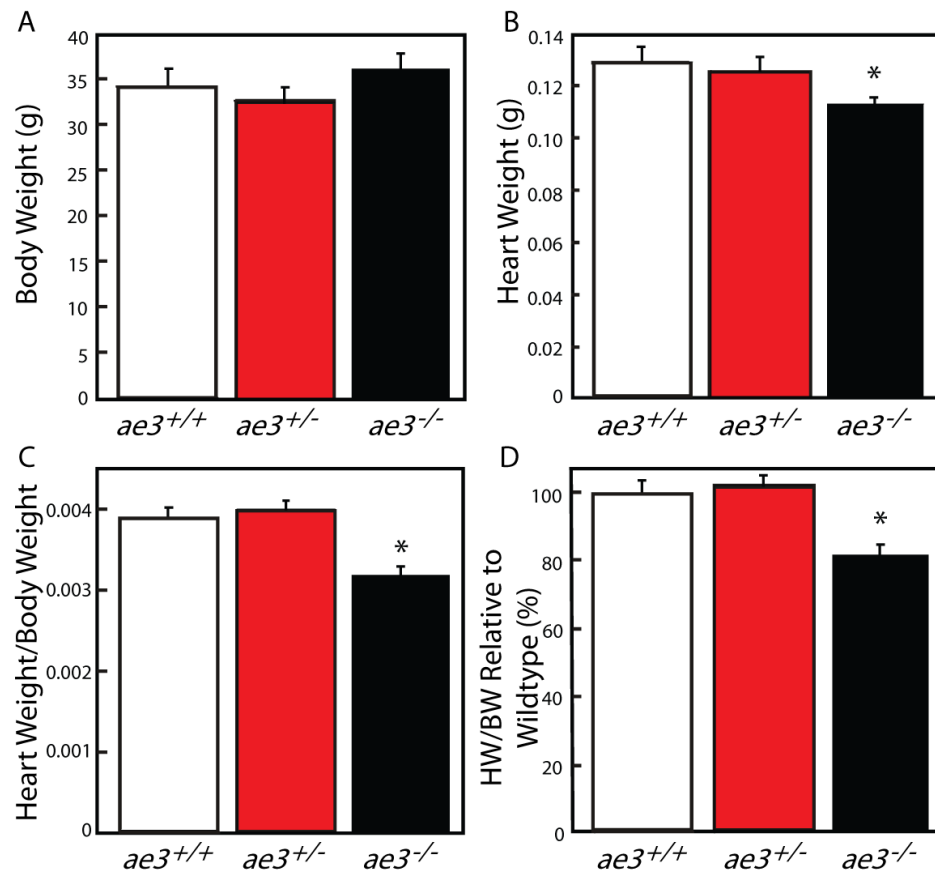


Fig. 4.1 Heart weight (wet) to body weight ratio of wildtype ($ae3^{+/+}$), heterozygote ($ae3^{+/-}$) and knock-out ($ae3^{-/-}$) mice. Mice lacking the $ae3$ gene were generated. Body weights (BW) of the $ae3^{-/-}$, $ae3^{+/-}$ and the $ae3^{+/+}$ littermates were measured. Hearts, surgically removed from anaesthetized mice and trimmed of extracardiac tissues, were measured to obtain the ventricular weight (HW). The HW/BW ratio, an index of hypertrophy, was calculated and expressed relative to $ae3^{+/+}$ animals. * $P < 0.05$, relative to $ae3^{+/+}$ (n=8).

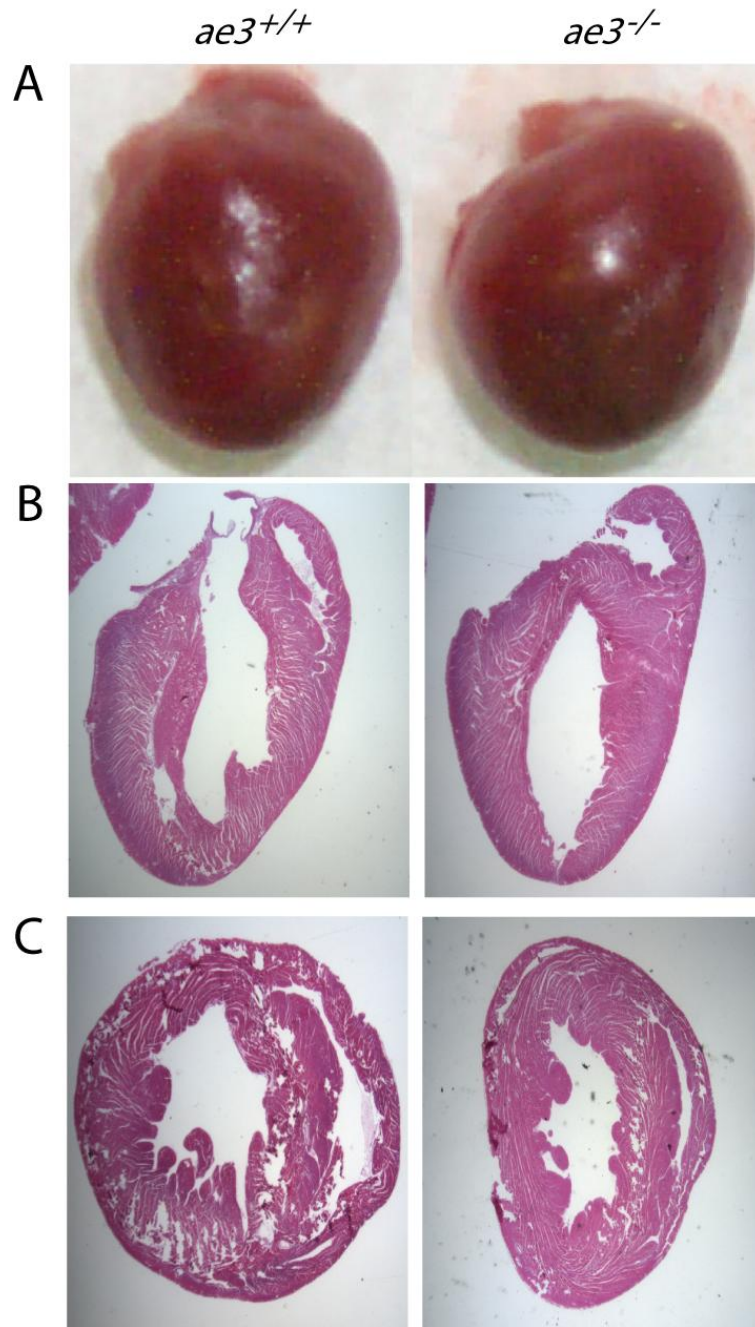


Fig. 4.2 Cross-sections of heart from wildtype (*ae3^{+/+}*) and knock-out (*ae3^{-/-}*) mice. Whole hearts (A) were removed from euthanized mice and longitudinal (B) and transverse (C) sections of the ventricle were performed to compare the chamber diameter of *ae3^{-/-}* and *ae3^{+/+}* hearts.

shown in Fig. 4.4. The concentrations of PE and ANGII were selected based on previous studies (11) which showed induction of hypertrophy in adult mice cardiomyocyte when the agents were applied at the chosen concentrations. Cell surface area of cardiomyocytes was evaluated 24 h following treatment, a period previously shown to adequately induce hypertrophy in adult mice cardiomyocytes (11). Our results demonstrate that PE and ANGII did not significantly induce hypertrophy in cardiomyocytes cultured for 3 h, 6 h, 12 h or 24 h prior to hypertrophic intervention (Fig. 4.5C). PE and ANGII significantly increased the cell surface area of cardiomyocytes cultured for a pretreatment period of 18 h (Fig. 4.5C). Images of myocytes pre-cultured for 3 to 18 h demonstrated similar morphology with the typical rod-shaped structure with very minimal rounding of the cells (Fig. 4.5A). However, cardiomyocytes treated after 24 h of culturing was accompanied by a lot of rounded myocytes (Fig. 4.5B). Thus, the 18 h pretreatment period was selected as the optimal condition for the induction of hypertrophy and was employed for the rest of the experiments. Each group is a set of five different experiments (n=5) containing between 100-200 cells per experiment per group.

Cardiomyocyte hypertrophy is characterized by an increase in cardiomyocyte surface area, resulting in an overall increase in heart size. Cardiomyocytes were isolated from adult WT and *ae3*^{-/-} mice and the cell surface assessed by morphometry. The cell surface area of *ae3* null cardiomyocytes was 20%±4% (n=6) lower than WT (Fig. 4.3). To determine the response of cardiomyocytes to pro-hypertrophic stimulation, adult cardiomyocytes were

cultured and treated with PE and ANGII 18 h later. Cell surface area was measured 24 h following treatment with hypertrophic agonists. PE and ANGII induced a 20-25%±4% (n=10) increase in the cell surface area of WT cardiomyocytes, but cardiomyocytes from *ae3^{-/-}* hearts were not susceptible to pro-hypertrophic stimulation by these agents (Fig. 4.6C). This suggests that AE3 has a role in the hypertrophic signaling pathway downstream of PE and ANGII.

4.2.4 Effect of hypertrophic stimulation on hypertrophic molecular markers

Cardiac hypertrophic development is associated with increased expression of marker genes, including ANP (59), β -myosin heavy chain (β -MHC) (48) and α -skeletal actin (57). mRNA and protein levels of these markers are elevated in hypertrophic hearts (14). Expression levels of ANP and β -MHC, were assessed by real-time qRT-PCR in cardiomyocytes were subjected to pro-hypertrophic stimulation. Transcript abundance of ANP and β -MHC were not significantly different between untreated cardiomyocytes from WT and *ae3^{-/-}* mice (Figs. 4.7A and 4.7B). Stimulation with PE and ANGII, however, led to 8-10 fold increase of ANP and β -MHC expression levels in cardiomyocytes from WT mice. In contrast, ANP and β -MHC increased only 1-2 fold in cardiomyocytes from *ae3^{-/-}* mice. These data suggest that pro-hypertrophic stimulation induces a much greater upregulation of hypertrophic marker genes in cardiomyocytes from WT mice than *ae3^{-/-}* cardiomyocytes.

Table 4.1. Echocardiographic analysis of WT and *ae3^{-/-}* mice.

Parameter	WT (n=3)	<i>ae3^{-/-}</i> (n=3)
Ejection fraction, %	65 ± 3	67 ± 7
Fractional shortening, %	35 ± 3	37 ± 7
IVSd, mm	0.70 ± 0.01	0.75 ± 0.04
LVIDd, mm	3.5 ± 0.1	3.4 ± 0.1
LVPWd, mm	0.67 ± 0.03	0.70 ± 0.03
IVSs, mm	1.08 ± 0.03	1.11 ± 0.09
LVIDs, mm	2.3 ± 0.1	2.1 ± 0.3
LVPWs, mm	1.05 ± 0.07	1.05 ± 0.12
MV E Velocity, mm/s	730 ± 50	710 ± 50
MV A Velocity, mm/s	390 ± 30	520 ± 40
MV E/A ratio	1.9 ± 0.1	1.4 ± 0.1*
E/E'	24 ± 3	21 ± 4
IVRT, ms	16 ± 0	17 ± 2
TEI index	0.63 ± 0.03	0.61 ± 0.02
Systolic Pressure, mm Hg	102 ± 7	100 ± 9
Diastolic Pressure, mm Hg	66 ± 6	64 ± 8
Flow, ml/min	11 ± 1	10 ± 1
Volume of blood, ml	36 ± 6	31 ± 5
Heart Rate, bpm	699 ± 1	721 ± 49

Values are expressed as means ± S.E.M. (n = 3 per group); P < 0.05. IVSd, diastolic intraventricular septal wall thickness; LVIDd, diastolic left ventricular internal diameter; LVPWd, diastolic left ventricular posterior wall thickness; IVSs, systolic intraventricular septal wall thickness; LVIDs, systolic left ventricular internal diameter; LVPWs, systolic left ventricular posterior wall thickness; MV E velocity, peak E wave mitral valve velocity; MV A velocity, peak A wave mitral valve velocity; MV E/A, ratio of peak E wave mitral valve velocity to peak A wave mitral valve velocity; E/E', ratio of peak E wave mitral valve velocity to E wave mitral valve tissue motion; IVRT, isovolumic relaxation time.

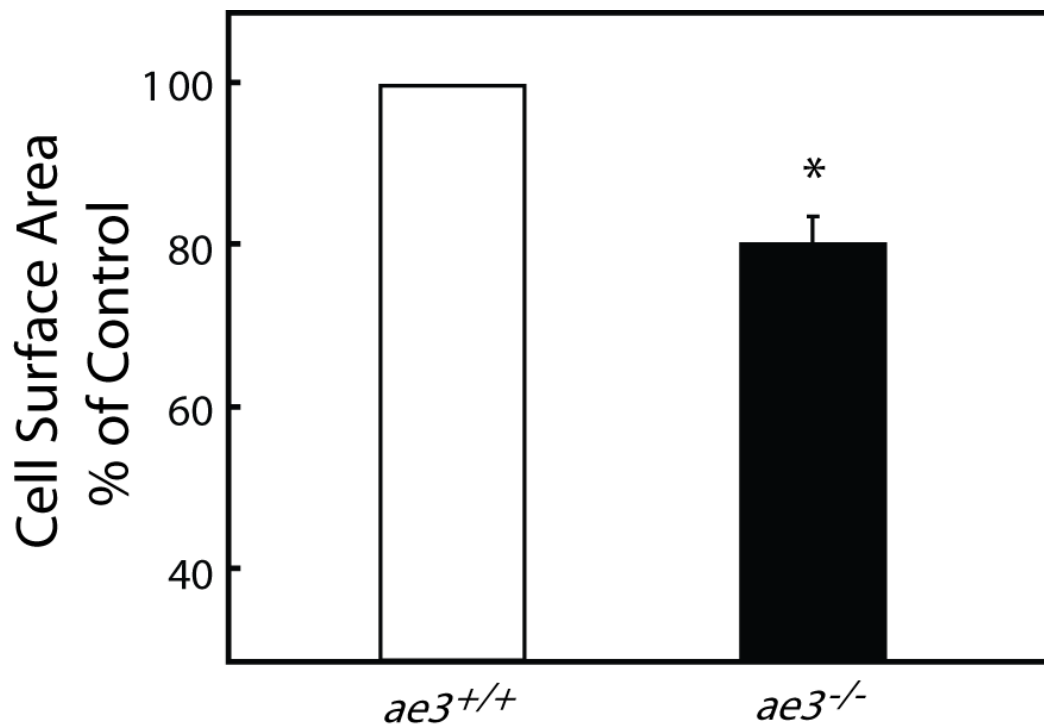


Fig. 4.3 Assessment of cardiomyocyte size. Cardiomyocytes were isolated from male adult hearts of both wildtype (*ae3^{+/+}*) and knock-out (*ae3^{-/-}*) mice. Total cell surface area of rod-shaped cardiac cells were determined by morphometry and calculated as percent. Data of knock-out cells were expressed as a percentage relative to the wildtype cells (Control).

* P<0.05 compared to wildtype (n=6).

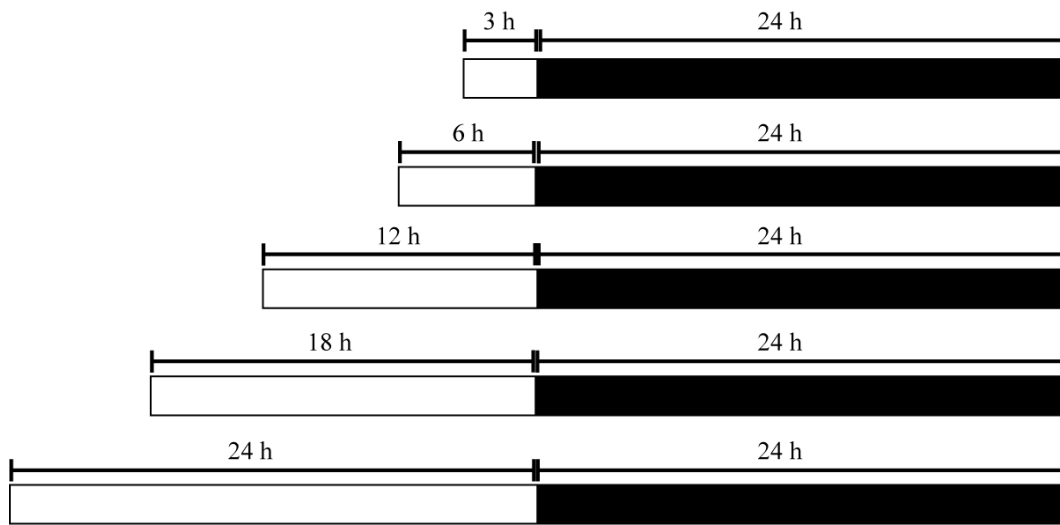


Fig. 4.4 Protocol for optimization of conditions for inducing hypertrophy. Cardiomyocytes isolated from male adult mice were incubated for 3 h, 6 h, 12 h, 18 h and 24 h (□) and subjected to hypertrophic agonist stimulation for further 24 h (■). Vehicle control groups were treated in a similar fashion as treatment hypertrophic groups. Hypertrophy was assessed by analysis of cell surface area of cardiomyocyte images taken pre- and post-treatment with the hypertrophic agonists.

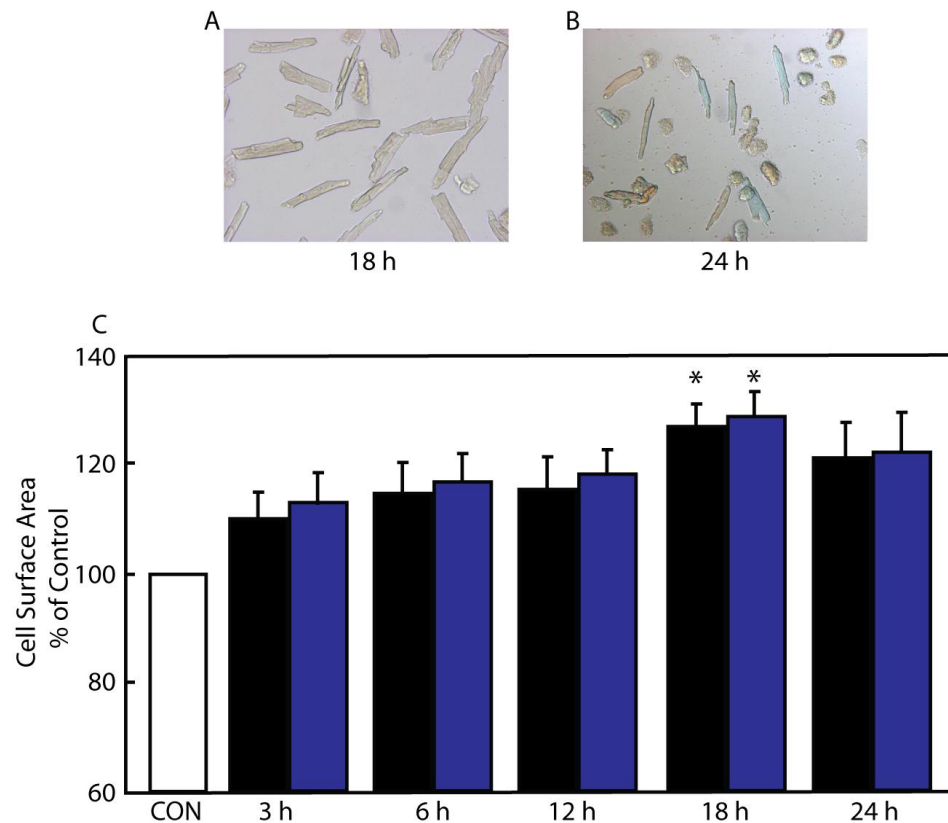


Fig. 4.5 Optimization of conditions for induction of cardiomyocyte hypertrophy. Cardiomyocytes were isolated from adult wildtype male mice hearts and cultured in a culture medium for 3, 6, 12, 18 and 24 h (timing referred to that outlined in Fig. 4.4) and subjected to hypertrophic intervention with 10 μ M phenylephrine (PE) (black bars) and 1 μ M angiotensin II (ANGII) (grey bars). A, Representative image of cardiomyocytes pre-cultured for 18 h taken after treatment with PE. B, Representative image of cardiomyocytes pre-cultured for 24 h taken after treatment with ANGII. C, Summary of data of cardiomyocytes pre-cultured for 3, 6, 12, 18 and 24 h and treated with PE and ANGII for 24 h. The cell surface area was expressed as a percentage of control groups (open bars). *P<0.05, relative to control group (n=5).

4.2.5 HTM gene expression in *ae3*^{-/-} cardiomyocytes

AE3 is implicated as part of a functional complex with NHE1 and CAII, referred to as the hypertrophic transport metabolon (HTM), whose activation has been proposed to induce cardiac hypertrophy (11, 15). To assess the possibility of functional compensation for loss of AE3 by altered expression of these partner proteins, we examined mRNA expression of NHE1 and CAII by real-time qRT-PCR. Baseline expression level of NHE1 in *ae3*^{-/-} mice was significantly elevated compared to the *WT* mice (Fig. 4.8A). Pro-hypertrophic stimulation with PE or ANGII did not influence the NHE1 transcript abundance in the *WT* or *ae3*^{-/-} cardiomyocytes (Fig. 4.8A). CAII transcript abundance was higher in cardiomyocytes from *ae3*^{-/-} mice than from *WT* mice (Fig. 4.8B). *ae3* ablation thus induces a compensatory increase in CAII expression. Pro-hypertrophic stimulation, however, markedly increased CAII levels in both *WT* and *ae3*^{-/-} cardiomyocytes (Fig. 4.8B).

Since the baseline expression level of CAII was elevated in *ae3*^{-/-} cardiomyocytes and was further enhanced by hypertrophic stimulants in *WT* cardiomyocytes, we evaluated CAII protein expression. Cardiomyocytes isolated from *ae3*^{-/-} and *WT* male adult mice hearts were probed for CAII on immunoblots (Fig. 4.9A). CAII resolved at ~27 kDa, consistent with the expected molecular weight of CAII. The steady-state level of CAII was higher in *ae3*^{-/-} cardiomyocytes than *WT* cardiomyocytes (Fig. 9B), consistent with the mRNA expression level (Fig. 8B). PE and ANGII increased CAII levels in the *WT*

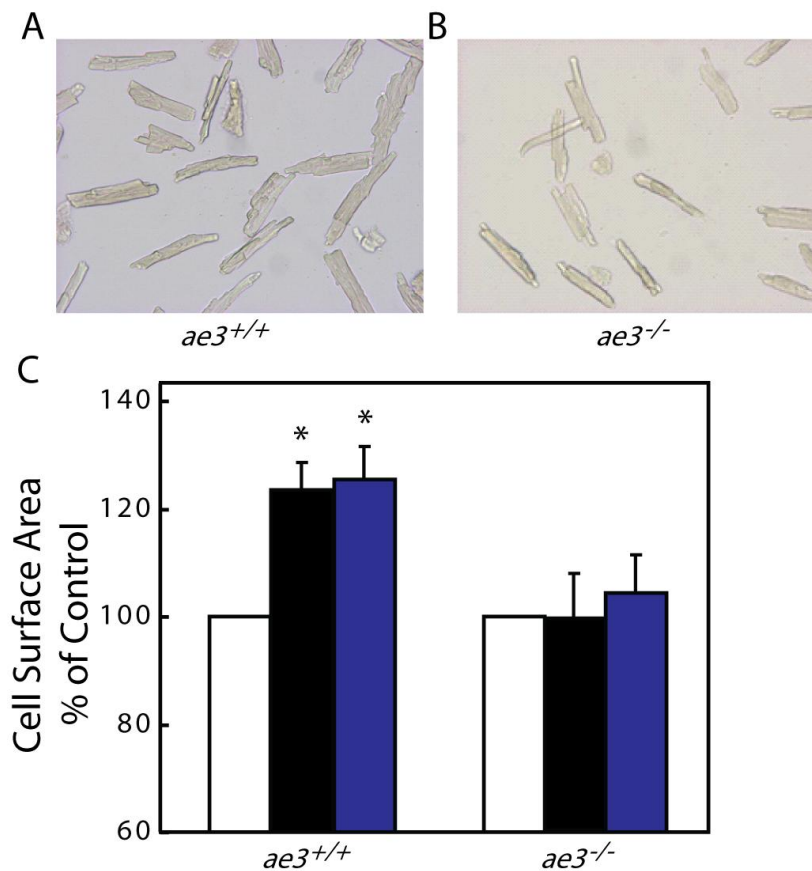


Fig. 4.6 Effect of hypertrophic stimuli on cardiomyocyte size. To determine the effect of ANGII and PE on hypertrophic development, cardiomyocytes (A, B) isolated from the ventricles of adult mice were subjected to ANGII (1 μ M) and PE (10 μ M) treatment for 24 h, following an 18 h pretreatment period. Images of the cardiomyocytes taken pre- and post-treatment using a QICAM fast cooled 12-bit color camera were quantified to measure the cell surface area. In the control group, equal volume of the vehicle was added. C, The cell surface area was expressed as a percentage of control groups (open bars) and compared to the ANGII (black bars) and PE (grey bars) treated groups. * $P < 0.05$, relative to control group (n=10).

cardiomyocytes. Contrastingly, CAII levels in *ae3^{-/-}* cardiomyocytes were not significantly affected by pro-hypertrophic stimulation (Fig. 4.8B).

4.2.6 Protein synthesis rate in *ae3^{-/-}* cardiomyocytes

Cardiac hypertrophy is also characterized by an increase in protein synthesis to accommodate cardiomyocyte enlargement (39). Protein synthesis was measured by determining the amount of radioactive [³H]-Phe incorporated into proteins in cardiomyocytes. Cardiomyocytes were isolated and cultured as described above and treated with PE and ANGII, followed by incubation with radiolabeled [³H]-Phe. The amount of [³H]-Phe incorporated into proteins in the presence of pro-hypertrophic stimuli was increased in cardiomyocytes from WT mice, but not in cardiomyocytes from *ae3^{-/-}* mice. We conclude that *ae3^{-/-}* mice do not respond to pro-hypertrophic agonists with increased protein synthesis (Fig. 4.10).

4.2.7 p*H*_i regulation in *ae3^{-/-}* cardiomyocytes

AE3 is involved in cardiomyocyte p*H*_i regulation (5, 19), but there are no AE3-specific inhibitors that would enable delineation of the role of AE3 in p*H*_i regulation. We thus examined the rate of recovery of p*H*_i from an imposed intracellular alkalinization in freshly isolated cardiomyocytes. Cardiomyocytes were cultured on laminin-coated glass coverslips for 2 h, then incubated with the pH-sensitive fluorescence dye, BCECF-AM. Cells were perfused with a HCO₃⁻-containing Ringer's buffer until steady-state p*H*_i was reached and the perfusion was switched to the HCO₃⁻-containing Ringer's buffer, containing TMA. The

presence of TMA induced a rapid intracellular alkalinization (Fig. 4.11A) until a new steady-state pH_i was reached. pH_i regulatory transporters spontaneously restored cell pH_i . Steady-state pH_i was measured as the pH_i 60 s prior to switching to the TMA-supplemented HCO_3^- -containing Ringer's buffer. The rate of pH_i recovery from imposed intracellular alkalinization was measured as the linear regression fitted to the initial minute of pH_i recovery. Baseline pH_i was identical in cardiomyocytes from WT and *ae3*^{-/-} mice (Fig. 4.11B). This implies that under basal physiological conditions, loss of AE3 does not affect the steady-state pH_i in cardiomyocytes. The rate of recovery of pH_i from alkalosis was, however, significantly slower in *ae3*^{-/-} cardiomyocytes than WT (Fig. 4.11C). This could be accounted for by the absence of AE3 whose activity acidifies the cell to counter a rise in pH_i .

4.2.8 Expression of pH_i regulators in *ae3*^{-/-} cardiomyocytes

We next assessed the expression level of the other pH_i regulatory transporters at the protein level. Protein concentration was determined by the Bradford Assay and 50 μg of each lysate was loaded. On immunoblots all the proteins migrated at the expected sizes, AE1 and NHE1 at ~100-110 kDa, and SLC26a6 at ~80 kDa (Figs 4.12-4.14). Lysates from AE1-expressing erythrocytes and HEK293 cells were used as positive controls and negative controls, respectively. AE1 expression was upregulated in *ae3*^{-/-} cardiomyocytes relative to WT, AE1 expression level was not significantly different in *ae3*^{+/-} lysates (Fig. 4.12). Expression of NHE1 was elevated in *ae3*^{-/-} cardiomyocytes compared to

WT, but remained unchanged in the heterozygotes (Fig. 4.13A-B). Expression of SLC26a6 protein was not affected by deletion of the *ae3* gene (Fig. 4.14A-B).

4.3 Discussion

Pathological cardiac hypertrophy renders the heart susceptible to cardiac failure. Accumulating evidence implicates NHE1 as a key candidate mediating pathological hypertrophy. Prolonged NHE1 activation produces intracellular alkalinization, therefore sustained activation can only occur in the presence of a counter acidifying mechanism. The present study examined the possibility that the $\text{Cl}^-/\text{HCO}_3^-$ anion exchange mediated by AE3 is responsible for the acidification mechanism. Our studies using AE3 deficient mice support a role for AE3 in cardiovascular pH regulation and the development of cardiomyocyte hypertrophy. Pharmacological antagonism of AE3 is thus a possible therapeutic direction in the prevention of maladaptive cardiac hypertrophy.

AE3 in the Hypertrophic Transport Metabolon- The role of AE3 in cardiac physiology is incompletely characterized, but several lines of evidence suggest that AE3 $\text{Cl}^-/\text{HCO}_3^-$ exchange is required to maintain pH_i homeostasis (19, 61, 64). Consistent with this, we found that the rate of recovery from an alkaline load was reduced in *ae3*^{-/-} cardiomyocytes, relative to WT. The hypertrophic transport metabolon is a proposed pathological pathway in which AE3, NHE1 and CAII are coordinately activated and promote hypertrophic growth (11, 15). Pro-hypertrophic agonists, including PE, ANGII and endothelin are coupled to PKC

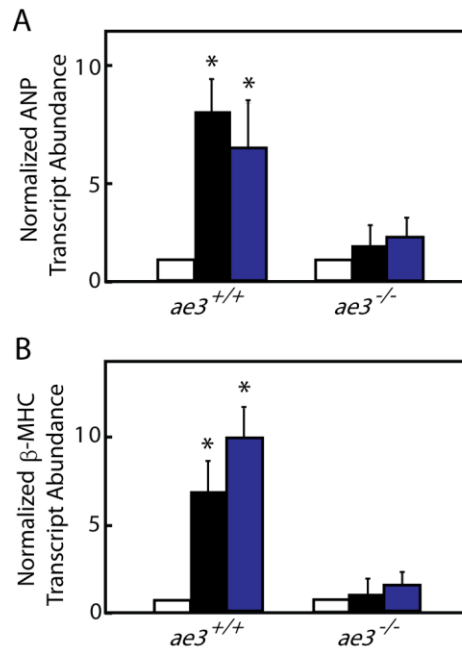


Fig. 4.7 Effect of hypertrophic stimuli on hypertrophic marker genes. Cardiomyocytes were isolated from *ae3*^{-/-} and *ae3*^{+/+} adult mice heart. Following 18 h culture period, ANGII (1 μ M, black bars) and PE (10 μ M, blue bars) were added for additional 24 h. To determine the mRNA expression levels of ANP, quantitative real-time PCR was performed in an ABI Prism 7900H Sequence Detection System. RNA prepared from cardiomyocytes was reverse transcribed and the resulting cDNA was subjected to qRT-PCR. Cycle threshold (Ct) value was obtained for ANP and GAPDH. Ct value of each sample was corrected for the respective GAPDH Ct values. Absolute differences in gene expression between samples based on the relation that a difference of 1 cycle corresponds to a difference of two-fold in template abundance. Relative transcript abundance was expressed as fold-change of ANP (A) and β -MHC (B) relative to control. * P<0.05, compared to control group (n=4).

activation. NHE1 and AE3 are both activated by agonists coupled to PKC activation (5, 25, 49). Co-activation of these pathways has the net effect of loading the cell with NaCl, with no change of cytosolic pH. Elevated cytosolic Na⁺ in turn reduces the efficacy of Ca⁺⁺-efflux by the plasma membrane Na⁺/Ca⁺⁺ exchanger, resulting in a rise in cytosolic Ca⁺⁺. Ca⁺⁺ is a pro-hypertrophic second messenger (28, 46) and also may promote hypertrophy in a feed-forward cascade by stimulation of PKC (34). Accumulating evidence suggests that both NHE1 and AE3 activities are influenced by physical and functional interactions with CAII (10, 43), which provides substrates for these transporters. Inhibition of CAII catalytic activity prevents PE-mediated cardiomyocyte hypertrophy (11). We propose that CAII, NHE1 and AE3 form a hypertrophic transport metabolon, where hypertrophy is promoted by the pathological activation of AE3 and NHE1, stimulated by interactions with CAII.

The functional relationship between AE3, CAII and NHE1 was further supported by our analysis of AE3 expression in *ae3*^{-/-} mice. Increased CAII transcript abundance and protein expression in *ae3*^{-/-} mice compared to WT mice suggest that there is compensation for a loss of AE3. This finding parallels results in retinal tissue from *ae3*^{-/-} mice, where there was increased CAII expression (6). There is also a significant increase in AE3 transcript abundance in *Car2* (*caii*^{-/-}) mice, compared to WT mice (15). The upregulation of NHE1 transcript abundance and increased protein expression provide further support for the HTM. Taken together, these data support a functional interaction between AE3 and CAII, where there is compensation of one for the loss of the other.

Loss of AE3 Prevents Cardiomyocyte Hypertrophy– This study lends support to the idea that AE3 is the $\text{Cl}^-/\text{HCO}_3^-$ exchanger isoform working in conjunction with NHE1 to promote cardiomyocyte hypertrophy. Non-specific inhibition of $\text{Cl}^-/\text{HCO}_3^-$ exchangers, using stilbene derivatives, prevented hypoxia-induced acidification in rat ventricular myocytes, as well as increases in intracellular Cl^- and Ca^{2+} concentrations (36, 40), suggesting a role of $\text{Cl}^-/\text{HCO}_3^-$ exchangers in cardiac pathology. When subjected to ischemia and reperfusion, hearts isolated from *ae3* null mice revealed no effect on cardiac performance demonstrated as contractility, ventricular developed pressure or end diastolic pressure relative to wildtype (54). Double knock-out *ae3/NKCC1* ($\text{Na}^+/\text{K}^+/\text{2Cl}^-$ co-transporter) mice, however, had elevated ischemia/reperfusion injury, which resulted in impaired cardiac contractility and overall cardiac performance (54). These findings were attributed to impaired Ca^{2+} handling in the double knock-out cardiomyocytes (54) compared to the single mutants. In a hypertrophic cardiomyopathy mouse model carrying a Glu180Gly mutation in α -tropomyosin (TM180), disruption of *ae3* did not prevent or reverse the hypertrophic phenotype (2). The TM180/AE3 double knockout mice had reduced cardiac function and compromised Ca^{2+} regulation, which accounted for the rapid decline to heart failure (2).

Taken together, these two studies suggest that AE3 loss is not cardioprotective, which contrasts with findings of the present study, which found that loss of AE3 renders cardiomyocytes less susceptible to pro-hypertrophic stimulation. Our data showed that the marked rise in cell surface area, protein synthesis, and fetal gene reactivation observed in response to hypertrophic

stimulation in cardiomyocytes from WT mice was not present in *ae3*^{-/-} mice. In the context of cardiomyocyte hypertrophy mediated by hormonal stimuli, our data demonstrate that loss of AE3 affords cardioprotection against cardiomyocyte hypertrophic development.

The discrepancy could be the result of the model of hypertrophy and the cardiac pathology being investigated. Hypertrophic cardiomyopathy is a genetic disorder which occurs as a result of mutations in the genes that encode the cardiac contractile proteins (23). This anomaly manifests as sudden cardiac death, arrhythmias, hypertrophy and heart failure (23). Overall, hypertrophic cardiomyopathy results in impairment of Ca²⁺ sensitivity by the myofibrils. In the present study, however, we employed a model of hypertrophy induced by PE or ANGII, which involves interaction of the ligands with their cell surface receptors, GPCR (62). The resultant intracellular response leads to increased cytosolic Ca²⁺ overload, which mediates a cascade of signaling pathway involving activation of PKC, which ultimately induces cardiomyocyte hypertrophy (12). Thus, the etiology, signaling pathway and pathophysiology of hypertrophic cardiomyopathy are distinct from that mediated by hormonal factors. These differences could account for the disparity between the influence of AE3 on hypertrophy in the present report and that shown in previous models of cardiovascular disease (2, 54). Since hypertrophic interventions by PE and ANGII failed to induce hypertrophy in the *ae3* null cardiomyocytes in our study, this may suggest that the PKC-coupled hypertrophic cascade requires functional AE3.

Phenotype of $ae3^{-/-}$ Mice– AE3 null mice have been reported to have no apparent defects, and the results of our analysis of the cardiac function of $ae3^{-/-}$ mice is comparable to these previous studies (2, 30, 54). Combined analysis of echocardiographic measurements of ventricular wall dimensions, chamber diameter and cardiac function between the two genotypes further suggests that loss of AE3 does not affect hypertrophy or cardiovascular performance. A significant decrease in the HW/BW ratio in $ae3^{-/-}$ mice is the result of a reduction in heart size, arising from a decrease in cardiomyocyte size. This suggests a critical role for AE3 in heart development.

Role of AE3 in control of cardiomyocyte pH_i – The finding that there is no difference in cardiomyocyte intracellular pH between $ae3^{-/-}$ and WT mice suggests that the loss of Cl^-/HCO_3^- exchange activity by $ae3$ deletion is compensated for by another Cl^-/HCO_3^- exchanger. Since there are several other Cl^-/HCO_3^- exchangers present in the heart, including the highly abundant SLC26A6, this is not surprising (7). The importance of AE3 in intracellular pH regulation was, however, evident in the reduced rate of pH_i recovery from imposed intracellular alkalosis in cardiomyocytes from $ae3^{-/-}$ mice compared to WT. This provides a possible explanation for the resistance of $ae3^{-/-}$ mice to pro-hypertrophic stimuli; $ae3^{-/-}$ cardiomyocytes have reduced acidifying activity to counter enhanced NHE1 activity associated with pro-hypertrophic stimulation.

Conclusion– We explored the role of AE3 in the development of cardiomyocyte hypertrophy and cardiovascular pH regulation, using AE3 deficient mice. Cardiomyocytes from $ae3^{-/-}$ mice were protected from increases in cell surface

area, protein synthesis, and fetal gene reactivation in response to hypertrophic stimulation. Steady-state cardiomyocyte pH_i in *ae3^{-/-}* mice was comparable to WT, but slower to recover from imposed intracellular alkalosis. Our findings demonstrate that AE3 and the rest of the hypertrophic transport metabolon is important in hypertrophic signaling pathways activated by PE and ANGII. Pharmacologically targeting AE3 activity in the event of hypertrophy is an attractive strategy to treat heart failure patients.

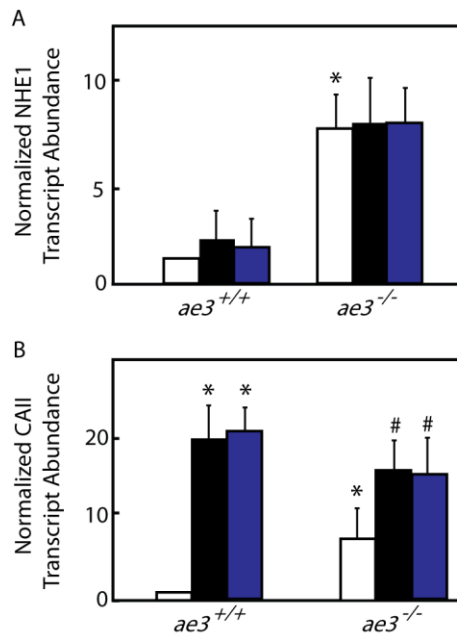


Fig. 4.8 Effect of hypertrophic stimuli on NHE 1 and CAII expression. Cardiomyocytes were isolated from *ae3*^{-/-} and *ae3*^{+/+} adult mice heart. Following 18 h culture period, ANGII (1 μ M, black bars) and PE (10 μ M, grey bars) were added for additional 24 h. To determine the mRNA expression levels of NHE1 or CAII, quantitative real-time PCR was performed in an ABI Prism 7900H Sequence Detection System. RNA prepared from cardiomyocytes was reverse transcribed and the resulting cDNA was subjected to qRT-PCR. Cycle threshold (Ct) value was obtained for NHE 1 or CAII and GAPDH. Ct value of each sample was corrected for the respective GAPDH Ct values. Absolute differences in gene expression between samples based on the relation that a difference of 1 cycle corresponds to a difference of two-fold in template abundance. Relative transcript abundance was expressed as fold-change of NHE1 (A) or CAII (B) relative to control (open bars). * $P < 0.05$, compared to *ae3*^{+/+} control group. # $P < 0.05$, compared to *ae3*^{-/-} control group (n=4).

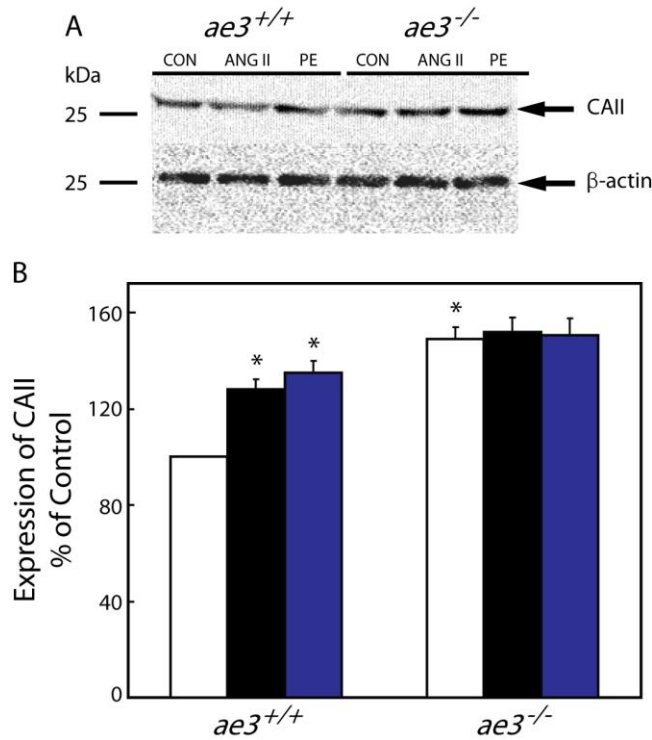


Fig. 4.9 Effect of hypertrophic stimulation of CAII expression. Cardiomyocytes isolated from wildtype (*ae3*^{+/+}) and knock-out (*ae3*^{-/-}) mice hearts were cultured for 18 h and subjected to vehicle (CON), angiotensin II (ANGII) and phenylephrine (PE) treatment for further 24 h. Lysates prepared from cardiomyocytes were probed for CAII expression by western immunoblotting. Immunoblots were stripped and probed for β -actin. A, Upper panel, representative immunoblot of lysates probed for CAII expression; lower panel, representative immunoblot stripped and reprobed for the expression of β -actin. B, Summary of data of CAII expression normalized for β -actin expression of CON (open bar), ANGII (black bar) and PE (grey bar) expressed as a percentage of CON of cardiomyocytes isolated from *ae3*^{+/+} and *ae3*^{-/-} mice hearts. * P<0.05, compared to control group (n=4).

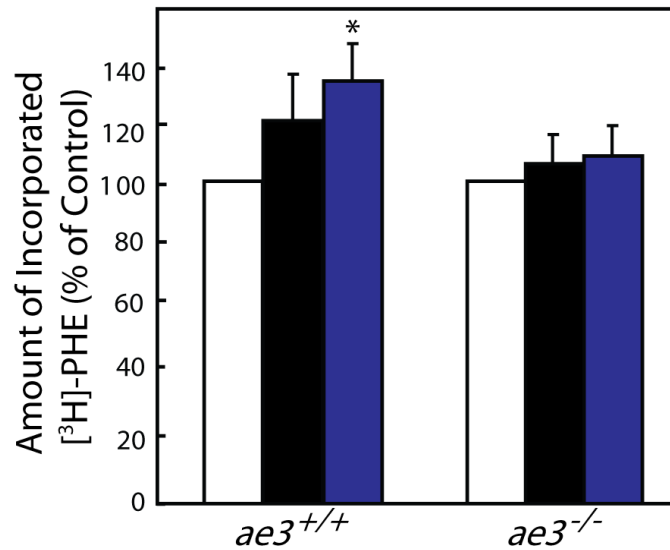


Fig. 4.10. Effect of hypertrophic stimuli on [³H]-Phe incorporation. Cardiomyocytes were isolated from both *ae3*^{-/-} and *ae3*^{+/+} adult mice heart. Following 18 h culture period, ANGII (1 μM, black bars) and PE (10 μM, grey bars) were added. Radiolabeled phenylalanine ([³H]-Phe, 1 μM), was added immediately after drug intervention and cells were incubated for further 24 h. Cells were harvested and proteins were precipitated by TCA precipitation. Following incubation on ice for 30 min proteins were pelleted by centrifugation at ~13,000 x g, for 15 min at 4 °C. Pellet was subjected to acetone wash for 3 times after the last wash the supernatant was carefully removed and the pellet was air-dried for 20 min at room temperature. Pellet was resuspended in buffer and scintillation fluid was added and the radioactivity counted in a liquid scintillation counter. The amount of incorporated [³H]-Phe was measured as decay per minute (dpm) and expressed relative to the vehicle control group as a percentage. * P<0.05 compared to control group (n=5).

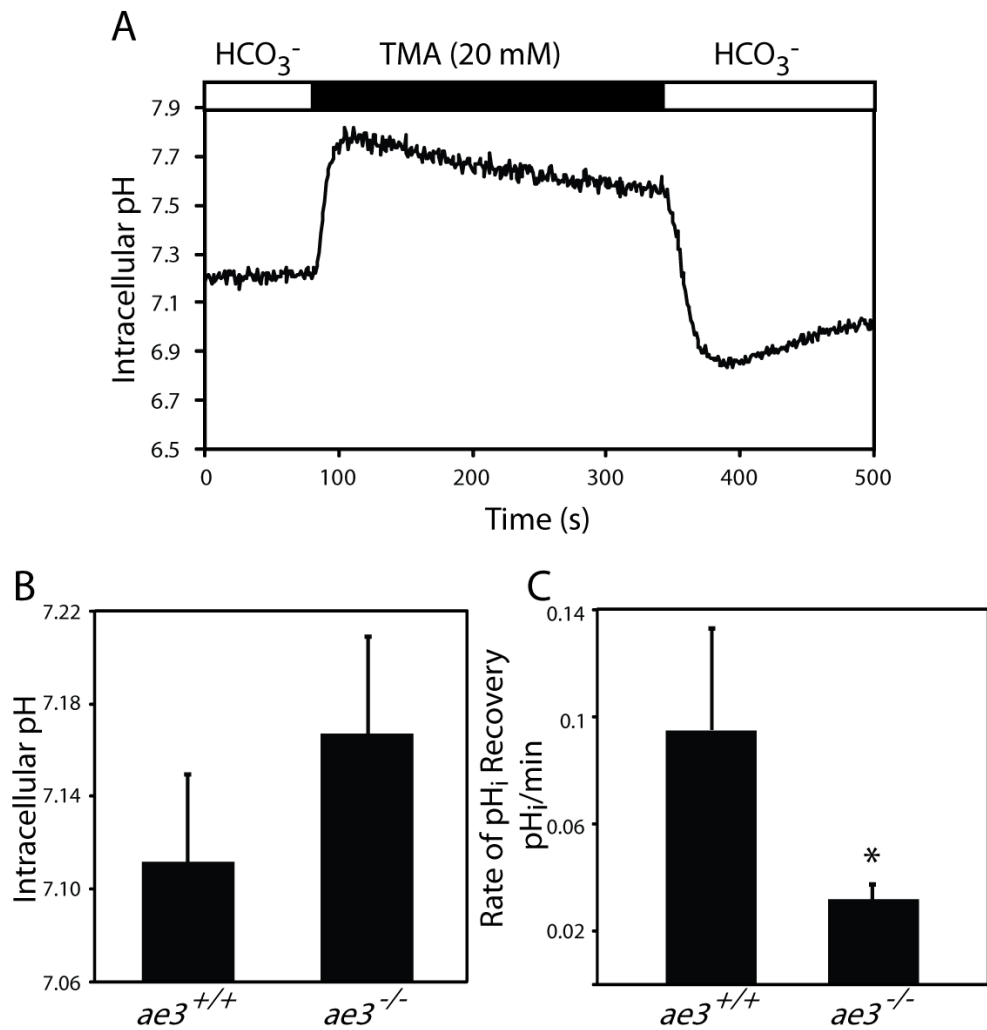


Fig. 4.11 Measurement of pH_i in freshly isolated cardiomyocytes. Freshly isolated cardiomyocytes plated on laminin-coated plates were loaded with $2 \mu\text{M}$ BCECF-AM for 30 min, placed in an Atof fluor cell chamber and mounted onto an inverted epifluorescence Leica DMIRB microscope. A, Representative trace of wildtype cardiomyocytes perfused with HCO_3^- -containing Ringer's buffer (open bar) until steady-state pH_i was reached and perfusion was switched to HCO_3^- -containing Ringer's buffer supplemented with 20 mM TMA (black bar). Perfusion was switched to the HCO_3^- -containing Ringer's buffer ~ 3 min later. At the end of the perfusion pH_i was clamped by the high K^+ /nigericin technique to

convert fluorescent intensities to pH_i . Steady-state pH_i was measured as the pH_i value prior to induction of intracellular alkalosis, A. The rate of recovery of pH_i from imposed alkalosis was assessed as the first minute of pH_i recovery fitted to a straight line. B, summary of data of steady-state pH_i and C, summary of data of the rate of pH_i recovery. * $P < 0.05$ compared to wildtype (n=4).

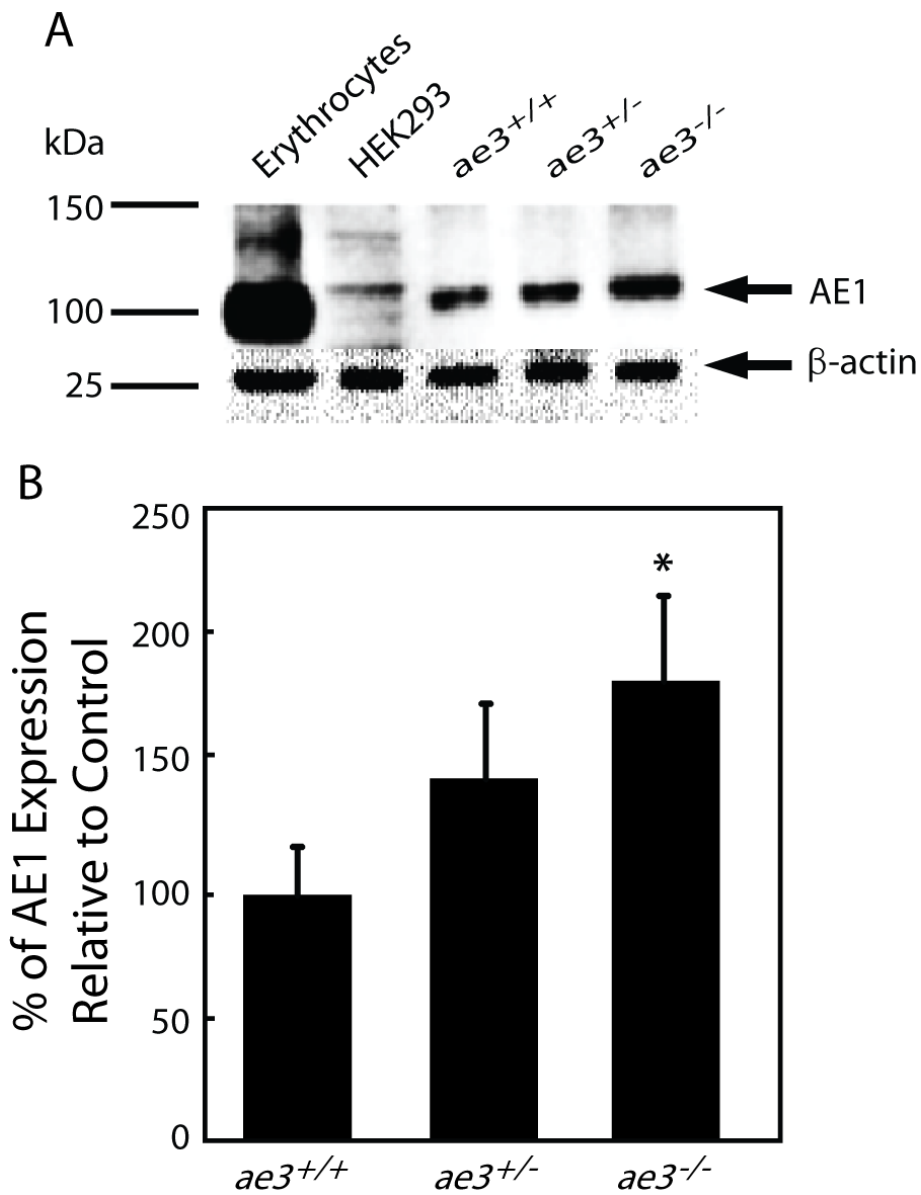


Fig. 4.12 Cardiac expression of AE1. Cardiomyocytes isolated from adult mice hearts, were lysed and probed on immunoblots for AE1. A, Upper panel is a representative immunoblot probed for AE1 of lysates from mouse erythrocytes, AE1-transfected HEK293 cells and cardiomyocyte lysates prepared from wildtype (WT), *ae3* heterozygote (*ae3*^{+/-}) and *ae3* null (*ae3*^{-/-}) mice. Lower panel is

summary of AE1 amount quantified by densitometry and expressed as a percentage relative to the WT group (n=4). *P<0.05 compared to the WT group.

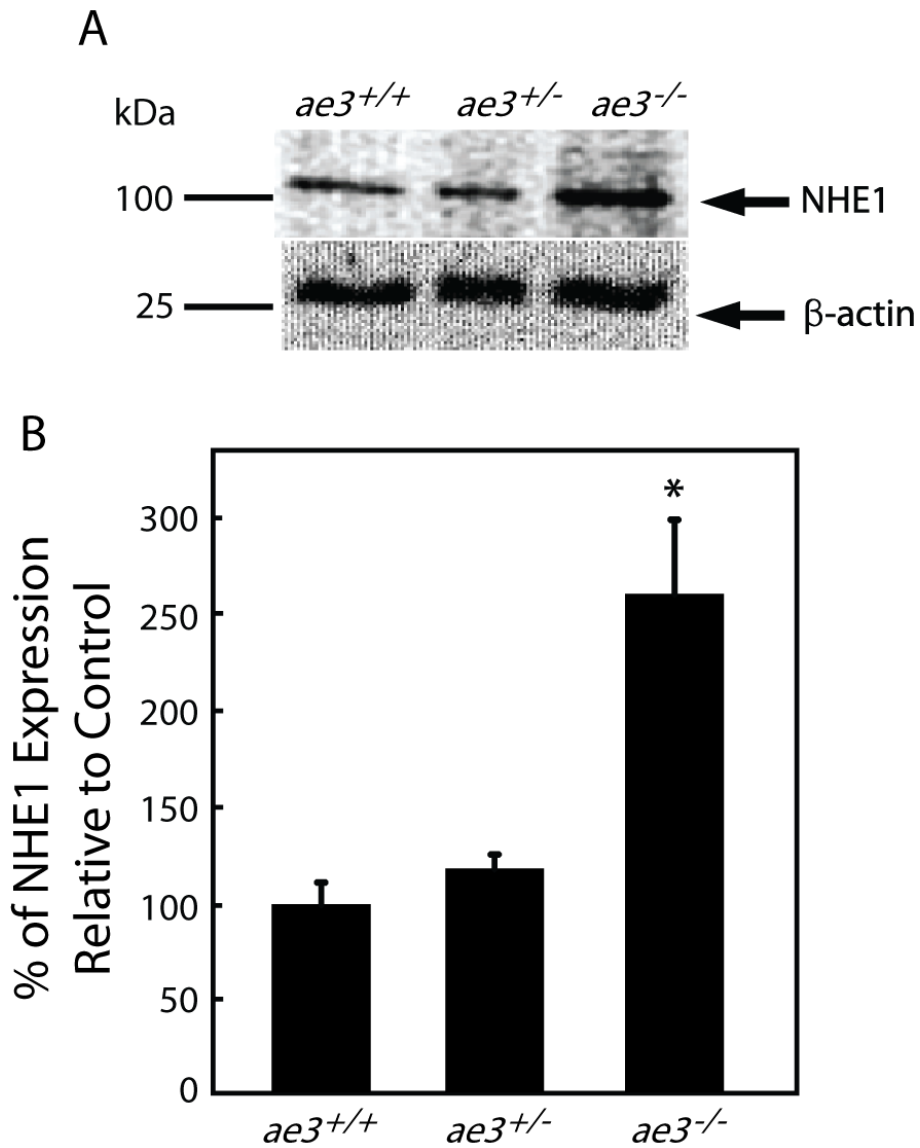


Fig. 4.13 Cardiac expression of NHE1. Cardiomyocytes isolated from adult mice hearts, were lysed and probed on immunoblots for NHE1. A, Upper panel is a representative immunoblot probed for NHE1 of cardiomyocyte lysates prepared from wildtype (WT), *ae3* heterozygote (*ae3*^{+/-}) and *ae3* null (*ae3*^{-/-}) mice. Lower panel is summary of NHE1 amount quantified by densitometry and expressed as a percentage relative to the WT group (n=4). *P<0.05 compared to the WT group.

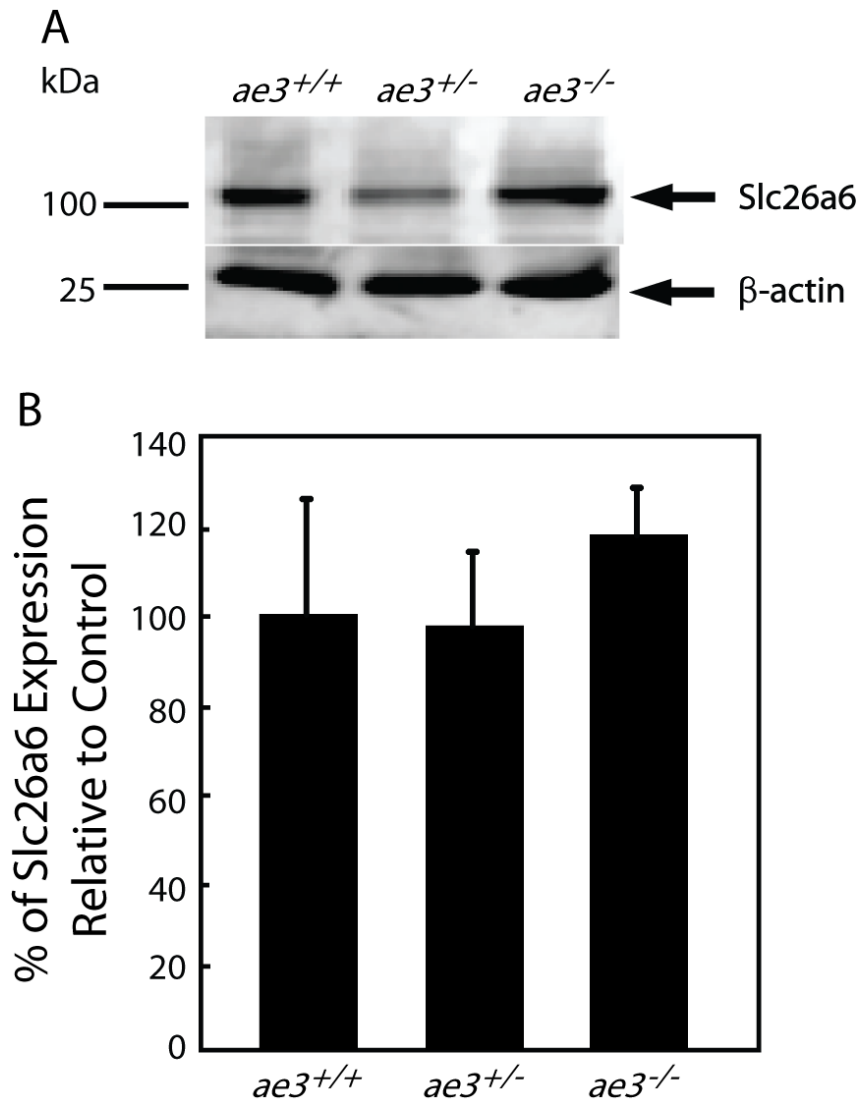


Figure 4.14. Cardiac expression of Slc26a6. Cardiomyocytes isolated from adult mice hearts, were lysed and probed on immunoblots for Slc26a6. A, Upper panel is a representative immunoblot probed for Slc26a6 of cardiomyocyte lysates prepared from wildtype (WT), *ae3* heterozygote (*ae3*^{+/-}) and *ae3* null (*ae3*^{-/-}) mice. Lower panel is summary of Slc26a6 amount quantified by densitometry and expressed as a percentage relative to the WT group (n=4). *P<0.05 compared to the WT group.

Bibliography

1. **Al-Samir S, Papadopoulos S, Scheibe RJ, Meissner JD, Cartron JP, Sly WS, Alper SL, Gros G, and Endeward V.** Activity and distribution of intracellular carbonic anhydrase II and their effects on the transport activity of anion exchanger AE1/SLC4A1. *J Physiol*, 2013.
2. **Al Moamen NJ, Prasad V, Bodi I, Miller ML, Neiman ML, Lasko VM, Alper SL, Wieczorek DF, Lorenz JN, and Shull GE.** Loss of the AE3 anion exchanger in a hypertrophic cardiomyopathy model causes rapid decompensation and heart failure. *J Mol Cell Cardiol* 50: 137-146, 2011.
3. **Alper SL.** Molecular physiology and genetics of Na⁺-independent SLC4 anion exchangers. *J Exp Biol* 212: 1672-1683, 2009.
4. **Alper SL.** Molecular physiology of SLC4 anion exchangers. *Exp Physiol* 91: 153-161, 2006.
5. **Alvarez BV, Fujinaga J, and Casey JR.** Molecular Basis for angiotensin II-induced increase of chloride/bicarbonate exchange in the myocardium. *Circ Research* 89: 1246-1253, 2001.
6. **Alvarez BV, Gilmour G, Mema SC, Shull GE, Casey JR, and Sauvé Y.** Blindness results from deficiency in AE3 chloride/bicarbonate exchanger. *PLoS ONE* 2: e839, 2007.
7. **Alvarez BV, Kieller DM, Quon AL, Markovich D, and Casey JR.** Slc26a6: A cardiac chloride/hydroxyl exchanger and predominant chloride/bicarbonate exchanger of the heart. *J Physiol* 561: 721-734, 2004.

8. **Alvarez BV, Kieller DM, Quon AL, Robertson M, and Casey JR.** Cardiac hypertrophy in anion exchanger 1-null mutant mice with severe hemolytic anemia. *Am J Physiol Heart Circ Physiol* 292: H1301-1312, 2007.
9. **Alvarez BV, Quon AL, Mullen J, and Casey JR.** Quantification of carbonic anhydrase gene expression in ventricle of hypertrophic and failing human heart. *BMC Cardiovasc Disord* 13: 2, 2013.
10. **Alvarez BV, Xia Y, Karmazyn M, and Casey JR.** Inhibition of phenylephrine-induced cardiac hypertrophy by a carbonic anhydrase inhibitor: a pathological pathway linking CAII, NHE1 and AE3fl. *J Mol Cell Cardiol* 37, 2004.
11. **Alvarez BV, Xia Y, Sowah D, Soliman D, Light P, Karmazyn M, and Casey JR.** A Carbonic Anhydrase Inhibitor Prevents and Reverts Cardiomyocyte Hypertrophy. *J Physiol* 579: 127-145, 2007.
12. **Barry SP, Davidson SM, and Townsend PA.** Molecular regulation of cardiac hypertrophy. *Int J Biochem Cell Biol* 40: 2023-2039, 2008.
13. **Becker HM and Deitmer JW.** Carbonic Anhydrase II increases the activity of the human electrogenic $\text{Na}^+/\text{HCO}_3^-$ cotransporter. *J Biol Chem* 282: 13508-13521, 2007.
14. **Bernardo BC, Weeks KL, Pretorius L, and McMullen JR.** Molecular distinction between physiological and pathological cardiac hypertrophy: experimental findings and therapeutic strategies. *Pharmacol Ther* 128: 191-227, 2010.

15. **Brown BF, Quon A, Dyck JR, and Casey JR.** Carbonic anhydrase II promotes cardiomyocyte hypertrophy. *Can J Physiol Pharmacol* 90: 1599-1610, 2012.
16. **Bui AL, Horwich TB, and Fonarow GC.** Epidemiology and risk profile of heart failure. *Nat Rev Cardiol* 8: 30-41, 2011.
17. **Casey JR, Sly WS, Shah GN, and Alvarez BV.** Bicarbonate Homeostasis in Excitable Tissues: Role of AE3 $\text{Cl}^-/\text{HCO}_3^-$ Exchanger and Carbonic Anhydrase XIV Interaction. *Am J Physiol Cell Physiol* 297: c1091-1102, 2009.
18. **Chen S, Khan ZA, Karmazyn M, and Chakrabarti S.** Role of endothelin-1, sodium hydrogen exchanger-1 and mitogen activated protein kinase (MAPK) activation in glucose-induced cardiomyocyte hypertrophy. *Diabetes Metab Res Rev* 23: 356-367, 2007.
19. **Chiappe de Cingolani GE, Ennis IL, Morgan PE, Alvarez BV, Casey JR, and Camilion de Hurtado MC.** Involvement of AE3 isoform of Na^+ -independent $\text{Cl}^-/\text{HCO}_3^-$ exchanger in myocardial pH_i recovery from intracellular alkalization. *Life Science* 78: 3018-3026, 2006.
20. **Cingolani HE.** Na^+/H^+ exchange hyperactivity and myocardial hypertrophy: are they linked phenomena? *Cardiovasc Res* 44: 462-467, 1999.
21. **Cingolani HE and Camilion De Hurtado MC.** Na^+/H^+ exchanger inhibition: a new antihypertrophic tool. *Circ Res* 90: 751-753, 2002.
22. **Cingolani HE and Ennis IL.** Sodium-hydrogen exchanger, cardiac overload, and myocardial hypertrophy. *Circulation* 115: 1090-1100, 2007.

23. **Coats CJ and Elliott PM.** Genetic biomarkers in hypertrophic cardiomyopathy. *Biomark Med* 7: 505-516, 2013.
24. **Engelhardt S, Hein L, Keller U, Klambt K, and Lohse MJ.** Inhibition of $\text{Na}^+\text{-H}^+$ exchange prevents hypertrophy, fibrosis, and heart failure in beta(1)-adrenergic receptor transgenic mice. *Circ Res* 90: 814-819, 2002.
25. **Farias F, Morgan P, de Cingolani GC, Maria C, and de Hurtado C.** Involvement of the Na^+ -independent $\text{Cl}^-/\text{HCO}_3^-$ exchange (AE) isoform in the compensation of myocardial Na^+/H^+ isoform 1 hyperactivity in spontaneously hypertensive rats. *Canadian journal of physiology and pharmacology* 83: 397-404, 2005.
26. **Fliegel L.** Molecular biology of the myocardial Na^+/H^+ exchanger. *Journal of molecular and cellular cardiology* 44: 228-237, 2008.
27. **Frey N, Katus HA, Olson EN, and Hill JA.** Hypertrophy of the heart: a new therapeutic target? *Circulation* 109: 1580-1589, 2004.
28. **Frey N, McKinsey TA, and Olson EN.** Decoding calcium signals involved in cardiac growth and function. *Nat Med* 6: 1221-1227, 2000.
29. **Gonzalez-Begne M, Nakamoto T, Nguyen HV, Stewart AK, Alper SL, and Melvin JE.** Enhanced formation of a HCO_3^- transport metabolon in exocrine cells of $\text{Nhe1}^{-/-}$ mice. *J Biol Chem* 282: 35125-35132, 2007.
30. **Hentschke M, Wiemann M, Hentschke S, Kurth I, Hermans-Borgmeyer I, Seidenbecher T, Jentsch TJ, Gal A, and Hubner CA.** Mice with a targeted disruption of the $\text{Cl}^-/\text{HCO}_3^-$ exchanger AE3 display a reduced seizure threshold. *Mol Cell Biol* 26: 182-191, 2006.

31. <http://www.who.int/mediacentre/factsheets/fs317/en/index.html>.
Cardiovascular diseases (CVDs): World Health Organization, 2011.
32. **Kang TC, An SJ, Park SK, Hwang IK, Suh JG, Oh YS, Bae JC, and Won MH.** Alterations in Na^+/H^+ exchanger and $\text{Na}^+/\text{HCO}_3^-$ cotransporter immunoreactivities within the gerbil hippocampus following seizure. *Brain Res Mol Brain Res* 109: 226-232, 2002.
33. **Karmazyn M.** Pharmacology and clinical assessment of cariporide for the treatment coronary artery diseases. *Expert Opin Investig Drugs* 9: 1099-1108, 2000.
34. **Karmazyn M.** Therapeutic potential of Na-H exchange inhibitors for the treatment of heart failure. *Expert Opin Investig Drugs* 10: 835-843, 2001.
35. **Karmazyn M, Sostaric JV, and Gan XT.** The myocardial Na^+/H^+ exchanger: a potential therapeutic target for the prevention of myocardial ischaemic and reperfusion injury and attenuation of postinfarction heart failure. *Drugs* 61: 375-389, 2001.
36. **Kawasaki H, Otani H, Mishima K, Imamura H, and Inagaki C.** Involvement of anion exchange in the hypoxia/reoxygenation-induced changes in pH_i and $[\text{Ca}^{2+}]_i$ in cardiac myocyte. *European journal of pharmacology* 411: 35-43, 2001.
37. **Kifor G, Toon MR, Janoshazi A, and Solomon AK.** Interaction between red cell membrane band 3 and cytosolic carbonic anhydrase. *J Membr Biol* 134: 169-179, 1993.

38. **Kim HJ, Myers R, Sihn CR, Rafizadeh S, and Zhang XD.** Slc26a6 functions as an electrogenic $\text{Cl}^-/\text{HCO}_3^-$ exchanger in cardiac myocytes. *Cardiovasc Res*, 2013.
39. **Kovacic S, Soltys CL, Barr AJ, Shiojima I, Walsh K, and Dyck JR.** Akt activity negatively regulates phosphorylation of AMP-activated protein kinase in the heart. *J Biol Chem* 278: 39422-39427, 2003.
40. **Lai ZF and Nishi K.** Intracellular chloride activity increases in guinea pig ventricular muscle during simulated ischemia. *American Journal of Physiology-Heart and Circulatory Physiology* 275: H1613-H1619, 1998.
41. **Li M, Naqvi N, Yahiro E, Liu K, Powell PC, Bradley WE, Martin DI, Graham RM, Dell'Italia LJ, and Husain A.** c-kit is required for cardiomyocyte terminal differentiation. *Circ Res* 102: 677-685, 2008.
42. **Li X, Alvarez B, Casey JR, Reithmeier RA, and Fliegel L.** Carbonic anhydrase II binds to and enhances activity of the Na^+/H^+ exchanger. *J Biol Chem* 277: 36085-36091, 2002.
43. **Li X, Liu Y, Alvarez BV, Casey JR, and Fliegel L.** A novel carbonic anhydrase II binding site regulates NHE1 activity. *Biochemistry* 45: 2414-2424, 2006.
44. **Lohi H, Lamprecht G, Markovich D, Heil A, Kujala M, Seidler U, and Kere J.** Isoforms of SLC26A6 mediate anion transport and have functional PDZ interaction domains. *Am J Physiol Cell Physiol* 284: C769-779, 2003.
45. **Lu J, Daly CM, Parker MD, Gill HS, Piermarini PM, Pelletier MF, and Boron WF.** Effect of human carbonic anhydrase II on the activity of the

human electrogenic $\text{Na}^+/\text{HCO}_3^-$ cotransporter NBCe1-A in *Xenopus* oocytes. *J Biol Chem* 281: 19241-19250, 2006.

46. **Marks AR.** Calcium and the heart: a question of life and death. *J Clin Invest* 111: 597-600, 2003.

47. **Members WG, Roger VL, Go AS, Lloyd-Jones DM, Benjamin EJ, Berry JD, Borden WB, Bravata DM, Dai S, Ford ES, Fox CS, Fullerton HJ, Gillespie C, Hailpern SM, Heit JA, Howard VJ, Kissela BM, Kittner SJ, Lackland DT, Lichtman JH, Lisabeth LD, Makuc DM, Marcus GM, Marelli A, Matchar DB, Moy CS, Mozaffarian D, Mussolino ME, Nichol G, Paynter NP, Soliman EZ, Sorlie PD, Sotoodehnia N, Turan TN, Virani SS, Wong ND, Woo D, and Turner MB.** Heart Disease and Stroke Statistics—2012 Update: A Report From the American Heart Association. *Circulation* 125: e2-e220, 2012.

48. **Miyata S, Minobe W, Bristow MR, and Leinwand LA.** Myosin heavy chain isoform expression in the failing and nonfailing human heart. *Circ Res* 86: 386-390, 2000.

49. **Moor AN and Fliegel L.** Protein kinase-mediated regulation of the Na^+/H^+ exchanger in the rat myocardium by mitogen-activated protein kinase-dependent pathways. *J Biol Chem* 274: 22985-22992, 1999.

50. **Mraiche F, Oka T, Gan XT, Karmazyn M, and Fliegel L.** Activated NHE1 is required to induce early cardiac hypertrophy in mice. *Basic Res Cardiol* 106: 603-616, 2011.

51. **Niederer SA, Swietach P, Wilson DA, Smith NP, and Vaughan-Jones RD.** Measuring and modeling chloride-hydroxyl exchange in the Guinea-pig ventricular myocyte. *Biophys J* 94: 2385-2403, 2008.
52. **Perez NG, Alvarez BV, Camilion de Hurtado MC, and Cingolani HE.** pH_i regulation in myocardium of the spontaneously hypertensive rat. Compensated enhanced activity of the $\text{Na}^+\text{-H}^+$ exchanger. *Circ Res* 77: 1192-1200, 1995.
53. **Piermarini PM, Kim EY, and Boron WF.** Evidence against a direct interaction between intracellular carbonic anhydrase II and pure C-terminal domains of SLC4 bicarbonate transporters. *J Biol Chem* 282: 1409-1421, 2006.
54. **Prasad V, Bodi I, Meyer JW, Wang Y, Ashraf M, Engle SJ, Doetschman T, Sisco K, Nieman ML, Miller ML, Lorenz JN, and Shull GE.** Impaired cardiac contractility in mice lacking both the AE3 $\text{Cl}^-/\text{HCO}_3^-$ exchanger and the NKCC1 $\text{Na}^+\text{-K}^+\text{-2Cl}^-$ cotransporter: effects on Ca^{2+} handling and protein phosphatases. *J Biol Chem* 283: 31303-31314, 2008.
55. **Pushkin A, Abuladze N, Gross E, Newman D, Tatishchev S, Lee I, Fedotoff O, Bondar G, Azimov R, Ngyuen M, and Kurtz I.** Molecular mechanism of kNBC1-carbonic anhydrase II interaction in proximal tubule cells. *J Physiol* 559: 55-65, 2004.
56. **Sterling D, Reithmeier RA, and Casey JR.** A Transport Metabolon. Functional Interaction of Carbonic Anhydrase II and Chloride/Bicarbonate Exchangers. *J Biol Chem* 276: 47886-47894, 2001.

57. **Suurmeijer AJ, Clement S, Francesconi A, Bocchi L, Angelini A, Van Veldhuisen DJ, Spagnoli LG, Gabbiani G, and Orlandi A.** Alpha-actin isoform distribution in normal and failing human heart: a morphological, morphometric, and biochemical study. *J Pathol* 199: 387-397, 2003.
58. **Takewaki S, Kuro-o M, Hiroi Y, Yamazaki T, Noguchi T, Miyagishi A, Nakahara K, Aikawa M, Manabe I, Yazaki Y, and et al.** Activation of Na⁺-H⁺ antiporter (NHE-1) gene expression during growth, hypertrophy and proliferation of the rabbit cardiovascular system. *J Mol Cell Cardiol* 27: 729-742, 1995.
59. **Tsutamoto T, Wada A, Maeda K, Hisanaga T, Maeda Y, Fukai D, Ohnishi M, Sugimoto Y, and Kinoshita M.** Attenuation of compensation of endogenous cardiac natriuretic peptide system in chronic heart failure: prognostic role of plasma brain natriuretic peptide concentration in patients with chronic symptomatic left ventricular dysfunction. *Circulation* 96: 509-516, 1997.
60. **Vandenberg JI, Metcalfe JC, and Grace AA.** Intracellular pH recovery during respiratory acidosis in perfused hearts. *Am J Physiol* 266: C489-497, 1994.
61. **Vaughan-Jones RD and Spitzer KW.** Role of bicarbonate in the regulation of intracellular pH in the mammalian ventricular myocyte. *Biochem Cell Biol* 80: 579-596, 2002.
62. **Xia Y and Karmazyn M.** Obligatory role for endogenous endothelin in mediating the hypertrophic effects of phenylephrine and angiotensin II in neonatal rat ventricular myocytes: evidence for two distinct mechanisms for endothelin regulation. *J Pharmacol Exp Ther* 310: 43-51, 2004.

63. **Xue J, Mraiche F, Zhou D, Karmazyn M, Oka T, Fliegel L, and Haddad GG.** Elevated myocardial Na⁺/H⁺ exchanger isoform 1 activity elicits gene expression that leads to cardiac hypertrophy. *Physiol Genomics* 42: 374-383, 2010.
64. **Yannoukakos D, Stuart-Tilley A, Fernandez HA, Fey P, Duyk G, and Alper SL.** Molecular cloning, expression, and chromosomal localization of two isoforms of the AE3 anion exchanger from human heart. *Circ Res* 75: 603-614, 1994.

Chapter 5

Summary and Future Directions

5.1 Summary

This thesis addressed two main objectives

1. The effect of CAII on the transport activity of the $\text{Cl}^-/\text{HCO}_3^-$ anion exchanger AE1 and
2. The role of the $\text{Cl}^-/\text{HCO}_3^-$ anion exchanger AE3 on the development of cardiomyocyte hypertrophy.

The first objective provided the basis for the second in that we were able to establish that anion exchangers require the presence of catalytically active CAII for maximal activity. AE1 was employed to investigate the role of CAII interaction on transport activity because it is considered to be the prototype of the $\text{Cl}^-/\text{HCO}_3^-$ anion exchanger AE family. Moreover, AE1 has a very high transport rate making it a very useful tool to study the transport characteristics of the anion exchangers (29). Abundant evidence shows that maximal transport activity of bicarbonate transporters requires the presence of catalytically active CAII (10, 29). CAII maximizes the anion exchange activity of $\text{Cl}^-/\text{HCO}_3^-$ anion exchangers by forming a physical linkage with the carboxyl tail of the anion exchangers (25, 36). Tomato lectin caused similar distribution of CAII and AE1 in ghost membranes (36). Moreover, CAII and AE1 co-solubilized and co-immunoprecipitated which suggested a complex between the two proteins; antibody directed against the carboxyl tail of AE1 blocked CAII from binding to AE1 and solid phase binding assay demonstrated that the carboxyl terminus tethered to glutathione-S-transferase (GST-Ct) bind to CAII at a saturably (36). Later, it was revealed that the binding motif of CAII was localized to an acidic-

rich region of AE1 containing the residues LDADD (35). Mutation of residues in this region led to lack of binding between AE1 and CAII which supports a complex formation between AE1 and CAII (29, 35). The first 17 amino acid residues of CAII, which is a very basic region, were shown to mediate binding to AE1 (34).

The acidic binding motif is highly conserved among the SLC4 family of transporters which led to the suggestion that CAII interacts with transporters (29). Subsequently, it was demonstrated that the binding of CAII to bicarbonate transporters facilitates the flux of HCO_3^- across the membrane (4, 10, 29). The physical and functional linkage between bicarbonate transporters has been termed bicarbonate transport (BT) metabolon which aims to maximize the transport activity of the transporters (19, 25). Despite the large body of evidence, which suggests the existence of bicarbonate metabolon, other studies have provided data in direct contention of this phenomenon (6, 17, 24).

The present study sought to further explore the concept of the BT metabolon. AE1 and AE3 share similar properties in their sequences and topology (29). Both anion exchangers can bind to CAII which increases their transport efficiency (29). Thus, data obtained from the AE1 studies could be extrapolated to AE3 anion exchanger.

To achieve the first objective wildtype CAII and catalytically inactive CAII, V143Y, were each fused to the C-terminus of AE1 and cloned into plasmid vectors. Constructs were transfected into HEK293 cells and the expression levels of AE1.CAII and AE1.CAII-V143Y were assessed by immunoblotting. The

functional consequences of the fusion of the two CAII isoforms to AE1 were evaluated in HEK293 cells by fluorimetry.

These observations lent credence to the existence of a bicarbonate transport (BT) metabolon. The physiological relevance of a BT is the efficient and maximal transport activity of the bicarbonate transporters. The confirmation of the BT metabolon provided the basis for our second objective that a functional interaction between NHE1, CAII and AE3 (3) will form a pathologically self-sustaining hypertrophic pathway and inhibition or loss of activity of one of the proteins in this complex will ameliorate the hypertrophic stimulation mediated by ANGII and PE. We tested the hypothesis that the loss of the AE3 $\text{Cl}^-/\text{HCO}_3^-$ anion exchanger would lead cause cardiomyocytes to become unresponsive to PE or ANGII-mediated hypertrophy.

Lack of specific pharmacological tools to inhibit AE3 transport activity prompted the use of AE3 null mice to investigate the role the protein plays in the hypertrophic signaling cascade of ANGII and PE. Experiments were undertaken in isolated cardiomyocytes from adult mouse heart and various indices of hypertrophy including cell surface area, hypertrophic molecular markers and protein synthesis were used to assess the effect of ANGII and PE. The data obtained are summarized below:

1. The loss of AE3 did not affect the body weight (BW) of the mice but caused a reduction of heart size (HW) relative to wildtype cardiomyocytes which translated into a decrease in the HW/BW ratio, an index of cardiac

hypertrophy. This provided the first evidence which suggested that AE3 is involved with cardiac developmental process.

2. To delineate further the involvement of AE3 in cardiac function, the hemodynamic properties of the mice heart were examined and our data revealed that under normal conditions, the loss of AE3 does not influence myocardial function.
3. Upon induction of hypertrophy in isolated cardiomyocytes from male adult mice, PE or ANGII caused a marked increase in cardiomyocyte surface area in wildtype myocytes, which was consistent with increased protein synthesis and reactivation of the fetal gene program revealed as elevation of hypertrophic marker genes, ANP and β -myosin heavy chain. The loss of AE3 however, rendered the cardiomyocytes unresponsive to the effects of PE or ANGII. This finding strongly supports the paradigm that AE3 is central to the hypertrophic signaling triggered by pro-hypertrophic agents.
4. Since it has been suggested that AE3 operates in concert with NHE1 and CAII to form a hypertrophic transport metabolon (HTM) (3), we hypothesized that disruption of AE3 would lead to an increase in the expression levels of CAII and NHE1. Our data indicate that CAII and NHE1 levels were increased at the mRNA and protein level which may suggest a compensatory response to the loss of AE3 supporting further the coupling of these three proteins in the hypertrophic cascade.

5. Additionally, hypertrophic intervention led to an increase in the expression level of CAII in both wildtype and *ae3* null cardiomyocytes. NHE1 levels were not influenced by hypertrophic agonists.
6. The AE3 $\text{Cl}^-/\text{HCO}_3^-$ anion exchanger is critical in myocardial pH_i homeostasis (32) by mediating intracellular acidification. Thus, loss of AE3 may cause imbalance of pH_i homeostasis. When the pH_i of cardiomyocytes was measured by fluorimetry, pH_i did not vary significantly between cardiomyocytes from wildtype and *ae3* null hearts. Under imposed intracellular alkalinization, the rate of recovery was much slower in the *ae3* null cardiomyocytes relative to wildtype cardiomyocytes. This supports the premise that AE3 is crucial in maintaining pH_i by acidifying the myocyte.
7. Two major acidifying pathways, AE3 and SLC26A6, are involved in pH_i homeostasis (32). Consequently, we assessed the effect of AE3 disruption on the expression level of SLC26A6, the major myocardial $\text{Cl}^-/\text{HCO}_3^-$ anion exchanger (2). Our data demonstrate that loss of *ae3* had no influence on the expression level of SLC26A6.

Taken together, our data provides insight into the mechanism by which pro-hypertrophic agonists mediate via activation of the HTM which comprises NHE1, AE3 and CAII. Pro-hypertrophic agonists stimulate their respective GPCRs, which leads to activation of downstream effectors including NHE1 (16). It has been shown that NHE1 activation is an early event in the pathway that results in myocardial hypertrophy (8, 9). Thus, we can infer from the present study that

there is an obligatory metabolic linkage of AE3 and NHE1 sustained activation such that AE3 can be induced as an early event in the hypertrophic cascade mediated by PE and ANGII. The loading of the cell with Na^+ as a result of NHE1 and AE3 activation following stimulation by PE and ANGII, will lead to intracellular Ca^{2+} overload via activation of the NCX and will induce further downstream changes culminating in hypertrophic development. Additionally, increased CAII expression upon treatment with PE and ANGII and subsequent enhancement of its activity will ensure adequate supply of substrates for AE3 and NHE1. In the absence of AE3, NHE1 will auto-inhibit (22, 37) and downstream targets which mediate hypertrophy will become inactive, which accounts for lack of influence of pro-hypertrophic intervention on *ae3* null myocytes in the present study.

We demonstrate from these findings that CAII catalytic activity is mandatory to maximizing the anion exchange of HCO_3^- transporters and that this interaction forms the basis of a hypertrophic transport metabolon between NHE1, AE3 and CAII, a pathologically self-sustaining complex whose activation induces hypertrophy which can progress to heart failure.

5.2 Future Directions

The findings from this thesis afford many opportunities for future studies to investigate further the functional consequence of the bicarbonate transport (BT) metabolon and its implication in physiology and pathophysiology. Highlighted below are some of the directions that the present study opens up for future considerations

5.2.1 An Intramolecular Transport Metabolon Fusion of Carbonic Anhydrase II to the C-terminus of the Cl⁻/HCO₃⁻ Exchanger, AE1

Although we were able to demonstrate by the present report that AE1 requires functionally active CAII, additional experiments can be performed to provide evidence to further support this phenomenon. Thus, to provide further evidence to support the existence of a BT metabolon in light of other contrary findings, the following investigations can be undertaken:

1. 'CAII-less' background

By examining the effect of CAII activity on AE1 transport activity in HEK293 cells, it was demonstrated that endogenous CAII is sufficient to maximize activity of the transporter ((29) and the present study). Thus, co-transfection of HEK293 cells with AE1 and exogenous CAII did not lead to enhanced AE1 transport activity compared to AE1 transfected cells. Since CAII is ubiquitously expressed, in order to fully delineate the effect of CAII interaction on bicarbonate transporters, a system that lacks endogenous CAII, which I term a 'CAII-less' system will be warranted. Employing a short hair-pin RNA (shRNA) technique to

knock-out endogenous CAII from HEK293 cells, such a system can be accomplished. Therefore, by generating HEK293 stable cell lines with no endogenous CAII background the effect of CAII on BT can be adequately evaluated.

2. Fusion of CAII and V143Y to the N-terminal tail of AE1

In the present study, wildtype CAII or mutant CAII-V143Y, was tethered to the surface of AE1 at the extreme C-terminal tail. For future considerations similar studies can be undertaken while the CAII isoforms are fused to the extreme N-terminus of AE1. This will address the possibility of steric hindrance which may be prevalent when CAII was fused to the extreme C-terminal of AE1. Also, the possibility of misfolding in the present study could be probed into further.

3. Fusion of CAII to functionally inactive AE1 mutants, LNANN or LAAA

Previous studies demonstrate that mutation of the CAII binding motif of AE1 led to a decrease in AE1 function which is attributed lack of physical link between AE1 and CAII (10, 29). To support the BT metabolon paradigm, catalytically active CAII can be fused to the AE1 mutants, LNANN or LAAA to assess whether the presence of CAII on the surface of the mutant AE1 will salvage transport activity.

4. Co-transfection of AE1 and plant CAII, β -carbonic anhydrase

All carbonic anhydrases belong to three distinct classes, α , β and γ with no sequence homology (27). Mammalian carbonic anhydrases belong to the α class; Most plant isoforms and some bacteria isoforms belong to the β class, while the

carbonic anhydrases isolated from archaeon sources belong to the γ class (13). The β and γ classes have distinct activity and kinetic properties compared to α -class and, these differences can be employed to study the effect of a β -carbonic anhydrase on AE1 transport activity. A plant source of β -carbonic anhydrase, *Methanobacterium thermoautotrophicum*, whose catalytic and kinetic properties have been characterized (27) can be cloned into a mammalian expression vector. β -carbonic anhydrase is less susceptible to inhibition by the sulphonamide compounds (27). Thus, in the presence of a sulphonamide compound such as acetazolamide, endogenous CAII activity will be inhibited. This enables the effect of CA activity to be tested in a background that otherwise has no activity. This study would further test the BTM model, since CAII from a non-mammalian could potentially augment the activity of a mammalian transporter, AE1, when endogenous CAII activity has been inhibited.

5. Extracellular component of the BT metabolon

Previous studies revealed that the BT metabolon contains an intracellular component involving a BT and CAII (10, 19, 29) as well as an extracellular component between a BT and CAIV, which is anchored to the outer surface of the plasma membrane by a glycosphosphatidylinositol linkage (1, 28). Thus, in a system in which both CAII and CAIV are expressed, such as in the heart, interaction between the BT, CAII and CAIV will form an intracellular and extracellular metabolon, respectively. The purpose of this interaction is to potentiate the rapid passage of CO₂ across the plasma membrane which may create a 'pull' (intracellular component) and a 'push' (extracellular component)

phenomenon. The presence of an extracellular BT metabolon can be ascertained by co-expression AE1.CAII or AE1.CAII-V143Y, and CAIV followed by examination of the catalytic activity of AE1 by fluorimetry.

6. Characterization of kinetic properties and catalysis of naturally-occurring metabolon

Bioinformatics studies have revealed that in some subfamilies of secondary carriers referred to as sulfate permease (SulP), are homologues that are either fused to or encoded within operons that also encode homologues of carbonic anhydrases (12). This may suggest that these carriers function as naturally-occurring metabolons that mediate the flux of bicarbonate or carbonate, thus they may be involved in pH_i regulation in the organisms expression them. Some of these carriers are found in prokaryotes (bacteria) where they may regulate functions imperative to survival of these organisms. A typical carrier is found in *Legionella pneumophila* (12), a gram negative, strictly aerobic bacterium belonging to the *Legionellaceae* family (11), which causes Legionnaires' disease, a severe form of pneumonia (30).

A study which aims to understand the role of the SulP carrier in *Legionella pneumophila* can be undertaken by cloning the carrier in bacterial expression vector as well mammalian expression vector. Catalytic and kinetic properties of the carrier can be characterized by employing techniques utilized in the present study.

Ultimately, bicarbonate transport assays can be employed as indicated in this thesis to characterize the bicarbonate transport activity of *Legionella*

pneumophila. Additionally, CA functional assays can be performed to evaluate the CA activity in the protein.

5.2.2 Role of AE3 in the development of cardiomyocyte hypertrophy

Data from the present report demonstrates that loss of AE3 renders the cardiomyocytes less susceptible to hypertrophy mediated by neurohormonal agents, PE and ANGII. Additional studies can be carried out to lend more credence to these findings.

1. *In vivo* study of hypertrophy and AE3

The present study employed an *ex vivo* approach to examine the effect of AE3 deletion on cardiomyocyte hypertrophic growth in presence of PE and ANGII. Although this strategy is well established and provides insight into the mechanism of induction of hypertrophy, it has not gone without its shortfalls. Data obtained from isolated cardiomyocytes may not directly extrapolate to what pertains to the physiological environment. Thus, to delineate further the role of AE3 transport activity in the heart *in vivo* approaches can be harnessed which may truly reflect the physiological environment of the heart. The approaches can include:

i. Transverse aortic constriction (TAC)

The TAC strategy has been employed in several studies in the mice to induce pressure overload which represents a pathological form of hypertrophy (21, 31). This procedure can be used to induce pressure overload in wildtype and *ae3* knock-out mice prior to assessment of physiological functional parameters of the heart such as echocardiography (ECG) and hemodynamic measurements *in vivo*.

Biochemical studies of the isolated heart to study expression levels of regulatory proteins in the development of hypertrophy can also be assessed.

A similar approach whereby the left anterior descending (LAD) artery is ligated can be utilized to examine the role of AE3 in other cardiac pathological conditions such as myocardial infarction (26).

ii. *Drug-induced cardiac hypertrophy by implantation of osmotic pump*

Another technique that is used to induce *in vivo* pathological hypertrophy is implantation of an osmotic pump which delivers pro-hypertrophic agonists (isoproterenol, ANGII, etc.) to the mice (33) at a constant rate. Further, similar studies as in the present thesis can be employed to investigate the role of AE3 in a non-evasive system using the osmotic pump. Observations from these experiments should be consistent with findings from the present thesis and also lend further support to the mechanism underlying hypertrophic mediation by the HTM.

iii. *Exercise-induced hypertrophy in $ae3^{-/-}$ mice*

Physiological hypertrophy can be induced in wildtype and *ae3* null mice by exercise-training (swim-training) to study whether AE3 plays a role in this form of hypertrophy.

2. Assessment of intracellular Ca^{2+} in the cardiomyocytes

Data in this thesis indicate that steady-state pH_i did not differ between cardiomyocytes from WT and *ae3* null mice. However, the rate of recovery of pH_i from induced alkalosis was slower in the *ae3* null cardiomyocytes relative to the wildtype cardiomyocytes. Employing similar fluorescent techniques,

cardiomyocytes can be loaded with a Ca^{2+} -sensitive dye such as fluo-4 (23) and BOCA-1 (15) to assess intracellular Ca^{2+} levels in wildtype or *ae3*^{-/-} cardiomyocytes in the presence or absence of pro-hypertrophic agents.

This is in keeping with our hypothesis that activation of the HTM proteins by hypertrophic agonist leads to intracellular Na^+ overload which induces an elevation of intracellular Ca^{2+} . Results from these experiments will shed more light on the mechanism of hypertrophic induction in WT cardiomyocytes compared to the *ae3* null mice.

We speculate that the level of cytosolic Ca^{2+} will be elevated in the WT cardiomyocytes relative to the *ae3*^{-/-} cardiomyocytes in response to hypertrophic stimulation. Thus, findings from these experiments will explain the failure of hypertrophic agonists to induce hypertrophy in *ae3*^{-/-} cardiomyocytes.

3. Induction of physiological hypertrophy

As mentioned earlier, myocardial hypertrophy can be categorized into physiological and pathological hypertrophy, which are mediated by distinct molecular pathways (5, 18). Since *ae3* null cardiomyocytes are unresponsive to pro-hypertrophic stimulation, which induces pathological hypertrophy, physiological hypertrophy can be activated to assess whether AE3 plays a role in that pathway. This can be achieved by incubating the cardiomyocytes with insulin-like growth factor, which activates the PI3K-PKB pathway (7). In addition, an exercise strategy can also be performed to stimulate physiological hypertrophy to delineate further the role of AE3.

4. Studying cardiac parameters and function in aged mice

The mice used in the study of the cardiac functional parameters (hemodynamic, ECG, etc.) in the present study were approximately three months old. No differences were observed in cardiac functionality between wildtype and *ae3* knock-out mice. Similar studies can be carried out in aged mice to evaluate whether *ae3* plays a role in cardiac function with age. As aged individuals are more susceptible to develop cardiac hypertrophy (14), it will be important to understand whether the loss of AE3 will be protective against hypertrophic agents in the aged mice.

5. Catalytic activity of SLC26A6 and NHE1

Intracellular pH is tightly regulated in the heart by interplay of transporters which mediate transport of H^+ or H^+ -equivalents by acidifying (AE3 Cl^-/HCO_3^- exchanger and SLC26A6) and alkalinizing (NHE1 and NBC) mechanisms (32). Our data showed that in the absence of AE3, NHE1 levels, the major alkalinizing pathway, were elevated but the predominant Cl^-/HCO_3^- exchanger in the heart, SLC26A6, levels were unaffected. The transport activities of NHE1 and SLC26A6 can be assessed in cardiomyocytes to delineate the underlying mechanism which normalized pH_i in the absence of AE3.

6. Interbreeding *ae3* null mice and activated NHE1 transgenic mice

A recent study showed that transgenic mice expressing constitutively active NHE1 are more susceptible to hypertrophic stimulation compared to transgenic mice expressing high levels of NHE1 (20). This thesis demonstrated that loss of *ae3* causes the heart to become unresponsive to hypertrophic stimulation. From these two studies it will be reasonable to speculate that double mutant mice, *ae3*^{-/-}

nhe1 mutant, generated by interbreeding activated NHE1 transgenic mice and *ae3* null mice, may be less responsive to hypertrophic stimulation. This stems from reasons already alluded to that sustained activity of NHE1 requires the presence of active AE3 (8, 9). Thus, for future considerations, double mutant mice can be generated and *in vivo* and *ex vivo* hypertrophic approaches can be employed to probe further the interaction between NHE1 and AE3 to understand their involvement in the pathways underlying cardiac hypertrophy.

Bibliography

1. **Alvarez B, Loisele FB, C.T. S, Schwartz GJ, and Casey JR.** Direct extracellular interaction between carbonic anhydrase IV and the NBC1 $\text{Na}^+/\text{HCO}_3^-$ co-transporter. *Biochemistry* 42: 2321-2329, 2003.
2. **Alvarez BV, Kieller DM, Quon AL, Markovich D, and Casey JR.** Slc26a6: A cardiac chloride/hydroxyl exchanger and predominant chloride/bicarbonate exchanger of the heart. *J Physiol* 561: 721-734, 2004.
3. **Alvarez BV, Xia Y, Sowah D, Soliman D, Light P, Karmazyn M, and Casey JR.** A Carbonic Anhydrase Inhibitor Prevents and Reverts Cardiomyocyte Hypertrophy. *J Physiol* 579: 127-145, 2007.
4. **Becker HM and Deitmer JW.** Carbonic Anhydrase II increases the activity of the human electrogenic $\text{Na}^+/\text{HCO}_3^-$ cotransporter. *J Biol Chem* 282: 13508-13521, 2007.
5. **Bernardo BC, Weeks KL, Pretorius L, and McMullen JR.** Molecular distinction between physiological and pathological cardiac hypertrophy: experimental findings and therapeutic strategies. *Pharmacol Ther* 128: 191-227, 2010.
6. **Boron WF.** Evaluating the role of carbonic anhydrases in the transport of HCO_3^- -related species. *Biochim Biophys Acta* 1804: 410-421, 2010.
7. **Chan AY, Soltys CL, Young ME, Proud CG, and Dyck JR.** Activation of AMP-activated protein kinase inhibits protein synthesis associated with hypertrophy in the cardiac myocyte. *J Biol Chem* 279: 32771-32779, 2004.

8. **Cingolani HE.** Na⁺/H⁺ exchange hyperactivity and myocardial hypertrophy: are they linked phenomena? [editorial]. *Cardiovasc Res* 44: 462-467, 1999.
9. **Cingolani HE and Ennis IL.** Sodium-hydrogen exchanger, cardiac overload, and myocardial hypertrophy. *Circulation* 115: 1090-1100, 2007.
10. **Dahl NK, Jiang L, Chernova MN, Stuart-Tilley AK, Shmukler BE, and Alper SL.** Deficient HCO₃⁻ transport in an AE1 mutant with normal Cl⁻ transport can be rescued by carbonic anhydrase II presented on an adjacent AE1 protomer. *J Biol Chem* 278: 44949-44958, 2003.
11. **Edelstein PH.** *Legionella**. In P. R. Murray (Ed.), *Manual of Clinical Microbiology*. Washington, DC: ASM Press, 2007.
12. **Felce J and Saier MH, Jr.** Carbonic anhydrases fused to anion transporters of the SulP family: evidence for a novel type of bicarbonate transporter. *J Mol Microbiol Biotechnol* 8: 169-176, 2004.
13. **Hewett-Emmett D and Tashian RE.** Functional diversity, conservation, and convergence in the evolution of the alpha-, beta-, and gamma-carbonic anhydrase gene families. *Mol Phylogenet Evol* 5: 50-77, 1996.
14. **Isoyama S, Wei JY, Izumo S, Fort P, Schoen FJ, and Grossman W.** Effect of age on the development of cardiac hypertrophy produced by aortic constriction in the rat. *Circ Res* 61: 337-345, 1987.
15. **Kamiya M and Johnsson K.** Localizable and highly sensitive calcium indicator based on a BODIPY fluorophore. *Anal Chem* 82: 6472-6479, 2010.

16. **Karmazyn M.** Therapeutic potential of Na-H exchange inhibitors for the treatment of heart failure. *Expert Opin Investig Drugs* 10: 835-843, 2001.
17. **Lu J, Daly CM, Parker MD, Gill HS, Piermarini PM, Pelletier MF, and Boron WF.** Effect of human carbonic anhydrase II on the activity of the human electrogenic $\text{Na}^+/\text{HCO}_3^-$ cotransporter NBCe1-A in *Xenopus* oocytes. *J Biol Chem* 281: 19241-19250, 2006.
18. **McMullen JR and Jennings GL.** Differences between pathological and physiological cardiac hypertrophy: novel therapeutic strategies to treat heart failure. *Clin Exp Pharmacol Physiol* 34: 255-262, 2007.
19. **McMurtrie HL, Cleary HJ, Alvarez BV, Loielle FB, Sterling D, Morgan PE, Johnson DE, and Casey JR.** The bicarbonate transport metabolon. *J Enzyme Inhib Med Chem* 19: 231-236, 2004.
20. **Mraiche F, Oka T, Gan XT, Karmazyn M, and Fliegel L.** Activated NHE1 is required to induce early cardiac hypertrophy in mice. *Basic Res Cardiol* 106: 603-616, 2011.
21. **Muller P, Kazakov A, Semenov A, Bohm M, and Laufs U.** Pressure-induced cardiac overload induces upregulation of endothelial and myocardial progenitor cells. *Cardiovasc Res* 77: 151-159, 2008.
22. **Nakamura TY, Iwata Y, Arai Y, Komamura K, and Wakabayashi S.** Activation of Na^+/H^+ exchanger 1 is sufficient to generate Ca^{2+} signals that induce cardiac hypertrophy and heart failure. *Circ Res* 103: 891-899, 2008.
23. **Paredes RM, Etzler JC, Watts LT, Zheng W, and Lechleiter JD.** Chemical calcium indicators. *Methods* 46: 143-151, 2008.

24. **Piermarini PM, Kim EY, and Boron WF.** Evidence against a direct interaction between intracellular carbonic anhydrase II and pure C-terminal domains of SLC4 bicarbonate transporters. *J Biol Chem* 282: 1409-1421, 2006.
25. **Reithmeier RAF.** A membrane metabolon linking carbonic anhydrase with chloride/bicarbonate anion exchangers. *Blood cells, Molecules and Diseases* 27: 85-89, 2001.
26. **Samsamshariat SA, Samsamshariat ZA, and Movahed MR.** A novel method for safe and accurate left anterior descending coronary artery ligation for research in rats. *Cardiovasc Revasc Med* 6: 121-123, 2005.
27. **Smith KS and Ferry JG.** A plant-type (beta-class) carbonic anhydrase in the thermophilic methanoarchaeon *Methanobacterium thermoautotrophicum*. *J Bacteriol* 181: 6247-6253, 1999.
28. **Sterling D, Alvarez BV, and Casey JR.** The extracellular component of a transport metabolon: Extracellular loop 4 of the human AE1 $\text{Cl}^-/\text{HCO}_3^-$ exchanger binds carbonic anhydrase IV. *J Biol Chem* 277: 25239-25246, 2002.
29. **Sterling D, Reithmeier RA, and Casey JR.** A Transport Metabolon. Functional Interaction of Carbonic Anhydrase II and Chloride/Bicarbonate Exchangers. *J Biol Chem* 276: 47886-47894, 2001.
30. **Tronel H, & Hartemann, P.** Overview of diagnostic and detection methods for legionellosis and *Legionella*. *Letters in Applied Microbiology* 48: 653-656, 2009.
31. **Ucar A, Gupta SK, Fiedler J, Erikci E, Kardasinski M, Batkai S, Dangwal S, Kumarswamy R, Bang C, Holzmann A, Remke J, Caprio M,**

- Jentsch C, Engelhardt S, Geisendorf S, Glas C, Hofmann TG, Nessling M, Richter K, Schiffer M, Carrier L, Napp LC, Bauersachs J, Chowdhury K, and Thum T.** The miRNA-212/132 family regulates both cardiac hypertrophy and cardiomyocyte autophagy. *Nat Commun* 3: 1078, 2012.
32. **Vaughan-Jones RD, Spitzer KW, and Swietach P.** Intracellular pH regulation in heart. *J Mol Cell Cardiol* 46: 318-331, 2009.
33. **Verma RK, Arora S, and Garg S.** Osmotic pumps in drug delivery. *Crit Rev Ther Drug Carrier Syst* 21: 477-520, 2004.
34. **Vince JW, Carlsson U, and Reithmeier RA.** Localization of the Cl⁻/HCO₃⁻ anion exchanger binding site to the amino-terminal region of carbonic anhydrase II. *Biochemistry* 39: 13344-13349, 2000.
35. **Vince JW and Reithmeier RA.** Identification of the Carbonic Anhydrase II Binding Site in the Cl⁻/HCO₃⁻ Anion Exchanger AE1. *Biochemistry* 39: 5527-5533, 2000.
36. **Vince JW and Reithmeier RAF.** Carbonic anhydrase II binds to the carboxyl-terminus of human band 3, the erythrocyte Cl⁻/HCO₃⁻ exchanger. *J Biol Chem* 273: 28430-28437, 1998.
37. **Wakabayashi S, Ikeda T, Iwamoto T, Pouyssegur J, and Shigekawa M.** Calmodulin-binding autoinhibitory domain controls "pH-sensing" in the Na⁺/H⁺ exchanger NHE1 through sequence-specific interaction. *Biochemistry* 36: 12854-12861, 1997.

Appendix

Generation of CAII Adenoviral Constructs

This work was included as part of a published paper:

Brown, B., Quon, A., Dyck, J. and Casey, J.R. (2012) Carbonic Anhydrase II Promotes Cardiomyocyte Hypertrophy, *Can. J. Physiol. Pharmacol.* **90**, 1599-610.

6.1 Introduction

Carbonic anhydrases (CAs) are a group of zinc metalloenzymes that play critical physiological roles. They are ubiquitously present in eukaryotes and prokaryotes and they are encoded by three unrelated genes 1. α -CAs are expressed mostly in vertebrates, algae and the cytoplasm of green plants, 2. β -CAs are expressed predominantly in bacteria, algae and chloroplasts of plants and 3. γ -CAs are found in archaea and bacteria (4, 10).

There are about 14 α -CAs identified thus far with diverse subcellular localization and tissue distribution. Cytosolic isoforms include CAs I-III and CA VII; four isozymes are membrane-bound (CAIV, CAIX, CAXII and CAXIV), CAV is located in the mitochondria and CAVI is the secreted form. CAs catalyze the reversible hydration of CO_2 to produce bicarbonate and proton. Since the primary buffer system in the human body is the $\text{CO}_2/\text{HCO}_3^-$, CAs are involved with cytosolic and whole-body pH regulation, regulation of acid/base homeostasis and fluid secretion.

In highly metabolic tissues such as the heart, whose function is accompanied by large production of CO_2 , CA catalytic activity is indispensable to maintain normal function. Of the 14 CA isozymes identified, CAII has the highest rate of catalysis (6, 7). Of particular physiological importance is the evidence proposing that CAs interact with bicarbonate transport proteins forming a transport metabolon, an interaction shown to maximize the transport rate of the transporters (9, 12, 13).

The adult myocardium expresses a number of CAs including CAIV, CAIX, CAXII and CAXIV (8, 11). Originally thought to be expressed exclusively in neonatal hearts CAII was recently shown to be expressed in the adult ventricular myocytes (1, 2, 14). The high metabolic activity of the myocardium results in a significant production of CO₂ which must be extruded in order to maintain pH_i homeostasis and normal function. Recently, it was shown that CAII is involved in the hypertrophic stimulation mediated by PE and ANGII (2). Inhibition of CAII activity prevented and reversed cardiomyocyte hypertrophy induced by PE and ANGII. This was attributed to the limitation of substrates for NHE1 and AE3 thus inhibiting the anion transport activity of the exchangers (2). Interestingly, PE and ANGII stimulation resulted in an increased expression of CAII an effect which was blunted by CAII inhibition. The CA inhibitors employed in this study, acetazolamide (ATZ) and ethoxzolamide (ETZ) may also inhibit other CAs in the myocardium which may suggest that other CAs other than CAII may be involved in hypertrophic signaling mediated by neurohormonal agents.

Thus, to understand the role of CAII in the myocardial response to hypertrophic stimuli, adenoviral transduction system was adopted to overexpress CAII in cardiomyocytes. Cardiomyocytes unlike other cell types do not lend themselves to standard transfection procedures. Therefore in order to deliver a gene of interest to study its properties, cardiomyocytes are infected with adenoviral construct carrying the target gene. The generation of the construct is based on a report established more than a decade ago that employs the use of

recombinant adenoviruses (5). This approach will provide a direct evidence of the involvement of CAII in the development of hypertrophy in cardiomyocytes.

In the present study we attempted to generate a recombinant adenoviral construct bearing wildtype CAII (Ad.WT-CAII) and mutant CAII (Ad.V143Y-CAII) for transfer into isolated cardiomyocytes. The effect of CAII in the development of cardiomyocyte hypertrophy mediated by hormonal stimulation can subsequently be assessed.

6.2 Results and Discussion

6.2.1 Generation of adenoviral constructs

To understand the role of CAII directly in cardiomyocyte hypertrophic development, adenoviral constructs carrying the gene that encodes wildtype human CAII (hCAII), pDAS1, was generated. Another construct bearing the catalytically inactive CAII mutant, V143Y, was also generated (pDAS2). The success of the cloning was confirmed by DNA sequencing through the entire length of the respective clones.

6.2.2 Expression of CAII proteins in cardiomyocytes

To confirm the presence of CAII in the adenoviral packaging cell lines, rat neonatal cardiomyocytes were transfected with pAdCAII-WT or pAdCAII-V143Y. As a negative control another group of cardiomyocytes were transfected with empty vector, pAdTrack-CMV. Forty-eight hours later, cells were harvested and lysates were probed for the presence of CAII using rabbit polyclonal anti-CAII antibody by western immunoblotting. Our results demonstrate that hCAII

and V143Y both resolved at the expected molecular weight, ~27 kDa, which suggests that the generation of the adenoviral package containing the CAII constructs, was successful (Fig. 6.1). Also a band resolved at the group transfected with empty vector which indicates the presence of endogenous CAII in cardiomyocytes (1) (Fig. 6.1).

The success of the cloning provided the basis to investigate the role of CAII in the phenylephrine (PE) or angiotensin II (ANGII)-mediated cardiomyocyte hypertrophy. The project was followed up by a graduate student in the Casey lab, Ms. Brittany Brown, who for her M.Sc. research showed that over-expression of wild-type CAII in neonatal rat ventricular myocytes did not affect cardiomyocyte hypertrophy development. Further, CAII-V143Y over-expression blunted hypertrophic development in response to pro-hypertrophic agonists, which led to the suggestion that CAII-V143Y behaves in a dominant negative fashion over endogenous CAII to suppress hypertrophy (3).

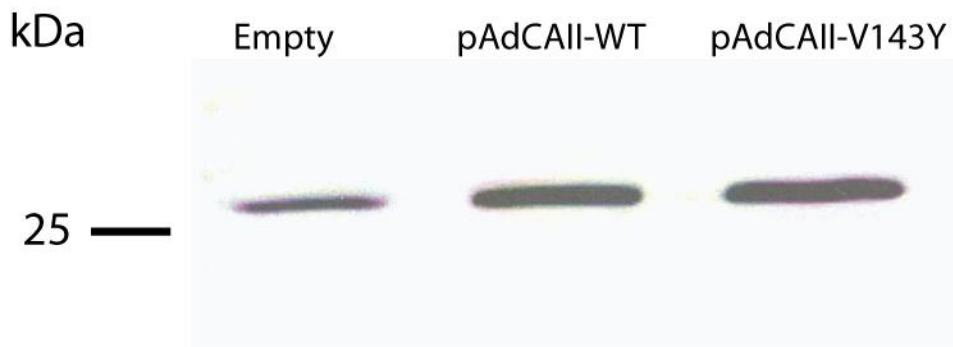


Fig. 6.1 Expression of adenoviral constructs in neonatal cardiomyocytes. Cardiomyocytes isolated from 7-day old rat pups were cultured and transfected with empty vector (Empty), adenoviral vector containing wildtype CAII (pAdCAII-WT) or adenoviral vector containing CAII mutant (pAdCAII-V143Y) 48 h later. Forty-eight hours later, cardiomyocytes were harvested lysed using lysis buffer. Samples were loaded and resolved on SDS-PAGE and proteins were transferred onto PVDF membranes. Immunoblots were incubated with rabbit polyclonal anti-CAII antibody for 16 h at 4 °C followed by incubation with donkey anti-rabbit IgG conjugated to horseradish peroxidase for 1 h at room temperature. Immunoblot was visualized using ECL reagents and Kodak Imaging Station 440CF.

Bibilography

1. **Alvarez BV, Quon AL, Mullen J, and Casey JR.** Quantification of carbonic anhydrase gene expression in ventricle of hypertrophic and failing human heart. *BMC Cardiovasc Disord* 13: 2, 2013.
2. **Alvarez BV, Xia Y, Sowah D, Soliman D, Light P, Karmazyn M, and Casey JR.** A Carbonic Anhydrase Inhibitor Prevents and Reverts Cardiomyocyte Hypertrophy. *J Physiol* 579: 127-145, 2007.
3. **Brown BF, Quon A, Dyck JR, and Casey JR.** Carbonic anhydrase II promotes cardiomyocyte hypertrophy. *Can J Physiol Pharmacol* 90: 1599-1610, 2012.
4. **Gilmour KM.** Perspectives on carbonic anhydrase. *Comp Biochem Physiol A Mol Integr Physiol* 157: 193-197, 2010.
5. **He TC, Zhou S, da Costa LT, Yu J, Kinzler KW, and Vogelstein B.** A simplified system for generating recombinant adenoviruses. *Proc Natl Acad Sci U S A* 95: 2509-2514, 1998.
6. **Kivela AJ, Parkkila S, Saarnio J, Karttunen TJ, Kivela J, Parkkila AK, Pastorekova S, Pastorek J, Waheed A, Sly WS, and Rajaniemi H.** Expression of transmembrane carbonic anhydrase isoenzymes IX and XII in normal human pancreas and pancreatic tumours. *Histochem Cell Biol* 114: 197-204, 2000.
7. **Mori K, Ogawa Y, Ebihara K, Tamura N, Tashiro K, Kuwahara T, Mukoyama M, Sugawara A, Ozaki S, Tanaka I, and Nakao K.** Isolation and

characterization of CAXIV, a novel membrane-bound carbonic anhydrase from mouse kidney. *J Biol Chem* 274: 15701-15705, 1999.

8. **Purkerson JM and Schwartz GJ.** Expression of membrane-associated carbonic anhydrase isoforms IV, IX, XII, and XIV in the rabbit: induction of CAIV and IX during maturation. *Am J Physiol Regul Integr Comp Physiol* 288: R1256-1263, 2005.

9. **Sterling D, Reithmeier RA, and Casey JR.** A Transport Metabolon. Functional Interaction of Carbonic Anhydrase II and Chloride/Bicarbonate Exchangers. *J Biol Chem* 276: 47886-47894, 2001.

10. **Supuran CT.** Carbonic anhydrases--an overview. *Curr Pharm Des* 14: 603-614, 2008.

11. **Vargas LA and Alvarez BV.** Carbonic anhydrase XIV in the normal and hypertrophic myocardium. *J Mol Cell Cardiol* 52: 741-752, 2012.

12. **Vince JW and Reithmeier RA.** Identification of the Carbonic Anhydrase II Binding Site in the Cl⁻/HCO₃⁻ Anion Exchanger AE1. *Biochemistry* 39: 5527-5533, 2000.

13. **Vince JW and Reithmeier RAF.** Carbonic anhydrase II binds to the carboxyl-terminus of human band 3, the erythrocyte Cl⁻/HCO₃⁻ exchanger. *J Biol Chem* 273: 28430-28437, 1998.

14. **Vuillemin M and Pexieder T.** Carbonic anhydrase II expression pattern in mouse embryonic and fetal heart. *Anat Embryol (Berl)* 195: 267-277, 1997.